Contribution to engine-out aircraft trajectory management and control

Hongying Wu

THÈSE

En vue de l'obtention du

DOCTORAT DE L'UNIVERSITÉ DE TOULOUSE

Délivré par :
Institut National des Sciences Appliquées de Toulouse (INSA Toulouse)

Discipline ou spécialité :

Automatique

Présentée et soutenue par :
Hongying WU

le : lundi 22 avril 2013

Titre :

Contribution to Engine-out Aircraft Trajectory Management and Control

---

JURY

Andreï DONCESCU, Alexandre Carlos BRANDÃO RAMOS
David ZAMMIT-MANGION, Minesh POUDEL
Félix MORA-CAMINO, Thierry MIQUEL

Ecole doctorale :
Systèmes (EDSYS)

Unité de recherche :
MAIAA/ENAC

Directeur(s) de Thèse :

Félix MORA-CAMINO

Rapporteurs :

Daniel CHOUKROUN, Weigang LI

ACKNOWLEDGEMENTS

This research was carried on in the laboratory: MAIAA (Laboratoire de mathématiques appliquées et d'informatique appliquée à l'aéronautique), Air Transport department at ENAC (Ecole Nationale de l'Aviation Civile).

First of all, I would like to express my sincere gratitude to my supervisor, Professor Felix Mora-Camino, who encourages, gives me instructive advising constantly during my graduate research. I am deeply grateful of his help in the completion of this thesis.

Secondly, I would like to thank jury for accepting to review my thesis. I would like to thank ENAC for providing the research project. I would also like to express my gratitude to the professors and teachers: Mr. Thierry Miquel, Mr. Antoine Drouin and Mr. Christian Le Roux, who have instructed and helped me a lot. Special thanks to all my classmates and colleagues: Lunlong Zhong, Hakim Bouadi, etc, who spent time in listening to me and helping me work out my problems.

Finally, thanks to my family for their continuous support and encouragement.

ABSTRACT

Engine-out is an undoubted critical situation for flight safety. The objective of this thesis is to improve the management of emergency manoeuvres for transportation aircraft once all engines go out at a given point during the flight. Here we consider the evolution of the gliding aircraft along a vertical plane possibly leading directly to a safe landing place. The gliding qualities of standard transportation aircraft are first analyzed and reachable areas from given initial situations are established. Once a safe reachable area exists the problem which is tackled here is to develop design principles for a guidance system which makes the aircraft perform a feasible glide trajectory towards such landing area. Reverse dynamic programming is used to build backwards sets of feasible trajectories leading to final conditions compatible with engine-out landing. To get an on-line device to produce efficient directives for the autopilot or the human pilot (through a flight director), a neural network is built from the generated database. Then simulation results are analyzed for validation and further improvements of the proposed approach are considered.

Keywords: Engine-out, Glide Flight, Reverse Dynamic Programming, Neural Networks

RÉSUMÉ

La panne de moteur est une situation critique pour la sécurité du vol. L'objectif de cette thèse est d'améliorer la gestion de la trajectoire avion d'urgence dans le cas d'une panne totale de moteur en un certain point de vol alors que l'avion a déjà pris une certaine vitesse et une certaine altitude après le décollage. Dans cette étude, on considère que la trajectoire de vol plané le long d'un plan vertical peut conduire directement à un lieu atterrissage sûr. Les performances d'un avion de transport sont d'abord analysées, et les lieus atteignables sont établis à partir d'une situation donnée initiale. Une fois une zone de sécurité accessible existe le problème qui est abordée ici est de développer un système de guidage qui permet à l'avion d'effectuer une trajectoire faisable vers la zone d'atterrissage. La programmation dynamique inverse est utilisée pour construire en arrière des ensembles de trajectoires faisables vers conditions finales compatibles avec panne de moteur. Afin d'obtenir un dispositif en ligne pour générer des directives efficaces pour le pilote automatique ou le pilote humain (par un directeur de vol), un réseau de neurones est construit à partir de la base de données générée. Ensuite, les résultats de simulation sont analysés pour validation, et d'autres améliorations de l'approche proposée sont prises en considération.

Mots clé: panne de moteur, vol plané, programmation dynamique inverse, réseau de neurones

CONTENTS

I General Introduction 1
I.1 General Considerations 3
I.2 General Objectives 4
I.3 Thesis Organization 4
II Engine-out Situations and Consequences 7
II.1 Introduction 9
II.2 Some Engine-Out Occurrences 9
II.3 Main Engine-Out Causes 11
II.4 Main Consequences of Engine-Out 13
II.4.1 The consequences on flight safety 13
II.4.2 The consequences on operational and control system 13
II.4.3 The consequences on the on-board digital systems 17
II.4.4 The consequences on aircraft environment 19
II.4.5 Consequences on other systems and equipments 25
II.5 Conclusion 25
III Engine-out Flight Dynamics for Transportation Aircraft 27
III.1 Introduction 29
III.2 The Reference Frames 29
III.2.1 Definitions of the considered reference frames 29
III.2.2 Rotation matrices between different reference frames 31
III.3 Aerodynamic Forces and Moments Applied to the Gliding Aircraft 32
III.4 Glide Dynamics Equations 34
III.5 The Effect of Wind on Glide Dynamics 35
III.5.1 Wind dependent ground speed and path angle 36
III.5.2 Wind dependent ground speed and angle of attack 39
III.6 Conclusion 46
IV Gliding Performances of Transportation Aircraft 47
IV.1 Introduction 49
IV.2 Glide Range Optimization 49
IV.3 Steady Straight Gliding Conditions 51

IV.4 Non Steady Equilibrated Glide Path Angle ……..…….. 55
IV.5 Steady Glide Turn Manoeuvres …….……. 60
IV.6 Conclusion …… 63
V Stability of Gliding Flight for Transportation Aircraft …….…….. 65
V.1 Introduction …….…….. 67
V.2 Stability along a Gliding Trajectory …….……...… 67
V.2.1 Characteristics of a steady glide reference trajectory …… 67
V.2.2 Case of a wind affecting mainly the angle of attack ……...…… 69
V.2.3 The general longitudinal case …….…….. 73
V.3 Stability during Glide with Undamped Pitch Dynamics ……...…… 77
V.3.1 Linear approximation of fast longitudinal dynamics ……. 77
V.3.2 Effect of wind on undamped short period dynamics …….…… 80
V.4 Simulation Results for Glide Stability Analysis ……. 81
V.4.1 Roots locus variation with wind speed pulses ……..…….. 81
V.4.2 Evolution of glide parameters under different wind speed scenarios ……... 82
V.5 Conclusion …….……. 85
VI Aircraft Trajectory Optimization Techniques: an Overview ……..…….. 87
VI.1 Introduction …….. 89
VI.2 Previous Research on Aircraft Trajectory Optimization ……. 89
VI.3 The General Trajectory Optimization Problem …….....…. 91
VI.4 Indirect Methods …….……. 93
VI.4.1 Optimality conditions …….…….. 93
VI.4.2 General features of indirect methods ……..……94
VI.5 Direct Methods ……. 96
VI.5.1 Direct Shooting Methods …….…… 97
VI.5.2 Direct Collocation Methods …….……. 100
VI.5.3 Limitation of direct methods ……. 100
VI.6 Dynamic Programming ……. 101
VI.6.1 Definition and scope of Dynamic Programming …….…… 101
VI.6.2 The optimization process of Dynamic Programming …… 101
VI.6.3 Applications to Aircraft Trajectory Optimization ……. 104
VI.7 Conclusion …….. 105

VII Vertical Glide Trajectory Generation through Dynamic Programming …….. 107
VII.1 Introduction …… 109
VII.2 Formulation of the Trajectory Optimization Problem …… 109
VII.2.1 Flight dynamics and flight domain constraints …… 109
VII.2.2 A first trajectory optimization problem formulation …….. 112
VII.2.3 Optimal trajectory problem formulation including final maneuverability … 113
VII.3 Analysis of the Trajectory Optimization Problem and Solution Strategy … 113
VII.4 Generation and Selection of Feasible Trajectories by Reverse Integration …..….. 115
VII.4.1 Selecting the space discretization …… 115
VII.4.2 Integrating the state equations and criterion discretization ……. 117
VII.4.3 Melting states at stages …… 119
VII.5 Dynamic Programming Selection Process .....…….. 123
VII.6 Numerical Results ……..…… 125
VII.7 Conclusion …… 129
VIII On-line Neural Control for Engine-out Gliding Aircraft ……..……. 131
VIII.1 Introduction …… 133
VIII.1.1 The need for a new Flight Director function ……..…..…… 134
VIII.1.2 Using a Neural Network as control parameter on-line generator …….. 134
VIII.2 Neural Networks ……..…… 134
VIII.2.1 Main characteristics of Feed Forward Neural Networks ……..…….. 134
VIII.2.2 Neural Networks applications in flight guidance ……..… 136
VIII.3 Neural Networks for Online Computation of Reference Pitch Angle ….….. 137
VIII.3.1 General features of the adopted Feed-forward Neural Networks ……. 137
VIII.3.2 The developed neural network structure ……. 139
VIII.3.3 Training and validation results ……. 140
VIII.4 Simulation Results …….. 143
VIII.4.1 Engine-out aircraft glide guidance without wind ……..…… 144
VIII.4.2 Engine-out aircraft glide guidance in the presence of wind …… 148
VIII.5 Engine-Out Emergency Management and System ……... 152
VIII.5.1 Integrating Engine-out guidance function into on-board systems …... 153
VIII.5.2 Tentative displays for controlled operation in Engine-Out situation … 155
VIII.6 Conclusion ……... 160

IX General Conclusion 161
IX.1 Main Objective of the Thesis 163
IX.2 Achievements 163
IX.3 Perspectives for Further Research and Development 164
Annex A Reference Aircraft Parameters 167
Annex B Non-linear Dynamic System Stability 171
B.1 Introduction 173
B.2 The State Models 173
B.3 Concepts of Stability at an Equilibrium Point 174
B.3.1 Stability of an equilibrium point (as defined by Lyapunov) 174
B.3.2 Asymptotic stability 175
B.3.3 Exponential stability 175
B.3.4 Global stability 176
B.3.5 Stability of a trajectory 176
B.4 The Lyapunov Method 176
B.4.1 Lyapunov candidate functions 176
B.4.2 Lyapunov Derivative 177
B.4.3 Local asymptotic stability 177
B.4.4 Global asymptotic stability 178
B.4.5 Examples of Lyapunov candidate function 179
B.4.6 Krasovskii method 179
B.5 Linear Systems Case 180
Annex C Examples of Numerical Integration Methods and Evaluation 181
C.1 Introduction 183
C.2 Euler's Method 183
C.3 Runge-Kutta Method 185
Annex D Feed-forward Neural Networks Training 189
D.1 Feed-Forward Neural Networks 191
D.2 Feed-forward Neural Network with Backward Propagation Algorithm 191
D.3 The Neural Network Training Process 194
Reference 197
Résumé 211

LIST OF FIGURES

Figure 2.1 Structure of hydraulic servo system ……. 14
Figure 2.2 Servo-control scheme of an aerodynamic surface ……..……. 14
Figure 2.3 A320 Hydraulic generation and distribution ……..…….. 16
Figure 2.4 Electrical power generation and distribution …….. 18
Figure 2.5 An example of arrangement of power supply …….. 18
Figure 2.6 The cabin temperature (pink curve) and outside temperature (yellow curve) … 21
Figure 2.7 Cabin pressure (pink curve) and outside pressure (yellow curve) ……. 22
Figure 2.8 The cabin temperature (pink curve) and outside temperature (yellow curve) with 20kw heating power ……...……..…… 22
Figure 2.9 Cabin pressure (pink curve) and outside pressure (yellow curve) with 20kw heating power …… 23
Figure 2.10 Cabin environment without air-conditioning …….……... 24
Figure 2.11 Cabin environment with an auxiliary heating system …….……. 24
Figure 3.1 Body frame with respect to the earth frame …… 30
Figure 3.2 Wind frame with respect to body frame …….. 31
Figure 3.3 Wind vector in vertical plane …… 40
Figure 4.1 Forces acting on a gliding aircraft …….……... 49
Figure 4.2 The green dot on Primary Flight Display …….…… 53
Figure 4.3 Example of steady state airspeed variation with respect to altitude …..…… 55
Figure 4.4 Evolution of γ with flight altitude …….……. 56
Figure 4.5 Steady gliding range ……... 57
Figure 4.6 Flight time duration of steady gliding at maximum path angle ……. 58
Figure 4.7 Gliding airspeed for different bank angles at different altitudes ….……. 61
Figure 4.8 Gliding path angle at different bank angles …… 62
Figure 4.9 Steady gliding turn radius at different bank angles and altitudes ……. 63
Figure 5.1 Steady glide airspeed with respect to altitude …….……. 68
Figure 5.2 Adopted wind effect on angle of attack ……. 71
Figure 5.3 Effect of a windshear on steady glide …… 72
Figure 5.4 Root locus of short period mode with different airspeed at different flight levels ... 79
Figure 5.5 Immediate Effect of Headwind on Short Period Root locus ……... 80

Figure 5.6 Immediate Effect of Tailwind on Short Period Root locus ……..…… 80
Figure 5.7 Roots loci for different wind scenarios ……. 81
Figure 5.8 Airspeed and ground speed under headwind pulses ……..…… 82
Figure 5.9 Evolution of pitch, glide and aerodynamic angles with headwind pulses …. 83
Figure 5.10 Pitch rate under headwind pulses ……...……..…… 83
Figure 5.11 Airspeed and ground speed under tailwind pulses …….……. 84
Figure 5.12 Evolution of pitch, glide and aerodynamic angles with tailwind pulses ….. 84
Figure 5.13 Pitch rate under tailwind pulses ……... 85
Figure 6.1 A classification of direct methods …….. 96
Figure 6.2 Discretization for direct shooting …….. 98
Figure 6.3 Stages and search space for Dynamic Programming …… 103
Figure 7.1 Ground distance to land *x* ……..…….…… 111
Figure 7.2 Space discretization for trajectory optimization …….…….. 117
Figure 7.3 Example of state generation after two reverse integrations ……..... 118
Figure 7.4 State generation process from one stage to the next ……. 120
Figure 7.5 Merging process at stage *k*+1 ……..……... 122
Figure 7.6 The states at stage *k*+1 after the merging process ……. 123
Figure 7.7 The optimal paths after selection at stage *k*+1 …….. 124
Figure 7.8 Examples of 3D optimal glide trajectories ……..…… 125
Figure 7.9 An example of computed 3D gliding trajectory ……. 126
Figure 7.10 Evolution of pitch angle of a computed gliding trajectory ……. 126
Figure 7.11 Safe glide domain from Reverse Dynamic Programming ……. 127
Figure 7.12 The computed safe total energy glide domain …….. 127
Figure 7.13 The computed safe altitude domain for gliding ……... 128
Figure 7.14 The computed safe speed domain for gliding …….. 128
Figure 7.15 Optimal trajectories with different gliding ranges ……. 129
Figure 8.1 Adopted structure for the feed-forward neural network ……. 138
Figure 8.2 Training/Validation intervals and associated fuzzy membership functions …. 140
Figure 8.3 Mean squared error evolution during training of neural network 5 ……... 141
Figure 8.4 Error distribution for validation of neural network 5 …….……. 141
Figure 8.5 Mean squared error evolution during training of neural network 7 ……... 142
Figure 8.6 Error distribution for validation of neural network 7 ….……. 142

Figure 8.7 Neural guidance structure during engine-out glide maneuver ….…….. 143
Figure 8.8 3D controlled glide trajectories with different ranges .....…. 144
Figure 8.9 Vertical controlled glide trajectories with different ranges …….. 145
Figure 8.10 Airspeed evolution with different gliding ranges ……. 145
Figure 8.11 Pitch angle variation along the different controlled glide trajectories ….. 146
Figure 8.12 3D gliding trajectories with 159 km and 165 km ranges …… 147
Figure 8.13 Vertical gliding trajectories with 159 km and 165 km ranges …… 147
Figure 8.14 Airspeed evolution with 159 km and 165 km gliding ranges ……..……. 148
Figure 8.15 Glide path angle with the effect of wind ……..…… 149
Figure 8.16 3D view of controlled glide trajectories with wind ……..…… 150
Figure 8.17 Vertical tracks of controlled glide trajectories with wind …..…… 151
Figure 8.18 Airspeed variations along controlled glide trajectories with wind …… 151
Figure 8.19 Pitch angle variations along controlled glide trajectories with wind …..... 152
Figure 8.20 Reference glide trajectory computation steps ……. 154
Figure 8.21 PFD engine-out information generation process ……..…… 155
Figure 8.22 Proposed indications on PFD for *on range* glide situation ……..……. 156
Figure 8.23 Proposed indications on PFD for *over range* glide situation ……..…….. 158
Figure 8.24 Proposed indications on PFD for *out of range* glide situation ……..……... 159
Figure B.1 Lyapunov stability …… 175
Figure B.2 Asymptotic stability ……. 175
Figure D.1 Artificial neuron ……..…….. 191
Figure D.2 The structure of a feed-forward ANN …… 192
Figure D.3 Flow chart of general feed-forward neural networks training ……..... 195

LIST OF TABLES

Table 2.1 Main reasons for engine-out ……..…… 12
Table 3.1 The ground speed (m/s) in different horizontal winds with airspeed of 150m/s... 40
Table 3.2 The ground speed (m/s) in different horizontal winds with airspeed of 110m/s... 41
Table 3.3 The ground speed (m/s) in different vertical winds …….……..…….. 41
Table 3.4 The ground speed (m/s) approximation ……. 42
Table 3.5 The angle of attack in different horizontal winds with airspeed of 150m/s 43
Table 3.6 The angle of attack in different horizontal winds with airspeed of 120m/s 43
Table 3.7 The angle of attack in different horizontal winds with airspeed of 100m/s 43
Table 3.8 The angle of attack in different horizontal winds with airspeed of 80m/s ….. 44
Table 3.9 The angle of attack in different vertical winds with airspeed of 150m/s ……. 44
Table 3.10 The angle of attack in different vertical winds with airspeed of 120m/s ….... 45
Table 3.11 The angle of attack in different vertical winds with airspeed of 100m/s ….... 45
Table 3.12 The angle of attack in different vertical winds with airspeed of 80m/s ……. 45

CHAPTER I

GENERAL INTRODUCTION

I.1 General Considerations

Along the last decades air transportation has been playing an important role to enable communication and the transport of goods and persons within a more and more globalized world economy. According to statistics of IATA (International Air Transport Association), 2.8 billion people flew on 38 million flights in 2011. This number is expected to increase significantly in the future. According to statistics of fatalities over decades, comparing different means of transportation (rail, water, road and air transportation), air transportation appears to be the safest transportation mode. Thanks to the endeavours of aircraft designers, aircraft manufacturers, airline operators, air traffic controllers, air transport regulations and others, the probability of aircraft accidents with human victims has been reduced to a very low value. Although aviation safety has been of the highest priority for organizations such as ICAO (International Civil Aviation Organization) and IATA, that does not impair some disasters to occur from time to time. In general these disasters take over all the aircraft passengers and crew with a high numbers of victims and then result in being very impressive for the public.

The current level of safety today is about one fatal accident per million flights[ICAO[1]]. This is a global goal which has been set by ICAO decades ago. Studies show that human factors are main contributors to air transport accidents [MELISSA J. P.], especially when some technical failures or several other adverse factors such as weather or maintenance problems appear. Pilots play a decisive role in the management of nonstandard situations for which on board automatic systems have not been designed to cope with. So designing automatic decision aid systems can help to manage efficiently critical situations such as engine-out.

Engines are essential for safe flight. Without their fault free operation, aircraft are unable to sustain flight. The failure of engines is an undoubted dramatic factor for safety since the safe flight domain of the aircraft is then subject to a dramatic shrinking while the availability of aerodynamic actuators is hampered by the deficit of available power. Many incidents and accidents are resulting from one engine failure and some from engine-out.

Here an undesirable and very special case, in which all engines go out at a given point during the flight, is considered. It is supposed that engine-out occurs once the aircraft has already gained some speed and altitude after take-off or is already at cruise or performing the first steps of descent for approach. So, here we do not consider the case in which engine-out occurs in the first steps of climb or the final approach. In both cases, the survivability of the aircraft is fully dependent on the skills of pilots and their immediate reaction to this catastrophic situation.

It appears that in engine-out situation any wrong decision made by pilot may lead to catastrophic consequences as it is the case with much less dangerous failure situations where a high percent of fatal accident is related to the action of pilot [ARENDT D.]. So it looks quite important to try to develop an emergency guidance capability for these situations. This new functionality could be integrated in the Guidance System next to the Flight Management System (FMS) of the aircraft in charge of selecting a proper landing site and calculate a feasible trajectory towards this site. Then the guidance system working in an emergency flight director mode would generate indications to the pilot to perform a safe descent are with some perspective of survival at the landing site.

I.2 General Objectives

To achieve this purpose there are major steps which should be performed in the research:

- Establish and analyze the flight dynamics of an air transportation aircraft with total engine failure (engine-out).
- Study the gliding characteristics and engine-out flying qualities of a transportation aircraft.
- Develop a method to establish the gliding domain from a given situation.
- Develop a method to determine optimized gliding trajectory towards a safe landing place.
- Develop an online advisory scheme for engine-out glide.

I.3 Thesis Organization

According to the objectives mentioned before, the thesis has been divided in several chapters:

- In chapter I the significance of trajectory optimization for all-engine-out is presented.
- In chapter II some situations and consequences of engine-out are analyzed.
- In chapter III the flight dynamics of engine-out aircraft are discussed to build the foundation of analysis for trajectory optimization.
- In chapter IV the gliding performances of an engine-out transportation aircraft are studied with the aim to find the reachable area.
- In chapter V the stability of gliding flight is discussed.
- In chapter VI a survey for optimization methods applied to aircraft trajectory optimization is performed.
- In chapter VII the chosen method for trajectory optimization of engine-out aircraft is introduced and numerical results are displayed. This allows to identify a safe glide domain and to build the corresponding data base.
- In chapter VIII an on-line advisory scheme for engine-out aircraft is built from the data base generated in chapter VII and numerical results as well as possible displays for the advisory system are provided.
- Finally the conclusion and perspectives for this study are presented in chapter IX.

CHAPTER II

ENGINE-OUT SITUATIONS AND CONSEQUENCES

II.1 Introduction

This chapter presents at first an overview of the main reported engine-out occurrences as well as a short analysis of known causes of engine-out. Then, it presents the main consequences of engine-out over airborne systems directly related with the sustainability of the flight in this situation. Indeed, this study is not devoted to aircraft design safety or to aircraft systems risk analysis, but instead to the conception of operational devices and methods turning this catastrophic situation into a bearable one with some perspective of survival. So, after describing the main components of the hydraulic systems of a transportation aircraft, the working of an aerodynamic actuator under servo-control with different pressure conditions is analyzed. This aspect is essential to check the remaining aircraft controllability with respect to the aerodynamic surfaces. Also is considered in this chapter, the evolution of the temperature and pressure of the cabin during a glide without or with reduced air conditioning, so that the resulting threat to passengers and crew health is evaluated.

II.2 Some Engine-Out Occurrences

In 1982, a British Airways 747 aircraft encountered a cloud of volcanic ash [ICAO[2]]and immerged itself into this cloud. After it flight into the cloud of volcanic, all engines lost their power. Fortunately they were restarted after the aircraft got out of the cloud of volcanic ash. Similarly, on 15 December 1989, a Boeing 747 of KLM (flight 867) [ICAO[2]], its engines stopped working after passing through a cloud of volcanic ashes emitted from Mount Redoubt when the aircraft flied to the airport of Anchorage, Alaska. After descending to 12 000 feet above Talkeetna Mountains, the engines restarted, so the aircraft land safely. But the company spent 80 million dollars in changing the four reactors for safety. That is nearly a third of the price of a new B747.

On 15/01/2009, the flight 1549, which was from New York City to Charlotte North Caroline [NTSB[1]]. Just after the flight took off from LaGuardia International Airport and climbing to 2800 feet (853m), it came across a group of big birds whose weight were from 2.6 to 4.8 kg. Some birds were sucked into the engine. It caused engine stop working.

Although without engine power the pilot made a success of performing an emergency landing on the Hudson River. Thanks to the proper decision and operation of pilot all lives onboard were saved, and nobody was seriously injured. The pilot was familiar with this aircraft and knew very well terrain of New York.

On 17/01/2008, in the final approach of flight 38, belonging to British Airway, which was about 220 meters high and 3.2 km from the runway, engines of this B777 were damaged because the temperature in engines kept higher than the 777's designed operating parameters [SLEIGHT P A]. When landed it missed runway and taxied on the grass of 350-400 m ahead of the runway. The problem was caused by the injection of fuel to the reactors, because the pump ports couldn't provide enough pressure.

On August 6, 2005 the flight 152F flew from Bari to Djerba. Because the Fuel Quantity Indicator (FQI) could not be triggered correctly, FQI shown that there was 2300kg fuel on board. In fact there wasn't enough fuel on board. But the crew were misguided by FQI and believed they had plenty of fuel[ANSV]. During the flight both engines stoped working due to lacking of enough fuel onboard. Further more, the alarms were not switched on because the aircraft was equipped with a gauge which is designed for a smaller aircraft. During descending the pilots failed to capture the runway. Finally the aircraft crashed on the sea with a large bank angle, which led to a splitting of the aircraft.

On August 24, 2001, the Flight 236 of Air Transat flying from Toronto to Lisbon exhausted all the fuel onboard over the Atlantic Ocean [AAPID]. The leakage of fuel caused this emergency situation. This was an A330 and with 306 people including 293 passengers and 13 crew aboard. Fortunately one of the flight crew had the experience of piloting gliders, the crew control the aircraft gliding for 120 km, and finally safely landed in the Azores. There was no life loss. Until now no other engine-out transportation aircraft has glide for a longer distance than this A330.

On November 23, 1996, an Ethiopian Airlines B-767 aircraft, whose flight Number is 961, from Addis to Abidjan was hijacked [HAMILTON J. A.]. After three and one-half hours flight, one engine failed to provide power because of lacking of fuel. The aircraft began to lose altitude from 39000(11887m) to 25000 feet (7620m). Then the second engine flamed out, and the aircraft had to lose altitude continually. The equipped Ram Air Turbine (RAT)

was extracted to provide emergency power to maintain the important functions and operations of the aircraft. With the loss of altitude and speed, RAT could not provide enough power, and the capacity of the batteries was limited. After electricity almost exhausted, the lighting system stops working. Further more the hijackers tried to control the aircraft to hit a resort. The pilots struggled with the hijackers, which led to an interruption of performing the emergency descending, and the aircraft crashed on the sea and split into 3 parts.

On 23 July, 1983, the flight 143 from Montreal to Edmonton ran out of fuel at 12000 feet (3658m) because of using different fuel measurement. Most aircraft of Air Canada use pounds as measurement unit, but this new generation Boeing aircraft used metric measurement. The personnel for refuelling didn't realize this, thus the aircraft just had part or required fuel before flying. When preparing for flight, the pilot also entered the weight in pounds. All of these led to all-engines-out during flight. The aircraft lost almost all electrical power and energy for the hydraulic systems, which were provided by engines. However the RAT was extracted automatically and provided energy to hydraulic system to make the aircraft controllable[WILLIAMS M.]. Finally the crew made a success of safe landing.

On July 19, 1989, the United Airlines Flight 232, a scheduled flight belonging to United Airlines, flew from Denver to Philadelphia.[CONROY M. T.] This was a Douglas DC-10 aircraft. Because the failure of the second engine destroyed all three of the hydraulic systems, the aircraft had power from other engines to fly, but lost surfaces control of flight. 112 people lost their lives.

II.3 Main Engine-Out Causes

An engine-out situation can be caused by different factors:

- Engine failure caused by;
    - Proper mechanical failure
    - Air pollution (ashes, dust, water, etc).
    - Collision with flying objects (birds)
- Engine shut down due to:
    - Fuel exhaustion
    - Voluntary or non voluntary shut down

They can be classified into five main types and shown in table 2.1. Main reasons for engine-out and related examples are listed there. It appears clearly that the way of the aircraft is operated during glide after engine-out occurs, has a direct impact on the survivability.

Table 2.1 Main reasons for engine-out:

Main Reasons	Basic Cause	Examples
Mechanical Problem	Problem of Engine itself	19/07/1989, DC-10, engine 2 failed and destroyed all three of the aircraft hydraulic systems.
	Other Mechanical problem	17/01/2008, B777, rejection of fuel to the reactor because of low pressure in the pump ports.
Fuel	Fuel Exhaustion	12/07/2000, A310, the right gear could not be retracted, so the fuel was consumed quickly than normal.
	Fuel Leak	24/08/2001, A330, the flight ran out of fuel because of fuel leak.
	Hijack	23/11/1996, B767, the aircraft stayed in the air for a long time, and ran out of fuel because of hijack.
	Fuel Contamination	03/1994, CL600, the engine stopped working because of fuel contamination
Human Error	Maintenance Mistake	06/08/2005, ATR 72-202, there was a problem with the Fuel Quantity Indicator, and the aircraft did not load enough fuel before taking-off.
Atmosphere Pollution, Weather	Volcanic Ash	15/09/1989, B747, the aircraft lost its four engines power after passing through the plume of volcanic ash.
	Extremely heavy rain or hail	08/1987, B737, during descending both of the aircraft engines experienced a flameout because of rain and hail. 04/1977, DC-9, during descend both engines lost rotation speed after encounter a thunderstorm [NTSB[2]] .
Others	Encounter Bird	15/01/2009, A320, encountered a group of birds, which caused loss of all engine power.

It is clear that if there was an optimized gliding trajectory calculated by the flight management computer or an available optimized control law, as well as a help to follow it, the safety level and the probability of survival would be increased. This is the main purpose of this thesis.

II.4 Main Consequences of Engine-Out

Obviously the transport aircraft cannot glide for a very long distance without engine power. Further more, engine is not only the power source for flying, but also main power source for other devices and systems on board, such as hydraulic systems, electric and electronic systems, cabin environment control systems, lighting, kitchen, etc. Thus all-engine-out constitutes an emergency situation for the aircraft. This situation has major impact on flight safety through flight sustainability and flight controls effectiveness.

II.4.1 The consequences on flight safety

Transportation aircraft can sustain flight thanks to their speed obtained from the power provided by the engines. Once all engines stop working, the flight range shrinks a lot, drag is increased, and speed at level of flight cannot be maintained. Most of time it becomes impossible to reach the destination airport but the aircraft can glide for some distance by utilizing its total energy which includes kinetic energy and potential energy. In some cases mentioned before the glide ability of the aircraft allowed to achieve a safe landing. It has been especially the case for Flight 236 on August 24, 2001, where the flight crew made the aircraft glide for 120km and land safely. The maximum glide range can be estimated according to initial flight situation (altitude, speed and mass), this issue is discussed in Chapter IV. Then the estimated maximum glide range can help the pilot to choose a suitable landing site. To land safely, some constraints must be satisfied during the whole glide period and especially at the end of the glide. In some cases mentioned before in which the final landing conditions were not satisfied, it led to accidents with some injuries and deaths as well as important aircraft damages. So a safe gliding trajectory must be identified and followed to make sure the aircraft is able to land safely. This is one of the main objective of the thesis, and is discussed in Chapter VII and VIII.

II.4.2 The consequences on operational and control system

On transportation aircraft, surfaces control operations are always actuated by hydraulic systems. These hydraulic systems (there are three of them in the majority of transportation aircraft) consist of a reservoir, accumulators, filters, power pumps, system relief valves and pressure regulators. The power pumps are used to extract energy from the engines and

convert this mechanical energy to hydraulic power. Thus the hydraulic pressure is kept at an operable level. For most large or medium-sized aircraft, the normal hydraulic pressure for operating is 3000 PSI. This power is distributed by means of hydraulic circuits to the different servo systems driving the aerodynamics actuators. A structure of hydraulic servo system is shown in figure 2.1.

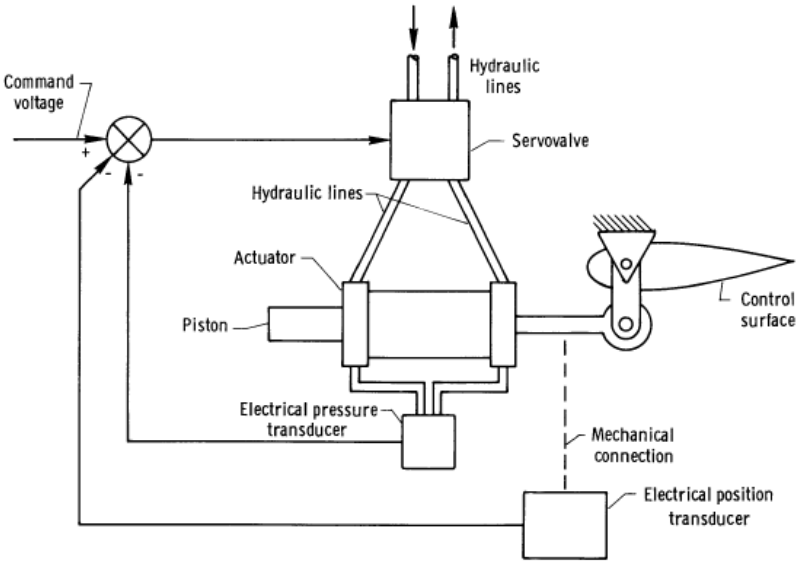

Figure 2.1 Structure of hydraulic servo system

The equivalent control scheme is given by figure 2.2:

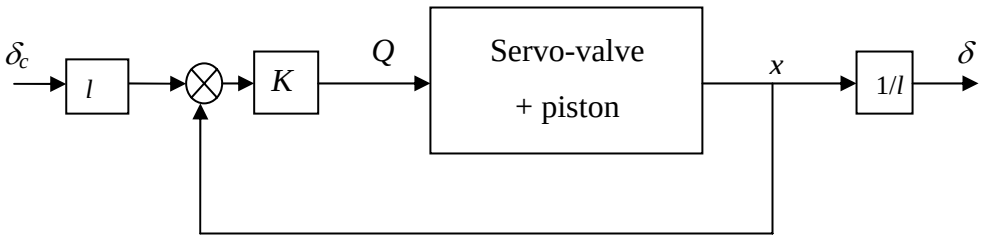

Figure 2.2 Servo-control scheme of an aerodynamic surface

Here x is the linear displacement of the piston , δ is the angular deflection of the surface, δ_c is the reference value for the deflection, l is the length of the lever with $\delta = x/l$, K is a pure

or a more complex gain and Q is the hydraulic flow through the piston. It can be shown [MORA-CAMINO. F[1].] that the flow through the piston of the servo-control is given by:

$$Q = A(\frac{dx}{dt} + \frac{1}{r}\frac{dF}{dt}) \tag{2.1}$$

where A is the surface of the main piston, r is the total stiffness (including anchor stiffness and hydraulic stiffness) and F is the force applied to the piston ($F = A \cdot \Delta p$) where Δp is the difference of pressure between the two chambers of the piston. Then the force equation applied to the moving part of the system is given by:

$$m\frac{d^2x}{dt^2} = F - f\frac{dx}{dt} - r_c x \tag{2.2}$$

where m is the mass of moving part (including control surface, mechanical links, transmissions and piston), f is the viscous friction of the moving part, r_c is the load stiffness which is proportional to the dynamic pressure. Then the open loop transfer function is given by:

$$H(p) = \frac{K/A}{p(\ (1 + r_c/r) + (f/r)p + (m/r)p^2\ )} \tag{2.3}$$

Now, supposing that the piston is commanded to change position between t_0 and t_1 according to $x(t) = \lambda \cdot (t - t_0)$ with $x_1 = \lambda \cdot (t_1 - t_0)$, then the work produced by the hydraulic fluid is given by:

$$W_h = \lambda \cdot f \cdot x_1 + (r_c/2) \cdot x_1^{\ 2} \tag{2.4}$$

In normal operation, hydraulic pressure is maintained by the pumps which convert the mechanical energy from engine to hydraulic power. When engine-out occurs the pumps will stop and the remaining hydraulic pressure will correspond mainly to the elastic energy of the fluid and will diminish with every control demand. Then when Δp becomes too small, according to relation (2.2) the force applied to the aerodynamic surface will be insufficient to control effectively its deflection.

Even thought the probability of all-engine-out is very low, it can occur as shown in the cases mentioned before. Its impact on hydraulic system might lead to a disaster. To maintain aircraft controllability, some devices can be introduced to compensate for the failure of the

engines and the ineffectiveness of the mechanical pumps. It is the case of the ram air turbine (RAT) or battery driven electric pumps. With the help of these complementary devices most control surfaces can be actuated, but the power provided by the complementary devices is much less than the power delivered by the engines. Then, Δp may have a value lower than normal, so the control ability is degraded.

For example, A320 aircraft has three hydraulic systems, marked with green, yellow and blue system respectively [Airbus[3]] [see figure 2.3].

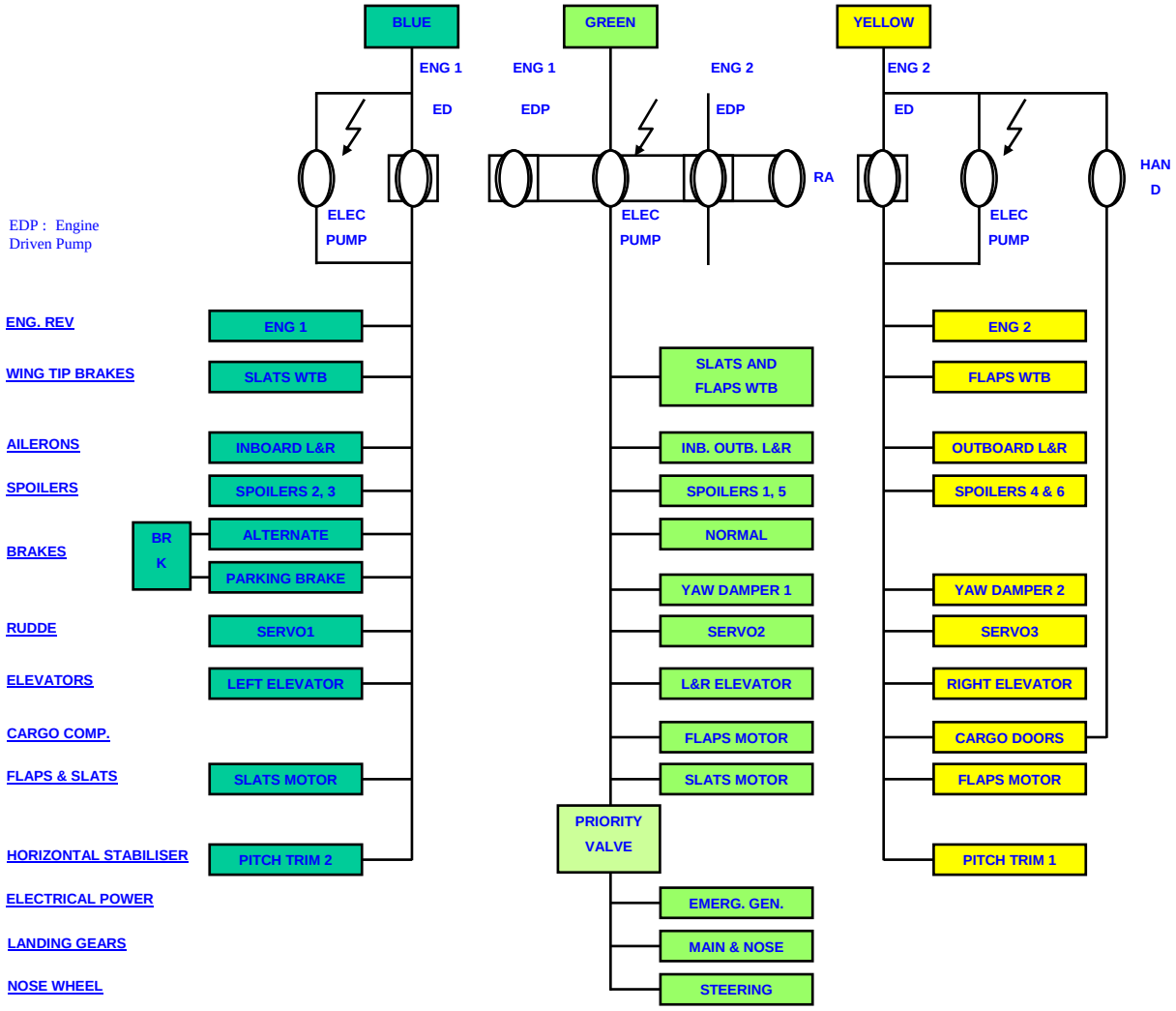

Figure 2.3 A320 Hydraulic generation and distribution

Each system has its own pump, which is connected to the corresponding engine. The green system pump is connected to the left engine with an output power of 48kw; on the other hand the yellow system pump is connected to the right engine also with an output power of 48kw. The blue system has an electric pump with an output power of 7.4kw, which start to work as long as any one of engines works. Each system serves for certain actuators of control surface. If just one engine stops working, the power transfer unit (PTU) can transfer energy power between the green and the yellow systems, thus the hydraulic system can work nominally. When all engines stop working, the RAT is extracted to work, but the output power is only 22kw. Comparing to the total output power of green system and yellow system, it is vey low. Thus not all hydraulic units are powered by it.

II.4.3 The consequences on the on-board digital systems

Modern transportation aircraft are equipped with electronic systems for communication, indication, computing and managing, controlling, etc. All of these equipments are designed to turn flying safer, more economic, and easier. Electric power supply is the essential factor for the normal operations of these equipments or devices. There are three primary sources of electric power: turbines, auxiliary power unit (APU) and emergency power source.

Normally the electric power is converted from engine mechanical energy by drive generator when aircraft is in air. Then it is distributed to different systems scattered over the whole aircraft as shown in figure 2.4 and figure 2.5.

When all engines stop working, especially caused by shortage of fuel, which means that the APU cannot be started to provide auxiliary power, batteries are switched on to provide electric power (some RATs can generate electric power also). Then some electric powered systems are shut down. This was the case with Flight 236 on August 24, 2001: the Flight Guidance Management Computer, the Multipurpose Control and Display Unit, the HF 1 radio, the Cockpit Voice Recorder, the Flight Data Recorder, Auto-Pilot 2, Flight Control Data Concentrator 1, flaps, pitch trim, rudder trim, Navigation Display 1, Auto Break/Anti Skid, Distance Measuring Equipment, and standby altimeter lighting [AAPID]. For most batteries equipping aircraft, they can support the operation of selected systems for about 30 minutes. Then with reduced operating functions, flight safety is lower than normal.

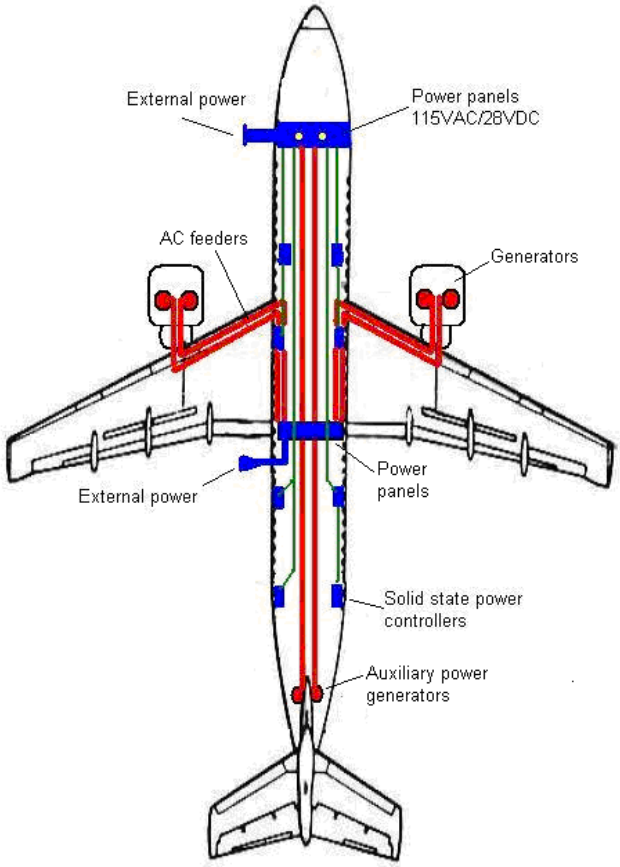

Figure 2.4 Electrical power generation and distribution

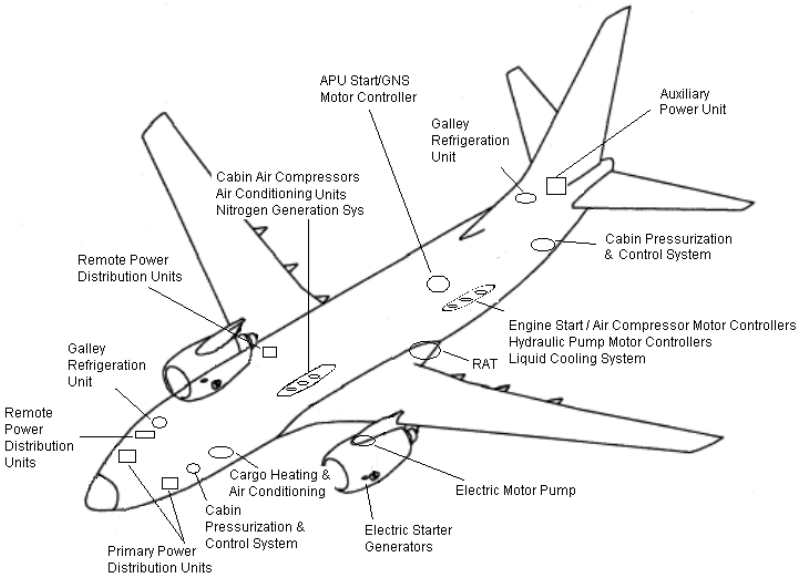

Figure 2.5 An example of arrangement of power supply

II.4.4 The consequences on aircraft environment

The higher the aircraft fly, the lower the air density is. Temperature and pressure are lower than those on the ground. Above 10000-meter height, the temperature is lower than -50°C, and the pressure is about one-fourth of see level standard air pressure. Human being cannot survive in that environment. During the whole flight, the oxygen, the pressure, and the temperature in the cabin should be kept on a certain domain for the sake of the health of passengers and crew. Before the technology of obtaining pressurized air from engine was used on aircraft, the transportation aircraft could not fly over 4000m altitude, unless every person was equipped with an oxygen mask.

Today transportation aircraft fly very often over 10000m at cruise. Once engines stop working, the cabin will loss pressure, and cabin temperature will decreases without the power and heat supplied by the engines to maintain the temperature in the cabin.

According to Newton's thermodynamic transfer law, the heat lose rate of cabin is expressed by equation (2.5).

$$\frac{dQ}{dt} = -h_f S_b (T_c - T_{0ut}) + n_p h_p + h_a \tag{2.5}$$

h_f – the coefficient of thermo exchange rate of the fuselage, 2.5W/ (m^2K)

S_b – the surface of the aircraft body (550m^2 –A320 d=4m, l=40m, V_c=500m^3)

T_c – the temperature of cabin

T_{out} – the outside temperature

n_p – the number of passengers and crews in the aircraft

h_a – the rate of thermo produced by avionics devices,

h_p – the rate of thermo produced by person, 0.1kW

Since according to the first principle of thermodynamics when gas expands it loses energy, too, the lost energy can be calculated by the following equation:

$$\rho T_{out} R dV = P_{out} d(V_c) \tag{2.6}$$

According to the first law of thermodynamics, the total lost energy can be obtained by:

$$m_c(t) C dT_c = -P_{out} dV + [-h_f S(T_c - T_{out}) dt + n_p h_p dt + h_a dt] \tag{2.7}$$

m_c – the mass of air in aircraft

ρ – density of air

R – 287 m^2 /s^2 ºK, or 1716 ft^2 /s^2 ºK

V_c – volume of cabin

P_{out} – outside pressure

P_c – the cabin pressure

C – specific heat of air

The aircraft is not a gas-tight container, the gas leak must be considered. The leak rate is a function of the difference between the inner pressure and the out pressure, which is written as:

$$q_{air} = \frac{dm_c}{dt} = C_p(P_c - P_{out}) \tag{2.8}$$

where C_p is the coefficient of leak, and q_{air} is the gas leak rate (kg/s). The Gaseous Equation of State is

$$P_c = \rho R T_c \tag{2.9}$$

and the differential of equation (2.9) is:

$$\frac{dP_c}{dt} \cdot V_c = m_c R \frac{dT_c}{dt} + RT_c \frac{dm_c}{dt} \tag{2.10}$$

Combining equations (2.6)-(2.10) together, the equations are rewritten as:

$$m_c(t) C \frac{dT_c}{dt} = -T_{out} R C_p (P_c - P_{out}) + [-h_f S(T_c - T_{out}) + n_p h_p + h_a] \tag{2.11}$$

$$V_c \frac{dP_c}{dt} = \frac{R}{C}\{-T_{out} R C_p (P_c - P_{out}) + [-h_f S(T_c - T_{out}) + n_p h_p + h_a]\} + T_c R C_p (P_c - P_{out}) \tag{2.12}$$

In the troposphere, the relation between the temperature and the pressure is:

$$p_{out} = p_0 \left(\frac{T_{out}}{T_0}\right)^{\frac{-g}{a_0 R}} \tag{2.13}$$

$$T_{out} = T_0 - 6.5z \tag{2.14}$$

a_0 – -6.5*10^{-3} ºK

T_0 – 288.15 ºK

z – the altitude of aircraft, which can be calculated by $\frac{dz}{dt} = V_h$

g – 9.80665 m/s^2

Now the state equations of cabin environment are:

$$\frac{dT_c}{dt} = -\frac{R^2 T_c (T_0 - 6.5z)}{P_c V_c C} C_p (P_c - p_0 (\frac{T_0 - 6.5z}{T_0})^{\frac{-g}{a_0 R}}) + \frac{RT_c}{P_c V_c C}[-h_f S(T_c - (T_0 - 6.5z)) + n_p h_p + h_a] \tag{2.15}$$

$$\frac{dP_c}{dt} = -\frac{R^2 (T_0 - 6.5z)}{V_c C} C_p (P_c - p_0 (\frac{T_0 - 6.5z}{T_0})^{\frac{-g}{a_0 R}}) + \frac{R}{V_c C}[-h_f S(T_c - (T_0 - 6.5z)) + n_p h_p + h_a] + \frac{RT_c C_p}{V_c} (P_c - p_0 (\frac{T_0 - 6.5z}{T_0})^{\frac{-g}{a_0 R}}) \tag{2.16}$$

$$\frac{dz}{dt} = V_h \tag{2.17}$$

Supposing all-engines-out occurs when aircraft cruise over 10000m high, and the descending rate is 10m/s, figure 2.6 shows cabin temperature curve and outside temperature curve with respect to time. Figure 2.7 shows cabin pressure curve and outside pressure.

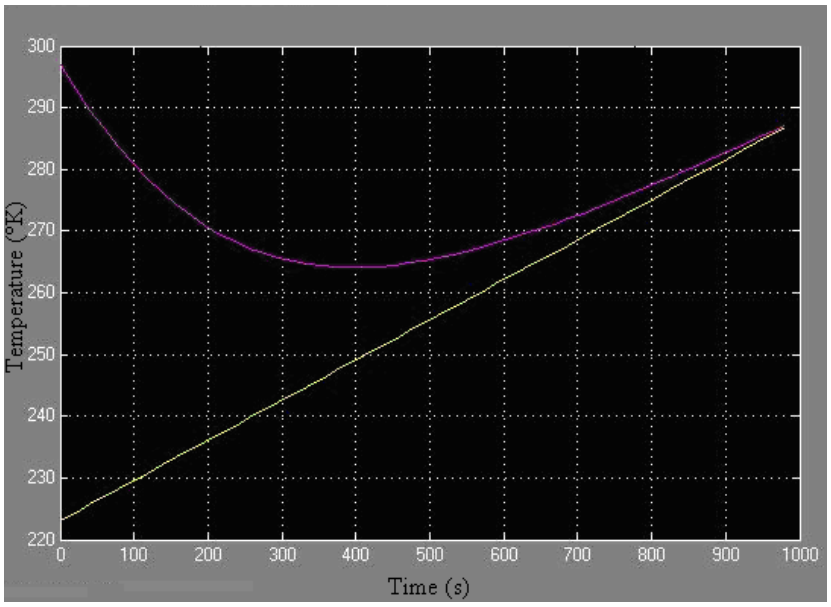

Figure 2.6 The cabin temperature (pink curve) and outside temperature (yellow curve)

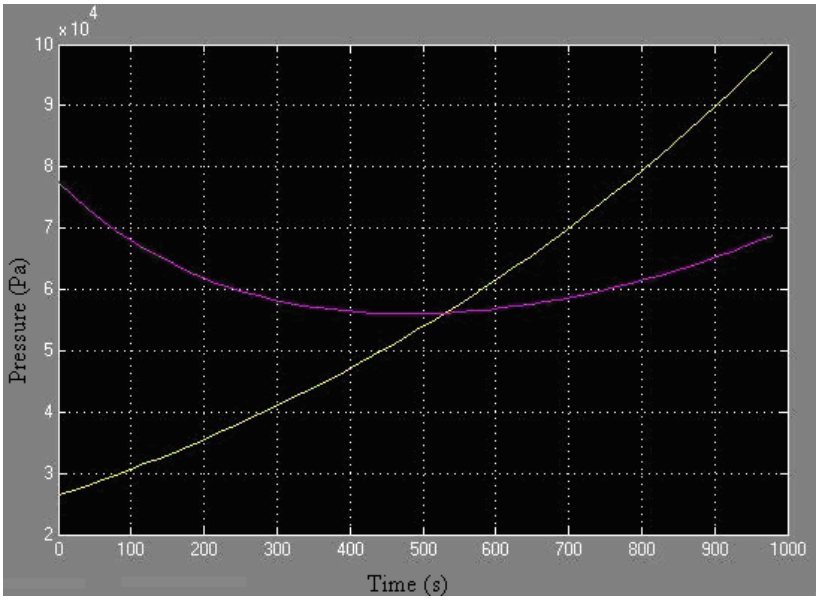

Figure 2.7 Cabin pressure (pink curve) and outside pressure (yellow curve)

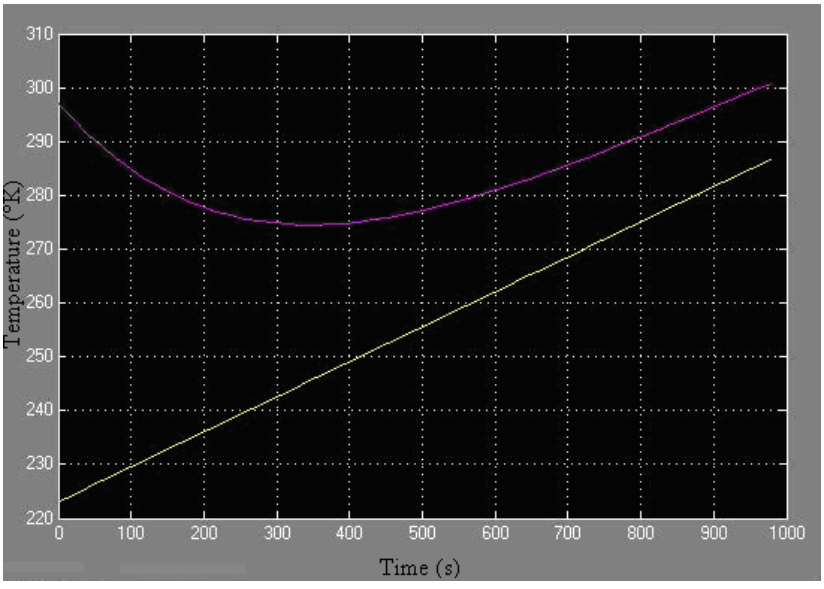

Figure 2.8 The cabin temperature (pink curve) and outside temperature (yellow curve) with 20kw heating power

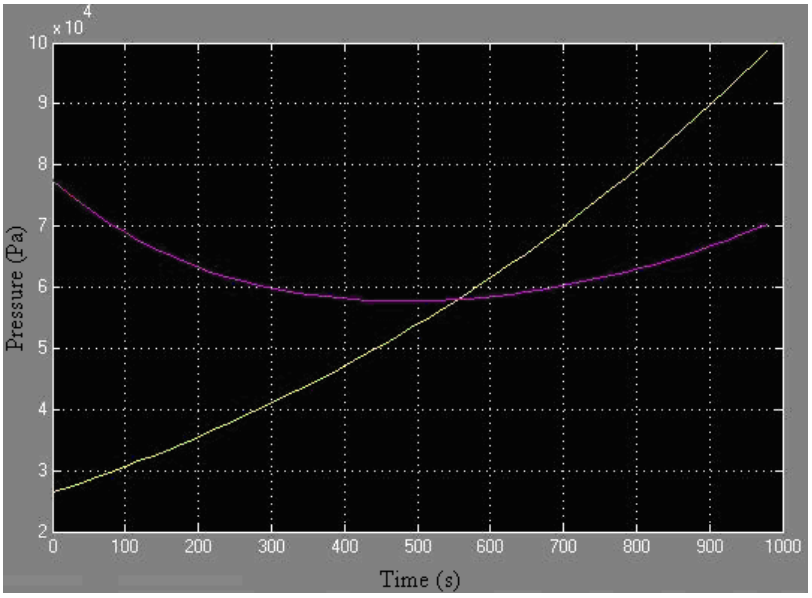

Figure 2.9 Cabin pressure (pink curve) and outside pressure (yellow curve) with 20kw heating power

The figures 2.6 and 2.7 are obtained under the condition that the air conditioning does not work. The aircraft glide from 10 km altitude to see level. Because of the large difference between cabin temperature and outside temperature at the beginning of gliding, heat transfer is faster, the same happens with cabin pressure. Thus the cabin temperature decreasing rate and pressure loss rate are high at cruise level. When the aircraft is below 4500m, the outside pressure become higher than the inside pressure and the cabin pressure increases again. To avoid the injuries or death caused by oxygen deficit, the oxygen masks should be dropped when the cabin altitude is over 4000m with no air conditioning [AAPID]. If there is some heating power the curves are modified. Figures 2.8 and 2.9 display the case in which a power of 20 KW is devoted to cabin heating.

From these figures it appears that the cabin temperature decreases quickly without air conditioning system and then increases a little bit slowly because of the variation of outside pressure and teperature during gliding. Normally the air conditioning power is 50kw, but in this case, where all engines stop working, the heating power decreases. Supposing the heating power is 20kw, the lowest cabin temperature remains above zero degree. The heating system has a small impact on cabin pressure, further more heating system cannot increase oxygen content of the cabin. Figure 2.10 and figure 2.11 show cabin environment variation (temperature and pressure) with respect to aircraft altitude.

It appears in both cases that if no sudden depressurization occurs, the cabin environment (temperature and pressure) will not be a critical issue during the glide towards the ground.

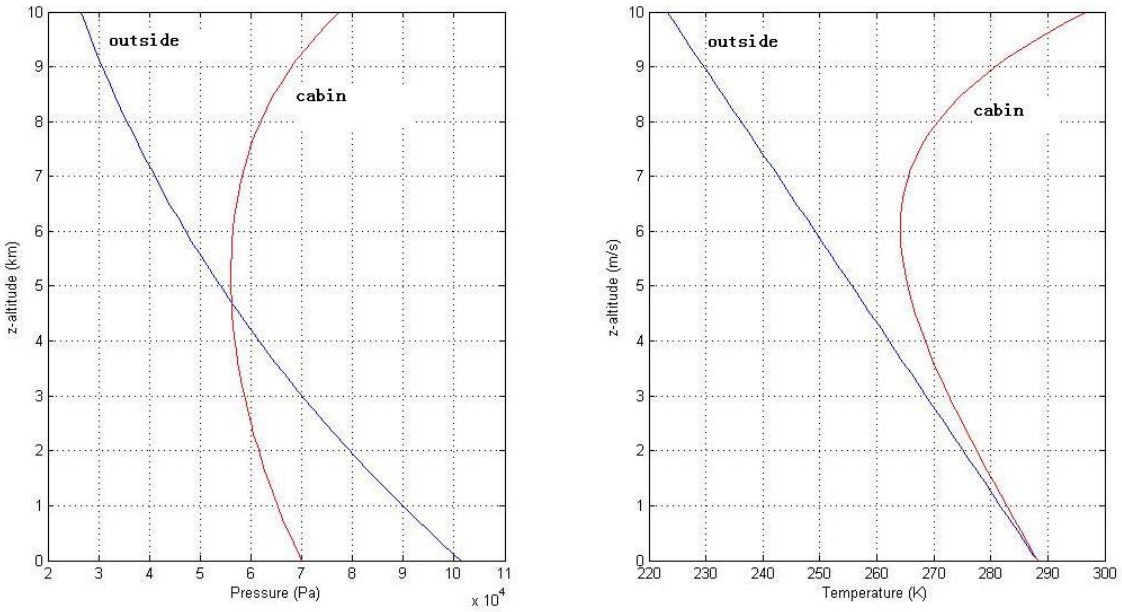

Figure 2.10 Cabin environment without air-conditioning

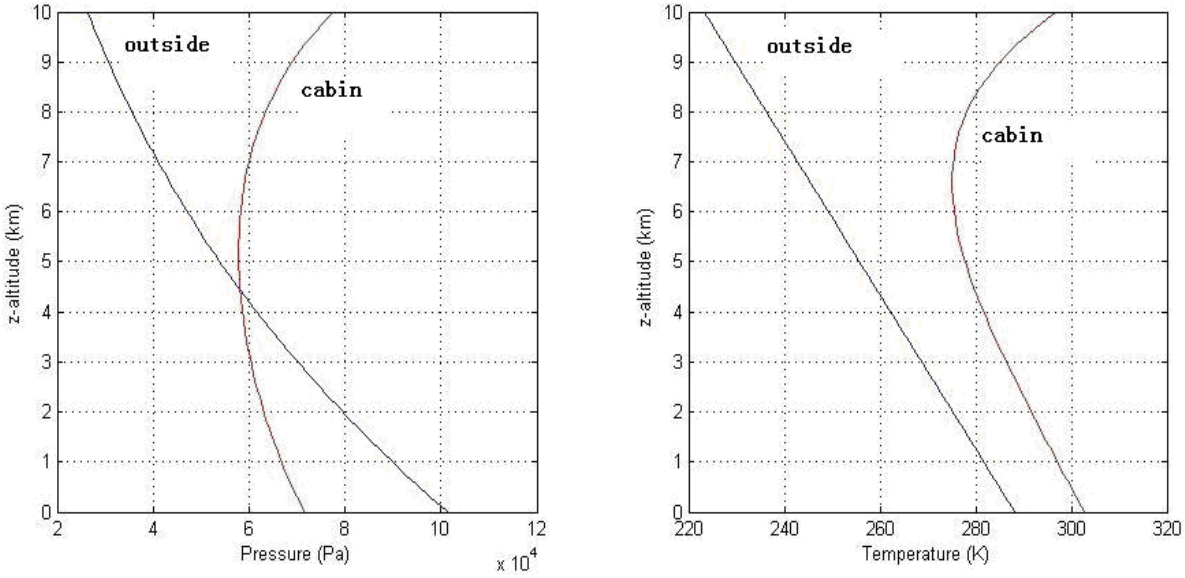

Figure 2.11 Cabin environment with an auxiliary heating system

II.4.5 Consequences on other systems and equipments

There are some other equipments or facilities using electric power, like lighting systems, passenger entertainment systems, kitchen, etc. If it is evening, darkness makes people panic under the emergency situation and it has a negative impact on evacuating and rescuing efficiency, especially when a serious accident occurs at landing.

II.5 Conclusion

There are no emergency procedures published by the aircraft manufacturers in the case of engine-out since this is considered to be an extremely improbable event (Probability < 10^{-9} /flight hours) with catastrophic consequences. Procedures exist in the case of a single engine failure in a multi-engine aircraft and up to two engine failures in a four-engine aircraft. Depending on the stage of the flight at which the engine failure occurs, different actions must be taken. At take-off, after reducing the rate of climb to limit the loss of speed, here the aid of an Head Up Display-HUD, appears to be desirable, the pilot can try to perform a manoeuvre to return to land at the same airport. If the partial engine failure happens at cruise, the adoption of an airspeed equal to the green dot speed should provide a maximum area to select an emergency airport to land.

From the study developed above the main effect on the on-board systems will be the loss of the main energy source leading to limitations for the pilot to control the aerodynamic surfaces efficiently all along the glide and specially near and at landing. Then auto-pilot functions will be limited while normal auto-guidance functions should be no more available. The consequences for the cabin environment are limited to uncomfortable temperature and pressure conditions but without criticality.

The effects caused by engine-out on power supply can be limited by the operation of auxiliary equipments such as the RAT and the APU, providing an auxiliary source of power for the flight computers and the control of some main aerodynamic surfaces.

CHAPTER III

ENGINE-OUT FLIGHT DYNAMICS FOR TRANSPORTATION AIRCRAFT

III.1 Introduction

In this chapter the flight dynamics of a gliding transportation aircraft are considered. They are not too much different from the flight dynamics of a powered transportation aircraft which have been established in the past with reference works such as [NELSON R. C.] [ETKIN B.] [MCLEAN D.] [PRATT R.]. At first sight, the main differences between the gliding and the powered aircraft are for the former one the absence of thrust and a balance of the drag force which is increased by the drag of the stopped engines.

Then in the first part of this chapter, after introducing the useful reference frames for the present study, as well as the external forces and moments applied to the gliding aircraft, the flight dynamics equations of the gliding aircraft are displayed.

In the second part of this chapter, since the gliding aircraft is particularly vulnerable with respect to the wind, the relations between attitude angles such as pitch angle, bank angle and angle of attack with respect to airspeed and wind speed are considered. The influence of the wind speed on the value of the angle of attack is investigated and a numerical application is developed.

III.2 The Reference Frames

Among the different reference frames [NELSON R. C.] to represent and analyze atmospheric flight dynamics, including aircraft attitude and trajectory, three of them are of main interest for this study: wind frame, body frame and Earth frame. The wind frame allows to express easily the aerodynamic forces and moments, the body frame is suitable to apply the dynamics principles and to write the flight dynamics equations while the Earth frame is adapted to the representation of the trajectory followed by the gliding aircraft.

III.2.1 Definitions of the considered reference frames

The three reference frames considered are linked to each other by kinematics relations and are defined with respect to each other. Figure 3.1 illustrates the relation between the Earth frame and the aircraft body frame.

a) The local Earth frame: G_E (X_E, Y_E, Z_E):

- The origin of the coordinates system coincides with the centre of gravity of the aircraft.
- X_E axis directs along a reference azimuth (true north or magnetic north generally).
- Z_E axis is oriented in the direction of the centre of the Earth.
- Y_E axis is perpendicular to the plane of X_E-Z_E and points to east. This coordinates system is also called *inertial axes* system. [NELSON R. C.]

b) The aircraft body frame: G_B, (X_B, Y_B, Z_B):

- This is a fundamental frame to establish the flight dynamics equations.
- X_B axis starts from the original O_B, which is the gravity centre of aircraft, towards the nose of the aircraft. This is the longitudinal axis of the aircraft, generally closing to its principal axis of inertia.
- Y_B is perpendicular to the plane of symmetry of the aircraft and is oriented to the right. The plane X_B-Z_B coincides with the symmetry plane of aircraft.
- Z_B axis is perpendicular to the horizontal plane X_B-Y_B downward.

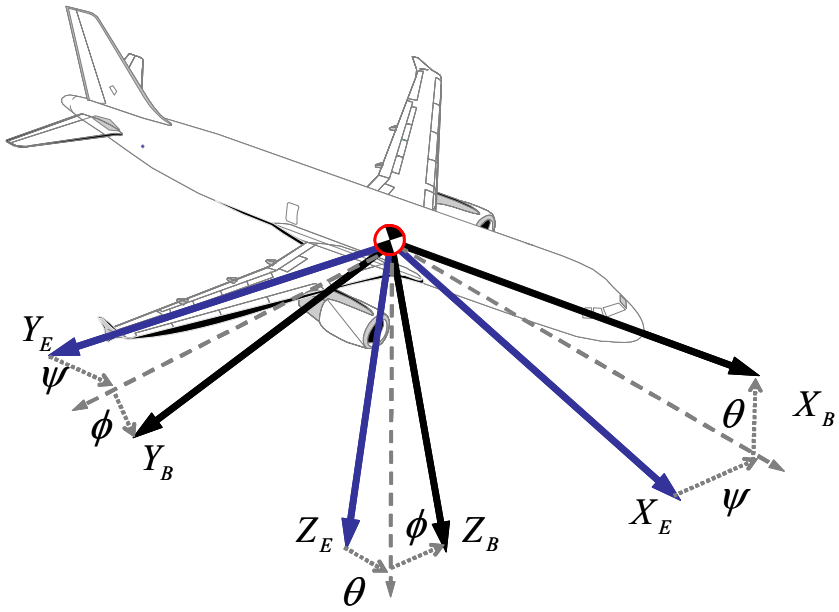

Figure 3.1 Body frame with respect to the earth frame

c) The wind frame: G_W (X_W, Y_W, Z_W), which is also named stability reference frame, is shown in Figure 3.2 with respect to the body frame.

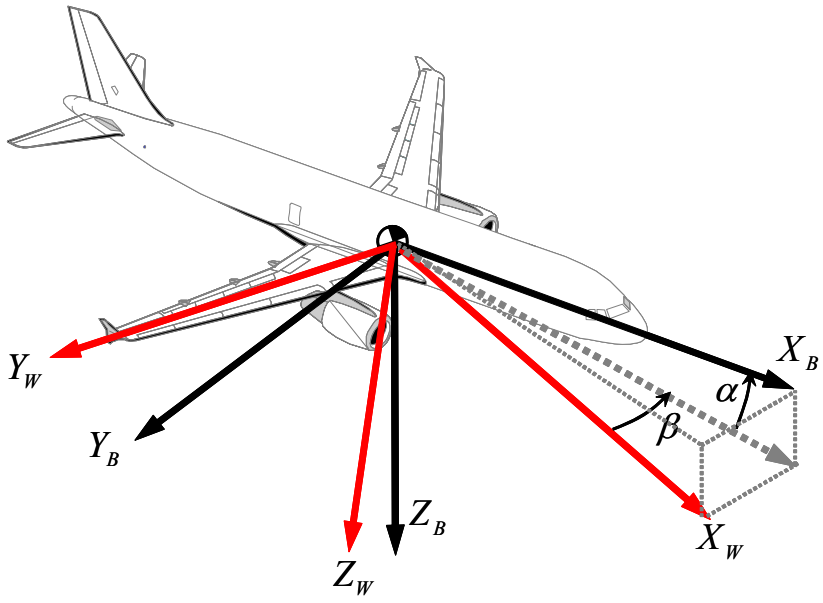

Figure 3.2 Wind frame with respect to body frame

- Both of the origins of the frames in figure 3.2 are at the aircraft centre of gravity (*CG*).
- X_W axis is defined parallel to the vector of speed.
- Z_W axis is perpendicular to the axis X_W and downward.
- Y_W axis is oriented to the right, and is perpendicular to the plane X_W-Z_W. These three axes are called *aerodynamic stability*, or *wind axes*.

III.2.2 Rotation matrices between different reference frames

The equations of flight dynamics are in general expressed in the more appropriable reference frame according to the objectives of the study. Therefore it may be necessary to transform flight dynamics equations from a coordinates frame to another. This is realized by a rotation operation around the centre of gravity of the aircraft, which is the common origin for the three main reference frames. The rotation matrix, T_{bw}, from the wind frame to the body frame is characterised by the angle of attack, α, and the sideslip angle, β. It is expressed as:

$$T_{bw} = \begin{bmatrix} \cos\alpha\cos\beta & -\cos\alpha\sin\beta & -\sin\alpha \\ \sin\beta & \cos\beta & 0 \\ \sin\alpha\cos\beta & -\sin\alpha\sin\beta & \cos\alpha \end{bmatrix} \tag{3.1}$$

To carry on the navigation calculations, the Earth frame appears to be more appropriable. The rotation matrix, T_{eb}, from the body frame to the Earth frame is characterised by the pitch angle, θ, the roll angle, ϕ, and the yaw angle (or heading), ψ, which is shown in the next expression:

$$T_{eb} = \begin{bmatrix} \cos\theta\cos\psi & \sin\phi\sin\theta\cos\psi - \cos\phi\sin\psi & \cos\phi\sin\theta\cos\psi + \sin\phi\sin\psi \\ \cos\theta\sin\psi & \sin\phi\sin\theta\sin\psi + \cos\phi\cos\psi & \cos\phi\sin\theta\sin\psi - \sin\phi\sin\psi \\ -\sin\theta & \sin\phi\cos\theta & \cos\phi\cos\theta \end{bmatrix} \tag{3.2}$$

III.3 Aerodynamic Forces and Moments Applied to the Gliding Aircraft

The aerodynamic forces to which the aircraft is submitted as a consequence of its motion in the atmosphere, are the drag, the lift, and the side force, which are along or against the axes X_w, Y_w, and Z_w respectively shown in figure 3.2. These forces are defined in terms of dimensionless aerodynamic coefficients C_D, C_L and C_Y:

$$D = \frac{1}{2}\rho V^2 S \cdot C_D(\alpha, \delta_e, M_a) \tag{3.3-a}$$

$$L = \frac{1}{2}\rho V^2 S \cdot C_l(\alpha, \delta_e, M_a) \tag{3.3-b}$$

$$Y = \frac{1}{2}\rho V^2 S \cdot C_Y(\beta, \delta_r, p, r, M_a) \tag{3.3-c}$$

where L is lift, D is drag, Y is side force, α is the angle of attack, δ_e is the elevator deflection, δ_r is the rudder deflection, p is the roll rate, r is the yaw rate, M_a is the Mach number, β is the angle of sideslip, ρ is the air density, S is the surface area of wing, and V is the airspeed.

It is here supposed that when the aircraft engines stop working, they pass to the windmill mode. Many aircraft equipped with a RAM air turbine (RAT). In those aircraft once all the engines stop working, the RAT starts to work. It is a small deployable windmill, which when activated extracts power from the air flow along the aircraft to provide an emergency residual power to feed the main hydraulic and electronic systems. It has a small impact on the overall drag of the aircraft[CORONADO H.]. However the windmill drag effect should be taken into account, so the global drag coefficient of the engine-out aircraft is slightly increased [LIU Z.][WANG Z.].

$$C_D^{'} = C_D(\alpha, \delta_e, M_a) + C_W(M_a) \tag{3.4-a}$$

$$D = \frac{1}{2}\rho V^2 S \cdot C_D^{'} \tag{3.4-b}$$

where C_D' is the drag coefficient, C_W is the drag coefficient caused by windmill effect.

A first approximation of C_w is:

$$C_W = \frac{n\sigma}{S} C_D \tag{3.5}$$

where σ is the engine main section, and n is the number of engines.

The aerodynamic moments referenced in the body frame are the rolling moment L, the pitch moment M, and the yawing moment N, which point to the axes X_B, Y_B, and Z_B respectively.

$$L = \frac{1}{2}\rho V^2 Sb \cdot C_L(\beta, \delta_a, p, r, \delta_r, M_a) \tag{3.6-a}$$

$$M = \frac{1}{2}\rho V^2 Sb \cdot C_M(\alpha, \delta_e, q, \dot{\alpha}, \dot{\delta}_e, M_a) \tag{3.6-b}$$

$$N = \frac{1}{2}\rho V^2 Sb \cdot C_N(\beta, \delta_a, \delta_r, p, r, M_a) \tag{3.6-c}$$

where δ_a is the ailerons deflection, q is the pitch rate, b is the typical length for the given aircraft, and M_a is Mach number.

Following Newton's second law, we can write the acceleration equations of the aircraft in the body frame. Since the aerodynamic forces are originally defined in the wind frame, their projections in the body frame produce the force components F_x, F_y, and F_z, along the three body axes according to:

$$\begin{bmatrix} F_x \\ F_y \\ F_z \end{bmatrix} = \begin{bmatrix} \cos\alpha\cos\beta & -\cos\alpha\sin\beta & -\sin\alpha \\ \sin\beta & \cos\beta & 0 \\ \sin\alpha\cos\beta & -\sin\alpha\sin\beta & \cos\alpha \end{bmatrix} \begin{bmatrix} -D \\ Y \\ -L \end{bmatrix} \tag{3.7}$$

III.4 Glide Dynamics Equations

The motion of a flying aircraft is a combination of translation and rotation movements, whose causes are the external forces and moment equations applied to it. Considering that the aircraft is a rigid body, the Newton forces equations are given by:

$$F_x - mg \sin\theta = m\left(\dot{u} + qw - rv\right) \tag{3.8-a}$$

$$F_y + mg \cos\theta \sin\phi = m\left(\dot{v} + ru - pw\right) \tag{3.8-b}$$

$$F_z + mg \cos\theta \cos\phi = m\left(\dot{w} + pv - qu\right) \tag{3.8-c}$$

where *u, v, w* are the components of inertial speed along the X_B, Y_B, and Z_B axes; *p, q, r* are the angular rates around the X_B, Y_B, and Z_B axes; Φ, θ, and Ψ are the Euler angles; *m* is the total mass of the aircraft.

The corresponding moment equations are given by:

$$L = I_x \dot{p} - I_{xz} \dot{r} + qr\left(I_z - I_y\right) - I_{xz} pq \tag{3.9-a}$$

$$M = I_y \dot{q} + rp\left(I_x - I_z\right) + I_{xz}\left(p^2 - r^2\right) \tag{3.9-b}$$

$$N = -I_{xz} \dot{p} + I_z \dot{r} + pq\left(I_y - I_x\right) + I_{xz} qr \tag{3.9-c}$$

The terms I_x, I_y and I_z are the mass inertia moments of the body about the X_B, Y_B, and Z_B axes, respectively. The term I_{xz} is an inertia product.

In the considered flight situation, engine-out, sooner or later it will be necessary to throw away the unnecessary fuel that overloads the gliding aircraft, so that the mass of the aircraft, *m* is expected to decrease to *m′*

$$m' = m - m_F \tag{3.10}$$

where m_F is the mass of the discharged fuel, and m' is the residual aircraft mass. The aircraft inertia moments, (I_x, I_y, I_z, I_{xz}), will also change according to this mass change from an initial value to another one (I_x', I_y', I_z', I_{xz}'):

$$\begin{bmatrix} I_x & 0 & -I_{xz} \\ 0 & I_y & 0 \\ -I_{xz} & 0 & I_z \end{bmatrix} \rightarrow \begin{bmatrix} I_x' & 0 & -I_{xz}' \\ 0 & I_y' & 0 \\ -I_{xz}' & 0 & I_z' \end{bmatrix} \tag{3.11}$$

To compute the new inertia moments, information about the position and shape of tanks as well as fuel and cargo mass distribution are necessary. At this point, some indirect estimation using identification techniques from Systems Identification theory [HAMEL P. G.[1,2]] [MAINE R. E.] could be useful at this stage.

The body angular rates are defined in the body frame, and the Euler angles (ϕ, θ, ψ) is defined with respect to the Earth frame. The relation between the body angular velocities and the Euler angle can be expressed by the Euler's equations (3.12):

$$\dot{\theta} = q\cos\phi - r\sin\phi \tag{3.12-a}$$

$$\dot{\phi} = p + q\sin\phi\tan\theta + r\cos\phi\tan\theta \tag{3.12-b}$$

$$\dot{\psi} = (q\sin\phi + r\cos\phi)\sec\theta \tag{3.12-c}$$

The speed components of the aircraft in the Earth frame can be then written as:

$$\begin{bmatrix} \dot{X} \\ \dot{Y} \\ \dot{Z} \end{bmatrix} = \begin{bmatrix} \cos\theta\cos\psi & \sin\phi\sin\theta\cos\psi - \cos\phi\sin\psi & \cos\phi\sin\theta\cos\psi + \sin\phi\sin\psi \\ \cos\theta\sin\psi & \sin\phi\sin\theta\sin\psi + \cos\phi\cos\psi & \cos\phi\sin\theta\sin\psi - \sin\phi\sin\psi \\ -\sin\theta & \sin\phi\cos\theta & \cos\phi\cos\theta \end{bmatrix} \begin{bmatrix} u \\ v \\ w \end{bmatrix} \tag{3.13}$$

All of these equations are fundamental for flight manoeuvre analysis and flight path designing when all engines are out. To analyze better the aircraft movements, a simulator model of the aircraft has been built in SIMULINK based on the equations given above.

III.5 The Effect of Wind on Glide Dynamics

At engine-out, the aircraft is very dependent of the wind speed and direction encountered along the glide. In that case, adopting a path angle or a pitch angle which in normal flight conditions will appear safe, can lead, as it will be shown, the aircraft at the verge of stalling.

III.5.1 Wind dependent ground speed and path angle

Here we consider three different speeds: ground speed - V_g, airspeed - V_a, and wind speed - V_w.

Ground speed represent the speed of the aircraft with respect to the Earth, airspeed represent the mean instantaneous aircraft speed with respect to the surrounding air, while wind speed is the mean speed of the air around the aircraft with respect to the Earth. So the relation between the three speed vectors is written as:

$$\underline{V}_g = \underline{V}_a + \underline{V}_w \tag{3.14}$$

Considering the inertial path angle γ_g and horizontal orientation ψ of the ground speed, the ground speed vector is rewritten in the Earth frame as:

$$\underline{V}_g = \begin{pmatrix} V_g \cos\gamma_g \cos\psi \\ V_g \cos\gamma_g \sin\psi \\ -V_g \sin\gamma_g \end{pmatrix} \tag{3.15}$$

where $V_g = \left\| \underline{V}_g \right\|$.

In the same way the airspeed vector is given with respect to the angle of attack α and the sideslip angle β in body frame as:

$$\underline{V}_{ab} = \begin{pmatrix} V_a \cos\alpha \cos\beta \\ V_a \sin\beta \\ -V_a \sin\alpha \cos\beta \end{pmatrix} \tag{3.16}$$

Furthermore this vector can be expressed in the Earth frame by using the rotation matrix given in Equation (3.2).

$$\underline{V}_{ae} = T_{eb} \begin{pmatrix} V_a \cos\alpha \cos\beta \\ V_a \sin\beta \\ -V_a \sin\alpha \cos\beta \end{pmatrix} \tag{3.17}$$

To simplify equation (3.17), some notations are introduced here:

$$c_1 = C_\alpha C_\beta C_\theta C_\psi + S_\beta (S_\phi S_\theta C_\psi - C_\phi S_\psi) + S_\alpha C_\beta (C_\phi S_\theta C_\psi + S_\phi S_\psi) \tag{3.18-a}$$

$$c_2 = C_\alpha C_\beta C_\theta S_\psi + S_\beta (S_\phi S_\theta S_\psi + C_\phi C_\psi) + S_\alpha C_\beta (C_\phi S_\theta S_\psi - S_\phi C_\psi) \tag{3.18-b}$$

$$c_3 = -C_\alpha C_\beta S_\theta + S_\beta S_\phi C_\theta + S_\alpha C_\beta C_\phi C_\theta \tag{3.18-c}$$

where C_α is the notation of $\cos\alpha$, S_β is the notation of $\sin\beta$,etc.

Then the airspeed vector in the Earth frame is rewritten as:

$$\underline{V}_{ae} = V_a \begin{pmatrix} C_\alpha C_\beta C_\theta C_\psi + S_\beta (S_\phi S_\theta C_\psi - C_\phi S_\psi) + S_\alpha C_\beta (C_\phi S_\theta C_\psi + S_\phi S_\psi) \\ C_\alpha C_\beta C_\theta S_\psi + S_\beta (S_\phi S_\theta S_\psi + C_\phi C_\psi) + S_\alpha C_\beta (C_\phi S_\theta S_\psi - S_\phi C_\psi \\ -C_\alpha C_\beta S_\theta + S_\beta S_\phi C_\theta + S_\alpha C_\beta C_\phi C_\theta \end{pmatrix} = V_a \begin{pmatrix} c_1 \\ c_2 \\ c_3 \end{pmatrix} \tag{3.19}$$

Thus combining those equations, the ground speed vector is given by:

$$\underline{V}_g = \begin{pmatrix} V_g \cos\gamma_g \cos\psi \\ V_g \cos\gamma_g \sin\psi \\ -V_g \sin\gamma_g \end{pmatrix} = T_{eb} \begin{pmatrix} V_a \cos\alpha \cos\beta \\ V_a \sin\beta \\ -V_a \sin\alpha \cos\beta \end{pmatrix} + \begin{pmatrix} V_{wx} \\ V_{wy} \\ V_{wz} \end{pmatrix} \tag{3.20}$$

And the ground speed value is calculated by:

$$\begin{aligned} V_g &= V_a \sqrt{\left[c_1 + \frac{V_{wx}}{V_a}\right]^2 + \left[c_2 + \frac{V_{wy}}{V_a}\right]^2 + \left[c_3 + \frac{V_{wz}}{V_a}\right]^2} \\ &= V_a \sqrt{1 + 2\underline{C}\frac{\underline{V}_w}{V_a} + \left\|\frac{\underline{V}_w}{V_a}\right\|^2} \end{aligned} \tag{3.21}$$

where $\underline{C} = [c_1 \quad c_2 \quad c_3]$ and $\underline{V}_w = [V_{wx} \quad V_{wy} \quad V_{wz}]^T$. Obviously vector $\underline{C}$ has a modulus equal to 1 and it has the direction of the airspeed vector. Furthermore the ground speed modulus is expressed as:

$$\left\|\underline{V}_g\right\|^2 = \left\|\underline{V}_a\right\|^2 + 2\underline{V}_a^T \underline{V}_w + \left\|\underline{V}_w\right\|^2 \tag{3.22}$$

Now defining parameter λ as:

$$\lambda = \frac{2\underline{V}_a^T \underline{V}_w}{V_a^2} + \left\| \frac{\underline{V}_w}{V_a} \right\|^2 \tag{3.23}$$

equation (3.21) is simplified as:

$$V_g = V_a \sqrt{1+\lambda} \tag{3.24}$$

When the wind speed modulus is small with respect to the one of the airspeed, the ground speed is approximated by airspeed V_a or $V_a \sqrt{1+\frac{2\underline{C}\underline{V}_w}{V_a}}$. So the ground speed can be expressed by:

$$V_g \approx V_a \sqrt{1+\frac{2}{V_a}((C_\alpha C_\theta C_\psi + S_\alpha S_\theta C_\psi)V_{wx} + (C_\alpha C_\theta S_\psi + S_\alpha S_\theta S_\psi)V_{wy} + (-C_\alpha S_\theta + S_\alpha C_\theta)V_{wz})} \tag{3.25-a}$$

or

$$V_g \approx V_a + ((C_\alpha C_\theta C_\psi + S_\alpha S_\theta C_\psi)V_{wx} + (C_\alpha C_\theta S_\psi + S_\alpha S_\theta S_\psi)V_{wy} + (-C_\alpha S_\theta + S_\alpha C_\theta)V_{wz}) \tag{3.25-b}$$

and the glide path angle γ_g with respect to the earth is obtained and shown in equation (3.26), and the glide path angle with respect to the air γ_a is shown in equation (3.27).

$$\gamma_g = -\arcsin\left[\frac{V_a}{V_g}(-\sin\theta\cos\alpha\cos\beta + \sin\phi\cos\theta\sin\beta + \cos\phi\cos\theta\sin\alpha\cos\beta) + \frac{V_{wz}}{V_g}\right] \tag{3.26}$$

$$\gamma_a = -\arcsin(-\sin\theta\cos\alpha\cos\beta + \sin\phi\cos\theta\sin\beta + \cos\phi\cos\theta\sin\alpha\cos\beta) \tag{3.27}$$

In the case in which the aircraft flies with a zero sideslip angle and without a roll movement, equation (3.26) is rewritten as:

$$\gamma_g = -\arcsin\left[\frac{V_a}{V_g}(-\sin\theta\cos\alpha + \cos\theta\sin\alpha) + \frac{V_{wz}}{V_g}\right] = -\arcsin\left[-\frac{V_a}{V_g}\sin\gamma_a + \frac{V_{wz}}{V_g}\right] \tag{3.28}$$

Supposing the aircraft flies in a still atmosphere under the conditions $\beta = 0$ and $\phi = 0$, the relation between γ, θ, and α is simply:

$$\gamma = \gamma_a = \gamma_g = \theta - \alpha \tag{3.29}$$

This is the classical formula used as a first approximation for flight dynamics analysis. Equation (3.24) can be rewritten as:

$$V_g \approx V_a\sqrt{1+\frac{2\underline{C}\underline{V}_w}{V_a}} = V_a\sqrt{1+\frac{2}{V_a}(\cos\gamma\cos\psi\cdot V_{wx}+\cos\gamma\sin\psi\cdot V_{wy}-\sin\gamma\cdot V_{wz})} \tag{3.30}$$

III.5.2 Wind dependent ground speed and angle of attack

In this paragraph we use the previously developed formulas to display through a numerical application the effect of different wind scenarios over the ground speed and the angle of attack.

a) Wind dependent ground speed and ground path angle

Here we take advantage of relations:

$$V_g = V_a\sqrt{\begin{aligned}&\left(C_\alpha C_\beta C_\theta C_\psi + S_\beta(S_\phi S_\theta C_\psi - C_\phi S_\psi) + S_\alpha C_\beta(C_\phi S_\theta C_\psi + S_\phi S_\psi) + \frac{V_{wx}}{V_a}\right)^2 \\ &+\left(C_\alpha C_\beta C_\theta S_\psi + S_\beta(S_\phi S_\theta S_\psi + C_\phi C_\psi) + S_\alpha C_\beta(C_\phi S_\theta S_\psi - S_\phi C_\psi) + \frac{V_{wy}}{V_a}\right)^2 \\ &+\left(-C_\alpha C_\beta S_\theta + S_\beta S_\phi C_\theta + S_\alpha C_\beta C_\phi C_\theta + \frac{V_{wz}}{V_a}\right)^2\end{aligned}} \tag{3.31}$$

and

$$\gamma_g = -\arcsin\left(\frac{V_a}{V_g}(\sin(\alpha-\theta)+\frac{V_{wz}}{V_g}\right) \tag{3.32}$$

Here we will consider no lateral effect, so we assume that $\beta = 0$, $\phi = 0$ and ψ = constant = 0 and $V_{wy} = 0$ then:

$$V_g = V_a\sqrt{\left((C_\alpha C_\theta + S_\alpha S_\theta)+\frac{V_{wx}}{V_a}\right)^2+\left((-C_\alpha S_\theta + S_\alpha C_\theta)+\frac{V_{wz}}{V_a}\right)^2} \tag{3.33-a}$$

or

$$V_g = \sqrt{V_a^2 + 2V_aV_w\cos(\theta - \alpha + \vartheta_w) + V_w^2} \tag{3.33-b}$$

where ϑ_w is the angle of wind speed vector with respect to the Earth frame, which is shown in figure 3.3.

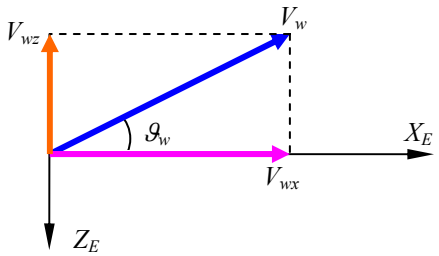

Figure 3.3 Wind vector in vertical plane

To understand better the importance of the wind effect over atmospheric flight, a numerical application has been perform. Here we have considered the following cases for the airspeed and the attitude angles:

1) V_a = 150 m/s with θ = 1°, α = 3°, 4.5°, 6.5°, 9.5°

2) V_a =110 m/s with θ = 1°, α = 3°, 4.5°, 6.5°, 9.5°

3) V_a =150 m/s, 120m/s, 100m/s, 80m/s, with θ = 1°, γ = - 4°, - 6°, - 8°, - 10°

With respect to the winds we consider the following situations:

I) Horizontal head winds of 0 m/s, ±10 m/s, ±20 m/s or ±30 m/s

Table 3.1 The ground speed (m/s) in different horizontal winds with airspeed of 150m/s

Wind speed / Angle of attack	-30m/s	-20m/s	-10m/s	0m/s	10m/s	20m/s	30m/s
3°	120.0228	130.0141	140.0065	150	159.9943	169.9892	179.9848
4.5°	120.0228	130.0141	140.0065	150	159.9943	169.9892	179.9848
6.5°	120.0228	130.0141	140.0065	150	159.9943	169.9892	179.9848
9.5°	120.0228	130.0141	140.0065	150	159.9943	169.9892	179.9848

Table 3.1 shows that the ground V_g speed can be approximated by the sum of airspeed V_a and wind speed V_w, $V_g \approx V_a + V_{wx}$, when the vertical component of wind is zero. The calculation is carried on again under the condition of V_a=110m/s, and the results are listed in table 3.2.

Table 3.2 The ground speed (m/s) in different horizontal winds with airspeed of 110m/s

Wind speed / Angle of attack	-30m/s	-20m/s	-10m/s	0m/s	10m/s	20m/s	30m/s
3°	80.0251	90.0149	100.0067	110	119.9944	129.9897	139.9856
4.5°	80.0769	90.0456	100.0205	110	119.9829	129.9684	139.956
6.5°	80.1897	90.1125	100.0506	110	119.9578	129.9221	139.8914
9.5°	80.4518	90.2681	100.1208	110	119.8993	129.814	139.7408

The same conclusion is obtained by table 3.2, which is $V_g \approx V_a + V_w$.

II) Vertical wind of 0 m/s, ±5 m/s or ±10 m/s

Table 3.3 The ground speed (m/s) in different vertical winds

Wind speed / Angle of attack	-10m/s	-5m/s	0m/s	5m/s	10m/s
3°	149.9843	149.9088	150	150.2576	150.6808
4.5°	149.7226	149.7779	150	150.3881	150.9409
6.5°	149.3736	149.6036	150	150.5615	151.2863
9.5°	148.8508	149.3428	150	150.8201	151.8006

The calculation results illustrate that the ground speed almost equal the airspeed, and the maximum approximation error is 1.8m/s. Comparing to 150m/s, this approximation error is small. Even when the airspeed is 80m/s and the aircraft descend with steep path angle of 9.5°, the maximum approximation error is 2.07m/s, whose relative error is about 2.5%, which is not very large.

Further more the calculations are carried on under the condition of wind with vertical and horizontal component, and the results prove that the ground speed can be approximated by $V_g \approx V_a + V_{wx}$ with small approximation error.

Table 3.4 The ground speed (m/s) approximation

Wind speed / Angle of attack	V_{wx}=-30m/s V_{wz}=-10m/s	V_{wx}=-20m/s V_{wz}=-5m/s	V_{wx}=-10m/s V_{wz}=10m/s	V_{wx}=0m/s V_{wz}=0m/s	V_{wx}=10m/s V_{wz}=-10m/s	V_{wx}=20m/s V_{wz}=5m/s	V_{wx}=30m/s V_{wz}=10m/s
3°	120.0033	129.9088	140.7357	150	159.9796	170.2166	180.5525
4.5°	119.7232	129.7868	141.0274	150	159.7224	170.3097	180.7384
6.5°	119.3897	129.649	141.4261	150	159.3695	170.4146	180.9588
9.5°	118.9766	129.4959	142.0436	150	158.8195	170.531	181.2307

b) Wind dependent angle of attack

Here we take advantage of relation:

$$\gamma_g = -\arcsin\left[\frac{V_a}{V_g}(-\sin\theta\cos\alpha + \cos\theta\sin\alpha) + \frac{V_{wz}}{V_g}\right] \tag{3.34}$$

to compute the corresponding value of the angle of attack for different airspeed, winds and path angles. The angle of attack is calculated by:

$$\alpha = \theta - \frac{V_g}{V_a}\arcsin(\sin\gamma_g + \frac{V_{wz}}{V_g}) \tag{3.35}$$

while with respect to the winds we consider the following situations:

I) Horizontal head winds of 0 m/s, ±10 m/s, ±20 m/s or ±30 m/s

1) V_a = 150 m/s with γ_g= - 4°, -6°, -8° or -10°

With the conclusion of table 3.1 and table 3.2, the ground speed can be approximated by airspeed and wind speed, $V_g \approx V_a + V_{wx}$. When the aircraft flies in different horizontal wind at certain glide path angle, the angles of attack are calculated according to equation (3.35), and the results are listed in table 3.5.

Table 3.5 The angle of attack in different horizontal winds with airspeed of 150m/s

Wind speed / Glide path angle	-30m/s	-20m/s	-10m/s	0m/s	10m/s	20m/s	30m/s
-4°	4.1991°	4.466°	4.7329°	5°	5.2671°	5.5344°	5.8017°
-6°	5.7968°	6.1976°	6.5987°	7°	7.4016°	7.8036°	8.2058°
-8°	7.3925°	7.9277°	8.4635°	9°	9.5372°	10.0751°	10.6139°
-10°	8.9853°	9.6556°	10.3272°	11°	11.6742°	12.35°	13.0273°

These results indicate that the large angle of attack is required when aircraft descents at a large glide path angle.

2) V_a =120 m/s with γ_g= - 4°, -6°, -8° or -10°

In this case the calculations are carried on as same as precede calculation except the airspeed varies to 120m/s, and the results are given in table 3.6.

Table 3.6 The angle of attack in different horizontal winds with airspeed of 120m/s

Wind speed / Glide path angle	-30m/s	-20m/s	-10m/s	0m/s	10m/s	20m/s	30m/s
-4°	3.9989°	4.3325°	4.6662°	5°	5.3339°	5.668°	6.0023°
-6°	5.4964°	5.9972°	6.4984°	7°	7.5021°	8.0046°	8.5078°
-8°	6.9914°	7.66°	8.3295°	9°	9.6716°	10.3444°	11.0185°
-10°	8.4832°	9.3203°	10.1592°	11°	11.843°	12.6884°	13.5364°

3) V_a =100 m/s with γ_g= - 4°, -6°, -8° or -10°

Table 3.7 The angle of attack in different horizontal winds with airspeed of 100m/s

Wind speed / Glide path angle	-30m/s	-20m/s	-10m/s	0m/s	10m/s	20m/s	30m/s
-4°	3.7988°	4.1991°	4.5994°	5°	5.4008°	5.8017°	6.2029°
-6°	5.1961°	5.7968°	6.3981°	7°	7.6025°	8.2058°	8.8099°
-8°	6.5907°	7.3925°	8.1955°	9°	9.8061°	10.6139°	11.4236°
-10°	7.9818°	8.9853°	9.9912°	11°	12.0119°	13.0273°	14.0466°

4) V_a =80 m/s with γ_g= - 4°, -6°, -8° or -10°

Table 3.8 The angle of attack in different horizontal winds with airspeed of 80m/s

Wind speed / Glide path angle	-30m/s	-20m/s	-10m/s	0m/s	10m/s	20m/s	30m/s
-4°	3.4988°	3.9989°	4.4993°	5°	5.501°	6.0023°	6.504°
-6°	4.7458°	5.4964°	6.2477°	7°	7.7533°	8.5078°	9.2635°
-8°	5.9901°	6.9914°	7.9946°	9°	10.0078°	11.0185°	12.0323°
-10°	7.2306°	8.4832°	9.7395°	11°	12.2654°	13.5364°	14.8137°

These results indicate that when the aircraft descend at a fix glide path angle in backwards wind the angle of attack is smaller. On the contrary if the aircraft descent in forwards wind the angle of attack increases the angle of attack. The effect of wind increases when the airspeed decreases. The increments and decrements of angle of attack caused by wind cannot be neglected comparing to the angle of attack in still atmosphere. So the impact of horizontal wind should be considered in the analysis.

II) Vertical wind of 0 m/s, ±5 m/s or ±10 m/s

1) V_a = 150 m/s with γ_g= - 4°, -6°, -8° or -10°

Table 3.9 The angle of attack in different vertical winds with airspeed of 150m/s

Wind speed / Glide path angle	-10m/s	-5m/s	0m/s	5m/s	10m/s
-4°	8.8409°	6.9171°	5°	3.0874°	1.177°
-6°	10.8573°	8.9241°	7°	5.0826°	3.1698°
-8°	12.8787°	10.9336°	9°	7.0756°	5.158°
-10°	14.9051°	12.9455°	11°	9.0661°	7.1413°

2) V_a = 120 m/s with γ_g= - 4°, -6°, -8° or -10°

Table 3.10 The angle of attack in different vertical winds with airspeed of 120m/s

Wind speed / Glide path angle	-10m/s	-5m/s	0m/s	5m/s	10m/s
-4°	9.806°	7.3974°	5°	2.6096°	0.2221°
-6°	11.828°	9.4065°	7°	4.6041°	2.2145°
-8°	13.8563°	11.4187°	9°	6.5956°	4.2011°
-10°	15.891°	13.434°	11°	8.5841°	6.1817°

3) V_a = 100 m/s with γ_g= - 4°, -6°, -8° or -10°

Table 3.11 The angle of attack in different vertical winds with airspeed of 100m/s

Wind speed / Glide path angle	-10m/s	-5m/s	0m/s	5m/s	10m/s
-4°	10.7737°	7.878°	5°	2.132°	-0.7331°
-6°	12.8019°	9.8894°	7°	4.1258°	1.2595°
-8°	14.8377°	11.9045°	9°	6.116°	3.245°
-10°	16.8815°	13.9234°	11°	8.1027°	5.2236°

4) V_a = 80 m/s with γ_g= - 4°, -6°, -8° or -10°

Table 3.12 The angle of attack in different vertical winds with airspeed of 80m/s

Wind speed / Glide path angle	-10m/s	-5m/s	0m/s	5m/s	10m/s
-4°	12.2305°	8.6°	5°	1.4158°	-2.1668°
-6°	14.2693°	10.6151°	7°	3.4088°	-0.173°
-8°	16.3178°	12.6348°	9°	5.3974°	1.8121°
-10°	18.3764°	14.6593°	11°	7.3815°	3.7884°

These tables show that adopting common values for the glide path angle, depending on the strength and direction of the wind, high angle of attack values can be obtained. It appears also, that when the airspeed of the aircraft is smaller, the effect of wind is more important. Then it

can be considered that the aircraft will be more vulnerable to wind by the end of the glide at already low speed and low height above the ground.

III.6 Conclusion

If engine-out flight dynamics look quite similar to the dynamics of a powered aircraft, what becomes fundamental in this case is the relation of the aircraft with the surrounding air and especially the surrounding wind. It has been shown in the last part of this chapter that the gliding aircraft can find itself in a critical situation with respect to stall while it has no way to react to this situation (for a powered aircraft, a surplus of thrust will reduce this danger-α floor mode). In the next chapter, the gliding performances of a transportation aircraft subject to the displayed flight dynamics will be considered.

CHAPTER IV

GLIDING PERFORMANCES
OF
TRANSPORTATION AIRCRAFT

IV.1 Introduction

Without engine power, aircraft can glide only a very limited distance which depends on the apparent total energy (potential energy and kinetic energy) the aircraft has at the start of glide. Within this reachable range landing sites can be identified and one of them is chosen by considering its surrounding terrain configuration as well as wind information.

In this chapter gliding performances of a transportation aircraft are analysed in order to determine gliding performances such as the maximum reachable area. For that, first we consider the formulation of an optimization problem to get the conditions for a maximum range glide. Then simplified approaches considering steady or quasi steady glide conditions are developed to estimate maximum range and to characterize straight glide at minimum rate of descent. Then steady gliding turn performances are considered.

IV.2 Glide Range Optimization

The forces that act on the aircraft while performing a vertical glide, which are shown in figure 4.1, can be expressed in the body vertical plane as:

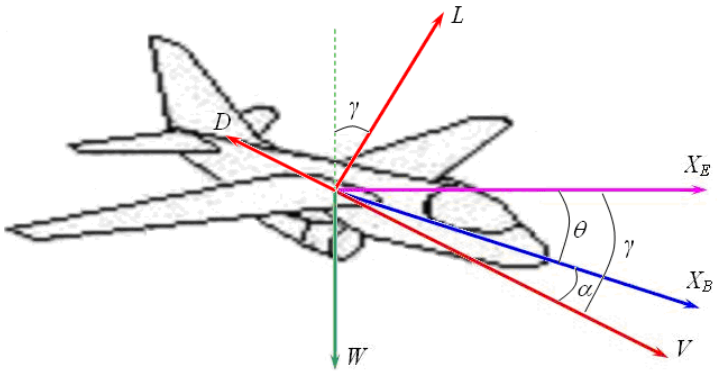

Figure 4.1 Forces acting on a gliding aircraft

$$m\dot{V} = -D - W\sin\gamma \tag{4.1-a}$$

$$m\,V\,\dot{\gamma} = L - W\cos\gamma \tag{4.1-b}$$

and with respect to the pitch moment we assume that:

$$I_y \dot{q} = M \approx 0 \tag{4.1-c}$$

The vertical flight dynamics reduced to the trajectory of the gliding aircraft are given by:

$$-D - W \sin\gamma = m\dot{V} \quad \text{and} \quad m V \dot{\gamma} = L - W \cos\gamma = 0 \tag{4.2}$$

while the position of the gliding aircraft vary according to:

$$\dot{x} = V \cos\gamma \quad \text{and} \quad \dot{z} = V \sin\gamma \tag{4.3}$$

Then to get the maximum range we can formulate the following optimization problem :

$$\max \int_{t_0}^{t_f} V \cos\gamma \, dt \tag{4.4}$$

with the state variables V, γ, z, the input α and the state equations:

$$\dot{V} = -D(z, V, C_D^{'}(\alpha))/m - g\sin\gamma \tag{4.5-a}$$

$$\dot{\gamma} = L(z, V, C_l(\alpha))/(mV) - (g/V)\cos\gamma \tag{4.5-b}$$

$$\dot{x} = V \cos\gamma \tag{4.5-c}$$

$$\dot{z} = V \sin\gamma \tag{4.5-d}$$

with the initial conditions:

$$V(0) = V_0,\ \gamma(0) = \gamma_0,\ x(0) = 0,\ z(0) = z_0 \tag{4.6-a}$$

the final condition which defines final time t_f:

$$z(t_f) = z_f \tag{4.6-b}$$

where z_f is the altitude of the targeted landing area, and the permanent feasibility conditions:

$$V_{\max}(z) \geq V(t) > (1+\varepsilon)\, V_{stall} = \sqrt{\frac{2mg}{\rho(z(t))\, S\, C_{l\max}}} \qquad \varepsilon \approx 0.3 \tag{4.7-a}$$

and

$$\alpha_{\min} \leq \alpha \leq \alpha_{\max} \tag{4.7-b}$$

Then the maximum range will be equal to $x^*(t_f)$.

In the case in which some huge ground obstacle (a narrow ridge of stiff mountains for example) must be overfly to reach a candidate landing area, criterion (4.4) can be replaced in a first stage by $\max \int_{t_0}^{t_c} V \sin\gamma \, dt$ where t_c is such that $\int_{t_0}^{t_c} V \cos\gamma \, dt = x_c$, with x_c being the position of the top of the ground obstacle. Otherwise a permanent constraint such as $z(t) \geq h(x(t))$, where h is a safe altitude at position x, should be introduced.

It is clear that no analytical solution is available to this problem. Its solution via Variational Calculus [BRUNT B. v.], also see Annex C, should also lead to an intricate two points boundary value problem while its numerical solution via discretization either in space or time, should lead to cumbersome calculations. So alternatively, approached analytical solutions can be developed by introducing simplifying assumptions. It will be the case when considering steady glide conditions.

IV.3 Steady Straight Gliding Conditions

The steady gliding flight of an aircraft is theoretically characterised by zero acceleration and angular velocities, and then by zero roll, pitch and yaw external moments.

Assuming that there is no side slip angle, that the components of the external forces in the fixed vertical plane compensated without instant acceleration, and that the aerodynamic moments are null, we get the following forces and moment conditions in the vertical plane:

$$m\dot{V} = -D - W\sin\gamma = 0 \tag{4.8-a}$$

$$m\,V\,\dot{\gamma} = L - W\cos\gamma = 0 \tag{4.8-b}$$

$$I_y\,\dot{q} = M = 0 \tag{4.8-c}$$

The corresponding glide path angle is given by:

$$\gamma = -\arctan(D/L) \tag{4.9}$$

The glide path angle, measured in radian, is very small so that the approximations:

$$\gamma = -D/L \tag{4.10-a}$$

$$L = W \tag{4.10-b}$$

are often acceptable.

Since the weight is constant during the glide, the maximum steady glide angle will be obtained with a minimum drag condition.

The glide path angle can be related to the drag and lift forces as:

$$\gamma = -\arctan(D/L) = -\arctan(1/f) \tag{4.11}$$

where f is the aerodynamic Lift-to-drag ratio. Then the maximum glide path angle (since the glide path angle is negative, in absolute value we have a minimum) will correspond to the maximum Lift-to-drag ratio which is an aerodynamic parameter independent of the wing loading W/S.

Recalling the drag force and lift force expressions for an engine-out situation relation (3.4-a) :

$$C_D^{'} = C_D + C_W = C_{D0} + C_W + KC_l^{\,2} = C_{D0}^{'} + KC_l^{\,2} \tag{4.12}$$

where $K=1/(\pi e\, b/S)$, the term b is the wing span, and S is the surface area of the aircraft wing, e is an empirical parameter called the Oswald efficiency factor [RAYMER D. P.], the glide path angle can be related to the drag and lift coefficients as:

$$\gamma = -\arctan\left(\frac{C_{D0}^{'} + KC_l^{\,2}}{C_l}\right) \tag{4.13}$$

The maximum glide path angle is a parameter of steady gliding flight performance characteristic. Since from equation (4.5) the maximum glide path angle of steady gliding occurs when the ratio of the drag coefficient to the lift coefficient is at minimum, then:

$$\frac{\partial(-\tan\gamma)}{\partial C_l} = \frac{-C_{D0}^{'} + KC_l^{\,2}}{C_l^{\,2}} = 0 \quad \text{with} \quad \frac{\partial^2(-\tan\gamma)}{\partial C_l^{\,2}} = 2C_{D0}^{'}/C_l^{\,3} > 0 \tag{4.14}$$

and we get:

$$C_l^{\,*} = \sqrt{C_{D0}^{'}/K} \tag{4.15}$$

Then the corresponding drag coefficient is given by:

$$C_D^{*} = 2 \cdot C_{D0}^{'} \tag{4.16}$$

and the maximum glide path angle is then expressed as:

$$\gamma^{*} = -\arctan\left(2\sqrt{KC_{D0}^{'}}\right) \tag{4.17}$$

In this situation we can write $W = \frac{1}{2}\rho(z)V^2 S\, C_l^*$ and the airspeed in this condition is such as:

$$V(z) = \sqrt{\frac{2W}{\rho(z)S}\sqrt{\frac{K}{C_{D0}^{'}}}} \tag{4.18}$$

This speed is known by pilots as “the green dot” speed [SHAVER C.][AIRBUS[2]].

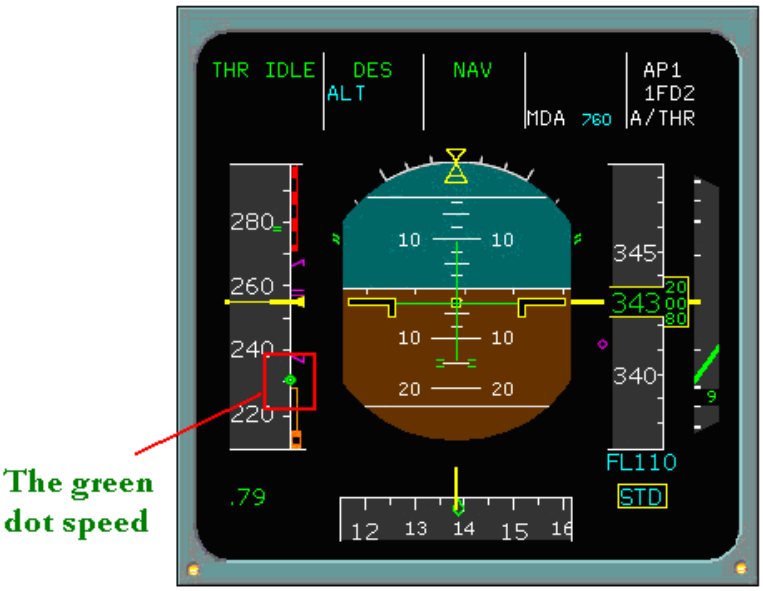

Figure 4.2 The green dot on Primary Flight Display

The dynamic pressure $Q = \frac{1}{2}\rho(z)V(z)^2$ is found to remain constant during the steady glide:

$$Q = Q^* = \frac{W}{S}\sqrt{\frac{K}{C_{D0}^{'}}} \tag{4.19}$$

So at constant maximum glide path angle, as shown in Figure 4.3, the airspeed decreases along the descending glide while air density is increasing. Depending on the glide starting at a high flight level (cruise), the speed variation along the glide can be very large. In general from cruise level after a glide of 10 km, a loss of about 1000 m is experimented and the speed variation is not negligible. Since the airspeed is decreasing during the glide, the stall constraint must be satisfied along the glide:

$$V > V_{stall} = \sqrt{\frac{2W}{\rho(z)\, S\, C_{l\max}}} \tag{4.20}$$

or

$$\sqrt{\frac{K}{C_{D0}^{'}}} > \frac{1}{C_{l\max}} \tag{4.21}$$

This condition which is independent of the flight level is a general aerodynamic condition for glide feasibility.

In this ideal situation, the glide range to sea level will be given by:

$$R_{th} = -z_0 / tg\gamma^* \tag{4.22}$$

where z_0 is the initial flight level expressed in meters.

Adopting a nonlinear model for the standard atmosphere [VINH. N. X.] the density can be expressed by an equation such as:

$$\rho(z) = \rho_0 \, e^{-\frac{g}{RT}z} \tag{4.23}$$

where:

$T = T_0 + a\ z$, with $T_0 = 288.15°K$,

$a_0 = -6.5 \times 10^{-3} °K/m$,

$R = 287 m^2/s^2 °K$,

$\rho_0 = 1.2250 kg/m^3$.

From equation (4.18) we have:

$$\frac{dV}{dz} = \frac{dV}{d\rho} \cdot \frac{d\rho}{dz} = \sqrt{\frac{2W}{S}\sqrt{\frac{K}{C_{D0}^{'}}}}\left(-\frac{1}{2}\rho^{-\frac{3}{2}}\right) \cdot \frac{d\rho}{dz} = \frac{1}{2}\sqrt{\frac{2W}{S}\sqrt{\frac{K}{C_{D0}^{'}}}}\,\frac{g + a_0 R}{RT_0}\,\rho_0^{-\frac{1}{2}}\left(\frac{T_0 + a_0 z}{T_0}\right)^{\frac{g}{2a_0R}-\frac{1}{2}} \tag{4.24}$$

Then, integrating relation 4.24 we get the variation of the speed along the steady state glide as shown in figure 4.3:

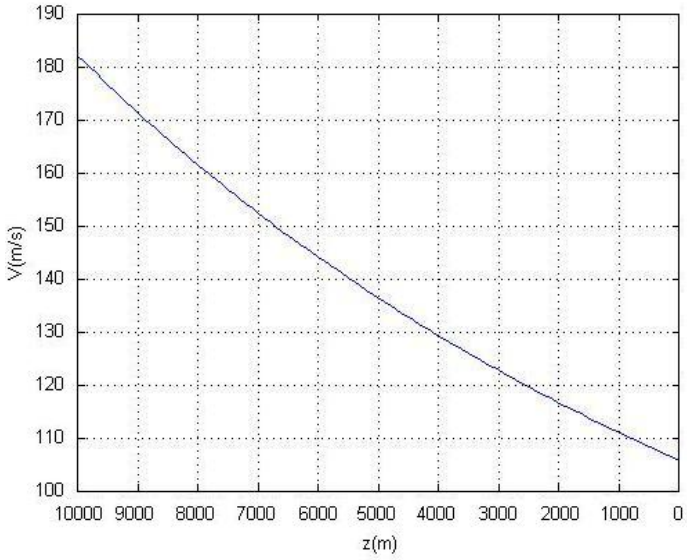

Figure 4.3 Example of steady state airspeed variation with respect to altitude

IV.4 Non Steady Equilibrated Glide Path Angle

Now if it is considered that longitudinal glide is non-steady (airspeed is no more constant) but vertical load factor (body axis) is constant, equations (4.8.a) and (4.8.b) become:

$$m\dot{V} = -D - W\sin\gamma \tag{4.25-a}$$

$$L - W\cos\gamma = 0 \tag{4.25-b}$$

and since:

$$\dot{V} = \frac{dV}{dt} = \frac{dV}{dz}\frac{dz}{dt} = V\sin\gamma\frac{dV}{dz} \tag{4.26}$$

we get:

$$-\tan\gamma = \left[\frac{L}{D}\left(1+\frac{V}{g}\frac{dV}{dz}\right)\right]^{-1} \tag{4.27}$$

Since the dynamic pressure is here given by:

$$Q = \frac{1}{2}\rho_0 e^{-\frac{g}{RT}z}V^2 \tag{4.28}$$

we write:

$$V\frac{dV}{dz}=\frac{1}{2}\frac{g}{RT}V^2=g\frac{Q}{\rho RT}=g\frac{Q}{p} \tag{4.29}$$

So the glide path angle is a function of the static pressure *p*, where *p* is a function of the altitude, *z*, as shown in equation (4.30):

$$p=p_0\left(\frac{T}{T_0}\right)^{-\frac{g}{a_0R}}=p_0\left(\frac{T_0+a_0z}{T_0}\right)^{-\frac{g}{a_0R}} \tag{4.30}$$

where $p_0=1.01325\times10^5 N/m^2$, $a_0=-6.5\times10^{-3}{}^\circ K/m$, $R=287m^2/s^2{}^\circ K$.

Now equation (4.27) can be written:

$$-\tan\gamma=\left[\frac{L}{D}\left(1+\frac{Q}{p(z)}\right)\right]^{-1} \tag{4.31}$$

Assuming the result of the previous section where the dynamic pressure was found to remain constant during steady glide, we get a new relation between the glide angle path and the altitude:

$$\gamma(z)=-\arctan\left(\left[\frac{1}{2\sqrt{C_{D0}{}'K}}\left(1+\frac{Q}{P_0\left(\frac{T_0+a_0z}{T_0}\right)^{-\frac{g}{a_0R}}}\right)\right]^{-1}\right) \tag{4.32}$$

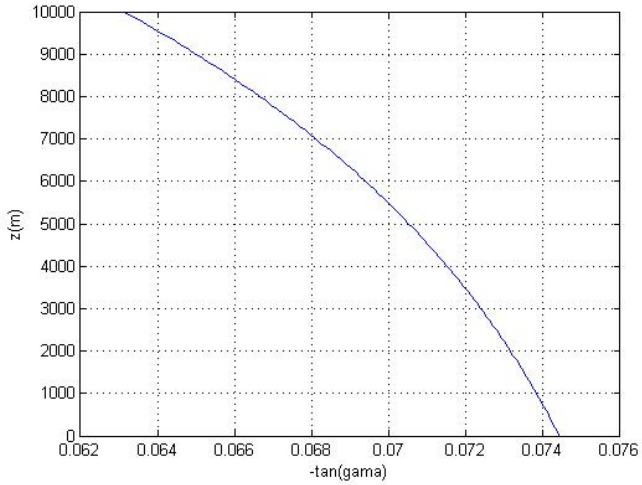

Figure 4.4 Evolution of γ with flight altitude

Figure 4.4 illustrates the fact that the value of '$-\tan\gamma$' increases slightly as the flight altitude is decreasing from 10000m to sea level.

The maximum flight range, R_a is then given by:

$$R_a = \int_{z_{t0}}^{z_t} \frac{1}{\tan\gamma^*(z)}\,dz = -\int_{z_{t0}}^{z_t} \frac{1}{2\sqrt{C_{D0}'K}} \left(1 + \frac{Q}{P_0\left(\frac{T_0 + a_0 z}{T_0}\right)^{-\frac{g}{a_0 R}}}\right) dz \tag{4.33}$$

or

$$R_a = -\frac{z}{2\sqrt{C_{D0}'K}} - \frac{W}{2SC_{D0}'}\frac{1}{P_0}\frac{T_0 R}{g + a_0 R}\left(1 + \frac{a_0}{T_0}z\right)^{\frac{g}{a_0 R}+1}\Bigg|_{z_{t0}}^{z_t} \tag{4.34}$$

This is illustrated in Figure 4.5 where it is clear that if the aircraft loses engine power at a higher altitude, it will be able to glide over an increased range which is nearly proportional to the initial difference of flight levels [WU H.[1]]. In the case of the accident occurred on 24/08/2001, the A330 aircraft glided for about 120 km.

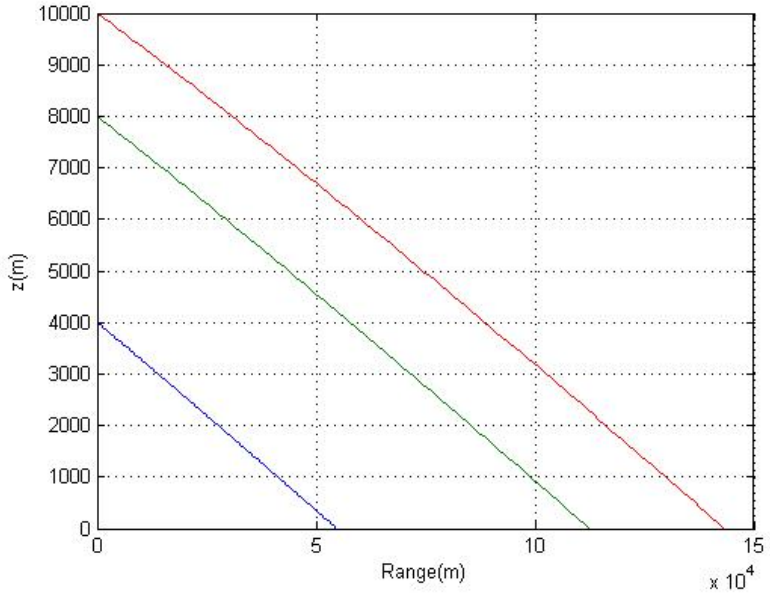

Figure 4.5 Steady gliding range

This range should be corrected with considering effect of the size and orientation of the windspeed.

The duration of the glide can be of interest since during an engine-out situation cabin air conditioning should be reduced or may be switch off to reserve on board remaining power to survival functions. Since $dt = (1/V\sin\gamma)\,dz$, the total glide time can be estimated from (4.32) when not considering the wind speed:

$$t = \int_{z_0}^{z_t} \frac{1}{V\sin\gamma(z)} dz = -\int_{z_0}^{z_t} \sqrt{\frac{\rho}{2Q}} \frac{1}{2\sqrt{C_{D0}{}'K}} \left(1 + \frac{Q}{P_0 \left(\frac{T_0 + a_0 z}{T_0} \right)^{-\frac{g}{a_0 R}}} \right) dz \qquad (4.35\text{-a})$$

or

$$t = -\left\{ \frac{RT_0}{a_0 R - g} \frac{\sqrt{\rho_0}}{\sqrt{2QC_{D0}{}'K}} \left(\frac{T_0 + a_0 z}{T_0} \right)^{-\frac{g}{2a_0 R}+0.5} + \frac{\sqrt{Q\rho_0}}{P_0\sqrt{2C_{D0}{}'K}} \frac{RT_0}{a_0 R + g} \left(\frac{T_0 + a_0 z}{T_0} \right)^{\frac{g}{2a_0 R}+0.5} \right\} \Bigg|_{z_0}^{z_t} \qquad (4.35\text{-b})$$

Figure 4.6 shows flight time for steady gliding at maximum path angle starting from different flight altitudes.

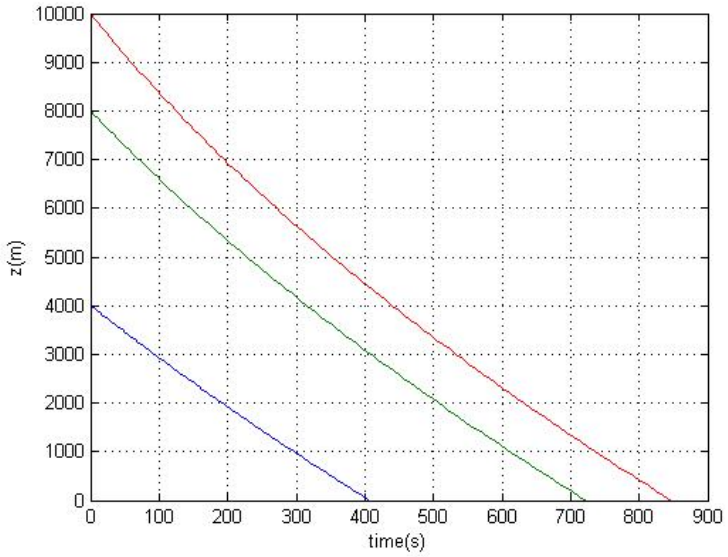

Figure 4.6 Flight time duration of steady gliding at maximum path angle

From equation (4.5-d) and (4.10), the vertical speed is rewritten as:

$$\dot{z} = V \sin\gamma = -\frac{VD}{W} \tag{4.36}$$

where $(-\dot{z})$ is the descent rate. Considering equation (3.4), (4-10) and (4.12), the minimum value of $(-\dot{z})$ is expressed as :

$$-\dot{z} = \frac{VD}{W} = \sqrt{\frac{2}{\rho}} \cdot \left(\frac{\sqrt{Q^3} S C'_{D0} + KW^2/(\sqrt{Q}S)}{W}\right) \tag{4.37}$$

where Q is the dynamic pressure $\frac{1}{2}\rho(z)V(z)^2$. The minimum rate of descent is such as:

$$\frac{\partial(-\dot{z})}{\partial Q} = \sqrt{\frac{2}{\rho}} \cdot \left(\frac{1.5\sqrt{Q} S C'_{D0}}{W} - \frac{KW}{2\sqrt{Q^3}S}\right) = 0 \tag{4.38}$$

It is easy to check that the second derivative of $-\dot{z}$ with respect to Q is positive, then when the aircraft adopts the dynamic pressure Q_{mr} given by :

$$Q_{mr} = \frac{W}{S}\sqrt{\frac{K}{3C'_{D0}}} \tag{4.39}$$

the aircraft will descent at minimum rate. This situation corresponds then to the maximum endurance glide.

This dynamic pressure is different from the maximum range glide dynamic pressure, which is given by equation (4.19). Thus the relation between the green dot speed V_{gr} (corresponding to the maximum glide range) and the speed for the minimum rate of descent V_{mr} (corresponding to the maximum endurance) is:

$$V_{gr} = \sqrt[4]{3} \cdot V_{mr} = 1.316 \cdot V_{mr} \quad \text{and} \quad V_{mr} = 0.7598 \cdot V_{gr} \tag{4.40}$$

Then, since in both cases the lift force must be close to the weight of the aircraft, this means that at the maximum endurance glide, the angle of attack will be higher than at the maximum range glide.

In the same way the glide path angle for the minimum rate $-\gamma_{mr}$ of descent is expressed as:

$$-\gamma_{mr} = \frac{2}{\sqrt{3}} \cdot (-\gamma^*) \tag{4.41}$$

Then the max endurance t_{mr} corresponding to the minimum rate of descent is:

$$t_{mr} = \int_{z_0}^{z_t} \frac{1}{V_{mr}(z)\sin\gamma_{mr}(z)} dz = \frac{3^{0.75}}{2} \int_{z_0}^{z_t} \frac{1}{V_{gr}(z)\sin\gamma^*(z)} dz = \frac{3^{0.75}}{2} \cdot t_{gr} = 1.13975 \cdot t_{gr} \tag{4.42}$$

where t_{gr} is gliding time corresponding to the green dot speed.

IV.5 Steady Glide Turn Manoeuvres

During glide, turning manoeuvres can be necessary to avoid some ground obstacle or to head towards the targeted landing area according to roll out possibilities. When the gliding aircraft performs a turn, the steady condition is very different from the straight glide condition.

The aircraft is supposed to maintain a steady roll angle ϕ, so the equations (4.1) are rewritten as:

$$-D - W\sin\gamma = 0 \tag{4.43-a}$$

$$L\cos\phi - W\cos\gamma = 0 \tag{4.43-b}$$

So the glide path angle is:

$$-\tan\gamma = \frac{D}{L\cos\phi} \tag{4.44}$$

Comparing these equations with equations (4.3), it appears that when the aircraft turns steadily the aircraft needs more lift. That means the dynamic pressure should be increased to keep the vertical force balance. The glide path angle is also very small so that we can consider approximations leading to equations :

$$-\gamma = \frac{D}{L\cos\phi} \tag{4.45-a}$$

$$L = \frac{W}{\cos\phi} \tag{4.45-b}$$

Now the glide path angle can be expressed as:

$$-\tan\gamma = \frac{D}{L\cos\phi} = \frac{C_D^{'}}{C_l\cos\phi} = \frac{C_{D0}^{'} + KC_l^2}{C_l\cos\phi} \tag{4.46}$$

The maximum glide path angle during a turn with bank angle ϕ is then given by:

$$\gamma_{glide-\max} = -\arctan\frac{2\sqrt{KC_{D0}^{'}}}{\cos\phi} \tag{4.47}$$

The constraint with respect to the stall becomes:

$$V > V_{stall} = \sqrt{\frac{2W}{\rho S C_{l\max}\cos\phi}} \tag{4.48}$$

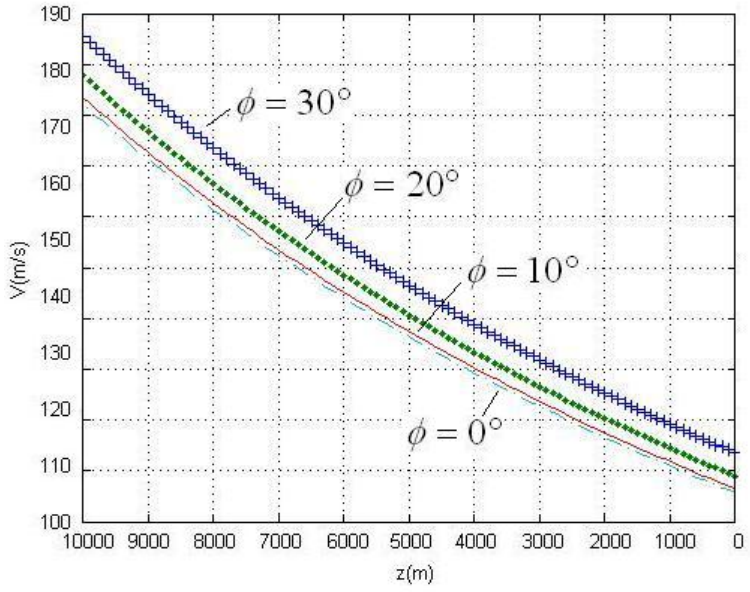

Figure 4.7 Gliding airspeed for different bank angles at different altitudes

Figure 4.7 shows the relations between glide airspeed and altitude at different bank angles. It appears that the more the bank angle is, the more the aircraft airspeed should be to maintain

steady glide conditions. Here also by supposing that the dynamic pressure Q remains constant during a steady gliding turn and adopting relation (4.28), we get:

$$-\tan\gamma(z)=\left[\frac{1}{2\cos\phi\sqrt{C_{D0}{}'K}}\left(1+\frac{Q}{P_0\left(\frac{T_0+a_0z}{T_0}\right)^{-\frac{g}{a_0R}}}\right)\right]^{-1} \tag{4.49}$$

Then, figure 4.8 shows the relation between the path angle and the bank angle at steady glide turn.

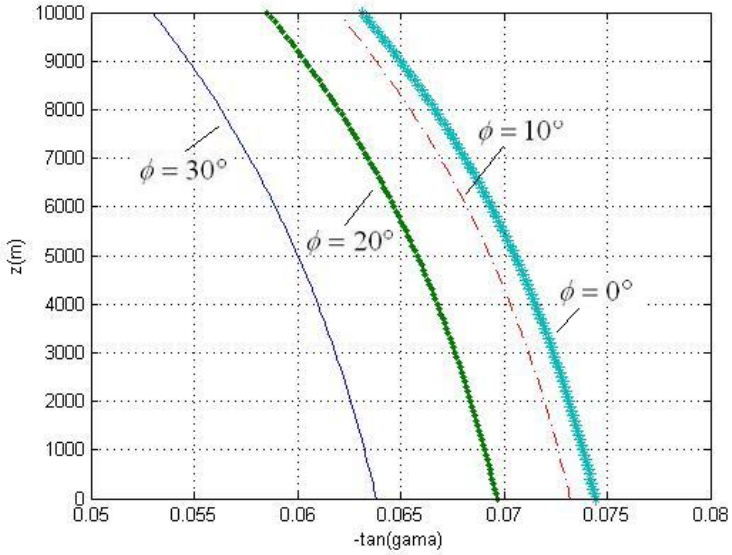

Figure 4.8 Gliding path angle at different bank angles

Assuming an equilibrated turn, we have:

$$\dot{\psi}=\frac{g}{V\cos\gamma}\tan\phi \tag{4.50}$$

Since $\frac{d\psi}{dz}=\dot{\psi}\cdot\frac{dt}{dz}$, to perform a change of heading of $\Delta\psi$ radians, the minimum loss of altitude Δz will be such as:

$$\int_{z_1}^{z_1-\Delta z} \frac{dz}{\sin(2\gamma(z))\cdot V(z)^2} = \frac{\Delta\psi}{2\cdot g\cdot\tan\phi} \tag{4.51}$$

The turning radius is such that $V\cos\gamma = R\dot{\psi}$, then:

$$R(z) = \frac{(V(z)\cos\gamma(z))^2}{g\tan\phi} \tag{4.52}$$

Figure 4.9 shows the relation among turn radius, altitude and the bank angle at steady gliding turn.

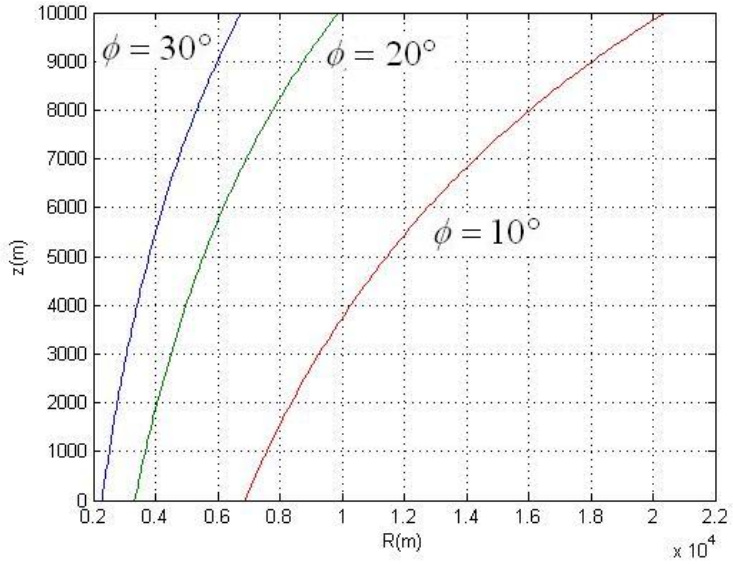

Figure 4.9 Steady gliding turn radius at different bank angles and altitudes

IV.6 Conclusion

In this chapter steady gliding performances of a transportation aircraft have been established in order to determine identify the flight glide domain of the engine-out aircraft. The formulation of an optimization problem to get the maximum range glide has led to intricate optimality conditions, so a simplified approach considering steady or quasi steady glide conditions have been developed to estimate the maximum range and to characterize straight glide at minimum rate of descent. Then steady gliding turn performances have been considered. Now, the question which arises is relative to the stability of the steady glide

trajectories, mainly when the gliding aircraft encounters wind perturbations, a situation which is likely to happen in an engine-out glide. This question is developed in the next chapter.

CHAPTER V

STABILITY OF GLIDING FLIGHT
FOR
TRANSPORTATION AIRCRAFT

V.1 Introduction

In this chapter the stability of glide flight around and towards steady glide trajectories is investigated. In general the atmosphere is not completely still and different configurations of wind producing glide perturbations can be encountered as the aircraft proceeds always nearer to the ground and likely with a smaller airspeed along its glide trajectory. This question is essential for the safety of the glide trajectory since it is directly related to the controllability of the glide situation by the pilot, the effectiveness of his control actions as well as his degree of implication in the glide management task. Annex B presents the main concepts related with the stability of nonlinear systems as well as the approach of Lyapunov to stability analysis of such systems.

Here two situations are considered depending if the engine-out situation affects (through the hydraulic and electric power systems) the pitch stability function of the gliding aircraft or not. In the first case the guidance dynamics stability around steady glide trajectories is investigated while in the second case, short period dynamics stability is considered.

The simulations displayed in this chapter are relative to a reference transportation aircraft and its reference data is displayed in Annex A.

V.2 Stability along a Gliding Trajectory

Here it will be supposed that during the period of the glide for which stability is studied, the pilot or the autopilot tries to maintain the pitch angle to the value corresponding to a steady glide. This will be made possible by the presence of the pitch stabiliser which will ease pitch control either manual or automatic. In this case the only independent input parameter which is available is the pitch angle θ, which can, even in an engine-out situation, be controlled by the pilot either through the hydraulic power provided by the RAT or the auxiliary power unit-APU, or through the trim control channel.

V.2.1 Characteristics of a steady glide reference trajectory

The vertical flight guidance equations written in the aircraft wind axis are given by:

$$\dot{V} = -\frac{1}{m}(D(V, z, \theta - \gamma) + m\, g\, \sin\gamma) \qquad \text{(5.1-a)}$$

$$\dot{\gamma} = \frac{1}{mV}(L(V, z, \theta - \gamma) - m\,g\,\cos\gamma) \tag{5.1-b}$$

while the COG coordinates follow the kinematics:

$$\dot{x} = -V\,\cos\gamma \tag{5.1-c}$$

$$\dot{z} = V\,\sin\gamma \tag{5.1-d}$$

Here it is considered that steady glide conditions are characterized by relations (see chapter IV):

$$\gamma_s = -\arctan\left(\frac{C_{D0}^{'} + K \cdot C_l(\alpha_s)^2}{C_l(\alpha_s)}\right) \tag{5.2-a}$$

$$V_s(z) = \sqrt{\frac{2W}{\rho(z)\,S\,C_l(\alpha_s)}} \tag{5.2-b}$$

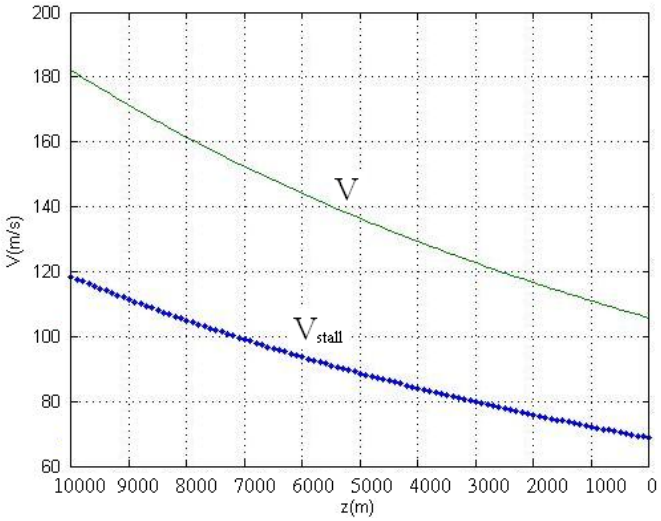

Figure 5.1 Steady glide airspeed with respect to altitude

The choice of γ_s corresponds a value of α_s solution of the nonlinear equation is:

$$K \cdot C_l(\alpha_s)^2 + \tan(\gamma_s) \cdot C_l(\alpha_s) + C_{D0}^{'} = 0 \tag{5.2-c}$$

and then a value for the pitch angle is given by:

$$\theta_s = \alpha_s + \gamma_s \tag{5.2-d}$$

V.2.2 Case of a wind affecting mainly the angle of attack

Then if the wind creates a variation of α equal to $\Delta\alpha$, the corresponding variation of γ, $\Delta\gamma$, will have such relation (3.27):

$$\gamma_g = -\arcsin\left(\frac{V_a}{V_g}(\sin(\alpha-\theta)+\frac{V_{wz}}{V_g}\right) = \gamma_s + \Delta\gamma \tag{5.3}$$

If we suppose that $V_a \approx V_g = V$ and that the angles are all small, we get:

$$\Delta\gamma \approx -\frac{V_{wz}}{V} \approx -\Delta\alpha \tag{5.4}$$

The vertical flight dynamics of a gliding aircraft can be written as:

$$\dot{V}_s + \Delta\dot{V} = -\frac{1}{m}(D(z_s+\Delta z, V_s+\Delta V, \alpha_s+\Delta\alpha)) + mg\sin(\gamma_s+\Delta\gamma) \tag{5.5-a}$$

$$(V_s+\Delta V)(\dot{\gamma}_s+\Delta\dot{\gamma}) = \frac{L(z_s+\Delta z, V_s+\Delta V, \alpha_s+\Delta\alpha)}{m} - g\cos(\gamma_s+\Delta\gamma) \tag{5.5-b}$$

$$\dot{x}_s + \Delta\dot{x} = -(V_s+\Delta V)\cos(\gamma_s+\Delta\gamma) \tag{5.6-c}$$

$$\dot{z}_s + \Delta\dot{z} = (V_s+\Delta V)\sin(\gamma_s+\Delta\gamma) \tag{5.6-d}$$

with at steady glide:

$$D(z_s, V_s, \alpha_s)) + mg\sin(\gamma_s) = 0 \qquad \text{with} \quad \dot{V}_s \approx 0 \tag{5.7-a}$$

$$L(z_s, V_s, \alpha_s)/m - g\cos(\gamma_s) = 0 \qquad \text{with} \quad \dot{\gamma}_s = 0 \tag{5.7-b}$$

$$\dot{x}_s = -V_s\cos\gamma_s \tag{5.7-c}$$

$$\dot{z}_s = V_s\sin\gamma_s \tag{5.7-d}$$

Then we can write the drag equation as:

$$\Delta\dot{V} = -\frac{1}{m}(D(z_s+\Delta z, V_s+\Delta V, (\alpha_s+\Delta\alpha)) + mg\sin(\gamma_s-\Delta\alpha) \tag{5.8-a}$$

which can be rewritten as :

$$\Delta\dot{V} = -\frac{1}{m}(\frac{\partial D}{\partial z}\Big|_s\cdot\Delta z + \frac{\partial D}{\partial V}\Big|_s\cdot\Delta V + \frac{\partial D}{\partial \alpha}\Big|_s\cdot\Delta\alpha) - mg\cdot\Delta\alpha + O_D^2(\Delta z, \Delta V, \Delta\alpha) \tag{5.8-b}$$

and neglecting the second order term as well as $\frac{\partial D}{\partial z}\big|_s \cdot \Delta z$, we get :

$$\Delta \dot{V} = -\frac{1}{m}(\frac{\partial D}{\partial V}\big|_s) \cdot \Delta V + (-\frac{1}{m}\frac{\partial D}{\partial \alpha}\big|_s - g) \cdot \Delta \alpha \tag{5.8-c}$$

The lift equation reduces here, where θ is maintained as constant, to:

$$\Delta \gamma = -\Delta \alpha \tag{5.9}$$

With respect to the longitudinal variation, we have:

$$\Delta \dot{x} = -(V_s + \Delta V)\cos(\gamma_s - \Delta \alpha) + V_s \cos \gamma_s \tag{5.10-a}$$

or

$$\Delta \dot{x} = -\Delta V \cos(\gamma_s) + O_x^2(\Delta V, \Delta \alpha) \tag{5.10-b}$$

and neglecting the second order term, we get :

$$\Delta \dot{x} = -\cos(\gamma_s)\, \Delta V \tag{5.10-c}$$

With respect to the vertical variation, we get:

$$\Delta \dot{z} = (V_s + \Delta V)\sin(\gamma_s - \Delta \alpha) - V_s \sin \gamma_s \tag{5.11-a}$$

or

$$\Delta \dot{z} = V_s\, \Delta \gamma + O_z^2(\Delta V, \Delta \alpha) \tag{5.11-b}$$

and neglecting the second order term, we get :

$$\Delta \dot{z} = V_s\, \Delta \gamma \tag{5.11-c}$$

It appears that the first order approximation of the variation from the steady glide conditions, equations (5.8-c), (5.10-c) and (5.11-c) represents a cascaded system and the stability of equations (5.8-c) will imply the stability of the trajectory around the steady glide trajectory. These conditions are such as:

$$\Delta \dot{V} = -\frac{1}{m}(\frac{\partial D}{\partial V}\big|_s) \cdot \Delta V + (-\frac{1}{m}\frac{\partial D}{\partial \alpha}\big|_s - g) \cdot \Delta \alpha \tag{5.12-a}$$

or

$$\Delta\dot{V} = a\,\Delta V + b\,\Delta\alpha \tag{5.12-b}$$

where

$$a = -\frac{1}{m}\frac{\partial D}{\partial V}\Big|_s < 0 \quad \text{and} \quad b = -\frac{1}{m}\frac{\partial D}{\partial \alpha}\Big|_s - g \tag{5.12-c}$$

It appears that the dynamics of this first order linear system are asymptotically stable.

When the wind effect over α is similar to a wind pulse (Figure 5.2) there is:

$$\Delta\alpha(t) = \Delta\alpha_0\big(u(t-t_0) - u(t-t_0+T)\big) \quad \text{with } T > 0 \tag{5.13}$$

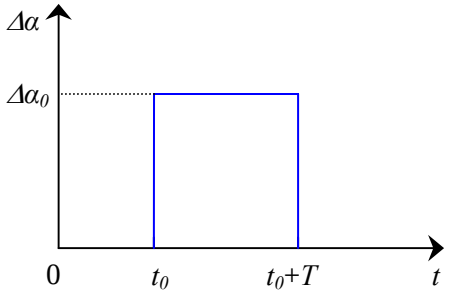

Figure 5.2 Adopted wind effect on angle of attack

where $u(\text{-})$ is the unit step function, we get $\Delta V(t)$ between t_0 and t_0+T:

$$\Delta V(t) = \frac{b}{a}(1 - e^{a\,(t-t_0)})\,\Delta\alpha_0 \tag{5.14-a}$$

with

$$\Delta\gamma(t) = -\Delta\alpha_0 \tag{5.14-b}$$

$$\Delta x(t) = -\cos(\gamma_s)\,\frac{b}{a}\cdot\Delta\alpha_0\cdot\left(t - t_0 + \frac{1}{a}\left(1 - e^{a(t-t_0)}\right)\right) \tag{5.14-c}$$

$$\Delta z(t) = -V_s\cdot\Delta\alpha_0\cdot(t - t_0) \tag{5.14-d}$$

and after t_0+T:

$$\Delta V(t) = \frac{b}{a}(1 - e^{a\,T})\,e^{a\,(t-T)}\Delta\alpha_0 \tag{5.15-a}$$

with

$$\lim_{t\to+\infty} \Delta V(t) = 0 \qquad \text{and} \quad \Delta\gamma(t) = 0 \tag{5.15-b}$$

and

$$\Delta x(t) \to -\cos(\gamma_s)\left(\frac{b}{a}\left(1-e^{a\,T}+\frac{1}{a}\left(1-e^{a\,(t-T)}\right)\right)\right)\Delta\alpha_0 \tag{5.16-a}$$

with

$$\lim_{t\to+\infty} \Delta x(t) = -\cos(\gamma_s)\left(\frac{b}{a}\left(1+\frac{1}{a}-e^{a\,T}\right)\right)\Delta\alpha_0 \tag{5.16-b}$$

and

$$\Delta z(t) = -V_s \cdot \Delta\alpha_0 \cdot T \tag{5.17}$$

From equations (5.15-b) and (5.17), it appears that the gliding aircraft after the crossing of the wind section returns asymptotically to a steady glide along a trajectory parallel to the unperturbed one. This is shown in figures 5.3-a and 5.3-b.

In figures 5.3, the red curves are for stable descend and the blue ones are for disturbed descend. Here the adopted wind perturbation is a kind of micro-downburst, since the lateral wind changes from head to tail while its vertical component is a downward pulse.

In the case in which the perturbation remains, according to equation (5.14-d), the drift between the unperturbed trajectory and the perturbed one goes increasing with time.

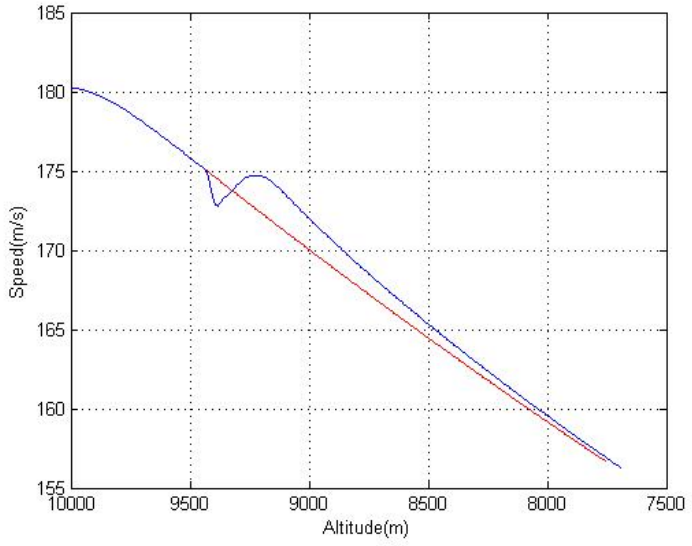

Figure 5.3-a Effect of a windshear on steady glide (V vs. z)

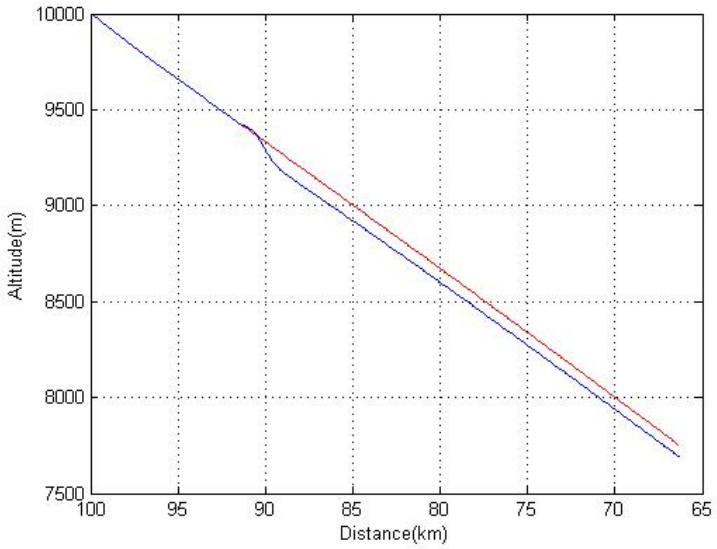

Figure 5.3-b Effect of a windshear on steady glide (z vs. x)

V.2.3 The general longitudinal case

Since the presence of wind makes change in general not only the angle of attack but also the intensity of airspeed, we consider here a more general case. For a general vertical wind perturbation, the vertical flight equations can be rewritten such as:

$$m\ddot{x} = D(z, V_a, \alpha)\cos(\theta - \alpha) + L(z, V_a, \alpha)\sin(\theta - \alpha) \qquad (5.18\text{-a})$$

$$m\ddot{z} = -D(z, V_a, \alpha)\sin(\theta - \alpha) + L(z, V_a, \alpha)\cos(\theta - \alpha) - mg \qquad (5.18\text{-b})$$

where

$$V_a = \sqrt{(\dot{x} - w_x)^2 + (\dot{z} - w_z)^2} \quad \text{and} \quad \alpha = \theta + \arctan\left(\frac{\dot{z} - w_z}{\dot{x} - w_x}\right) \qquad (5.19)$$

What we want to determine here is the stability of the glide trajectories around steady glide trajectories. We consider the aircraft once it has gone through a turbulent section following equations (5.18) to (5.19) is already away from any steady glide trajectory. Then we want to answer the question that given a gliding aircraft where the pitch angle is maintained constant, does its free evolution can lead to a new steady glide trajectory or not?

To answer this question, we consider a Lyapunov function [Annex B] corresponding to the evaluation of the distance between a general glide trajectory and a steady glide trajectory.

Consider now any steady glide trajectory which, according to results of chapter IV is characterized by the following equations and conditions:

$$\dot{x}_s = V_s \cos\gamma_s \tag{5.20-a}$$

$$\dot{z}_s = V_s \sin\gamma_s \tag{5.20-b}$$

with

$$D(z_s, V_s, \theta_s - \gamma_s)\cos\gamma_s + L(z_s, V_s, \theta_s - \gamma_s)\sin\gamma_s \approx 0 \tag{5.20-c}$$

$$-D(z_s, V_s, \theta_s - \gamma_s)\sin\gamma_s + L(z_s, V_s, \theta_s - \gamma_s)\cos\gamma_s - mg \approx 0 \tag{5.20-d}$$

where V_s, γ_s and θ_s are chosen according relations (5.2-a), (5.2-b) and (5.2-d).

Here we adopt as candidate Lyapunov function, the function Π of expression:

$$\Pi = \frac{1}{2}\left((V\sin\gamma - V_s(z)\sin\gamma_s)^2 + (V\cos\gamma - V_s(z)\cos\gamma_s)^2\right) \tag{5.21}$$

Effectively if it can be proven that there exists a steady glide trajectory characterized by V_s and γ_s so that $\lim_{t\to+\infty}\Pi = 0$ then:

$$\lim_{t\to+\infty} V(t) = V_s(t) \text{ and } \lim_{t\to+\infty}\gamma(t) = \gamma_s \tag{5.22}$$

which would characterize the convergence towards a steady glide trajectory.

Taking into account that $\dot{\gamma}_s = 0$, we have:

$$\dot{\Pi} = V\dot{V} - (\dot{V}V_s + V\dot{V}_s)\cos(\gamma_s - \gamma) + V_s\dot{V}_s \tag{5.23}$$

Considering that $\gamma_s - \gamma$ remains small and that the cosine can be approximated by 1, we get:

$$\dot{\Pi} \approx (V - V_s)(\dot{V} - \dot{V}_s) \tag{5.24}$$

In the first approach, we consider the evolution of the glide with respect to the original steady glide trajectory. Supposing that before instant t_0 there is no wind we have $V(t_0) = V_s(t_0)$. Then at time $t_0 + dt$ with $dt > 0$, as the consequence of wind we can have two situations:

- either $V(t_0+dt) > V_s(t_0+dt)$:

  Since $V(t)$ is a smooth function of time, we must have $\dot{V}(\tau) > \dot{V}_s(\tau)$ for some τ such as: $0 < \tau < dt$ and $(V(t_0+\tau) - V_s(t_0+\tau))(\dot{V}(t_0+\tau) - \dot{V}_s(t_0+\tau)) > 0$.

- or $V(t_0+dt) < V_s(t_0+dt)$, then we must have $\dot{V}(\tau) < \dot{V}_s(\tau)$ for some τ such as: $0 < \tau < dt$ and again $(V(t_0+\tau) - V_s(t_0+\tau))(\dot{V}(t_0+\tau) - \dot{V}_s(t_0+\tau)) > 0$.

This result displays the natural instability of the glide trajectory with respect to the *original* steady glide trajectory.

Now, introducing explicitly the effect of wind in the stability analysis, we can write:

$$\dot{V} = -\frac{1}{m} D(z, V_a, \theta - \gamma_a) - g \sin\gamma_a \tag{5.25-a}$$

$$\dot{V}_s = -\frac{1}{m} D(z, V_s, \theta - \gamma_s) - g \sin\gamma_s \tag{5.25-b}$$

where according to relation (3.25-b):

$$V_a \approx V - V_{wx} + \gamma_a \cdot V_{wz} \tag{5.26}$$

Now introducing $\Delta V = V - V_s$, we can write:

$$\dot{V} = -\frac{1}{m} D(z, V_s + \Delta V - V_{wx} + \gamma_a \cdot V_{wz}, \theta - \gamma_a) - g \sin\gamma_a \tag{5.27}$$

We can write with a first order approximation:

$$\begin{aligned} &D(z, V_s + \Delta V - V_{wx} + \gamma_a \cdot V_{wz}, \theta - \gamma_a) \\ &\approx D(z, V_s, \theta - \gamma_s) + \frac{\partial D}{\partial V_a}\Big|_s \cdot (\Delta V - V_{wx} + \gamma_a \cdot V_{wz}) + \frac{\partial D}{\partial \alpha}\Big|_s (\gamma_a - \gamma_s) \end{aligned} \tag{5.28}$$

and

$$\begin{aligned} \dot{\Pi} = (V - V_s)(\dot{V} - \dot{V}_s) = \Delta V \cdot \Delta\dot{V} \approx -\frac{1}{m}\frac{\partial D}{\partial V_a}\Big|_s \cdot \Delta V^2 \\ -\left(\frac{1}{m}\frac{\partial D}{\partial V_a}\Big|_s (-V_{wx} + \gamma_a \cdot V_{wz}) + \frac{1}{m}\frac{\partial D}{\partial \alpha}\Big|_s (\gamma_a - \gamma_s) + g(\gamma_a - \gamma_s)\right) \cdot \Delta V \end{aligned} \tag{5.29}$$

The sign of $\dot{\Pi}$ cannot be predicted according to the above relation since if the first term is negative but the second term can take any sign. Then without any particular providence, the convergence of a passive gliding aircraft towards the original steady glide trajectory is not insured. This is also shown by the simulations displayed in figures 5.3-a and 5.3-b.

However, if the pilot could know the wind components and choose an aerodynamic path angle γ_a such as:

$$\gamma_a = \frac{\left(m\lambda - \frac{\partial D}{\partial V_a}\Big|_s\right)\Delta V + \left(\frac{\partial D}{\partial V_a}\Big|_s V_{wx} + \frac{\partial D}{\partial \alpha}\Big|_s \gamma_s + mg\gamma_s\right)}{\frac{\partial D}{\partial V_a}\Big|_s V_{wz} + \frac{\partial D}{\partial \alpha}\Big|_s + mg} \quad \text{with} \quad \lambda > 0 \tag{5.30}$$

then :

$$\dot{\Pi} = -\lambda\, \Delta V^2 \tag{5.31}$$

and the glide trajectory should be attracted by a steady glide.

Then to join a steady glide trajectory, the pilot or the autopilot should drive the aircraft by modifying the pitch angle along the glide.

The feasibility of such endeavor can be analyzed by considering the following optimization problem:

$$\min_{\theta(t)} \frac{1}{2}\int_0^{t_f} \left((V\sin\gamma - V_s(z)\sin\gamma_s)^2 + (V\cos\gamma - V_s(z)\cos\gamma_s)^2\right)dt \tag{5.32-a}$$

with

$$\dot{V} = -\frac{1}{m}D(z,V,\theta-\gamma) - g\sin\gamma \tag{5.32-b}$$

$$\dot{\gamma} = \frac{L(z,V,\theta-\gamma)}{m\,V} - \frac{g}{V}\cos\gamma \tag{5.32-c}$$

$$\dot{z} = V\sin\gamma \tag{5.32-d}$$

$$\dot{x} = V\cos\gamma \tag{5.32-e}$$

with

$$V_{\max}(z) \geq V(t) > (1+\varepsilon)\, V_{stall} = \sqrt{\frac{2mg}{\rho(z(t))\, S\, C_{l\max}}} \qquad \varepsilon \approx 0.3 \tag{5.32-f}$$

$$\alpha_{\min} \leq \theta - \gamma \leq \alpha_{\max} \tag{5.32-g}$$

and

$$z(t) \geq h(x(t)) \tag{5.32-h}$$

with the initial conditions:

$$V(0) = V_0,\ \gamma(0) = \gamma_0,\ x(0) = 0,\ z(0) = z \tag{5.32-i}$$

and the final conditions:

$$V(t_f) = V_s(z(t_f)), \quad \gamma(t_f) = \gamma \tag{5.32-j}$$

Here t_f is the unknown convergence instant from initial conditions (5.32-i). Other candidate functions for the optimization criterion could be considered while final conditions (5.32-j) should remain unchanged. With respect to the numerical resolution, the same considerations than in Chapter IV.2 about the difficulty to solve this problem can be made.

V.3 Stability during Glide with Undamped Pitch Dynamics

Now since here we suppose that the pitch stability function is no more active, we have to study the natural flight dynamics of the aircraft while gliding towards or around a steady glide trajectory. Then in this section we are interested on the short term pitch dynamics of the aircraft with the main objective of assessing the risk of stall due to wind perturbations. We consider that the position of the trimmable horizontal stabiliser remains under control of the pilot, however since its dynamics are very slow with respect to the short period they are not considered in this study.

V.3.1 Linear approximation of fast longitudinal dynamics

Let the general longitudinal dynamics of an aircraft be written as:

$$\dot{V} = -\frac{1}{m} D(z, V_a, \dot{\alpha}, \theta - \gamma) - g \sin\gamma \tag{5.33-a}$$

$$V\, \dot{\gamma} = \frac{L(z, V_a, \dot{\alpha}, \theta - \gamma)}{m} - g \cos\gamma \tag{5.33-b}$$

with the pitch dynamics

$$\dot{\theta} = q \tag{5.33-c}$$

$$\dot{q} = \frac{1}{J} M(z, V_a, \dot{\alpha}, \theta - \gamma, \delta_e) \tag{5.33-d}$$

where q is the pitch rated, J is the pitch inertia moment and M is the pitch aerodynamic moment. Consider the state and input variations around a point on a steady gliding trajectory given by:

$$\underline{X} = [\Delta V \quad \Delta\alpha \quad \Delta\theta \quad \Delta q]^T \qquad \text{and} \qquad U = \Delta\delta_e = 0 \tag{5.34}$$

The linearized flight dynamics are given by [NELSON R. C.] :

$$\begin{bmatrix} 1 & 0 & 0 & 0 \\ 0 & V + \frac{1}{m}\frac{\partial L}{\partial \dot{\alpha}} & 0 & 0 \\ 0 & 0 & 1 & 0 \\ 0 & -\frac{1}{J}\frac{\partial M}{\partial \dot{\alpha}} & 0 & 1 \end{bmatrix} \begin{bmatrix} \Delta\dot{V} \\ \Delta\dot{\alpha} \\ \Delta\dot{\theta} \\ \Delta\dot{q} \end{bmatrix} = \begin{bmatrix} -\frac{1}{m}\frac{\partial D}{\partial V} & -\frac{1}{m}\frac{\partial D}{\partial \alpha} + \frac{L}{m} & -g\cos(\theta-\alpha) & 0 \\ -\frac{1}{m}\frac{\partial L}{\partial V} & -\frac{1}{m}\frac{\partial L}{\partial \alpha} - \frac{D}{m} & -g\sin(\theta-\alpha) & V - \frac{1}{m}\frac{\partial L}{\partial q} \\ 0 & 0 & 0 & 1 \\ \frac{1}{J}\frac{\partial M}{\partial V} & \frac{1}{J}\frac{\partial M}{\partial \alpha} & 0 & \frac{1}{J}\frac{\partial M}{\partial q} \end{bmatrix}_e \begin{bmatrix} \Delta V \\ \Delta\alpha \\ \Delta\theta \\ \Delta q \end{bmatrix} \tag{5.35}$$

or

$$E\,\dot{\underline{X}} = A\,\underline{X} + \underline{B}\,U \tag{5.36}$$

So the eigenvalues of control system are the roots of the following equation, which indicates two mode of flight, phugoïd mode and short period mode:

$$|sE - A| = \begin{bmatrix} s + \frac{1}{m}\frac{\partial D}{\partial V} & \frac{1}{m}\frac{\partial D}{\partial \alpha} - \frac{L}{m} & g\cos(\theta-\alpha) & 0 \\ \frac{1}{m}\frac{\partial L}{\partial V} & sV + \frac{s}{m}\frac{\partial L}{\partial \dot{\alpha}} + \frac{1}{m}\frac{\partial L}{\partial \alpha} + \frac{D}{m} & g\sin(\theta-\alpha) & -V + \frac{1}{m}\frac{\partial L}{\partial q} \\ 0 & 0 & s & -1 \\ -\frac{1}{J}\frac{\partial M_m}{\partial V} & -\frac{s}{J}\frac{\partial M_m}{\partial \dot{\alpha}} - \frac{1}{J}\frac{\partial M_m}{\partial \alpha} & 0 & s - \frac{1}{J}\frac{\partial M_m}{\partial q} \end{bmatrix} = 0 \tag{5.37}$$

Furthermore the free longitudinal short period mode dynamics are given by equations:

$$\begin{bmatrix} V + \frac{1}{m}\frac{\partial L}{\partial \dot{\alpha}} & 0 \\ -\frac{1}{J}\frac{\partial M_m}{\partial \dot{\alpha}} & 1 \end{bmatrix} \begin{bmatrix} \Delta\dot{\alpha} \\ \Delta\dot{q} \end{bmatrix} = \begin{bmatrix} -\frac{1}{m}\frac{\partial L}{\partial \alpha} - \frac{D}{m} & V - \frac{1}{m}\frac{\partial L}{\partial q} \\ \frac{1}{J}\frac{\partial M_m}{\partial \alpha} & \frac{1}{J}\frac{\partial M_m}{\partial q} \end{bmatrix} \begin{bmatrix} \Delta\alpha \\ \Delta q \end{bmatrix} \tag{5.38}$$

whose characteristic polynomial $P(s)$ is given by:

$$P(s) = a\,s^2 + b\,s + c \tag{5.39}$$

with

$$a = V \tag{5.40-a}$$

$$b = \frac{QS}{m} C_{l\alpha} + \frac{QSC_D}{m} - \frac{QS}{J} \frac{C_{ma}}{2V_a} C_{mq} V - \frac{QS}{J} \frac{C_{ma}}{2V_a} C_{m\dot{\alpha}} V \tag{5.40-b}$$

and

$$c = -\frac{QS}{J} [\frac{C_{ma}}{2V_a} C_{mq} \frac{QSC_{l\alpha} + QSC_D}{m} + C_{m\alpha} V] \tag{5.40-c}$$

The main independent operational parameters appearing in the characteristic polynomial are ground speed V, the airspeed V_a and the dynamic pressure Q or equivalently the speed and the flight level z.

In the case of a reference aircraft (see Annex A for reference data) the root locus of the short period mode when the airspeed varies with $V_a \in [V_{\min}, V_{\max}]$ with $V_{\min} = V_{stall}(z)$ and $V_{\max} = 250 m/s$ at different flight levels is displayed in figure 5.4.

It appears that the lower the airspeed is, the closer the root is to the imaginary axis of the complex plane with an increasing tendency for oscillation while dynamic stability remains guaranteed. Also, with a decreasing flight level along the glide trajectory, the root locus goes closer to the real axis with an increasing damping resulting from increased air density.

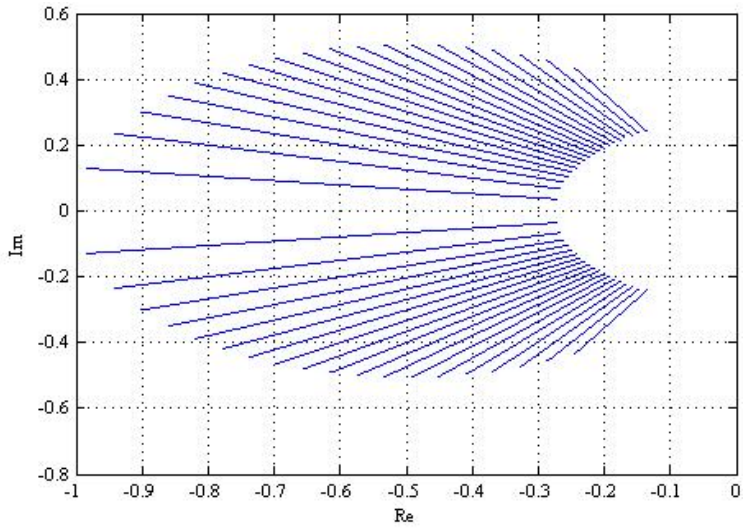

Figure 5.4 Root locus of short period mode with different airspeed at different flight levels

V.3.2 Effect of wind on undamped short period dynamics

When a gliding aircraft encounters a sudden headwind, the airspeed increases accordingly while the effect on the ground speed is progressive according to the drag equation.

The corresponding change in the roots locus is displayed in figure 5.5. The main effect on this roots locus is to move it away from the imaginary axis. When the aircraft fly at low altitude, the root locus may even reach the real axis.

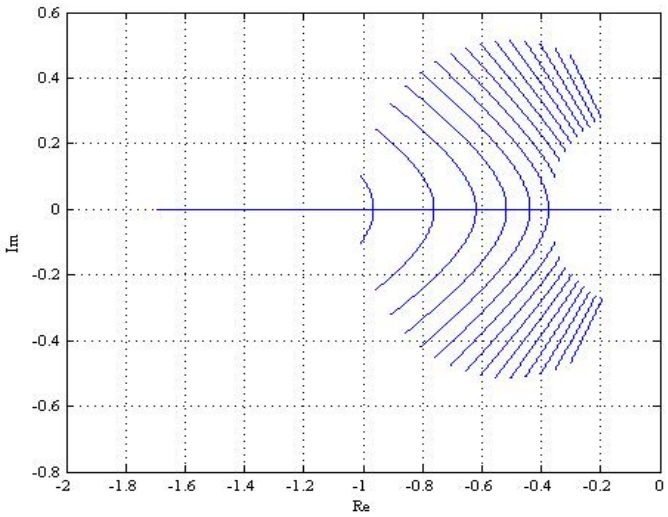

Figure 5.5 Immediate effect of headwind on short period root locus

On the other hand if the aircraft encounters a sudden tailwind, the airspeed decreases immediately. So the roots locus changes accordingly as shown in figure 5.6.

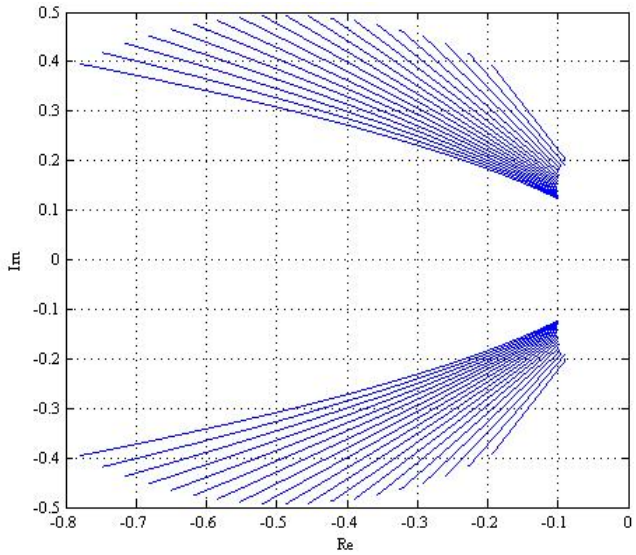

Figure 5.6 Immediate effect of tailwind on short period root locus

In that case the effect of tailwind is to decrease the short period damping with a different effect of altitude.

It appears that in both cases (headwind and tailwind), within the nominal airspeed range, dynamic stability remains guaranteed.

V.4 Simulation Results for Glide Stability Analysis

The analysis performed in the previous paragraph has been carried out by using a linear approximation of the short period dynamics. Here a full nonlinear mathematic model of a reference aircraft is simulated using Matlab-Simulink. It is supposed that the all-engines-out situation starts at a flight level of 7000 meters, with an airspeed equal to 180 m /s and with an initial glide path angle equal to -0.075*rad*. Different wind scenarios during the glide manoeuver are considered.

V.4.1 Roots locus variation with wind speed pulses

Here the roots locus is displayed for the following wind speed scenarios with horizontal pulses:

- Blue locus: headwind pulse with amplitude of 30m/s
- Red locus: headwind pulse with amplitude of 15m/s
- Black locus: no wind
- Cyan locus: tail wind pulse with amplitude of 15m/s
- Magenta locus: tail wind pulse with amplitude of 30m/s

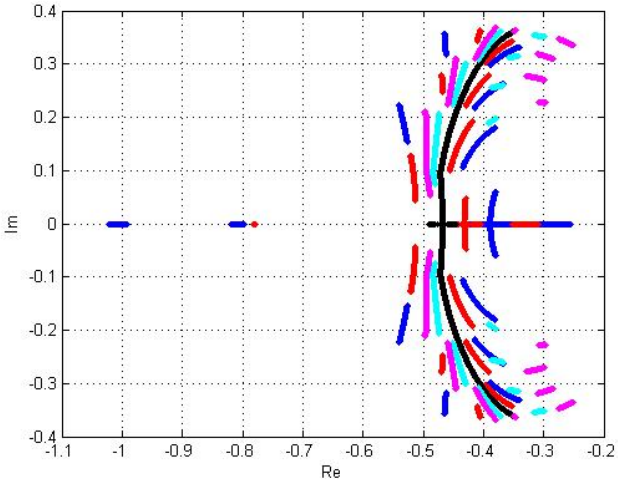

Figure 5.7 Roots loci for different wind scenarios

Figure 5.7 shows that when the aircraft encounter the head or the tail of a wind pulse, the airspeed changes suddenly, which leads to a shift in the position change of the root locus. Then, the roots locus is here divided into different segments according to the length of the pulses. It appears here also that short period dynamic stability remains guaranteed in all considered situations.

V.4.2 Evolution of glide parameters under different wind speed scenarios

Figure 5.8 shows the impact of a strong headwind of 30m/s on the glide trajectory. In this case the headwind appears under the form of pulses, shown in figure 5.8 with a magenta curve, and airspeed and ground speed are shown in blue curve and red curve respectively. Then other parameters vary accordingly.

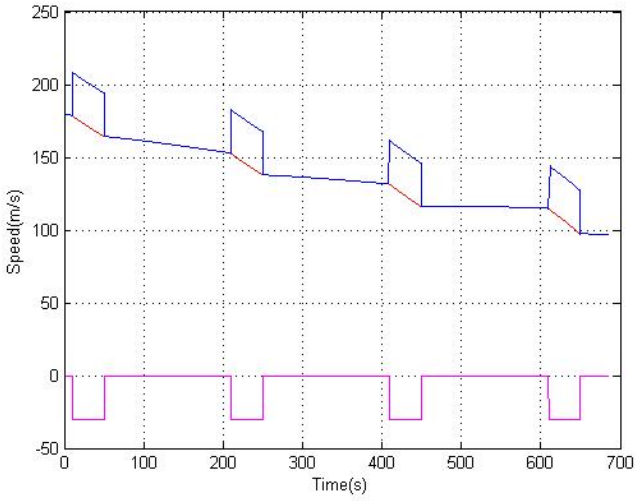

Figure 5.8 Airspeed and ground speed under headwind pulses

Figure 5.9 displays the corresponding evolution of the pitch angle (red curve), the angle of attack (blue curve) and glide path angle (magenta Curve). The corresponding values of the pitch angle rate are given in figure 5.10.

In figures 5.8, 5.9 and 5.10 the natural short period longitudinal stability is manifest even with strong wind disturbances except in situations where the aircraft is close to the ground. Indeed, if the aircraft is very close to the ground, a sudden disappearance of the headwind may lead to a stall followed by a crash on the ground. Every change of wind leads changes of pitch angle rate, but this change attenuates quickly.

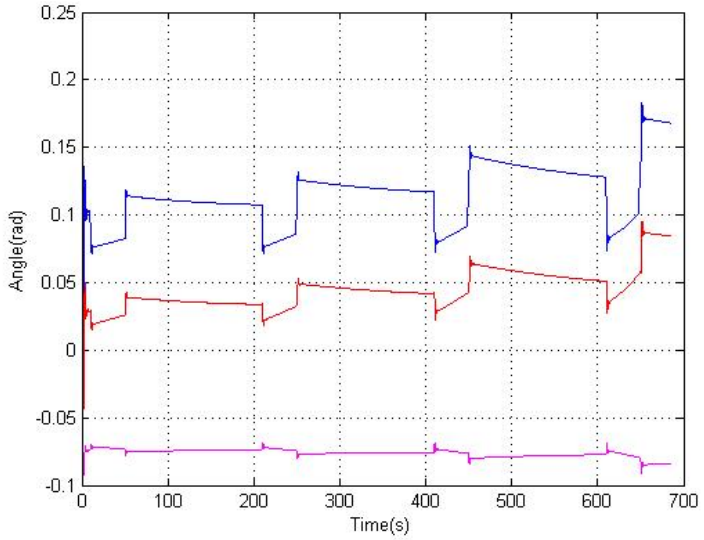

Figure 5.9 Evolution of pitch, glide and aerodynamic angles with headwind pulses

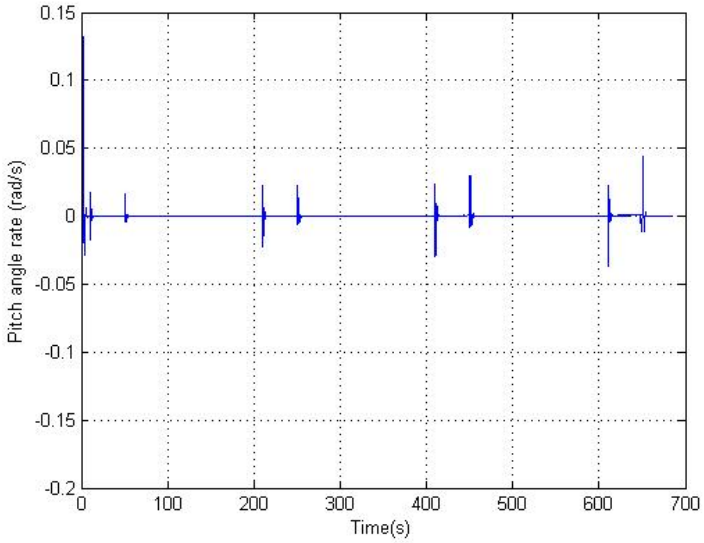

Figure 5.10 Pitch rate under headwind pulses

Figures 5.11, 5.12 and 5.13 displays the influence of tailwind pulses on the glide parameters.

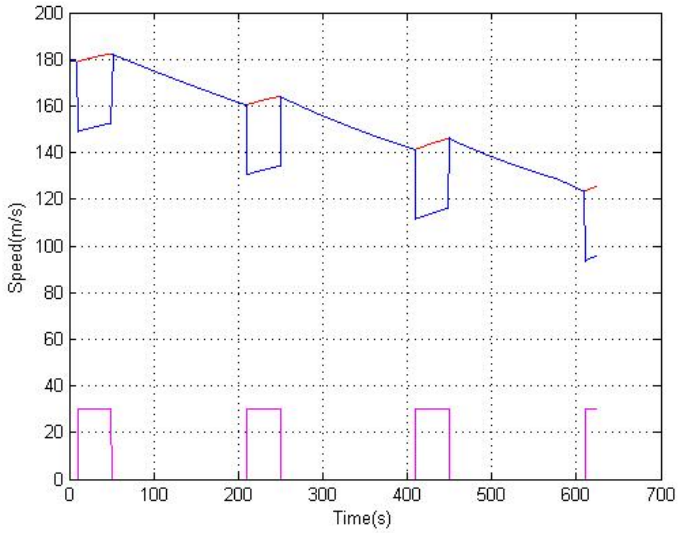

Figure 5.11 Airspeed and ground speed under tailwind pulses

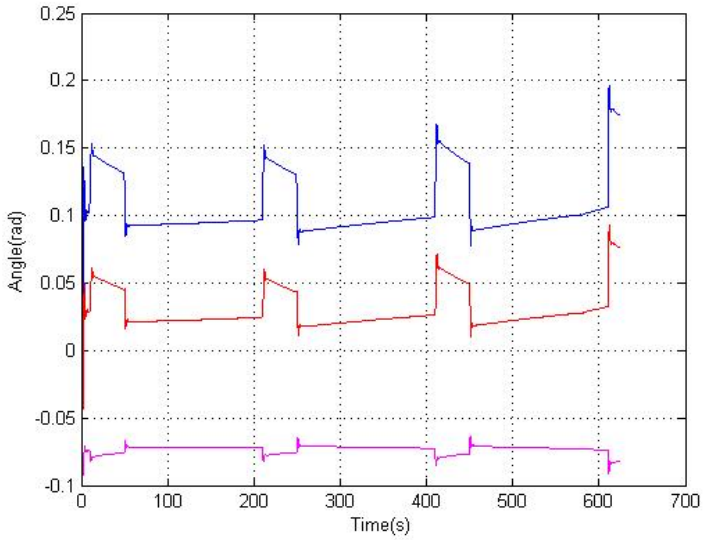

Figure 5.12 Evolution of pitch, glide and aerodynamic angles with tailwind pulses

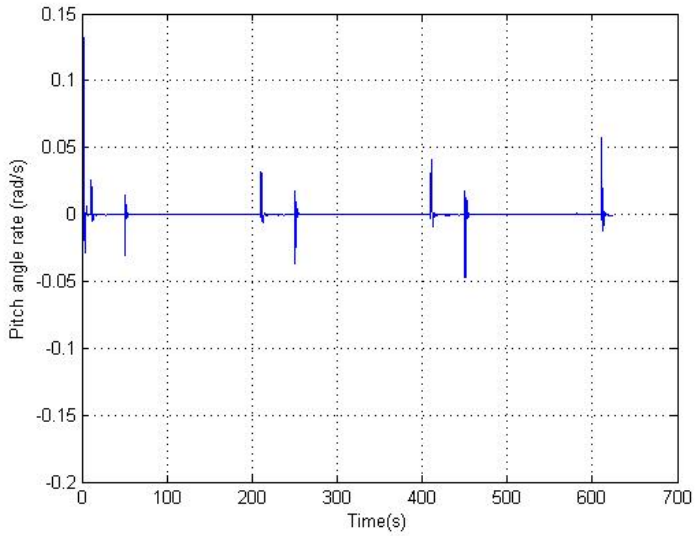

Figure 5.13 Pitch rate under tailwind pulses

Similar comments as in the case of headwind pulses can be produced.

V.5 Conclusion

This chapter has displayed an analysis of glide stability under wind perturbations. The perturbations considered also deterministic corresponds to extreme situations in which pure wind speed pulses are applied to the gliding aircraft. Other scenarios including in particular stochastic components of wind speed could be of interest in future studies.

In the case in which the pitch stabilizer is out of service as a consequence of the engine extinction, it appeared of interest to consider the short mode stability issue directly related with the risk of stall and to the difficulty of mastering the gliding aircraft by the pilot.

In the case in which the pitch stabilizers operates, the issue considered has been relative to the glide stability around steady glide trajectories.

If in the first situation, natural stability properties of commercial airplanes leads in general to manageable glide conditions by the pilot, in the second situation, it appears that the direct intervention of the pilot is necessary to return to a steady glide situation.

In the following chapter an overview of trajectory optimization methods will be developed with the aim of identifying a practical method to compute effectively safe glide trajectories for a transportation aircraft.

CHAPTER VI

AIRCRAFT TRAJECTORY OPTIMIZATION TECHNIQUES: AN OVERVIEW

VI.1 Introduction

Trajectory optimization is the process of generating a feasible trajectory which minimizes (or maximize) a performance index or optimization criterion. Trajectory optimization can be seen as an optimal control problem where the trajectory to be optimized is represented by the state history. The trajectory can be understood as a state trajectory for any dynamical system as well as the space trajectory of a mobile in the space. The generation of a flight trajectory that provides the best performance with respect to costs and service, plays an important role in the design of atmospheric vehicles such as transportation aircraft as well as in their daily operation.

The techniques which are today developed to solve optimization problems fall into two large classes: [BETTS J. T.[1,2]][STRYK O. von]

- The techniques taking profit of the optimality conditions derived from optimal control theory that lead to solution by either analytical or numerical procedures[DESOER C.A.].

- The techniques that solve an approximation to the optimal-control problem through the use of nonlinear programming through numerical procedures[SUN W.].

The techniques of the first class are said *indirect* in the sense that they find a solution to the optimality conditions at which the first order differential of the augmented performance measure (Hamiltonian), or variation, is zero. The techniques of the second class are said *direct* in the sense that they try to maximize (or minimize) directly the performance measure.

VI.2 Previous Research on Aircraft Trajectory Optimization

A very large effort has been developed to design numerical techniques able to solve the trajectory optimization problem when considering either space of atmospheric flight applications[CHEN Y.H.][NGO A. D.][SHI Y.].

Although an accurate and more detailed flight model allows to better estimate the aircraft performances, in general it will be more difficult to be used with numerical techniques for

trajectory optimization. However, since when an aircraft trajectory is given, it is in general possible to get through numerical inversion of such accurate flight model the corresponding inputs [GAO C.] even for complex flight maneuvers, these more detailed models can be useful to check the feasibility of the trajectory resulting from the solution of a trajectory optimization problem. For example, in [SEYWALD H.] the trajectory optimization problem was first solved using a direct multiple shooting technique for a three degree of freedom aircraft flight model and then an inverse simulation using a higher-fidelity five degree of freedom aircraft flight model was used to analyze the feasibility of the open-loop optimal control trajectory obtained using the first simplified model. In many situations, the size of the three-dimensional aircraft trajectory optimization problem has been reduced by introducing a total energy state [CALISE A. J. [1]].

Here a wide scope of problems directly related with aircraft trajectory optimization which have been formulated in general as optimal control problems are reviewed:

- Minimum-fuel optimization with fixed arrival time has been considered in [DICKMANNS E.D.] for wide body transportation aircraft where tradeoffs have been established between minimum fuel consumption and required arrival time. There the flight guidance dynamics have been adapted by introducing a total energy state considering the sum of potential energy and kinetic energy. This problem has also been considered in [LAWDEN D.F.] and treated as an optimal control problem using an aircraft model in the vertical plane, where the effect of decreasing weight of the aircraft with fuel consumption has been taken into account. Fuel consumption optimization for maximizing the range of aircraft is discussed in [ARDEMA M. D.]. And minimum fuel burn descents is studied in [ANDREEVA-MORI A.].

- The optimal landing problem has received a lot of attention and recently studies about continuous descent approaches (CDA) have led to the definition of trajectory optimization problems at descent and approach for transportation aircraft [*Sourdine II Consortium*] [SUZUKI S.]. Other optimization approaches have considered the effect of noise on communities in a multi criteria framework [THE 2005 CONGRESS] while the take-off and landing problems in the presence of wind shear have been studied in [MIELE A.[1]] and [MIELE A.[2]]. Note that the

trajectory to be selected is often represented as a four-dimensional flight path, with time as the fourth dimension in addition to the three-dimensional representation of a path.

- Minimum-time trajectories either for transportation aircraft [CLEMENTS J. C.], or [IYER R. V.] have been developed.
- The aircraft terrain-following (TF) problem is analyzed in [ASSEO S. J.]. In general, the terrain following problem is formulated as an optimal control problem where short term-safety related and long term path-following objectives are combined.
- The generation of wind-optimal trajectory for cruising aircraft has been considered in [JARDIN M. R.] [MCGEE T. G.]. Since windshear has an impact on flight safety, the corresponding optimal penetration landing trajectories are discussed in [MIELE A.[3]]
- Aircraft trajectory planning problems have also been studied in the context of air traffic management. [CAMPBELL S. E.] [MORA-CAMINO F.[2,3]] [DOUGUI N.E.] [SOLER M.] There, aircraft trajectory optimization is in general solved using hybrid approaches involving mathematical programming formulations and tools, allied with control concepts and/or Artificial Intelligence techniques (Neural networks, Genetic Algorithms). For example in [CAMPBELL S. E.] a Mixed Integer Programming technique is associated to a receding horizon control approach to limit contrail formation. In [MORA-CAMINO F.[3]], the minimum time merging maneuver is characterized using Pontryagin's Minimum Principle leading to the formulation of a mixed integer programming problem which is solved using Reverse Dynamic Programming allied with Neural Networks.

VI.3 The General Trajectory Optimization Problem

A general form of the trajectory optimization problem can be given by:

$$\min \Phi(\underline{x}, \underline{u}, t_f) \quad \text{with} \quad (\underline{x}, \underline{u}) \in X \tag{6.1}$$

where

$$\Phi(\underline{x},\underline{u},t_f) = F(\underline{x}(t_0),\underline{x}(t_f),t_f) + \int_{t=t_0}^{t=t_f} f(\underline{x},\underline{u},t)\,dt \tag{6.2}$$

is the performance index, F and f being functions capturing the performance of the system along the time period considered, and

$$X = \left\{ \underline{x},\underline{u},t_f \,\middle|\, \dot{\underline{x}}(t) = g(\underline{x}(t),\underline{u}(t),t), \underline{x}(t_0) = \underline{x}_0,\ h(\underline{x}(t),\underline{u}(t),t) \le h_{\max}, l(\underline{x}(t_f),t_f) \le l_{\max} \right\} \tag{6.3}$$

is a general set of constraints.

The differential constraints $\dot{\underline{x}}(t) = g(\underline{x}(t),\underline{u}(t),t)$ are state equations and $\underline{x}(t_0) = \underline{x}_0$ is an initial condition on the state of the system.

Here $\underline{x}$ is the state vector with $\underline{x}(t) \in R^n$, $\underline{u}$ is the control vector with $\underline{u}(t) \in R^m$, t_0 is the initial time, considered given here while t_f, which is the final time, may be a parameter to be optimized.

The set of differential equations with initial condition, $\dot{\underline{x}}(t) = g(\underline{x}(t),\underline{u}(t),t)$, $\underline{x}(t_0) = \underline{x}_0$, is the set of state equations which describe the evolution of the trajectory of the state vector from its initial conditions. It is for example the case when a flight plan for a commercial aircraft is optimized with the objective to arrive at a given destination airport with minimum fuel with nominal reserve.

The set of inequalities $h(\underline{x}(t),\underline{u}(t),t) \le h_{\max}$, or path constraints, can take different forms such as the classical one :

$$\underline{x}_{\min} \le \underline{x}(t) \le \underline{x}_{\max} \quad \text{and} \quad \underline{u}_{\min} \le \underline{u}(t) \le \underline{u}_{\max} \tag{6.4}$$

while the set of constraints $l(\underline{x}(t_f),t_f) \le l_{\max}$ can take, among other realizations, either the form $t_f \le t_f^{\max}$ (a maximum terminal time) or $\underline{x}(t_f) = \underline{x}_f$ (a terminal constraint on the value of the state).

It is also supposed in general that functions F, f, g and h are smooth functions.

Example: An example of such class of problems can be given by the 2D trajectory optimization for a train which can be formulated as:

$$\dot{x} = v \tag{6.5-a}$$

$$\dot{v} = -g\sin(\gamma(x)) - (a + b\,v + c\,v^2) + \alpha - \beta \tag{6.5-b}$$

where x is the train position, v is its speed, $\gamma(x)$ is the track slope at position x, the term $(a + b\,v + c\,v^2)$ represents the friction from the track and the air, α is the acceleration (specific thrust) produced by the engine and β is the deceleration from the brakes.

- Initial conditions: initial state is given by: $x(t_0) = x_0$ and $v(t_0) = v_0$.

- Final conditions: After a time period $T = t_f - t_0$, the train should be at final state: $x(t_f) = x_f$ and $v(t_f) = v_f$.

Control inputs are subject to the following constraints:

$$0 \le \alpha \le \alpha_{\max}\ 0 \le \beta \le \beta_{\max} \tag{6.6}$$

The total amount of burned fuel is supposed to be given by:

$$\int_{t_0}^{t_f} \alpha(t) \cdot v(t) \cdot dt \tag{6.7}$$

where $\alpha(t) \cdot v(t)$ is the developed power.

Then the optimal solution should lead the train from initial to final conditions at a minimum amount of burned fuel.

VI.4 Indirect Methods

Indirect methods are involved in matching the optimality conditions derived from the Pontryagin's minimum (or maximum) principle [STRYK O. von].

VI.4.1 Optimality conditions

The optimal control problem is an infinite dimensional problem and indirect methods try to find a solution to the optimality conditions resulting from the optimality principle called Pontryagin's minimum principle (or maximum principle)[NOTTROT R.] [ROSS I. M.] which is based on a generalization of results from the calculus of variations. This approach introduces the Hamiltonian function as an auxiliary function defined as:

$$H = f + \underline{\lambda}' \cdot g + \underline{\mu}' \cdot h \tag{6.8}$$

where $\underline{\lambda}$ is the co-state vector associated to the state equations and $\underline{\mu}$ is the Lagrange multipliers vector associated to the path constraints.

The optimality conditions are given by the state and co-state dynamics:

$$\underline{\dot{x}} = (\partial H / \partial \underline{\lambda})' \quad \underline{\dot{\lambda}} = -(\partial H / \partial \underline{x})' \tag{6.9}$$

where

$$\underline{u}(\underline{x}, \underline{\lambda}) = \arg\min_{\underline{u}} H \tag{6.10}$$

with initial and final , or transversal, conditions which can be written as:

$$\left(\frac{\partial}{\partial \underline{x}} F(\underline{x}(t_f), t_f) - \underline{\lambda}(t_f) \right)' \cdot \underline{\Delta x}(t_f) + \left(H(\underline{x}(t_f), \underline{u}(t_f), \underline{\lambda}(t_f), t_f) + \frac{\partial}{\partial t} \left(F(\underline{x}(t_f), t_f) \right) \right) \cdot \Delta t_f = 0 \tag{6.11}$$

In general this set of optimality conditions results in what is called a Two Point Boundary Value Problem. A summary of all necessary conditions for a large class of trajectory optimization problemsis available in [BRYSON A.E.]

VI.4.2 General features of indirect methods

These methods are called in general shooting methods since initial guesses must be performed.

- **Single Shooting Methods**:

For the single shooting an initial guess must be made about the values of unknown initial and terminal conditions, and then the state/co-state dynamics are integrated from t_0 to t_f. Then the errors in initial and terminal boundary conditions are assessed and the guess about the values of unknown initial and terminal conditions are modified. The process is iterated until all boundary conditions are satisfied with a sufficient accuracy.

- **Multiple-Shooting Methods:**

In this case the time interval is divided into segments and a guess is made for unknown initial conditions at the start time of each segment. Then the state/co-state dynamics are integrated on each segment and the errors at each segment interface and boundary conditions are assessed. Guesses at initial conditions at the start time of each segment are updated and the process is iterated until all boundary conditions are satisfied with a sufficient accuracy.

The solution of trajectory optimization problems with indirect methods requires the establishment of the first order optimality conditions. This task can be problematic since some

functions may be very complex or may be represented in a numerical way (numerical tables with interpolation algorithms, neural networks, etc.) , making that the computation of partial derivatives involved in the first order optimality conditions can be very cumbersome. Then the solution of the resulting two-point boundary value problem through a multidimensional zero finding algorithm must be considered. Several algorithms are available for an efficient solution of these problems.

When applying these methods, another major difficulty arises in the requirement of supplying very accurate initial guesses for the co-state variables. In general these variables do not have a physical meaning, but the trajectory may be very sensitive to even small changes in the co-state values. When close problems have to be solved, since limited knowledge is available on the structure of the optimal solution, the whole process must be restarted.

Shooting methods can be seen as a way to solve a simple root finding problem with in general a reduced number of variables. However, the Hamiltonian dynamics can be numerically unstable in either directions of time where the effect of the error in the initial/final guess grows when integrating from t_0 to t_f. Then, even for simple problems, indirect shooting methods can be unsuccessful. For example if we consider the following problem:

$$\min \frac{1}{2}\int_{t_0}^{t_f}(q\,x^2 + r\,u^2)dt \quad \text{with } \dot{x} = a\,x + b\,u \quad \text{and} \quad x(t_0) = x_0\,,\ \ x(t_f) = x_f \tag{6.12}$$

where $q > 0, r > 0, b \neq 0$. In agreement with the Maximum Principle, here the Hamiltonian dynamics are given by:

$$\begin{bmatrix}\dot{x}\\ \dot{\lambda}\end{bmatrix} = A\begin{bmatrix}x\\ \lambda\end{bmatrix} \quad \text{with} \quad A = \begin{bmatrix}a & -b^2/r\\ -q & -a\end{bmatrix} \tag{6.13}$$

where A is an unstable matrix.

While introducing many more variables, multiple-shooting methods perform an integration over shorter time intervals, limiting the tendency to diverge of the Hamiltonian dynamics. Another difficulty of indirect optimization methods is the requirement for a detailed mathematical analysis of each problem since in general, any small changes in the dynamics or in the boundary constraints may lead to a very different solution structure, requiring a

complete revision of the previous derivation of the solution. Author such as [FAHROO F.[1]] [HULL D. G.] have discussed this whole issue.

VI.5 Direct Methods

With the development of digital computers in the middle of the 20th century, direct trajectory optimization methods were developed in the 70s and 80s. The main attractiveness of this class of methods is the possibility to solve very complex optimization problems with a minimum mathematical analysis effort since only the physical equations (6.3) need to be coded by the user of such methods. However, these methods require efficient algorithms to solve mathematical programming problems with thousands of variables and linear/nonlinear constraints.

A general classification of direct methods is displayed in figure 6.1:

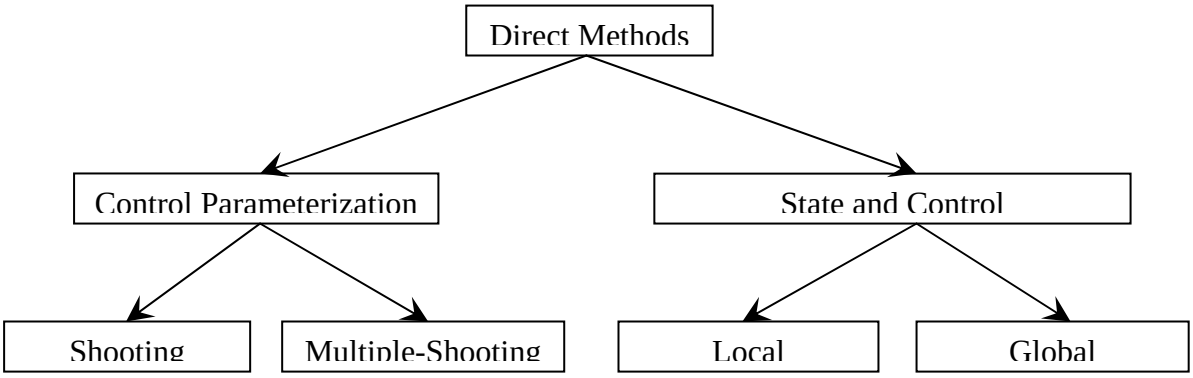

Figure 6.1 A classification of direct methods

Local collocation make use of implicit or explicit integration techniques while global collocation uses pseudospectral methods [FAHROO F.[2]] [BOLLINO K. P.] where Lagrange and Chebychev Polynomials are used in these methods to approximate the state Variables. The procedure for approximating the state and control variables is based on Legendre polynomials built on Chebychev nodes.

In general, direct optimization methods are composed of three main steps:

1. converting the dynamic system into a problem with a finite set of variables and algebraic constraints,

2. solving the finite-dimensional problem using a parameter optimization method,

3. assessing the accuracy of the finite-dimensional approximation and if necessary repeating the transcription and optimization steps.

Direct trajectory optimization methods are divided into two subclasses depending if it is only the controls or the controls and the states which are parameterized: direct shooting methods [BOCK H.G.] and direct collocation methods [HARGRAVES C.R.], [HULL D. G.]. Both classes of methods are characterized by the approximation of the optimal control time history by using control approximations such as piecewise constants, piecewise linear functions or others such as spline approximations.[BHATTACHARYA R.]

Besides the control discretization, path constraints must be also discretized. The algorithms only satisfy path constraints at discrete points called path constraint evaluation points. In the case of convex path constraints, they are approximated by a set of interior point constraints. The control approximation and the discretization of path constraints processes are not critical in general to get an acceptable approximation of the optimal trajectory since the error often made by calculating a suboptimal solution from the discretized version of the trajectory optimization problem can be made much smaller than the consequences of modeling errors. It can be of interest to show when studying the limit case of direct optimization methods, that the generated solution is equivalent to the solution found by an indirect method. There are also many available methods to calculate the time histories of the co-state variables based on the solution generated with a direct optimization method [HARGRAVES C.R.].

VI.5.1 Direct Shooting Methods

Direct shooting methods are based on the integration of the trajectory during the optimization process. Such an integration is usually performed numerically with standard solvers from initial value problems. The main steps of a direct shooting method are the following:

- Choose a control approximation for the control inputs:

$$u(t) = \sum_{n=0}^{N} w_n \ \phi_n(t) \tag{6.14}$$

  where $\phi_k \ \ k = 0, \cdots, N$ is an arbitrary base of functions, in general polynomials;

- Choose values for coefficients $w_n \quad n = 0, \cdots, N$;
- Integrate the state equations from t_0 to t_f and compute the corresponding performance;

- Iterate the above steps until the optimization criterion is optimized and the constraints are satisfied.

They are often based on indirect shooting methods originally developed to solve boundary value problems. In the perspective of direct shooting methods, the control time histories are discretized using a parameter dependent control approximation (see relation 6.14). Path constraints are discretized as well, and their matching is only checked at the path constraint evaluation points.

Figure 6.2 presents a control discretization and corresponding trajectory with a path constraint. Here the initial state is a scalar optimization parameter while the control is summarized by a vector of discrete optimization parameters while the path constraint is transformed into a vector of interior point constraints.

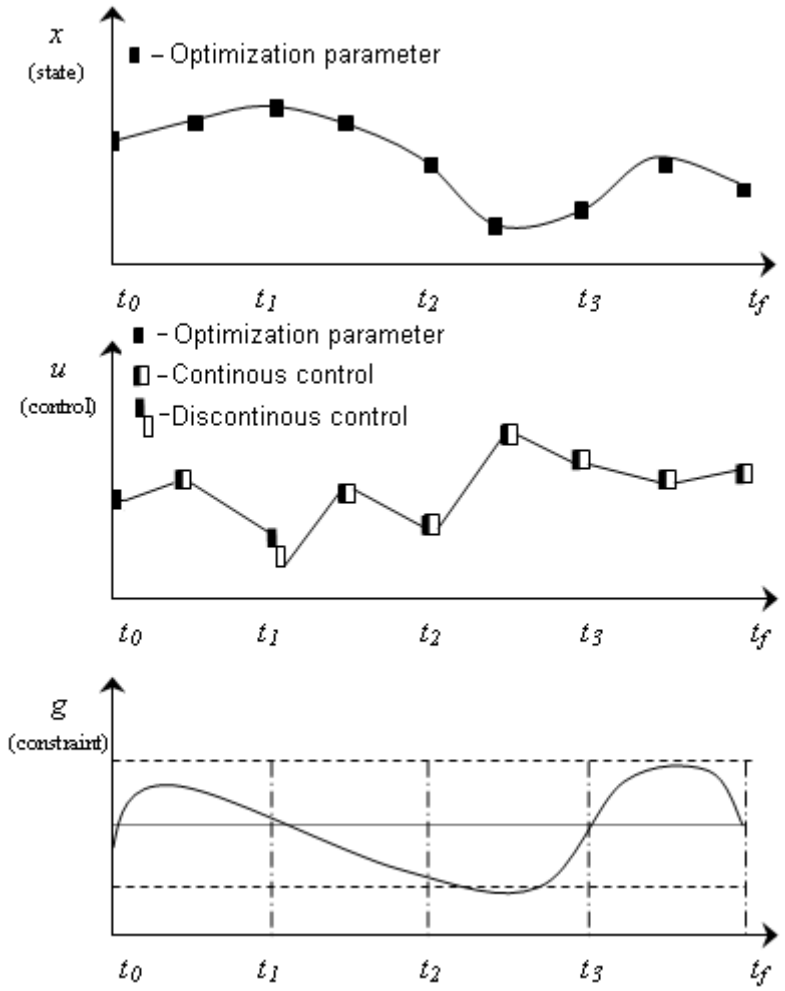

Figure 6.2 Discretization for direct shooting

The main advantage of this class of methods is that there is no need to establish complex optimality conditions or to integrate co-state equations. However, the major problem of shooting methods is a great sensitivity of the terminal constraints with respect to changes in the initial conditions. A first approach to reduce this sensitivity is to shoot from both sides of the interval and try to match the two trajectories at an intermediate point. Such methods are sometimes referred to as *shooting to a fitting point*.

In order to reduce the sensitivity of the terminal constraints with respect to changes in the initial conditions even further, multiple shooting techniques have been developed where additional points are inserted to restart the integration at intermediate points. The main steps of this class of techniques are:

- Divide the time period into time segments such as $t_0 < t_1 < \cdots < t_K = t_f$ where the corresponding time points are called grid or mesh points;
- Parametrize the control input within each time segment:

$$u^k(t) = \sum_{n=0}^{N} w_n^k \ \phi_n^k(t) \qquad k = 1, \cdots, K \tag{6.15}$$

- Introduce continuity constraints such as:

$$x(t_k^-) = x(t_k^+) \quad k = 1, \cdots, K-1 \tag{6.16}$$

- Compute total performance as the sum of the performance on each time segment;
- Enforce initial and final constraints and repeat the previous steps until the optimization criterion is optimized and the constraints are satisfied.

Multiple shooting techniques in general improve the quality of the solution obtained with respect to single shooting techniques but they need to add continuity constraints at time segment limits and increase the size of the numerical problem. Note that with this approach, discontinuous control solutions can be obtained while the true optimal control is continuous. The introduction of the multiple shooting points improve the numerical stability by preventing the growth of the error introduced by wrong initial guesses, coarse discretization and round-off, through possible instable dynamics.

Either single or multiple shooting, these methods generate often non accurate solution through a rather inefficient computation process while convergence is not guaranteed. Difficulties arise also with control bounds while path constraints are difficult to be included in

the problem and state equations are difficult to be solved via explicit integration. See Annex C for an example of explicit integration method used in direct multiple shooting techniques.

VI.5.2 Direct Collocation Methods

In contrast to the direct shooting methods, direct collocation methods are also approximating the state time histories by using e.g. Hermite-Simpson polynomials. [BUCHANAN J. L.] The basics for collocation methods were first proposed by Dickmanns and Well in 1974 in the framework of indirect collocation[DICKMANNS E.D.]. It was extended to a direct collocation method by Hargraves and Paris in 1987 [HARGRAVES C.R.]. A major improvement to collocation methods was made by Betts [BETTS J. T.[2]] with the introduction of an automatic mesh refinement algorithm and an quadratic method that is specialized on solving very large, sparse problems including several ten-thousand parameters and constrains. The special property of the method is that it is able to exploit the sparsity in the gradients of the cost function and of the constraint vector as well as of the Hessian matrix by directly calculating the Hessian matrix using sparse finite differencing. The main advantages of direct collocation methods with respect to direct multiple shooting methods are: a reduced computer times, reduced number of collocation intervals and a larger convergence radius.

VI.5.3 Limitation of direct methods

Multiple-shooting methods can be run with an ordinary differential equations solvers including step-size control algorithms. Then the method is almost independent of the original discretization grid and should provide a suboptimal solution since using the convergence solution in a simulation will produce a feasible trajectory satisfying all which satisfies all path constraints at the evaluation nodes as well as all boundary condition. Nevertheless, the integration process will generate a computational burden, mainly when considering the heavy numerical calculation of the gradients which are necessary to be computed to solve the associated nonlinear programming problem.

The direct collocation approach can be considered to perform an implicit integration of the trajectory without step-size control. An important difficulty with direct collocation methods arises when the computed solution does not reflect the physical behavior of the dynamic

system. The computed solution can be validated by simulation. If the resulting dynamics does not satisfy the path and boundary constrains, more collocation intervals must be introduced and when there are large changes in the dynamics many collocation intervals must be inserted.

VI.6 Dynamic Programming

Now we present one of the more powerful and clean approach to solve optimization problems.

VI.6.1 Definition and scope of Dynamic Programming

Dynamic Programming is a mathematical formalism developed by R. Bellman during the early 1950's [BELLMAN R.E.[1]] to optimize sequential decision making processes. Dynamic Programming was very quickly widely applied in many fields of Engineering [BELLMAN R.E.[2]] and Economics [BECKMAN M. J.] decision making optimization. Historically, Dynamic Programming was developed to optimize multi-stage decision processes and it has been indeed applied to many classes of multistage decision processes, providing in general practical solutions [BERTSEKAS D. P.[1]]. Current efforts in the field of Dynamic Programming are directed to its application to more and more different optimization problems which can be reformulated as multi-stage decision processes. Today, the fields of application of Dynamic Programming cover business, managerial, military and engineering problems. Some of the main fields are: Allocation processes[BERTSEKAS D. P.[2]], Cargo loading [DREYFUS S. E.], Cascade processes [NANDALAL K. D. W.], Control Processes, Equipment Replacement, Inventory and Stock Level, Reliability, Stochastic Allocation, Transportation Fleet Management, Game Theory and Investment. Of course, many convincing applications of Dynamic Programming to space and atmospheric trajectory optimization problems have been developed since that time.

VI.6.2 The optimization process of Dynamic Programming

When considering the previous classification of trajectory optimization methods, Dynamic Programming can be considered to be a particular class of methods presenting important features of direct and indirect methods at the same time.

- With respect to direct approaches, the availability of high speed computers and efficient mass data processing systems has turned possible the treatment of continuous

systems in a multi-stage manner opening the way to the application of Dynamic Programming rationale to trajectory optimization problems.

- With respect to indirect approaches, Dynamic Programming makes use of a selection process in the progressive construction of the solution based on the optimality principle of Bellman which is a sequential expression of the Hamilton-Bellman-Jacobi equation which is directly related to the Calculus of Variations [PONTRYAGIN L. S.].

For example, in the case of the following optimization problem:

$$\min_{\underline{u}(t),\, t\in[t_0,\, t_1]} \quad \psi\,(\underline{x}(t_1),\, t_1) + \int_{t_0}^{t_1} \phi\,(\underline{x}(t),\, \underline{u}(t),\, t)\, dt \tag{6.17}$$

with

$$\dot{\underline{x}} = a\,(\underline{x}(t),\, \underline{u}(t),\, t) \quad \text{and} \quad \underline{x}(t_0) = \underline{x}_0 \tag{6.18}$$

the Bellman's optimality principle is such as:

$$J^*(\underline{x}(t), t) = \min_{\underline{u}(\theta),\, t\le\theta\le t+\Delta t} \left(\int_t^{t+\Delta t} \phi(\underline{x}(\theta), \underline{u}(\theta), \theta)\cdot d\theta + J^*(\underline{x}(t+\Delta t), t+\Delta t) \right) \tag{6.19}$$

with

$$J^*(\underline{x}(t_1), t_1) = \psi\,(\underline{x}(t_1), t_1) \tag{6.20}$$

The application of Dynamic Programming presents computational problems related with topics such as accuracy, stability and partial solution storage. However it appears that in many situations, what is a complicating factor inducing computer burden with other optimization techniques, can be used to save computation time and storage needs while allowing to increase the solution accuracy by allowing to take benefit of problem peculiarities.

Contrarily to previous analyzed methods, the optimization process developed by Dynamic Programming is very easy to catch by the human mind and it is easy to derive in general, when necessary, some heuristics producing at low computational cost, suboptimal solutions.

Dynamic Programming is a systematic search procedure for finding the optimal decision sequence. Its multi-stage decision process is characterized by three important features:

- To achieve the objective of the process a sequence of decisions must be performed.
- The decisions at one stage are related with the decisions taken at the previous stages which lead to them since they affect its performance.
- Non optimal local solutions are rejected all along the way to the solution according to the adopted optimization criterion.

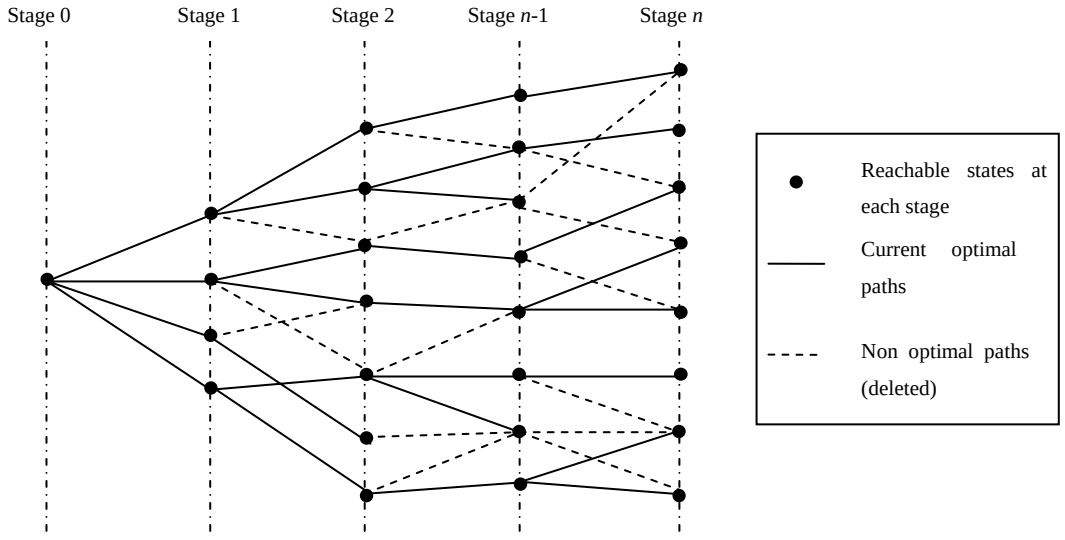

Figure 6.3 Stages and search space for Dynamic Programming

For the Dynamic Programming approach being feasible, it is necessary that the decision problem presents an optimization criterion and constraints with additive structures. Nonlinearities and non convexity are tackled by Dynamic Programming without any particular difficulty. To proceed with Dynamic Programming, *stages* must be defined. This leads to the time or space discretization in the case of continuous dynamics optimization problems. To each stage, a set of feasible *states* defines the search space at that stage.

The presence of constraints in the problem, a situation which in general complicates the solution search with variational methods as well as with collocation methods, facilitates the solution generation of the Dynamic Programming approach since the constraints reduce the size of the decision sets over which the search must be performed. The systematic search procedure developed by Dynamic Programming approaches can lead to a very large number of calculations and often a trade-off between computation efficiency and solution accuracy

may become necessary to match with the capability of present computers. However, this situation has been changing with the introduction of new techniques [JACOBSON D. H.], [BERTSEKAS D. P.[3]] and computers with enhanced performances.

VI.6.3 Applications to Aircraft Trajectory Optimization

Many applications of Dynamic Programming in the field of aircraft trajectory optimization have been performed along the last decades. For example in [WALLER M.C.], the interest to use Dynamic Programming to generate optimal aircraft trajectories, is analyzed. The advantages and disadvantages of the general Dynamic Programming approach are discussed. The main focus of the study is over the representation of the solution space and the size of the grid spacing which are factors that affect directly the accuracy of the solution as well as the computation volume. Then conditions to determine the required size of the solution space and the grid spacing are presented.

The Dynamic Programming approach has been also applied to tactical problems involving atmospheric hazards or environment considerations. For example in [BOTKIN N. D.] the generation of safe aircraft trajectories in the presence of windshear using Dynamic Programming has been discussed while in [NG Hok K.] convective effects are avoided using a Dynamic Programming based flight routing process. In [VISSER H.G.], Dynamic Programming is applied to Air Traffic Management issues related with terminal space capacity and safety. It appears that this technique is quite compatible with stochastic environments as well as with cooperative or non-cooperative multi-agent situations, which are important characteristics of air traffic operations. Then it is expected that extensions of the classical Dynamic Programming approach should be of great interest in the field of Air Traffic Management.

Finally, the rationale behind the construction of flight plans by the Flight Management System of modern transportation aircraft follows the main ideas of Dynamic Programming applied to a mix of fuel cost and travel time. However, until today, the resultant computational burden has led to the adoption of a near optimal 4D trajectory generation process even if some studies [HAGELAUER P.] about the feasibility and the interest of this approach for optimal flight plan generation.

VI.7 Conclusion

Other techniques, in general from Artificial Intelligence (Genetic Algorithms [RAUWOLF G.A.] [COVERSTONE-CARROLL V. L.] and other nature inspired optimization techniques [YANG X.X.] [WANG H.]), rapidly-exploring random tree method [CHENG P.], particles swarm optimization [XIE F.Q.] [SU M.] [WU H.[2]], etc, have been applied more recently to trajectory optimization problems. These techniques develop a stochastic search process based on general primitives and their effectiveness is based on the massive character of their computation. In general no insight in the structure of the solution is provided by these techniques which are in general quite complex to be programmed. Then a long and mainly empirical process of validation and tuning must be performed with limited guarantee of success in enlarged conditions.

From the analysis performed in this chapter, it appears that Dynamic Programming presents interesting characteristics to achieve gliding aircraft trajectory optimization:

- the optimization process is totally transparent while its follows Bellman's optimality principle,
- the optimal trajectory is constructed step by step,
- non optimal partial trajectories are deleted as soon as possible.

However, two difficulties to be faced when applying Dynamic Programming is the volume of calculations and the size of the memory necessary to store partial solutions. In the next chapter, it will be shown how a Dynamic Programming gliding trajectory optimization scheme can be constructed.

CHAPTER VII

VERTICAL GLIDE TRAJECTORY GENERATION THROUGH DYNAMIC PROGRAMMING

VII.1 Introduction

In this chapter the Dynamic Programming approach is developed with the aim of producing optimal glide trajectories starting at cruise level to bring the aircraft near the chosen landing site with an acceptable flight situation to make the landing attempt hopeful. In this situation, a Reverse Dynamic Programming process appears of interest. A first step to achieve this development is to choose a new independent variable, the distance to land so that the dynamic programming stages can be defined in accordance with flight performance and safety considerations. Then the choice of an adequate optimization criteria, as well as state constraints, is discussed to meet effectively the essential objectives of the manoeuvre. Then it appears that the design of the Reverse Dynamic Programming process must go through different empirical choices so that the computational burden it generates remains feasible even in an off line context. These choices are discussed in detail before final numerical results are provided by this method.

VII.2 Formulation of the Trajectory Optimization Problem

In this section some of the issues related with the optimal management of the trajectory of a transportation aircraft gliding from a given initial flight situation towards a safe landing place with acceptable landing conditions are considered. Contrary to the classical max range gliding problem, by the end of the gliding maneuver, the aircraft must be in conditions (speed and attitude) to perform a safe touch down at landing. It means that at arrival close to the ground, the ground speed of the aircraft must be between a minimum and a maximum value and that the vertical speed is sufficiently reduced.

VII.2.1 Flight dynamics and flight domain constraints

The flight guidance equations of the gliding aircraft, written in the aircraft wind axis, which are retained here are given by equations (7.1):

$$\dot{V} = -\frac{1}{m}(D(V,\rho,\theta-\gamma) + m\,g\,\sin\gamma) \tag{7.1-a}$$

$$\dot{\gamma} = \frac{1}{mV}(L(V,\rho,\theta-\gamma) - m\,g\,\cos\gamma) \tag{7.1-b}$$

$$\dot{x} = -V\cos\gamma \tag{7.1-c}$$

$$\dot{z} = V\sin\gamma \tag{7.1-d}$$

In this case the only independent input parameter which is available and candidate to be a control parameter, is the pitch angle, θ. The pitch angle can, even in an engine-out situation, be controlled by the pilot either through the hydraulic power provided by the RAT or the auxiliary power unit-APU, to actuate the elevator, or through the trim control channel to change the position of the horizontal trim stabilizer.

Here we consider that the initial flight conditions are such as:

$$x(0) = x_0,\ h(0) = h_0, V(0) = V_0, \gamma(0) = \gamma_0 \tag{7.2}$$

and that the ideal final landing conditions are such as:

$$h(t_f) = h_G(x(t_f)), V(t_f) = V_1, \gamma(t_f) = \gamma_1 \tag{7.3}$$

where V_1 and γ_1 should allow a safe landing at altitude $h_G(x(t_f))$ where function h_G is representative of the ground topography bellow the considered gliding approach.

Since final time is unknown and is only characterized by the satisfaction of the final conditions, the replacement of independent parameter t by the space variable x allows to diminish the complexity of the problem since now final x_f is known once the landing site has been chosen. Also, distance to land is a very important clue for the pilot in charge of controlling the glide of the engine-out aircraft. Moreover, this approach should facilitate the consideration of ground separation constraints (aircraft height with respect to the ground). This could make easier also the consideration of the effect of wind over the glide trajectory since intensity and direction of main stream winds is mainly related to space. Then, we have to rewrite the flight guidance equations of the gliding aircraft taking as independent variable the distance to land.

Then, from equations (7.1) with :

$$dt/dx = -1/(V\cos\gamma) \tag{7.4}$$

we get:

$$z' = -tg\,\gamma \tag{7.5-a}$$

$$V' = \frac{1}{mV\cos\gamma}(D(V,\rho,\theta-\gamma) + mg\sin\gamma) \tag{7.5-b}$$

$$\gamma' = -\frac{1}{mV^2\cos\gamma}(L(V,\rho,\theta-\gamma) - mg\cos\gamma) \tag{7.5-c}$$

where " ′ " represents the derivative with respect to the longitudinal position x of the aircraft (see figure 7.1). This can be rewritten in a global form as:

$$\underline{X}' = f(\underline{X},\theta) \quad \text{with} \quad \underline{X}^T = (z, V, \gamma) \tag{7.5-d}$$

where θ is the unique control parameter.

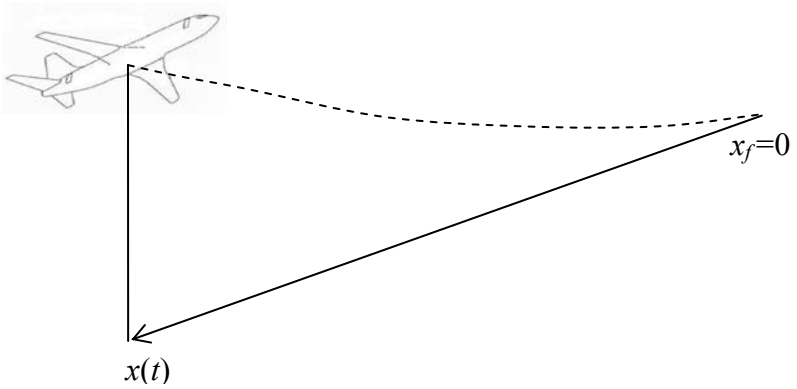

Figure 7.1 Ground distance to land x

The additional state constraints are:

$$V_{\max}(z) \geq V(x) \geq V_{\min}(z) \quad x \in [x_0, x_f],\ z \in [z_0, z_f] \tag{7.6-a}$$

$$\max\{\theta_{\min}, \alpha_{\min} + \gamma(x)\} \leq \theta(x) \leq \min\{\theta_{\max}, \alpha_{\max} + \gamma(x)\} \tag{7.6-b}$$

$$z(x) \geq h_G(x) \quad x \in [x_0, x_f] \tag{7.6-c}$$

Constraint (7.6-a) prevents from stalling or over-speed, constraint (7.6-b) prevents from stalling and constraint (7.6-c) prevents from some flight into terrain-FIT situation at an

intermediary point of the glide. To close this feasible space, an additional height constraint can be added where at least $z(x)$ could be such as:

$$z(x) \le z(x_0) \tag{7.6-d}$$

where x_0 is the initial ground distance to the landing place.

VII.2.2 A first trajectory optimization problem formulation

Our problem is here to generate a flyable trajectory for the engine-out aircraft towards some landing place where it must arrive with acceptable landing conditions. The generation of such trajectory is quite difficult considering the necessity to satisfy not only the final conditions but also to guarantee flight sustainability all along the trajectory. Even the issues of its existence, of its uniqueness or multiplicity, are difficult to be decided.

A classical method to generate trajectories has been to formulate optimization trajectory problems and to adopt the optimal trajectory as the generated one. Here, among many possible different formulations of a trajectory optimization problem a formulation which should ease the existence of a feasible trajectory should be adopted. This can be done by considering that the final constraints are practically satisfied when the final speed and the final path angle are inside a small interval centered on the target value (here $v_{\min}$, $v_{\max}$, $g_{\min}$ and $g_{\max}$ are positive margins):

$$V_1\,(1 - v_{\min}) \le V(x_f) \le V_1\,(1 + v_{\max}) \tag{7.7-a}$$

$$\gamma_1\,(1 - g_{\min}) \le \gamma(x_f) \le \gamma_1\,(1 + g_{\max}) \tag{7.7-b}$$

while the final height is as close as possible to the landing height. This leads to adopt as surrogate optimization criterion $(h(x_f) - h_G(x_f))^2$. The margins around the speed and path angle values can be modified to get a feasible solution while the corresponding values remain acceptable for flight sustainability. We could have adopted as objective either minimizing a measure of the difference between V (or γ) and the target value V_1 (or γ_1) with $h(x_f)$ within a given interval around $h_G(x_f)$, but from the operational view point the proposed formulation appears more convenient. In fact, if "final" speed and path angle are within the proposed

interval, the pilot should have the capability to perform final adjustments to perform a touch down manoeuvre as safe as possible.

Then the trajectory optimization problem could be written as:

$$\min \left(h(x_f) - h_G(x_f)\right)^2 \tag{7.8}$$

under constraints 7.2 and 7.4 to 7.7.

VII.2.3 Optimal trajectory problem formulation including final maneuverability

The previous optimality criterion has been chosen mainly for insuring a final flying condition compatible with some final adjustments by the pilot at the time of landing. However, for the pilot to be able to maneuver the aircraft at the final stage of landing a necessary condition is that the remaining hydraulic energy is enough to move as fast as necessary the main actuators. Since each time some new setting is to be achieved by the actuators (mainly le elevator) some hydraulic energy is lost, it appears of interest to adopt feasible trajectories where the settings of the actuators are as much as possible following smooth values. Then with the objective of getting a smooth flyable trajectory which avoids wasting unnecessarily the remaining hydraulic energy used to control the aerodynamic actuators (elevator, THS, flaps and aero brakes) along the engine-out glide trajectory, a different optimization criterion (or cost function) is adopted here:

$$J = \int_{x_f}^{x_0} \phi(\theta, V, V_z)\, dx \tag{7.9}$$

with this time the additional final constraint $h(x_f) - h_G(x_f) = 0$. In relation (7.9), function ϕ is a mesure of the variability of the trajectory and the control parameter which will be chosen later.

VII.3 Analysis of the Trajectory Optimization Problem and Solution Strategy

The solution of this non linear, strongly constrained trajectory optimization problem is difficult from the numerical point of view and a direct on line computation of its solution does

not appear to be feasible. For instance, according to the analysis in chapter VI, an approach based on the minimum principle (indirect methods) doubles the dimension of the states [CLARKE F.] and should result in a very difficult two point boundary problem since the resulting Hamiltonian has not an affine structure with respect to the input parameter. The direct methods, which in general transform the trajectory optimization problem into a large non convex linear programming problem, may converge to a sub-optimal solution, after a large computational effort where the proposed trajectory solution appears only at the end of the computational process.

Then, according to chapter VI, the main features of the Dynamic Programming solution approach appear to provide some good perspectives. Dynamic programming build step by step families of optimal trajectories shaped in a tree shaped solution graph until final state is reached, then providing the entire optimal trajectory from initial to final state. This progressive process of selection and generation of further steps for the candidate trajectories allows disregarding scores of non optimal solutions as soon as possible. However to be effective from the computational point of view, the search space must be discretized to face a finite dimensional problem. For that the decision space (here the values adopted for the independent parameter, the pitch angle value) and the resulting state space (speed, path angle and altitude) should be discretized. The discretized state equations written as:

$$\underline{X}_{k+1} = f_k(\underline{X}_k, \theta_l) \qquad (\ .10)$$

will generate new states at the next stage, and those which satisfy constraints (7.6-a) and (7.6-c) will be considered. Then at stage k+1 many states will be generated from a unique state at stage k. These states will be scattered within the feasible space defined by constraints (7.6-a, 7.6-c, 7.6-d) and the γ interval given by $[\theta_{\min} - \alpha_{\max}, \theta_{\max} - \alpha_{\min}]$. Then to avoid to have to consider as new seeds all these states some clustering should be performed in view of controlling the overall computational effort to find a solution. This issue will be discussed in the next section.

When considering in a real situation the trajectory optimization problem, it appears that the only stable information is relative to the final situation since current flight variables and position are changing at quick rate. So adopting the hypothesis of a successful glide towards

this place, it appears appropriate to consider the reverse trajectory optimization problem which consists in finding a feasible glide trajectory ending at this landing place and starting at the current aircraft situation (state ($z(t_0)$,$V(t_0)$, $\gamma(t_0)$) and ground distance $x(t_0)$).

Then, calculations start from the landing point, which satisfies the final constraints, and is carried on in a reverse way with state equations (7.5) by using the Dynamic Programming technique and satisfying constraints (7.6). So, a 'tree' rooted at landing situation will be constructed from one stage to the next until reaching the current position.

VII.4 Generation and Selection of Feasible Trajectories by Reverse Integration

According to the considerations developed in the previous section, here Dynamic Programming is used to generate a feasible glide trajectory towards a safe landing place. To insure the satisfaction of the final landing configuration given by the final constraints (7.3), whose satisfaction is a critical condition, a reverse approach is adopted. Then the gliding trajectory is computed backward from these final conditions through the feasible glide set defined by constraints (7.6) and the space discretized state equations (7.5).

VII.4.1 Selecting the space discretization

Here we adopt as setting time for the pitch control chain including the pilot a time period of 1 second. Then we chose near the landing site as discretization step the horizontal distance travelled by the aircraft during one second so that on-time pitch angle values will be available at the start of the final landing maneuver to touch down. Then while the aircraft is far from the landing site, higher time intervals can be adopted since there is no excessive urge. This will allow diminishing also the computational burden. For example, while the horizontal distance to land is higher than 20 kilometers, we adopt a constant time step of five seconds, which diminish linearly to 1 second at a distance of 5 kilometers:

$$\Delta t = 5 \sec \; if \; x - x_f \geq 20000\, m \tag{7.11-a}$$

$$\Delta t = 5 + 4 \cdot \frac{x - 20000}{15000} \sec \; if \; 20000\, m > x - x_f \geq 5000\, m \tag{7.11-b}$$

$$\Delta t = 1\,\text{sec}\ if\ x - x_f < 5000\,m \tag{7.11-c}$$

Since this travelled distance varies also according to ground speed, we chose a spatial discretization step which varies with its value. To apply exactly this approach, it should be already necessary to have the speed profile all along the selected trajectory, and this is not the case. Then we adopted a simplified ground speed profile V_G^{ref} where the ground speed is linearly decreasing with the distance to land:

$$V_G^{ref}(x) = V_G(x_f) + \frac{V_G(x_0) - V_G(x_f)}{x_0 - x_f} \cdot (x - x_f) \tag{7.12-a}$$

or approximately:

$$V_G^{ref}(x) = V(x_f) + \frac{V(x_0) - V(x_f)}{x_0 - x_f} \cdot (x - x_f) \tag{7.12-b}$$

Then, the space discretization steps can be chosen successively as:

$$x_{s+1} - x_s = \Delta x_s = V_G^{ref}(x_s) \cdot \Delta t(x_s) \tag{7.13}$$

and the spatial discretization is computed from:

$$x_{s+1} = x_s + V_G^{ref}(x_s) \cdot \Delta t(x_s) \tag{7.14}$$

from $x_{s=0} = x_f$ until $x_s = x_{cr}$. Here x_{cr} is the horizontal distance to the landing site at the start of the glide maneuver.

Then near the landing site the spatial discretization step is near 75 m (V≈150 Kt and Δt=1s) while 20 kilometers away the spatial discretization step is about 500 m (V≈ 200 Kt, Δt=5 s) and 100 kilometers away, the spatial discretization step is about 1000 m (V≈ 400 Kt, Δt=5 s). This means that to cover a glide of over 100 km, we will need less than 300 hundred stages in the Dynamic Programming process. Figure 7.2 displays such an example of space discretization along a gliding area.

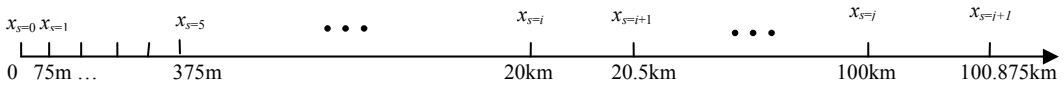

Figure 7.2 Space discretization for trajectory optimization

VII.4.2 Integrating the state equations and criterion discretization

As mentioned before, the final landing point with condition of (7.8) is the starting point of reverse integration, where the final landing constraints are satisfied. Then the integrations are carried on from this given point $(h(x_f), V(x_f), \gamma(x_f))$ according to state equations (7.5) under different input parameters, θ, over successive space intervals $[x_k, x_{k+1}]$ as computed in (7.14), to reach the next stage state. So the i^{th} state vector at stage k is defined as:

$$\underline{X}_{ki} = (z_{ki}, V_{ki}, \gamma_{ki})^T \tag{7.15}$$

From the i^{th} state $\underline{X}_{ki}$ at stage k, for each possible value of θ, θ_l , supposed maintained fixed along the space domain [x_i , x_{i+1}], a new state $\underline{X}_{k+1,i,l}$ is generated at stage k+1, according to:

$$\underline{X}_{k+1,i,l} = \underline{X}_{k,i} + \int_{x_k}^{x_{k+1}} \begin{bmatrix} -tg\,\gamma \\ \dfrac{1}{mV\cos\gamma}(D(V,\rho(z),\theta_l-\gamma)+mg\sin\gamma) \\ -\dfrac{1}{mV^2\cos\gamma}(L(V,\rho(z),\theta_l-\gamma)-mg\cos\gamma) \end{bmatrix} dx \tag{7.16}$$

If a generated state $\underline{X}_{k+1,i,l}$ does not satisfy all the constraints (7.6), it should be deleted.

Equation (7.16) is rewritten as:

$$\underline{X}_{k+1,i,l} = \int_{x_x}^{x_{k+1}} f(\underline{X},\theta_l)\,dx \qquad with\ \underline{X}(x_k) = \underline{X}_{k,i} \tag{7.17}$$

The above integration has been performed using the Trapezoid method with a constant spatial step equal to 5 meters (0.005km). It can be easily check that $f(\underline{X},\theta_l)$ is Lipschitz with some φ such that the following Euclidian norms are such as:

$$\left\| f(\underline{X},\theta_l) - f(\underline{X}_{k,i},\theta_l) \right\| \le \varphi \cdot \left\| \underline{X} - \underline{X}_{k,i} \right\| \tag{7. 18}$$

where $\underline{X}$ is any feasible state in the flight domain of the gliding aircraft and $\underline{X}_{k,i}$ is any feasible state generated in the Dynamic Programming search process. The value for φ is calculated through the Jacobian matrix $(\partial f / \partial \underline{X})$. Then according to the performance of the adopted trapezoid method, after n integration steps of length h ($n \cdot h = x_{k+1} - x_k$), an upper bound to the integration error is such that [CARTWRIGHT J. H. E.]:

$$\left\| \underline{X}_{k+1,i,l} - \underline{X}^{exact}_{k+1,i,l} \right\| \le \left(\frac{(1+h\varphi)^n - 1}{\varphi} \right) \cdot \frac{T_{n+1}}{h} \tag{7. 19}$$

where T_{n+1} is the truncation error after the last integration stage. Its expression is given in annex C.

In figure 7.3 an example of reverse integration using the retained numerical integration technique with a space step of 500 m is displayed. Here the initial state is such as $z(x_f) = 20m, V(x_f) = 75m/s$ and $\gamma(x_f) = -3^0 \approx -0.05rad$. After a first integration seven states corresponding to seven different values of θ are generated, but after a second integration, only 42 states can be distinguished where 49 are expected.

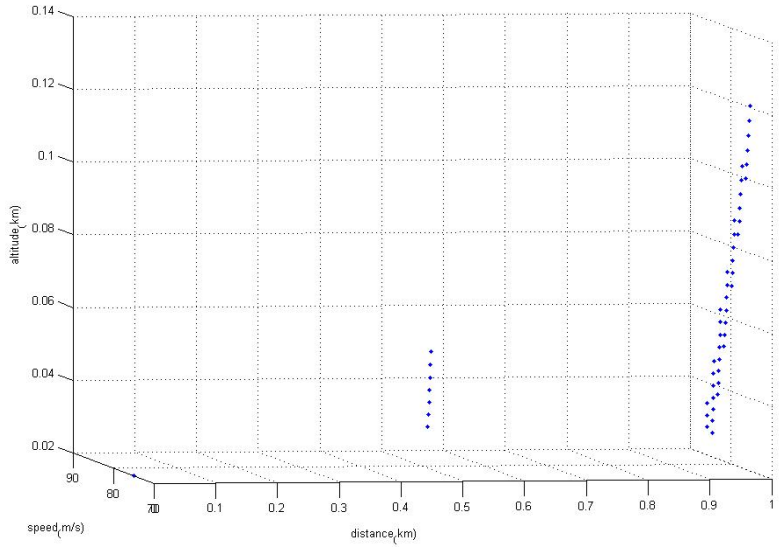

Figure 7.3 Example of state generation after two reverse integrations

To make effective the dynamic programming approach, the optimality criterion must also be discretized along the space. Here we write:

$$J = \int_{x_f}^{x_0} \phi(\theta, V, V_z)\, dx = \sum_{k=0}^{K-1} \int_{s_k}^{s_{k+1}} \phi(\theta, V, V_z)\, dx = \sum_{l=1}^{K} S_l \tag{7. 20}$$

where $s_1 = x_f$, $s_K = x_0$ and θ_k is the value of the pitch angle in the k^{th} space interval where the first one stats at the landing point.

For simplicity, we adopt the following expression for S_k:

$$S_k = \frac{|\theta_{k+1} - \theta_k|}{t_{s=k} - t_{s=k+1}} + \lambda_V \left(\frac{|V_{k+1} - V_k| + V_{zk} \cdot |\gamma_{k+1} - \gamma_k|}{x_{s=k} - x_{s=k+1}} \right) \tag{7. 21}$$

where λ_V is a positive parameter. The first term of S_k is relative to the temporal variability of the pitch angle along the trajectory and is someway related to the elevator deflection and then to the hydraulic power applied to it. The second term of S_k is related with the spatial variability of the trajectory followed by the gliding aircraft. Then, this surrogate criterion penalizes differently the mean temporal variation of the pitch angle and the mean spatial variation of the speed and the vertical speed over each stage.

VII.4.3 Melting states at stages

Figure (7.3) shown us that from one stage to the next the number of states to be theoretically considered is multiplied by the generating factor *L*, the *L* of the different values that the pitch angle can take, so that at the end of the k^{th} stage, the theoretical number of states is $(L)^{k-1}$ and the total number of states is N_k given by:

$$N_k = \frac{(L)^k - 1}{L - 1} \tag{7. 22}$$

However, for some of these values the flight variables are no more feasible and no new state is created at the next stage, thus limiting the generation of states at stage *k* to $n_k \leq (L)^{k-1}$. In many other cases, some new states are very close and it appears of interest, to limit the

computation burden to be delt with by the Dynamic Programming process, to merge them so that the number of states at this stage can be reduced before generating new stages for the following stage.

A heuristic melting procedure is developed to merge the states generated for the next stage. Figure 7.4 shows the basic process of generation.

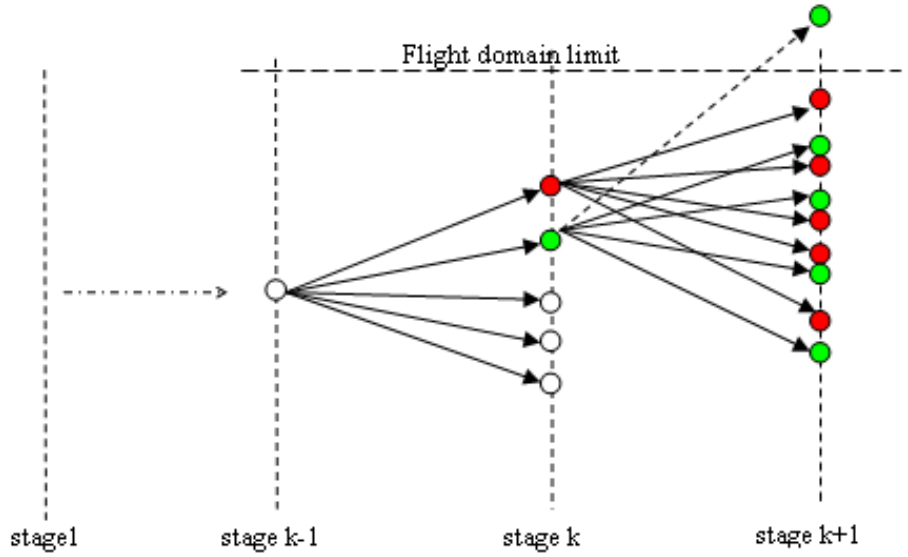

Figure 7.4 State generation process from one stage to the next

Here we consider that the discretization of the span of values considered for the pitch angle is such that the n_j^{k+1} states generated for stage k+1 from state j at stage k are not close between each other.

Otherwise, the adopted scaling for the pitch angle ($\{\theta_{\min} = \theta_1, \cdots, \theta_l < \theta_{l+1}, \cdots, \theta_L = \theta_{\max}\}$) should be revised. Here $\theta_{\min}$ and $\theta_{\max}$ are respectively the minimum and the maximum considered values for the pitch angle during the emergency glide, we took -10° and +15° for numerical application.

We say that two states p and q at the same stage are close if they are such as:

$$\Delta_{pq} = \sqrt{\frac{(V_p - V_q)^2}{W_V} + \frac{(z_p - z_q)^2}{W_z} + \frac{(\gamma_p - \gamma_q)^2}{W_\gamma}} \leq \varepsilon_{k+1} \qquad (7.\ 23)$$

where ε_{k+1} is a very small positive number, part of an increasing sequence so that the merging will be more effective with the distance to the landing site. Here W_V, W_z and W_γ are positive weights such as:

$$W_V = {V_{\max}}^2 \cdot \lambda_V \qquad W_z = {z_{\max}}^2 \cdot \lambda_z \quad \text{and} \quad W_\gamma = {\gamma_{\max}}^2 \cdot \lambda_\gamma \qquad (7.\ 24)$$

where $V_{\max}$, $z_{\max}$ and $\gamma_{\max}$ are scaling parameters and λ_V, λ_z and λ_γ with $\lambda_V + \lambda_z + \lambda_\gamma = 1$ are positive relative weightings.

The n_1^{k+1} feasible states generated for stage k+1 from a first state j=1 of stage k are now considered to be a set of macro states E_{k+1} for stage k+1. Let $\tilde{n}_{k+1} = n_1^{k+1} = |E_{k+1}|$. Then the merging procedure is run along the generating procedure according to the following algorithm applied to the set $E_k = \{\underline{e}_j^k, j = 1\ to\ n_k\}$ of the remaining states at stage k where $\underline{e}_j^k = (z_j^k, V_j^k, \gamma_j^k)^T$.

Begin

Do $E_{k+1} = Gen(\underline{e}_1^k)$, $\tilde{n}_{k+1} = |E_{k+1}|$

Do for $l = 1\ to\ \tilde{n}_{k+1}$

$\Gamma^{-1}(\underline{e}_l^{k+1}) = \underline{e}_1^k$

End

Do for j = 2 to n_k

$F_j = H = Gen\ (\underline{e}_j^k) = \{\underline{f}_l^{k+1}, l = 1\ to\ n_j^{k+1}\}$

Do for $l = 1\ to\ n_j^{k+1}$

$\Gamma^{-1}(\underline{f}_l^{k+1}) = \underline{e}_j^k$

End

Do for $l = 1\ to\ n_j^{k+1}$

Do for $s = 1$ *to* $\tilde{n}_{k+1}$

Compute Δ_{sl}

if $\Delta_{sl} \le \varepsilon_{k+1}$ then $H_j = H_j - \left\{\underline{f}_l^{k+1}\right\}$ and $\Gamma^{-1}(\underline{e}_s^{k+1}) = \Gamma^{-1}(\underline{e}_s^{k+1}) \bigcup \left\{\underline{e}_j^{k}\right\}$

End

$n_j^{k+1} = \left|H_j\right|$

End

Let $E_{k+1} = E_{k+1} \bigcup H_j$ and $n_{k+1} = \left|E_{k+1}\right|$

End

Finally, we get the set E_{k+1} of the remaining states generated for stage k+1. Here $Gen(\underline{e}_j^k)$ is the generation procedure which generates the next states from state $\underline{e}_j^k$ by reverse integration and by checking the flight domain constraints. $\Gamma^{-1}(\underline{e})$ represents the set of predecessors in the search graph (a tree after selection at the current stage) of the Dynamic Programming process.

Figures 7.5 and 7.6 illustrate the proposed merging process.

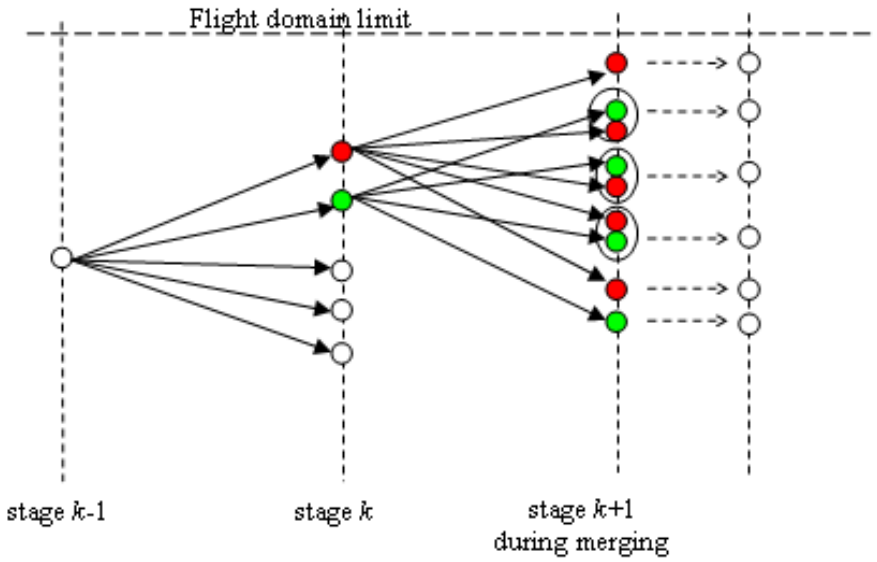

Figure 7.5 Merging process at stage k+1

The complexity of the above algorithm is rather low since its order at stage k for merging at stage k+1 is polynomial ($O(n_k{}^2 L^2)$.

Let us define the feasibility factor μ as the mean value over the stages of the ratio between the feasible states generated at a stage and the total number of generated states at this stage. Let us define the merging factor σ as the mean value over the stages of the ratio between the number of states after merging and the number of feasible states.

Then the mean ratio over the stages between n_{k+1} and n_k is given by $\mu \cdot \sigma \cdot L$.

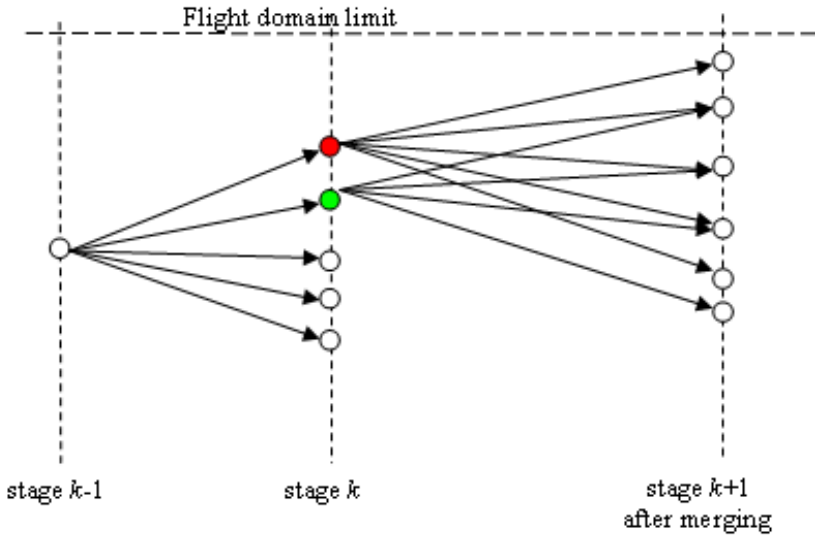

Figure 7.6 The states at stage k+1 after the merging process

VII.5 Dynamic Programming Selection Process

Let now be J_{j*}^k be the best performance obtained to join the initial state $\underline{e}_1^1$ at stage 1 to the state j , at stage k, $\underline{e}_j^k$, $k \geq 2$:

$$J_{j*}^k = \min_{Paths\ from\ \underline{e}_1^1\ to\ \underline{e}_j^k} \left(\sum_{l=1}^{k-1} S_l \right) \tag{7. 25}$$

and let π_{j*}^k be this optimal path.

Then, the optimal path, or reverse trajectory, linking state $\underline{e}_1^1$ to state $\underline{e}_h^{k+1}$ uses state $\underline{e}_{j*}^k$ such as:

$$J_{j*}^k + S_k(j*,h) = \min_{\underline{e}_l^k \in \Gamma^{-1}(\underline{e}_h^{k+1})} \left\{ J_{l*}^k + S_k(l,h) \right\} \tag{7. 26}$$

where the predecessor function Γ^{-1} has been updated at the merging process and where:

$$S_k(l,h) = \frac{\left|\theta_{k+1}^h - \theta_k^l\right|}{t_{s=k} - t_{s=k+1}} + \lambda_V \left(\frac{\left|V_{k+1}^h - V_k^l\right| + V_{zk}^l \cdot \left|\gamma_{k+1}^h - \gamma_k^l\right|}{x_{s=k} - x_{s=k+1}} \right) \tag{7. 27}$$

Only one solution , $\underline{e}_{j*}^k$, will be retained for equation (7.26). Then, the optimal path, or trajectory, leading back from state $\underline{e}_1^1$ to state $\underline{e}_h^{k+1}$ is given by $\pi_{j*}^k \bigcup (\underline{e}_{j*}^k, \underline{e}_h^{k+1})$. This selection process will construct, stage by stage a spanning arborescence. The result of this process is illustrated in figure 7.7 with respect to figure 7.6.

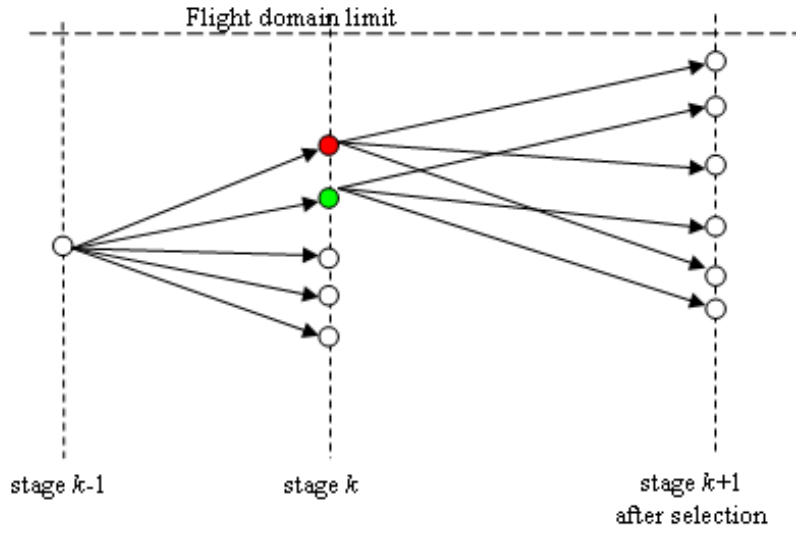

Figure 7.7 The optimal paths after selection at stage *k*+1

With respect to computational burden, the number of states to be treated by the whole selection process is of order $O((\mu \cdot \sigma \cdot L)^{K-1})$.

VII.6 Numerical Results

The Dynamic Programming approach described in the previous sections has been applied in the case of a wide body transportation aircraft with a mass of 120t which starts its engine-out glide at cruise level (FL 330) with an airspeed of 360 Kt at a distance up to 150km from a possible safe landing place. Then, about 400 stages have been considered to cover the whole distance. The altitude of the landing place has been taken equal to 0m.

The since the generating factor L has been taken equal to about10 a very large number of states has been expected, turning possibly unfeasible the numerical application. However, the total number of generated has been about 15×10^{9}. When considering stages statistics, it appeared that the resulting merging factor is very small, $\sigma = 0.2$, and that the feasibility factor, $\mu = 0.6$, is also rather small, so that the mean effective generating factor has been found to be about 1.2. This has resulted in computing times of up to 2 hours on a personal computer to generate through the above described Dynamic Programming process a whole optimal arborescence for this range. With different values for the parameters of the Dynamic Programming process, the computer time has gone up to 2 days.

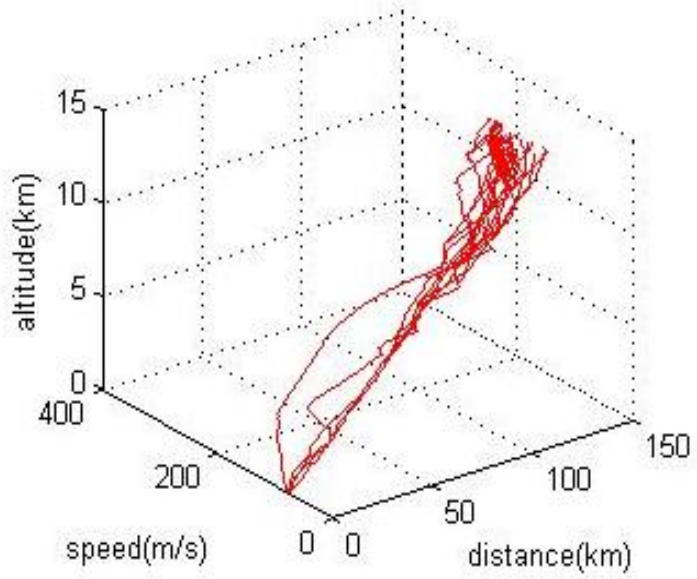

Figure 7.8 Examples of 3D optimal glide trajectories

Figure 7.8 provide some trajectories extracted from the optimal arborescence. These trajectories “end”(in fact start) at FL 290 to FL 360 at a distance of 150 km from the landing site and with different “final” (in fact initial) airspeeds (from 320 Kt to 500 Kt). It appears that the initial airspeed and altitude influence a lot the shape of glide trajectory.

Figure 7.9 displays a 3D optimal glide trajectory while 7.10 provides the corresponding evolution of the pitch angle.

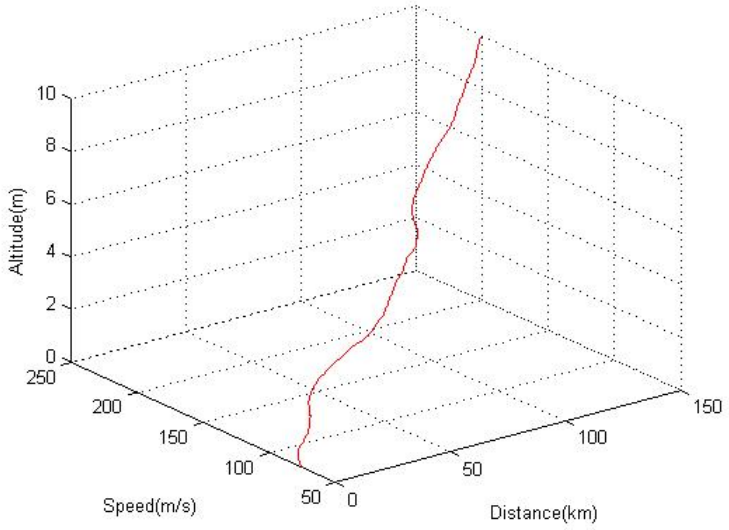

Figure 7.9 An example of computed 3D gliding trajectory

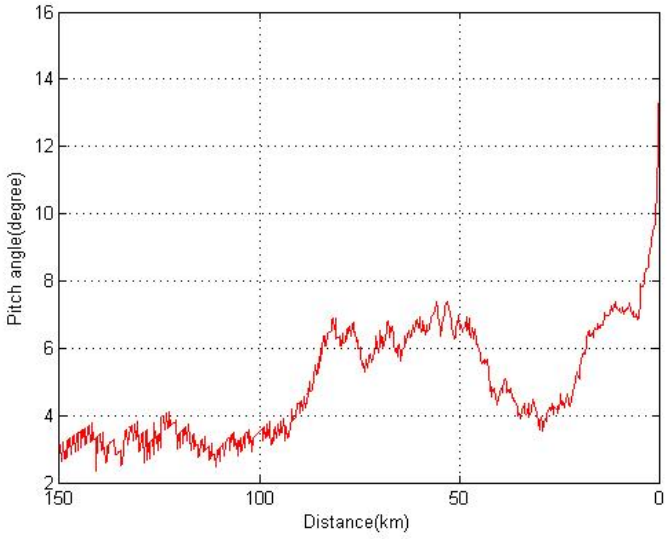

Figure 7.10 Evolution of pitch angle of a computed gliding trajectory

Figure 7.11 displays an example of a whole generated optimal arborescence. It appears that it forms a dense volume starting at point ($z = 50\,m, V = 75\,m/s, x = 0\,m$) with a path angle of -3°. This volume can be seen as representing the *glide domain* of this aircraft, similarly to the *flight domain* of an undamaged aircraft.

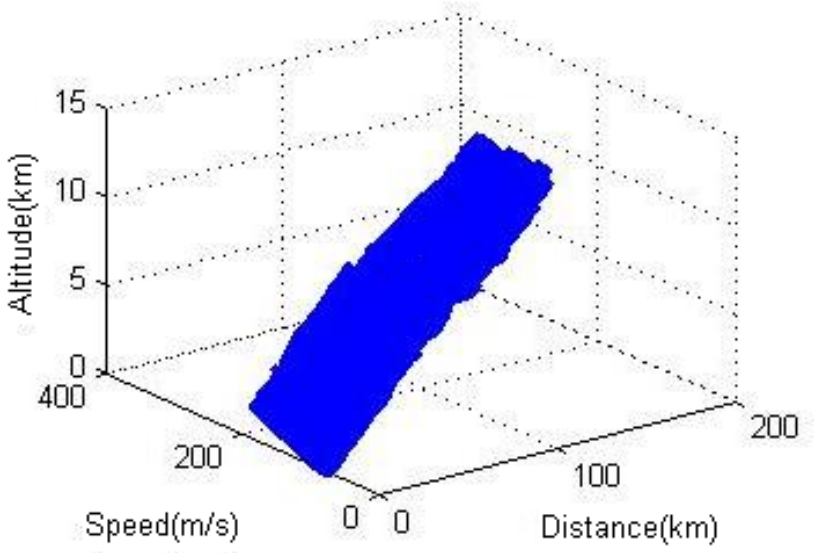

Figure 7.11 Safe glide domain from Reverse Dynamic Programming

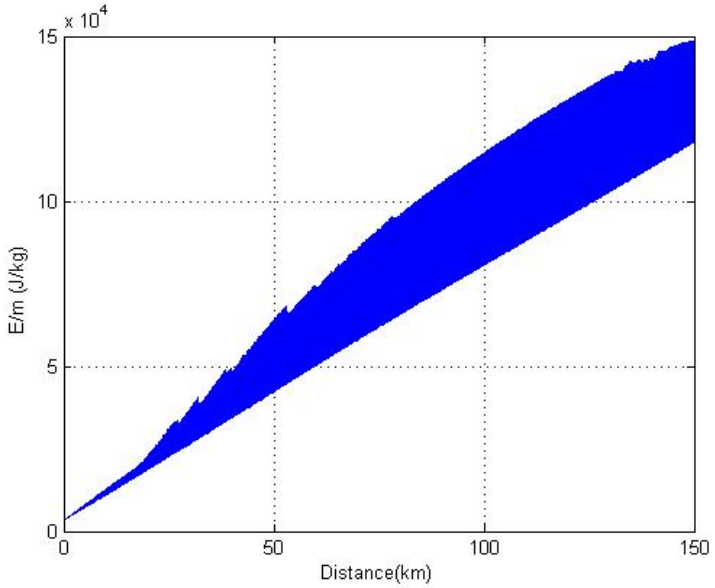

Figure 7.12 The computed safe total energy glide domain

If now considering total energy along the generated arborescence, this safe glide domain can be represented in terms of total energy. For the above data we get for example the safe total energy glide domain displayed in figure 7.12:

The computed altitude domain and speed domain are displayed in figure 7.13 and figure 7.14:

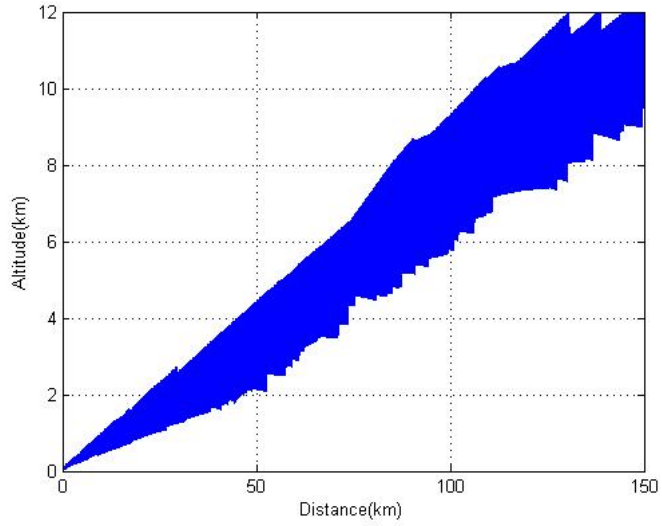

Figure 7.13 The computed safe altitude domain for gliding

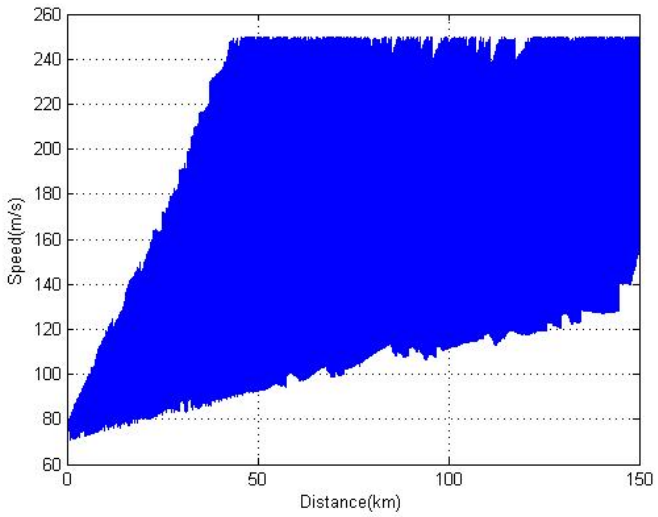

Figure 7.14 The computed safe speed domain for gliding

In the next chapter it will be shown how these domains can be used for the management of the aircraft trajectory after an engine-out event.

The generated arborescence can be considered as a data base and from it can be extracted shorter optimal trajectories reaching when possible the desired initial altitude and speed through different ranges. Figure 7.15 displays some trajectories with different ranges starting practically at almost the same flight level and airspeed.

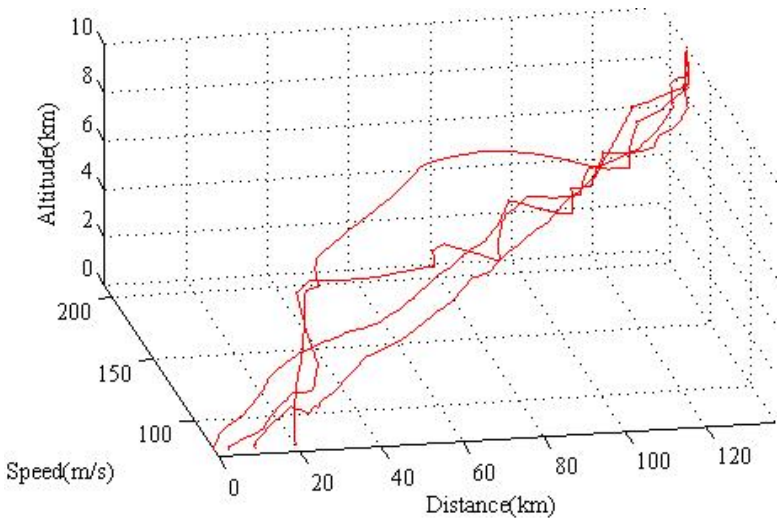

Figure 7.15 Optimal trajectories with different gliding ranges

Then it appears that the generated arborescence can also be of some help at the time of choosing a possible landing site.

VII.7 Conclusion

In this chapter, the development of a Reverse Dynamic Programming process to generate optimal glide trajectories has been detailed. In particular the different means adopted to secure the volume of computation and memory necessary to build solutions have been discussed and their efficiency has been appraised. It is the case in particular with:

- the proposed space discretization,
- the chosen numerical integration technique and space step,
- the developed melting states technique,

- the state deletion rule at a given stage.

When displaying the numerical results, it appears that what was considered at first a difficulty for applying the Reverse Dynamic Programming approach, can be in fact in the considered operational context, a major opportunity. Effectively, the developed Reverse Dynamic Programming process, to be as exhaustive and exact as possible to provide an optimal solution needs to sweep all the feasible glide domain, generating not only the particular optimal solution but also a full set of optimal trajectories, or a data base, covering the feasible glide domain and corresponding to different initial flight conditions.

In chapter VIII a neural network device will be introduced to take full profit of the generated feasible glide data base to propose a new function to help the pilot to perform a safe long glide manoeuvre in an engine-out situation.

CHAPTER VIII

ON-LINE NEURAL CONTROL FOR ENGINE-OUT GLIDING AIRCRAFT

VIII.1 Introduction

In chapter VII a Reverse Dynamic Programming approach was design to generate optimal gliding trajectories starting at cruise conditions. It appears that its direct application to on-line gliding control was unfeasible considering the involved computational burden. However, the Reverse Dynamic Programming process generates during its search process a whole database providing information about a large number of possible trajectories which constitute a tight mesh covering, for a given aircraft mass, its safe glide domain.

It is worth to observe that during near steady gliding for an engine-out aircraft, the guidance performance cannot be more than the piloting performance since the only control parameter left to modify the aircraft motion is the pitch angle.

So in this chapter a new tool is developed to take profit of this data base with the aim of providing on-line, piloting indications to the pilot. The objective is to help the pilot to take adequate piloting actions so that the aircraft follows a safe glide trajectory leading to target site with some probability of landing with success. This tool is based on a feed-forward neural network which has to be trained and validated with the generated glide trajectory data base. Numerical simulations are performed to demonstrate this concept.

VIII.1.1 The need for a new Flight Director function

It also happens that perturbations (wind in general) and past piloting errors make practically impossible to follow exactly an optimal glide trajectory from the start to the end (landing site). Then it appears that a new piloting function to help the pilot, or to generate pitch reference values to a still working autopilot, is very desirable. In the case of manual gliding control, this new function could be implemented in the flight director system. In that case this new function, let us call it PAG ("*Pitch At Glide*") should generate on-line pitch attitude tendency information to the pilot which will be eased in his task to make the aircraft adopt the right pitch attitude at the current height, speed and distance to the landing site. This will be most valuable when the pilot is far from the landing site and has few clues to manage the glide. When the aircraft reaches the vicinity of the landing site, the pitch information submitted to the pilot could be provided to a Head Up Display, if installed, so that the pilot can take more effectively into account outside information (distance to a safe spot, trees, buildings and other ground obstacles) to take his final decisions.

VIII.1.2 Using a Neural Network as control parameter on-line generator

As what has been told above, during near steady gliding for an engine-out aircraft, the only available adjustable control parameter is the pitch angle. Other means such as flaps, spoilers used or not as airbrakes and landing gears can also be used, but they are not adjustable. It can also be supposed that the trimmable horizontal stabilizer will remain fixed to its reference position since its control consumes too much hydraulic power. Then, once the position of these surfaces are chosen, given the starting conditions for gliding (mass, altitude, speed and distance) there is a causality relationship between the pitch history and the performed trajectory in a still atmosphere and to each point of an optimal glide trajectory generated by the Reverse Dynamic Programming process, is associate a unique quintuplet $(z, x, V, \gamma, \theta)$. Even in a perturbed atmosphere this causality between the pitch angle and the followed trajectory will be partially maintained. Observe also that according to the Reverse Dynamic Programming process such a quintuplet can at most be attached to a unique optimal trajectory from that point to the landing site conditions. So it appears of interest to try to build a numerical device integrating the whole generated data and producing on line the most adequate pitch angle reference value. All these considerations lead to consider the design of a neural network generator for the current reference value for the pitch angle [WU H.[3]].

So this chapter will display a proposal for the design of such a new function using a neural network structure.

VIII.2 Neural Networks

In this paragraph we recall briefly the main characteristics of feed-forward neural networks which are useful for our problem and provide an overview of neural networks applications in the field of aircraft flight control.

VIII.2.1 Main characteristics of Feed Forward Neural Networks

Artificial neural networks consist of a large number of interconnected elementary treatment units or neurons, which individually perform elementary operations on the signal which is submitted as input to each of them [VEELENTURF L.P.J.]. This treatment is characterized by an activation function which can be written in the general form as:

$$y = f(\sum_{g=1}^{N_e} w_g \; x_g + b \;) \tag{8.1}$$

where $f(\cdot)$ represents the activation function, w_g is the weight associated to its g^{th} connection with signal x_g, g = 1 to N_e, where N_e is the number of incident neurons and b is an activation threshold or bias. There is some analogy existing with the organization of biological neurons in the brain at this level: the interconnections correspond to axons and dendrites, the connection weights correspond to the synapses and the activation function models the electrochemical activity of biological neuron [WERBOS P. J.].

There is an enormous variety of artificial neural networks, corresponding to different choices with respect to the connection structure between neurons and to the activation functions carried out at the level of each neuron. The performances of an artificial neural network are directly related to the manner in which neurons are interconnected to build the structure. Loop-free networks and recurrent networks can be distinguished. The loop-free networks are static structures where the connections between neurons are realized in an unidirectional way, that is to say, the inputs of the neurons in the output layer, passing from the possible intermediate neurons layer or hidden layer, without backward connection. The loop free neural networks are called universal approximates in [HORNIK K.]. It has been demonstrated from different approaches in [BARRON R.] [CYBENKO G.] [FUNAHASHI K.][HORNIK K.] that a loop-free multilayer neural network can approach any continuous function with an arbitrary precision. For example, Hornik *et al* established indeed the following theorem:

Theorem: Let $\phi(x)$ be a continuous, non constant, bounded and monotone increasing function. Let S be a compact domain in R^n and $f(x_i, ..., x_n)$ be a real continuous function defined on S. So, for a given real number ε, which is positive strictly, there are an integer number N and real constants c_i, θ_i and $w_{i,j}$, i=1,…, N, j =1,…, n such that the following condition is satisfied:

$$\max_{x \in s} \left| f(x_i, ..., x_n) - \hat{f}(x_i, ..., x_n) \right| < \varepsilon \tag{8.2}$$

where $$\hat{f}(x_i, ..., x_n) = \sum_{i=1}^{N} c_i \phi \left(\sum_{j=1}^{n} w_{i,j} x_j - \theta_i \right) \tag{8.3}$$

Equation (8.3) represents the input-output relation realized by a feed-forward neural network with one hidden layer. For the neural network with multiple hidden layers, similar results can also be obtained from this theorem. Yet this theoretical result does not provide any practical indications on the network size and on the number of parameters necessary for approaching effectively function $f(x_i, ..., x_n)$. This issue should be solved in general through a try and error approach where the number of neurons and parameters is increased gradually.

Then, artificial neural networks can get, through a learning process, the capability of catching causality encountered between the input and the output of a physical system. This property is termed as *generalization*. Feed-forward networks have successfully be used in many fields, such as diagnostic with expert systems [LOONEY C. G.], pattern recognition [BISHOP C. M.] [BASU J. K.], combinatorial optimization [SMITH K.] and control, including nonlinear inverse control [CHEN L.], adaptive control [CHIDRAWAR S.][CHEN F.C.] and differential flat control [LU W.[1,2]]. Feed-forward neural networks have been applied in many other fieds and in the last decades they have been combined with other artificial intelligence techniques such as Fuzzy Logic and Genetic algorithms.

VIII.2.2 Neural Networks applications in flight guidance

Neural networks have been considered to be effective numerical tools to solve many problems related to the design of airborne systems in military and civil aviation. Many academic studies have been performed and some effective realizations, mainly in the military aviation field have been achieved. Examples of studies directly or indirectly related to flight guidance are:

- Estimation of aircraft aerodynamic coefficients by using neural interpolation [FETEIH S.]
- Identification of aircraft flight dynamics parameters [SAGHAFI F.].
- Computation of parameter values through neural networks for models devoted to analyze flight performance, see [XIE Y.].
- Contribution of neural networks to solve different flight control and management problems, such as in [BURGIN G. H.], where an artificial neural network is used to adjust the gain of a stability augmentation system to insure stability and another one is used to optimize the parameters of a flight path.

- Nonlinear adaptive flight control through neural networks, such as in [CALISE A. J.[2]].
- Trajectory tracking where nonlinear inversion is turned feasible by feed forward neural networks when the property of differential flatness [FLIESS M.] is considered[LU W.[3]].
- Homing control for missile guidance using Hopfield networks, such as in [STECK J.E.].
- Diagnose of aircraft engine for fault detection and identification [KOBAYASHI T.] .

From this short overview it looms that a safe application of neural network technology on board aircraft consists in using off-line trained neural networks to react to a situation which can be tackled by the neural network through its generalization power. In some special cases, additional on-line training can also be considered with interest.

VIII.3 Neural Networks for Online Computation of Reference Pitch Angle

Here the structure and the learning technique of the proposed neural network pitch angle reference generator are described briefly.

VIII.3.1 General features of the adopted Feed-forward Neural Networks

Our proposal here, has been to take profit of the amount of data generated by the Reverse Dynamic Programming search process, considering different situations and parameters such as aircraft initial distance to landing site x; altitude z; speed V and glide path angle γ to obtain pitch angle directives.

Here a feed-forward neural network is used to approximate the relations between the situation of aircraft (z, x, V, γ) and the desired directives (θ), which is implied in the database obtained in chapter VII through Reverse Dynamic Programming. Thus the database is used to train a specialized neural network designed to generate pitch angle directives (in fact the target current reference value for the pitch angle θ) at each point along the descent so that the glide trajectory leads safely to the landing location. Figure 8.1 shows the structure of neural network for calculating pitch angle θ, where the inputs of the neural network are x, z, V, and γ, and the output of the neural network is pitch angle, θ, which is sent to flight director as flight control reference. The aircraft mass m has not been considered in this study and has been kept

constant, but for real application of the proposed device, aircraft mass *m* should be considered as an input and the training of the neural network should be extended to consider aircraft mass variation. Here the number of neurons in the hidden layer, N_h, must be determined empirically by restarting the learning process with a different number N_h if the learning error remains too large or the validation is not conclusive.

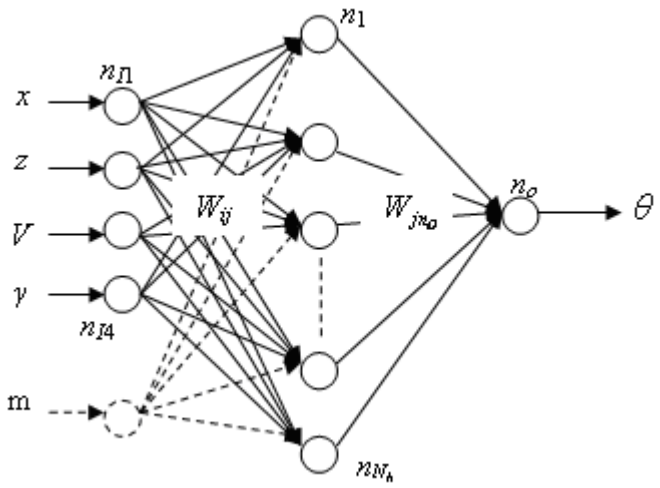

Figure 8.1 Adopted structure for the feed-forward neural network

The activation function which has been adopted has been the sigmoid function ($f(x)=1/(1+exp(-x))$ [HORNIK K.][CYBENKO G.] since it has given good results in other studies [LU W.[3]]. Every connection between two neurons *i* and *j* has a weight W_{ij} and every neuron has its own threshold *b*. The output of each hidden neuron *j* is then given by:

$$n_j = f_j\left(\sum_{k=1}^{4} w_{ij}\ n_{I\,i} + b_j\right) \quad j = 1,\cdots,N_h \tag{8.4-a}$$

while the global output of the neural network is given by:

$$\theta = n_o = f_o\left(\sum_{j=1}^{N_h} w_{jno} n_j + b_o\right) \tag{8.4-b}$$

where f_j and f_o are sigmoid functions, n_j is the output of neuron j in hidden layer, and θ or n_o is the output of neural network.

Here the data base generated by the Reverse Dynamic Programming process is taken into profit to provide the training data and the validation data for building the appropriate neural network. Figure 7.3 displays an example of training data generated from reverse dynamic programming. Training has been performed using the back propagation algorithm [see Annex D] written in Matlab.

VIII.3.2 The developed neural network structure

Even though a hidden-layer neural network can approach theoretically any nonlinear function, the enormous volume of data generated by the Reverse Dynamic Programming process covers a wide range of flight situations from cruise level to landing. The first attempts to build a global neural network covering the maximum range of an engine-out gliding aircraft have been unsuccessful, since after convergence of the learning process large errors remained between the pitch values computed by the neural network and the values provided by the training data. This was specially the case near the landing site and far from the landing site. In the first case the adoption of this reference value could be disastrous, while adopting erroneous pitch angles and consequently erroneous path angles, will lead to reduce the gliding range.

To try to improve the training performance the training data base has been divided into different local data bases, storing data according to the distance to the landing site. The maximum glide range has been covered by nine overlapping intervals has shown in figure 8.2. To each of these intervals is associated a trapezoidal fuzzy membership function [FAYE R.M.] $f_i(x), i = 1\,to\,9$, where x is the horizontal distance to the landing site. These functions are also represented in figure 8.2. There have been designed so that:

$$\sum_{i=1}^{i=9} f_i(x) = 1 \quad \forall x \in [0, d_{\max}] \tag{8. 5}$$

where d_{max} is the maximum gliding range.

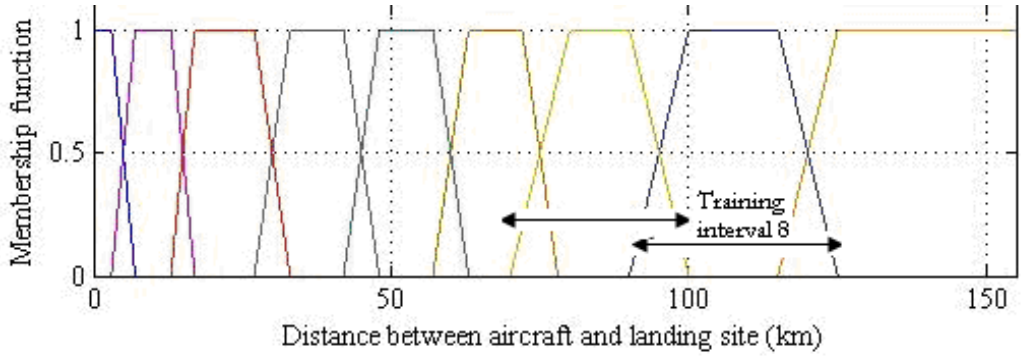

Figure 8.2 Training/Validation intervals and associated fuzzy membership functions

Then nine local feed-forward neural networks have been trained and validated. Since two adjacent local databases share some common training or validation data, the overall output of the designed neural network structure to any input data set (x, z, V, γ) is given by:

$$\hat{\theta} = \sum_{i=1}^{i=n} \hat{\theta}_i \cdot f_i(x) \tag{8.6}$$

where only two terms of the sum can be at most different from zero at the same time, so that in real time operation at most two local neural networks are active according to the distance to the planned landing site. Here $\hat{\theta}_i$ is the output from local neural network number i and $\hat{\theta}$ is the global estimation of the required pitch angle at the current flight situation. Additional subdivisions inside each sub interval is considered, for example different total energy intervals have been considered. Their introduction which would have the direct effect of multiplying the number of neural networks necessary to cover the whole glide domain as well as the current number of active sets, has not brought significant improvement in the accuracy of the resulting neural network structure. Moreover, in practical applications an additional training layer considering different mass values for the gliding aircraft should be introduced, then the actual complexity of proposed the neural network structure devoted to the on-line generation of reference values for the pitch angle can be considered already quite complex.

VIII.3.3 Training and validation results

The data generated by Reverse Dynamic Programming has been subdivided into nine local training databases and nine validation databases covering intervals of space whose size

increases with the distance to the planned landing place. Data corresponding to a common distance interval has been randomly subdivided into training data (90%) and validation data (10%).

Figures 8.3 and 8.5 display respectively the evolution of the total mean square error during training iterations (epochs) for neural networks number 5 and 7. The dispersion of the errors at the validation stage for neural networks number 5 and 7 are respectively displayed in figures 8.4 and 8.6.

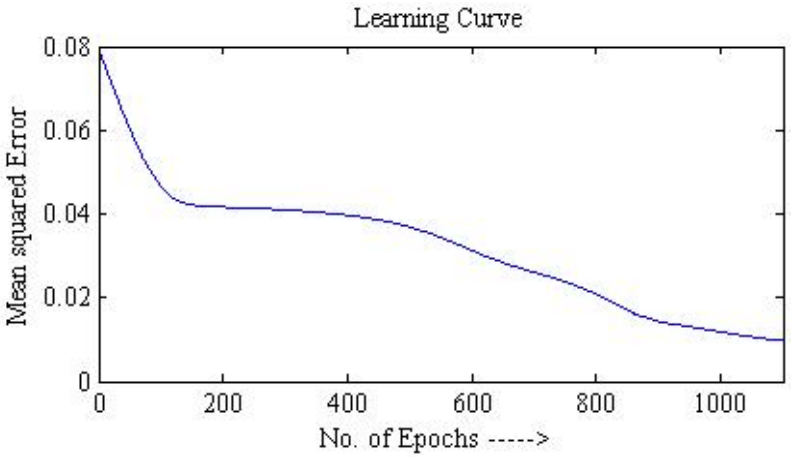

Figure 8.3 Mean squared error evolution during training of neural network 5

Figure 8.4 Error distribution for validation of neural network 5

Figure 8.5 displays an example of evolution of the total mean square error during the training experience of neural network 7. The dispersion of errors at the validation stage for neural network number 7 are displayed in figure 8.6:

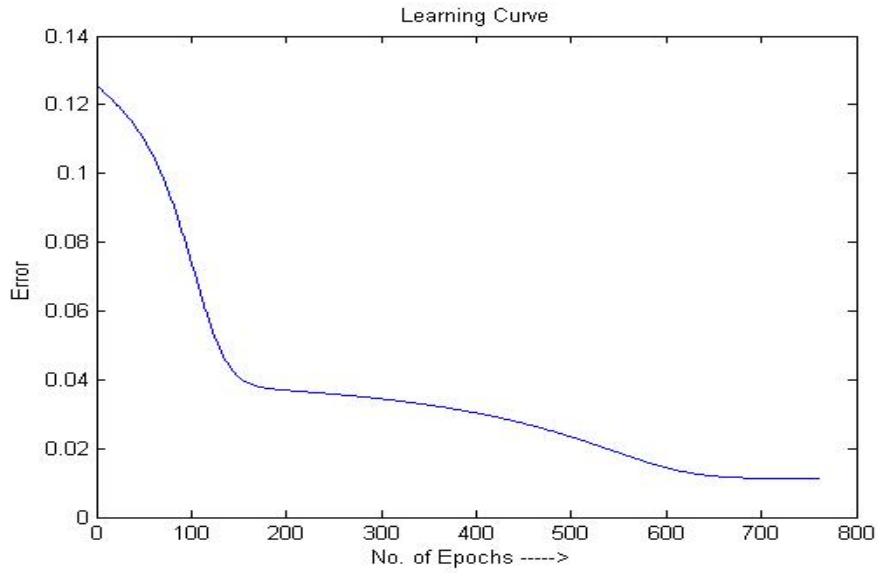

Figure 8.5 Mean squared error evolution during training of neural network 7

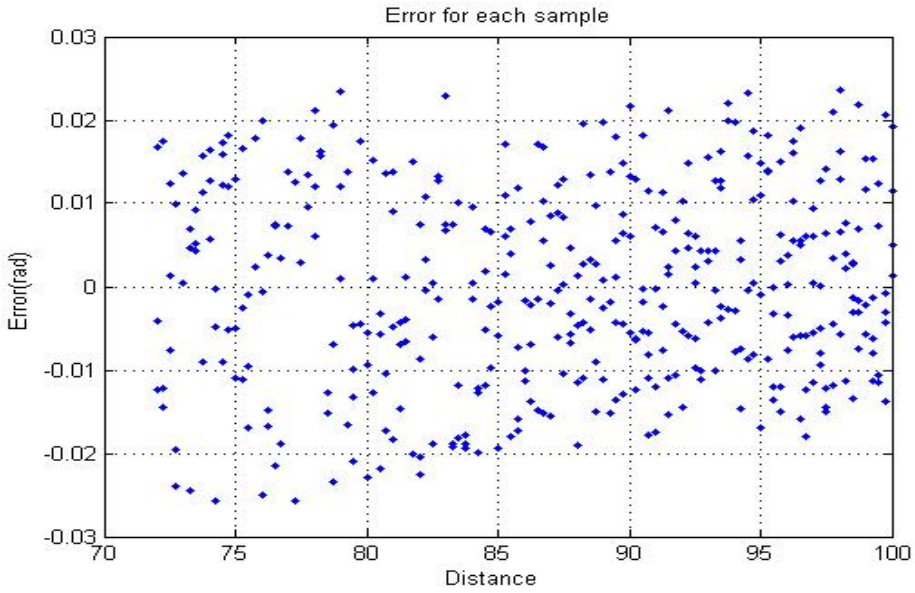

Figure 8.6 Error distribution for validation of neural network 7

It appears that the design and training of the proposed neural network structure has been quite difficult to perform, however acceptable accuracy has been finally obtained so that this tool could be considered useful for on line operation.

Comparing the error distributions of all the different neural networks which have been trained, it was found that all the distributions had similar characteristics. For example, as shown in figure 8.4, the errors which are at the left end of the interval tend to be negative, while the errors which are at the right end of the interval tend to be positive. So the averaging process between outputs of successive neural networks resulting from common data, relation (8.6), tends to compensate for these error tendencies.

VIII.4 Simulation Results

In this section the simulation results are presented where the proposed neural network tool is used to generate, starting from different initial flight situations, and successive values for the pitch angle until the glide maneuver is completed. It is supposed that the pilot follows perfectly the pitch angle reference values provided by the system according to the on-line control structure displayed in figure 8.7.

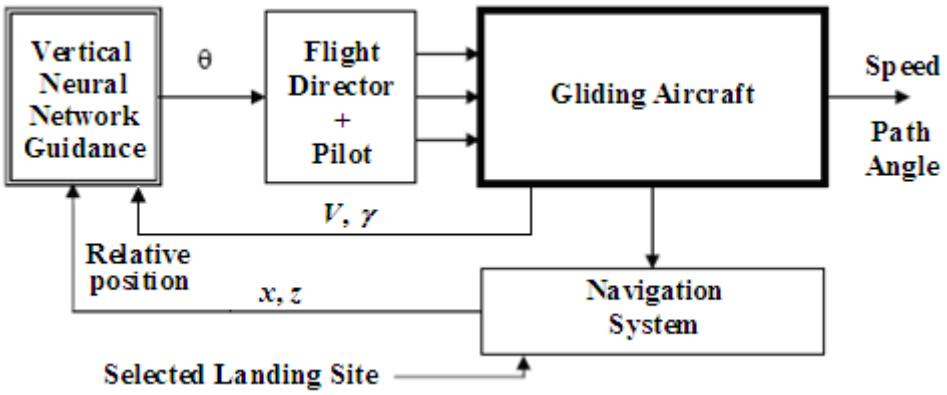

Figure 8.7 Neural guidance structure during engine-out glide maneuver

The very end of the glide, including the flap maneuver at landing, is not considered here, since in general it is directly performed by the pilot in manual mode. Recall there that the Reverse Dynamic Programming process has concentrated on smooth glide trajectories which save hydraulic power in view of final landing maneuvers execution.

The simulations have been carried out in Matlab and the data used corresponds to an reference transportation aircraft, see annex A.

Two different classes of flight conditions have been considered: no-wind and horizontal wind conditions.

VIII.4.1 Engine-out aircraft glide guidance without wind

In this section we focus on the no-wind condition. In this case, the initial situation of the aircraft is cruising at an altitude of about 11000m with a speed of 440 Kt (220 m/s), then the aircraft must glide over different distances ranging from 110km to 159km to arrive at the landing place. In this case, the max gliding range is about 159 km (see figure 8.8).

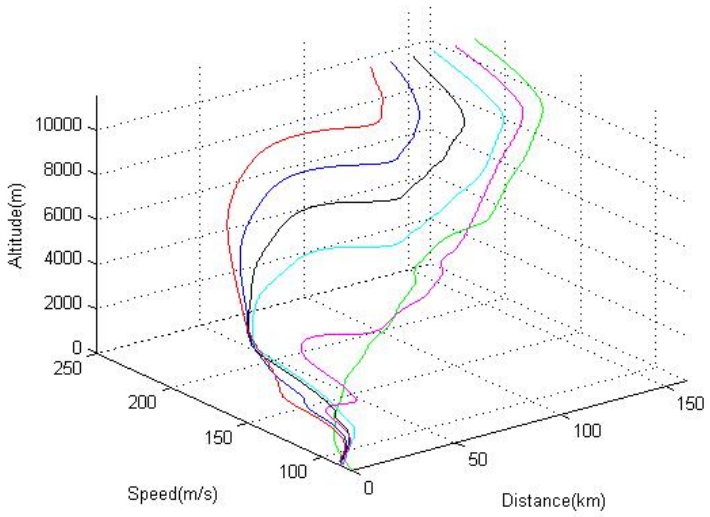

Figure 8.8 3D controlled glide trajectories with different ranges (110 km to 159 km)

The simulation results are displayed in the following figures.:

- Figure 8.8 provides a 3D view of the different produced gliding trajectories ranging from 110km to 159km: red (110 km), blue (120km), black (130km), cyan (140km), magenta (150km), green (159 km).

- Figure 8.9 provides a 2D view (x, z) of the same trajectories.
- Figure 8.10 provides the evolution of airspeed along the same trajectories.
- Figure 8.11 displays the evolution of pitch angle computed by the neural network, which produces the different gliding trajectories.

It appears that the shorter the gliding distance is, the rougher the 3D gliding trajectory is, with large variations of speed.

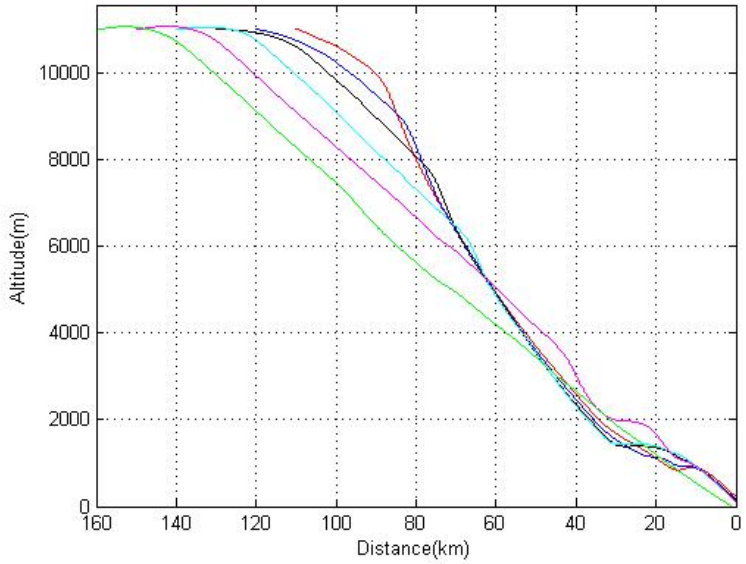

Figure 8.9 Vertical controlled glide trajectories with different ranges (110 km to 159 km)

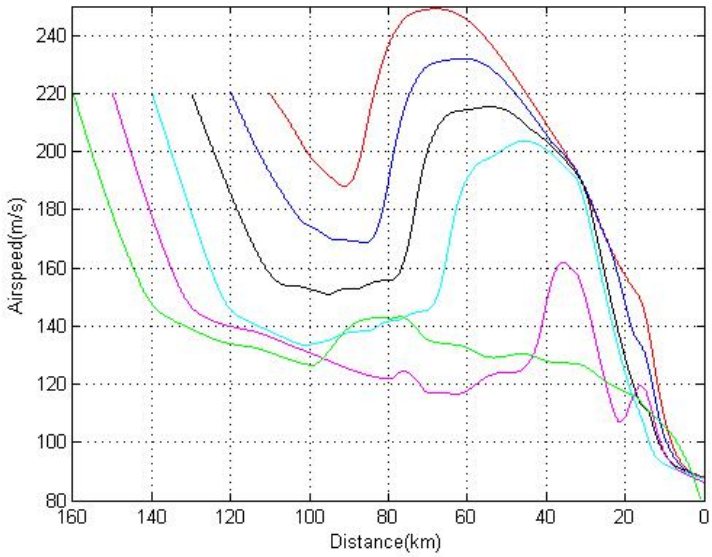

Figure 8.10 Airspeed evolution with different gliding ranges (110 km to 159 km)

From figure 8.10 it appears that when the glide range is short, the proposed solution computed by the neural network leads to higher speeds at lower altitude, so that total energy is reduced at a higher rate through increased friction (drag).

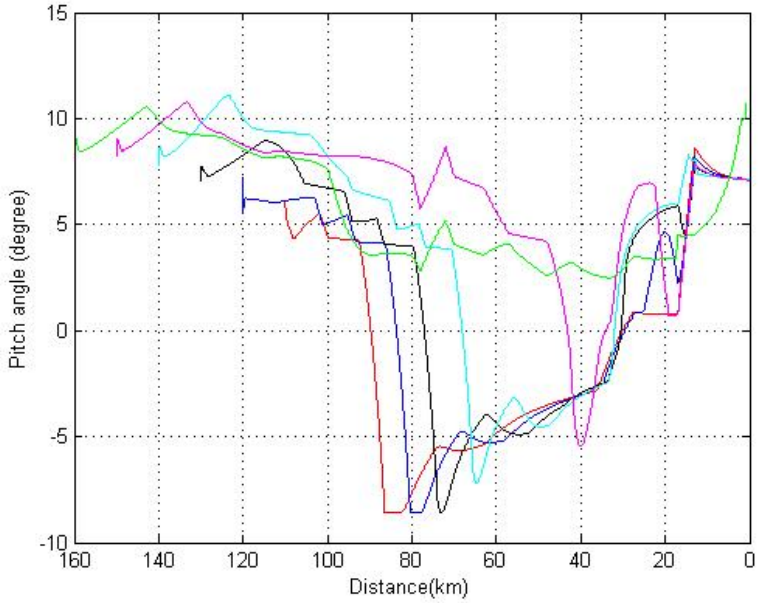

Figure 8.11 Pitch angle variation along the different controlled glide trajectories (110 km to 159 km)

From figure 8.11, it appears that depending of the glide range, the pitch angle evolution along the glide can be very different, while it evolves from minimum (-10°) to maximum values (+10°). So, this advocates for an external help to the pilot to choose its value along the glide trajectory.

In figures 8.12, 8.13, 8.14 and 8.15, the case of the maximum range glide and the case of the out of range glide are compared.

- maximum rang glide :159 km: black trajectory
- of the out of range glide:165km: magenta trajectory

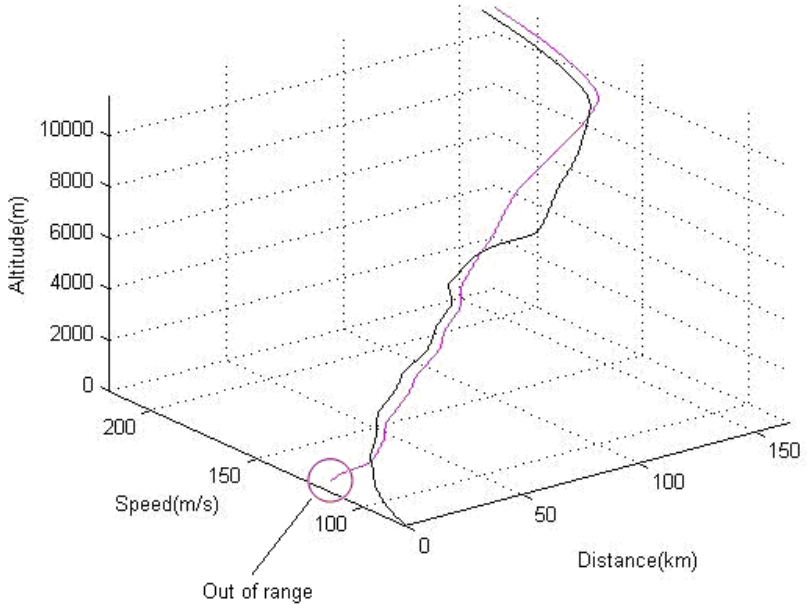

Figure 8.12 3D gliding trajectories with 159 km and 165 km ranges

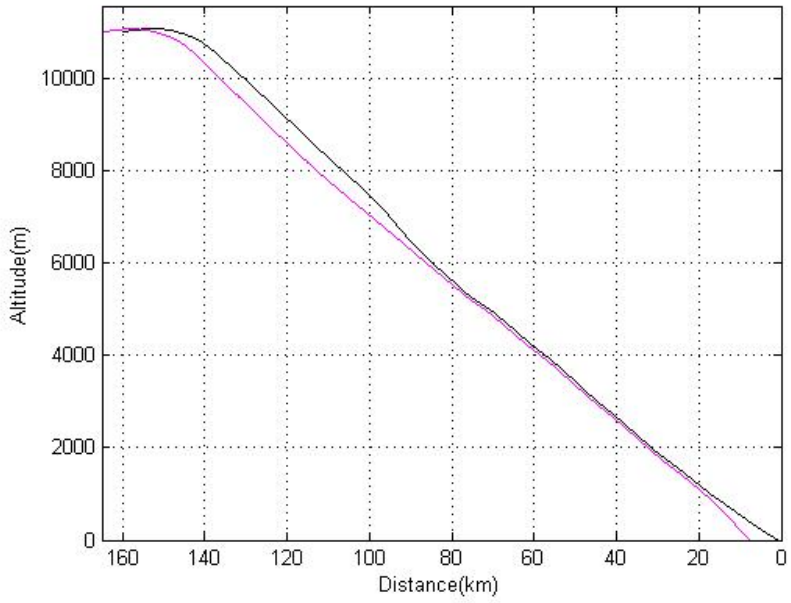

Figure 8.13 Vertical gliding trajectories with 159 km and 165 km ranges

From figures 8.12 and 8.13 it appears that the maximum glide range for the given aircraft (cruise level and speed, aircraft mass) is about 159 km.

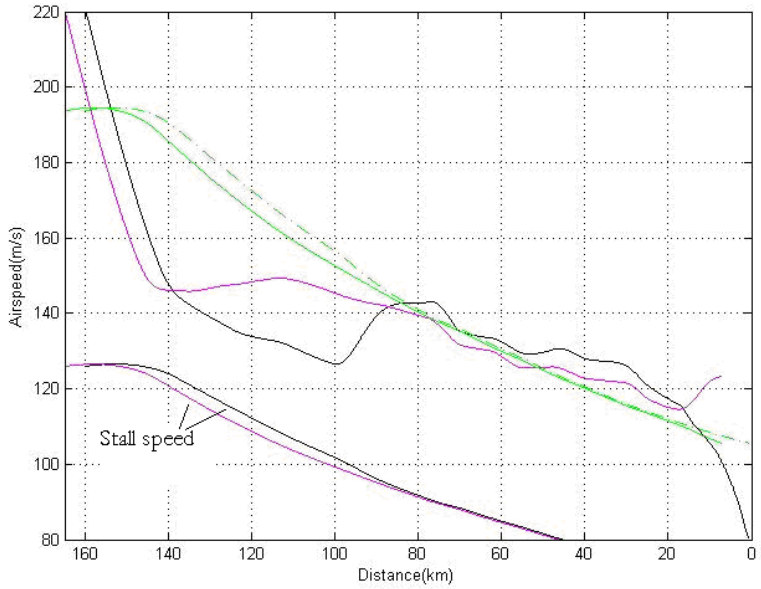

Figure 8.14 Airspeed evolution with 159 km and 165 km gliding ranges

In figure 8.14 has been added the green dot speed (green speed curve corresponding to 165km gliding and dotted green curve corresponding to 159km gliding) which theoretically provide the maximum glide range. The trajectory resulting from the neural network choice of the pitch angle does not follow the green dot speed for about half of the glide range. This can be explained by the fact that at the start of the glide, the speed of the aircraft (440 Kt) is different from the green dot speed at that altitude (390 Kt). In figure 8.14, the stall speed along each glide trajectory has been computed and it can be seen that the glide speed remains in both cases well above it.

VIII.4.2 Engine-out aircraft glide guidance in the presence of wind

In general, the atmosphere is not totally still and engine-out glide has a large probability to be achieved in a windy atmosphere. In general the structure of wind flows is complex and suffers modifications with time. Even if today many models for wind exist, wind prediction ahead of an aircraft is definitely not available. What can be known with an acceptable accuracy, by comparing on-board measurements (Pitot data and angle of attack measurement) on one side and inertial speed from inertial measurement unit hybridized with GPS on the other side, is the current wind speed at the actual position of the aircraft.

The neural network generator has been trained in a no wind situation from data produced by the Reverse Dynamic Programming process applied to the vertical guidance equations written in the wind frame. It will be obviously unfeasible to generate new training data for many different wind situations which could be met over the gliding area. So, here we are led to propose an empiric solution approach where the processed data in the no wind situation can be turned someway useful.

In figure 8.15, the parameters of vertical flight in an horizontal wind situation are introduced: γ_a is flight path angle with respect to atmosphere; γ_g is flight path angle with respect to the earth; V_a is airspeed; V_w is wind speed, and V_g is ground speed.

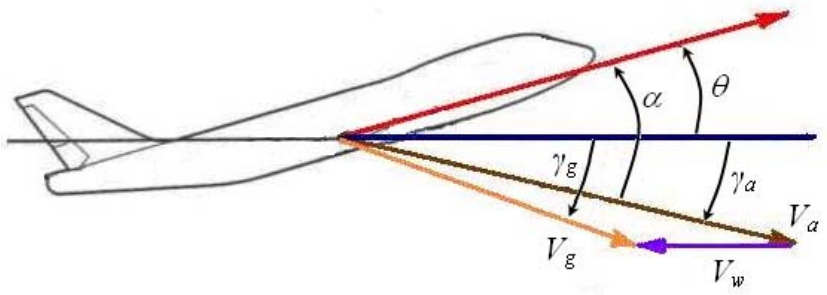

Figure 8.15 Glide path angle with the effect of wind

From this figure it becomes apparent that the presence of a horizontal wind shorten (tailwind) or increase (headwind) what could be called the wet aircraft glide trajectory. So, assuming that the wind speed remains constant all along the glide, the relation between the wet distance x_a and the real distance x is such as (here we take $\cos\gamma_a \approx \cos\gamma_g \approx 1$):

$$\frac{x_a}{V_a} = \frac{x}{V_g} = T \tag{8.7}$$

where T is the common current estimate of the duration of the glide. Then we will use as an input to the neural network generator x_a given by:

$$x_a = \frac{V_a}{V_g} \cdot x \tag{8.8}$$

Then along the glide the coefficient between x and x_a will change according to the current airspeed and the current wind speed, while input γ_a is equal to (θ - α) where θ and α are obtained from on-board measurements.

The proposed approach has been applied to the same aircraft as before, starting from an altitude of 6000m with an initial ground speed of 180m/s at a distance of 75 km from the proposed landing place. It has been supposed that the aircraft glides in a constant horizontal atmosphere. The following different wind speeds have been considered: -15m/s, -10m/s, -5m/s, 0m/s, 10m/s, 20m/s and 30m/s respectively. Negative speeds correspond to headwind while positive speeds correspond to tail winds.

Figure 8.16 illustrates the 3D view of the seven resulting trajectories (red: -15m/s; blue: -10m/s; black: -5m/s; cyan: 0m/s; magenta: 10m/s; green: 20m/s; yellow: 30m/s), while figure 8.17 and 8.18 display 2D views of altitude and airspeed variation with respect to the distance to the landing place.

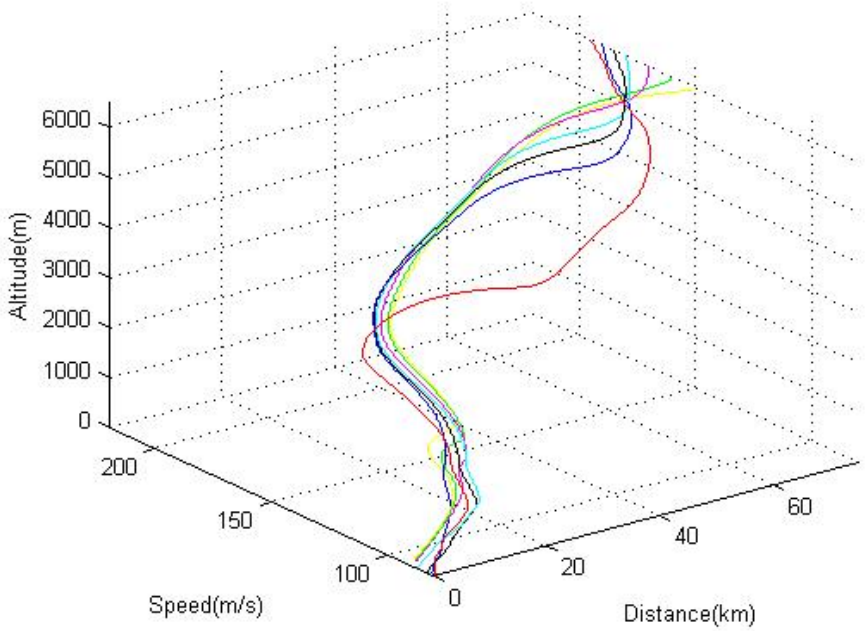

Figure 8.16 3D view of controlled glide trajectories with wind

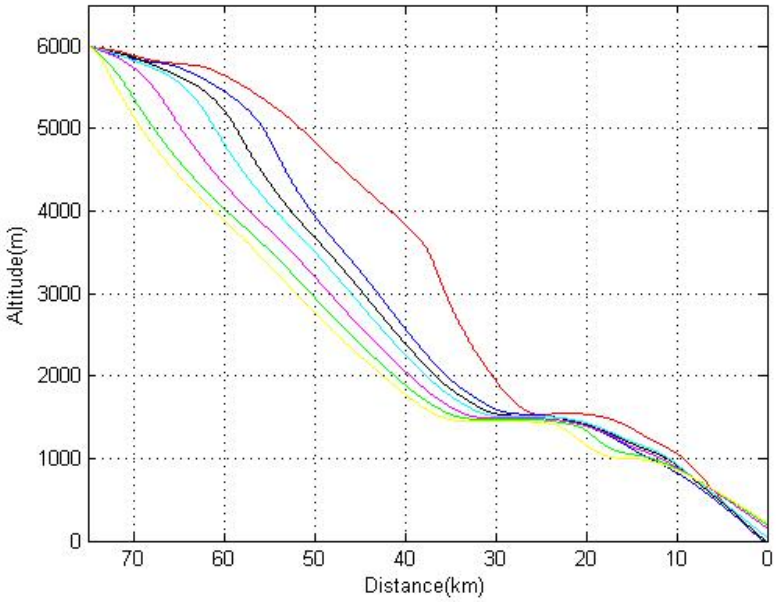

Figure 8.17 Vertical tracks of controlled glide trajectories with wind

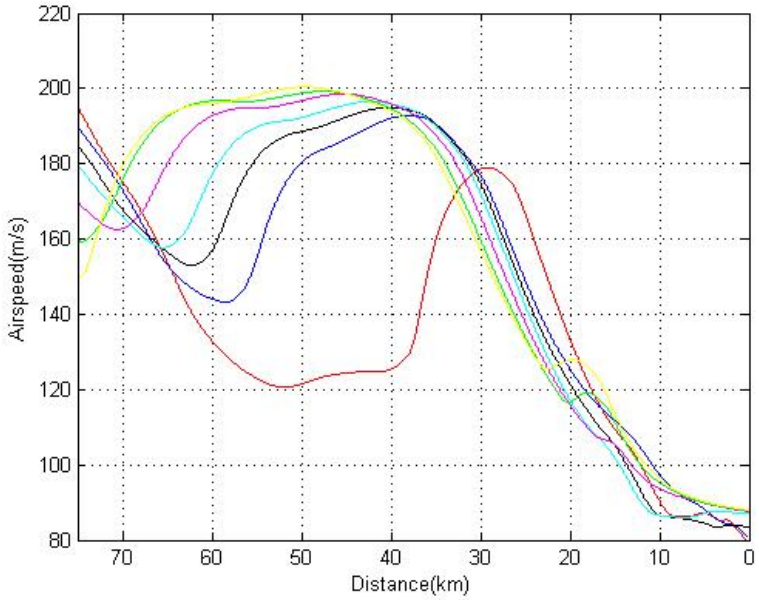

Figure 8.18 Airspeed variations along controlled glide trajectories with wind

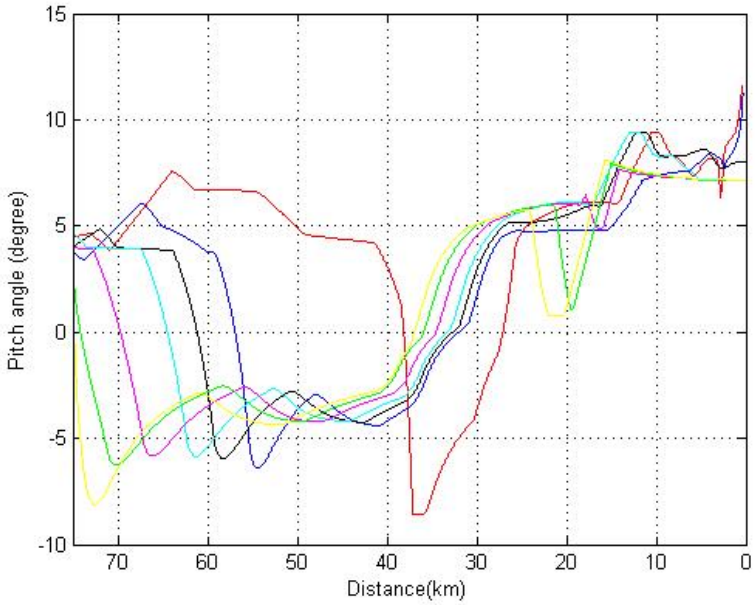

Figure 8.19 Pitch angle variations along controlled glide trajectories with wind

From the above figures it appears that, within the adopted assumption (constant horizontal wind), the proposed empirical solution provides feasible solutions for controlling the glide trajectory in an atmosphere with wind, allowing the aircraft to arrive with a safe speed margin near the proposed landing place. From these figures, it is clear also that wind has an important influence on the shape of the controlled glide trajectory and that in fact, depending on its intensity all along the glide trajectory, the whole endeavour can be achieved with success or not.

VIII.5 Engine-Out Emergency Management and System

From the developed study, the idea that a new function delivered by the Flight Director system and devoted to provide indications to aid the pilot to perform safe engine-out glide trajectory control, takes shape.

Here it is supposed that after engine-out is effective, there remains enough electrical energy (APU, batteries) to run during the whole glide the computers devoted to flight

management, included the navigation function which remains operative, data channels computers, fly by wire computers and cockpit displays including Flight Director. It is also supposed that although the Auto-guidance functions are inoperative as well as many flight envelope protections, the flight augmentation function remains active.

VIII.5.1 Integrating Engine-out guidance function into on-board systems

To escape safely from an in flight engine-out event which occurs, two types of decisions must be taken efficiently:

- the choice of a landing place
- a succession of piloting decisions so that guidance towards the chosen safe landing place is achieved.

Although the question of choosing the landing place has not been tackled directly in this thesis it can be considered that the data base which represents the safe glide domain can be used by the Flight Management System, together with its navigation data base (including eventually a terrain data base) and its performance data base, to perform the selection of a reachable landing place, preferably of course a runway. Then an initial reference glide trajectory can be established and informed to the pilot on the Navigation Display with predicted time and distance to emergency landing. This whole process, which should be realized by an enhanced Flight Management System, is sketched in figure 8.20.

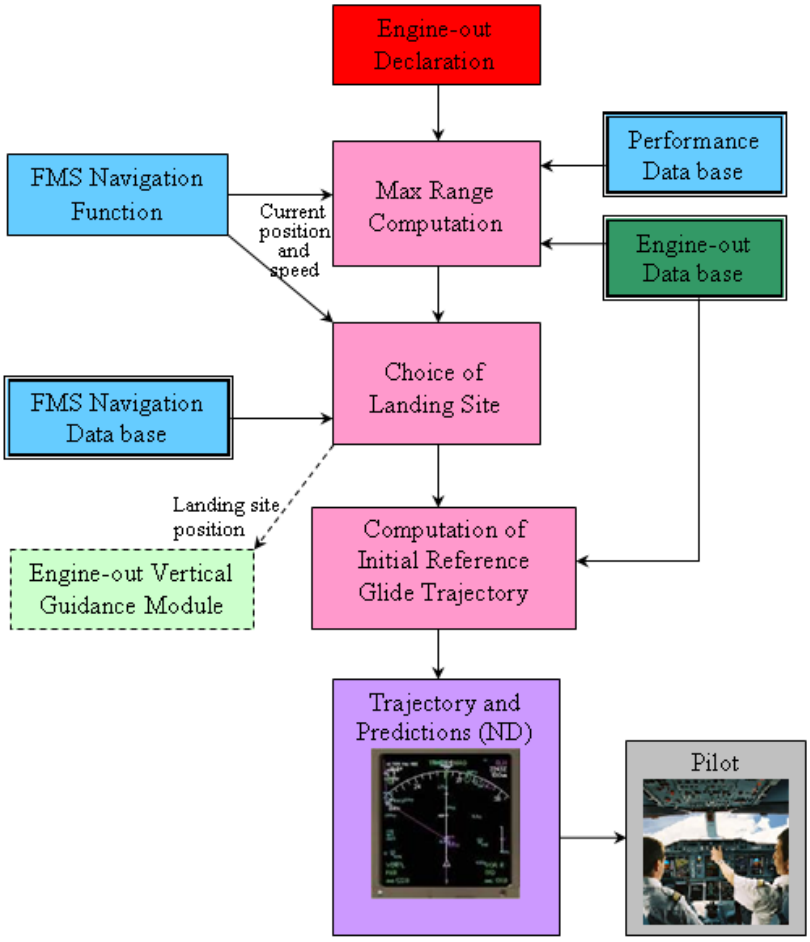

Figure 8.20 Reference glide trajectory computation steps

Then, a neural network device, similar to the one proposed in this chapter, can be used to generate on-line indications to the pilot. This on-line operation is essential since the aircraft is during the glide submitted to un-modeled perturbations while the actions taken by the pilot are not perfect. Then according to the current flight situation, which is in general different from the one derived from the initial reference glide trajectory, the neural network based engine-out vertical guidance module provides the pilot with an updated value for the reference pitch angle. This information can be integrated either in the Flight Director displays of the Primary Flight Display or in an Head Up Display, if available. It looks quite interesting to get at the final stage of the glide this information, as well as tendency information, on a Head Up Display.

The process generating the information which is produced on-line for the pilot and presented to him in the Primary Flight Display is shown in figure 8.21.

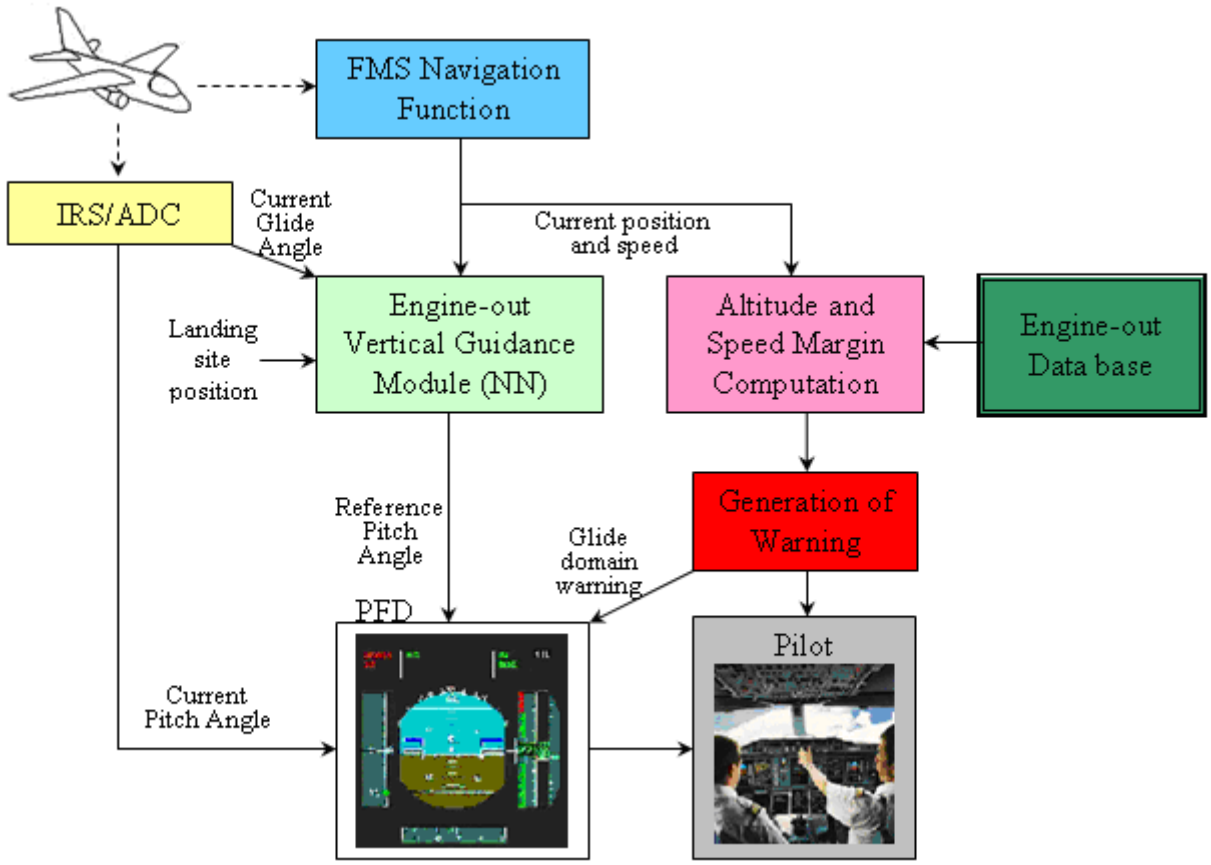

Figure 8.21 PFD engine-out information generation process

VIII.5.2 Tentative displays for controlled operation in Engine-Out situation

In this section, the possible information are presented to be displayed on the Primary Flight Display when the structure sketched in the previous section, based on the Engine-out Data Base and the Neural Network Vertical Guidance device, is put to work. Here we consider three situations:

a- Glide into domain situation

In this case the aircraft is inside the safe glide domain and the information displayed to the pilot on the PFD is the following:

- The active emergency manual mode: *Pitch at glide* (PAG), which is indicated at the normal position of longitudinal automated guidance modes in the Flight Mode Annonciator .
- The estimated landing situation: *On range* , which is indicated at the normal position of landing capacity information in the Flight Mode Annonciator .
- The reference pitch angle value represented by the pitch bar of the Flight Director.
- The current pitch angle given by the artificial horizon.
- On the speed indicator the current Conventional Airspeed, with its tendency. Also, the green dot speed corresponding to max range is displayed.
- On the Flight Level indicator, the current flight level with its upper and lower flight levels current limits with respect to the glide domain.
- The current vertical speed.

Here no information with respect to the lateral situation is included since this question has not been considered in this study.

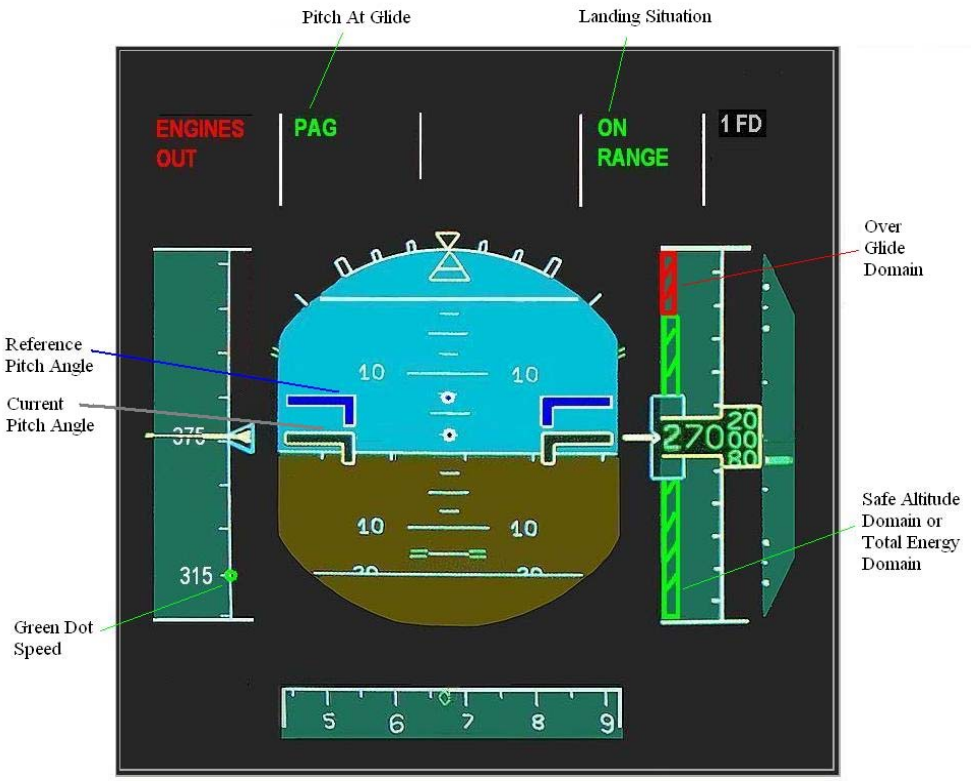

Figure 8.22 Proposed indications on PFD for *on range* glide situation

b- Over glide domain situation

In this case the aircraft is over the safe glide domain because its total energy (altitude and speed) is too large. For example, it may be too high and too fast near the tentative landing place to achieve a steady glide towards it. In that case a possible solution is for the pilot to extent the airbrakes. This will make the aircraft loose at high rate altitude and speed. Then when the aircraft enters within the safe glide domain, airbrakes will be retracted by the pilot and the manual mode *Pitch At Glide* will be announced. Then the aircraft has returned to the *glide into domain* situation.

In the transient *over glide domain* situation, the information displayed to the pilot on the PFD is the following:

- The active emergency mode: *Air brakes Descent* (ABK), with the *Pitch At Glide* mode indicated as armed at the normal position of longitudinal automated guidance modes in the Flight Mode Annonciator .
- The estimated landing situation: *Over range* , which is indicated at the normal position of landing capacity information in the Flight Mode Annonciator .
- The reference pitch angle value represented by the pitch bar of the Flight Director and which is maintained constant at a negative value (-10° in figure 8.23) compatible with speed constraints during this phase.
- The current pitch angle given by the artificial horizon.
- On the speed indicator the current Conventional Airspeed, with its tendency and the upper current limit with respect to the glide domain. Also, the green dot speed corresponding to max range is displayed.
- On the Flight Level indicator, the current flight level with its upper flight level current limits with respect to the glide domain.
- The current vertical speed.

Here also no information with respect to the lateral situation is included since this question has not been considered in this study.

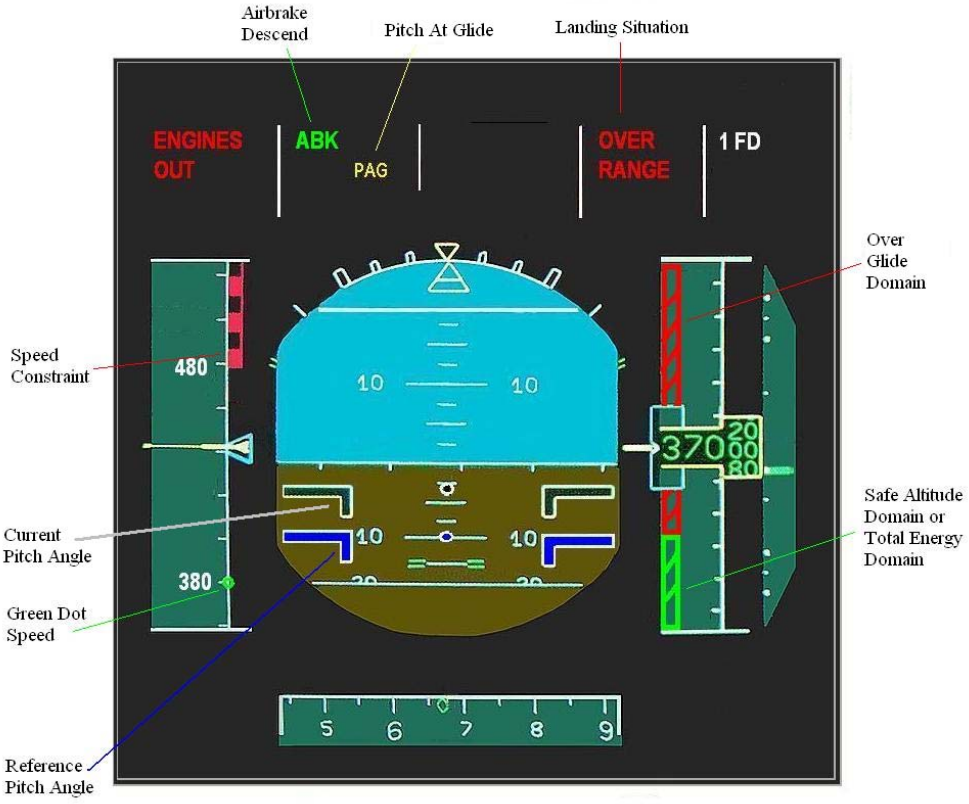

Figure 8.23 Proposed indications on PFD for *over range* glide situation

c- Glide below domain situation

In this case the aircraft is bellow the safe glide domain and the intended landing place cannot be reached anymore. A new final destination must be chosen, either with the help of an enhanced Flight Management System or directly by the pilot. Meanwhile it is supposed that the pilot adopts a speed near the max endurance speed (a margin may be taken to avoid too high values for the angle of attack) and the information displayed to the pilot on the PFD is the following:

- The active emergency manual mode: *Max Endurance Glide* (MEG), which is indicated at the normal position of longitudinal automated guidance modes in the Flight Mode Annonciator .
- The estimated landing situation: *Out of range* , which is indicated at the normal position of landing capacity information in the Flight Mode Annonciator .
- No reference pitch angle value is displayed in that case.

- The current pitch angle given by the artificial horizon.
- On the speed indicator the current Conventional Airspeed, with its tendency and the lower current limit with respect to the glide domain. Here the green dot represents the max endurance speed (with a possible margin to avoid stall) to be adopted by the pilot through the choice of the pitch angle.
- On the Flight Level indicator, the current flight level with the lower flight level current limit with respect to the glide domain.
- The current vertical speed.

Here also, no information with respect to the lateral situation is included since this question has not been considered in this study.

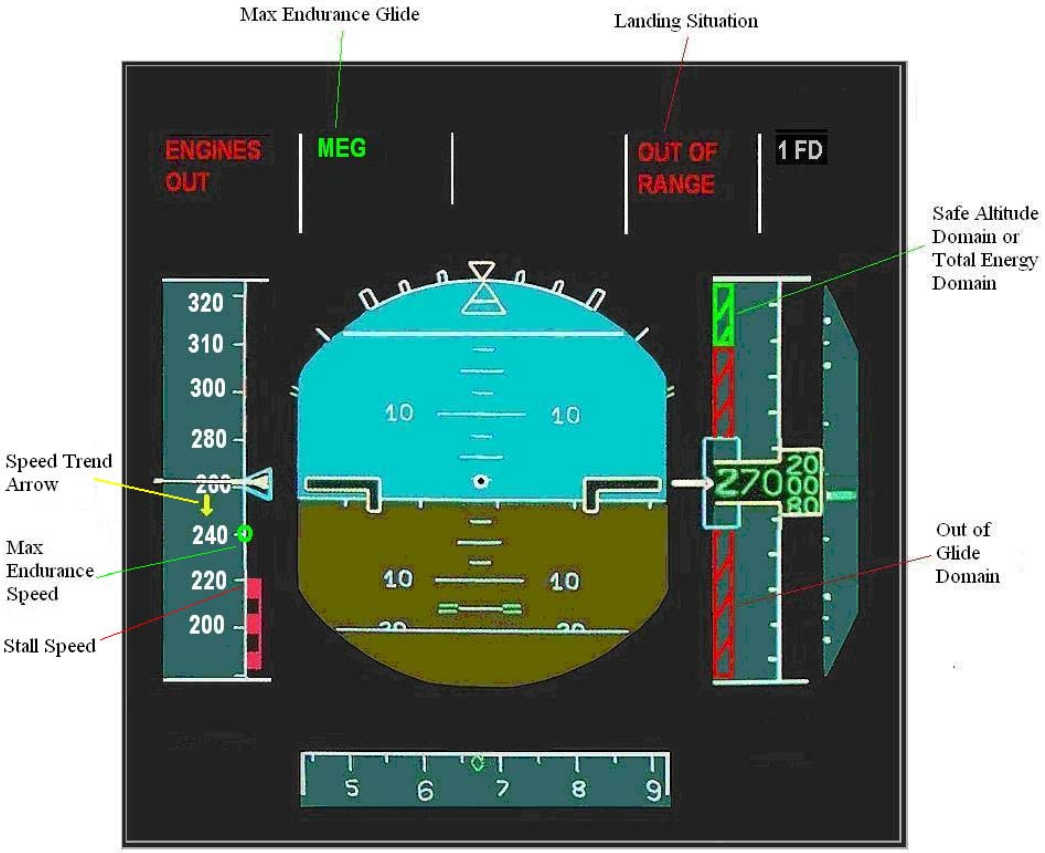

Figure 8.24 Proposed indications on PFD for *out of range* glide situation

VIII.6 Conclusion

In this chapter, a new tool has been developed to take profit of the data base generated by the Reverse Dynamic Programming process described in the previous chapter. The objective has been to design a new device whose function, similarly to the functions of a flight Director in normal flight, is to help the pilot to take adequate piloting actions so that the aircraft follows a safe glide trajectory leading to target site with some probability of landing with success. This tool has been based on a feed-forward neural network structure which has been designed, trained and validated with the aim of covering the whole glide domain of the aircraft in an engine-out situation.

It has been found that the effective training and subsequent validation of the neural network structure are intricate tasks and must be achieved through the design of several local feed-forward neural networks whose overall unification is performed through a fuzzy operator. However, the resulting computational module, which is basically an input-output device, can be operated on-line to provide useful advice to the pilot in a responsive way.

Several simulation results have been produced with different ranges or with different winds (head winds as well as tail winds). It appears that the necessary pitch angle to be adopted along a safe glide trajectory suffers large variations during the maneuver and depends also on the glide range and the estimated wind conditions.

Finally, a tentative display of the generated information to the pilot is proposed. It is proposed to provide this information to the pilot through the Primary Flight Display. The computed pitch reference value is reported and compared with the current pitch angle while information about the engine-out situation, the glide situation (over range, on range and out of range) and the speed and flight level limitations are displayed in the Flight Mode Anonciator (Engine status, landing capability), the Speed Indicator and the Flight Level Indicator. According to the landing capability information to employ the air brakes is also provided as well as advice to acquire and maintain maximum endurance attitude.

CHAPTER IX

GENERAL CONCLUSION

IX.1 Main Objective of the Thesis

The search for a safer air transportation operation within the Civil Aviation System is a never ending enterprise for engineers, operators and rule makers. Along the last decades new devices such as Ground Proximity Warning Systems, Anti Collision Avoidance Systems and others have been made available for the transportation aircraft operated by Civil Aviation at high cost through complex development processes involving concept definition, safety , feasibility and integration studies, effective design, tests and validation. The effective introduction of these systems, often urged by accidents whose occurrence was related to the lack of equivalent equipments, has been in general difficult .

The purpose of this study has been to make an initial contribution to the management and control of a critical situation, engine-out, which can be considered according to statistics a rare event but which has known recently some spectacular occurrences with diverse endings. The proposed contribution is relative to the feasibility of an advisory system which should provide to the pilot reference attitude information so that “safe” gliding trajectories can be performed. This should be also a factor limiting the stress of the pilot during this critical situation and leading him to enter the final landing phase with better moods.

IX.2 Achievements

First, the on-board consequences of an engine-out situation for a transportation aircraft have been considered to get a view as well of the remaining capabilities for flight control as of the cabin conditions for passengers and crew.

Then engine-out glide has been considered from the point of view of flight dynamics and flight domain constraints and finally from the point of view of flight performances including maximum range glide and maximum endurance glide. The concept of steady glide has been investigated and its stability with respect to wind perturbations has been studied, showing that in this situation, actions from the pilot are necessary to maintain a safe glide trajectory.

Then, after reviewing the main trajectory optimization techniques available in the scientific literature to deal with the generation of efficient aircraft trajectories, Reverse Dynamic

Programming has been adopted to generate optimal glide trajectories meeting all flight domain limitations. The Reverse Dynamic Programming process has been effectively adapted to the considered problem, needing the introduction of many practical settings to make feasible the resulting computational task. The adoption of the Reverse Dynamic Programming approach has led, when applied, to the generation of a whole data base about safe glide trajectories starting at different initial flight situations.

Finally, a neural network structure has been built using this data base to develop an on-line decision system to help the pilot choose the right pitch angle all along the glide trajectory leading to a landing situation with some survivability perspective. A tentative interface between the proposed emergency function and the pilot has been also sketched.

IX.3 Perspectives for Further Research and Development

This initial study could be developed in different directions so that an efficient and robust management and advisory system for engine-out situations can be turned available. Important issues such as:

- the choice of an on range safe landing site,
- the effectiveness of lateral maneuvers during engine-out glide, including their consequences with respect to total energy, speed and maximum range,
- the development of wind estimation techniques, useful even in normal flight, and the integration of these estimates in the advisory decision making module,
- the development of on-board flight parameter estimators, including current values of inertial parameters (mass and inertia moments) and aerodynamic parameters (additional drag from the failed-off engines),
- the adoption of improved versions for the proposed Reverse Dynamic Programming method,
- the development of a neural network development tool to better process the trajectory data base provided by the Reverse Dynamic Programming process and improve the computation of the pitch angle reference value.
- the development by specialists of an effective Man Machine Interface to provide the useful information to the pilot during an engine-out glide.

- the integration at low cost and complexity of this new function into the on-board computers coping with Flight Protections.

It is worth to observe that many of the above proposals can have positive consequences for the improvement of the efficiency of other pre-existing functions coping with flight management and protection.

ANNEX A

REFERENCE AIRCRAFT PARAMETERS

Values of the parameters (reference transportation aircraft)

This research is based on data relative to a standard transportation aircraft. The adopted values of the main parameters considered in the computation of flight performance and simulation studies in this thesis, are the following:

- m = 120000kg, the weight of aircraft;
- $I_{yy} = 9.72*10^6$, mass inertia moments of the body about the Y_B;
- $I_{xx} = 5.55*10^6$, mass inertia moments of the body about the X_B;
- $I_{zz} = 14.5*10^6$, mass inertia moments of the body about the Z_B;
- $I_{xz} = -3.3*10^4$, inertia product;
- b=43.9m, wing span;
- $S = 260m^2$, surface area of wing;
- $c_{ma} = 6.61$;
- $C_{l0} = 0$;
- $C_{l\alpha} = 4.982$;
- $C_{l\delta e} = 0.435$;
- $C_{lq} = -0.7$;
- $C_{l\alpha'} = -0.3$;
- $C_{m0} = -0.025$;
- $C_{m\alpha} = -1.246$;
- $C_{m\delta e} = -1.46$;
- $C_{mq} = -15$;
- $C_{m\alpha'} = -5$;
- $C_{d0} = 0.0175$;
- $k = 0.06$;
- $C_{Lp} = -13$;
- $C_{Np} = -1.5$;

ANNEX B

NON-LINEAR DYNAMIC SYSTEM STABILITY

B.1 Introduction

The notion of stability plays a key role in the study of the dynamics of physical systems. This property can be established or refuted through numerical resolution of the differential equations describing its dynamics and by the analysis of temporal trajectories calculated explicitly from different initial conditions. This approach is particularly arduous, and some theoretical results have been established to analyze directly the stability of a dynamic system through its mathematical model. A major contribution was provided in this area in 1892 by the Russian scientist Alexander Lyapunov Mikhalovich. He introduced the main basic concepts and theoretical results on the stability of dynamical systems described by a finite set of differential equations. Here, a simplified and shortened version of his work is presented.

Lyapunov theory has been recognized and employed just since 1960 when the concept of state model was adopted by the Automation and Cybernetics researchers.

B.2 The State Models

The dynamic evolution of a continuous system is modelled here by differential equations which consider the derivative with respect to the time of the vector $\underline{x}(t)$, denoted as $\dot{\underline{x}}(t)$. The vector $\underline{x}(t)$ represents the minimum information about the state of the system, which is called system state vector, necessary to describe its physical state over a given time span. Its derivative is expressed as a function of its instantaneous value and the influence of the external input vector $\underline{u}(t)$ as:

$$\dot{\underline{x}}(t) = F(\underline{x}(t), \underline{u}(t)) \tag{B.1}$$

Here $\underline{x}(t) \in R^n$, $\underline{u}(t) \in R^m$, n, m are integers and F is a continuous function of R^{n+m} in R^n . So, knowing the initial state of the system and the sequence of control inputs it is possible to calculate the system state at any moment after Initial time by using equation (B.1).

For a physical system, the differential representation is built according to the involved laws of Physics. In the following of this annex, the considered system behavior is given by an autonomous model such as:

$$\dot{\underline{x}} = f(\underline{x}(t)) \tag{B.2}$$

in which there can be no entries, or when the level of the inputs for the state model (B.1) is given by a state feedback expression such as:

$$\underline{u}(t) = h(\underline{x}(t)) \tag{B.3}$$

where h is the function of R^n in R^m.

For a given initial condition $\underline{x}(t_0)=\underline{x}_0$, the differential equation (B.2) implies (Cauchy's theorem) a unique trajectory in R^n called the *system trajectory in the state space*.

Often, these state trajectories develop toward some fixed points called *equilibrium states*. It is said that $\underline{x}$ is an equilibrium state for the system given by equation (B.2) if:

$$\underline{x}(t_1) = \underline{x}_e \Rightarrow \forall t \geq t_1 \quad \underline{x}(t) = \underline{x}_e \tag{B.4}$$

A necessary condition is that:

$$f(\underline{x}_e) = 0 \tag{B.5}$$

B.3 Concepts of Stability at an Equilibrium Point

B.3.1 Stability of an equilibrium point (as defined by Lyapunov):

The equilibrium state $\underline{x}_e$ is said to be *stable* according to Lyapunov if $\forall \varepsilon > 0$ there exists a non-empty neighborhood $V_{x_e}(\varepsilon)$ of $\underline{x}_e$ such as:

$$\underline{x}(0) \in V_{\underline{x}_e}(\varepsilon) \Rightarrow \left\|\underline{x}(t) - \underline{x}_e\right\| < \varepsilon \quad (\forall\, t > 0) \tag{B.6}$$

where $\| \ \|$ is the Euclidean norm in R^n.

Otherwise, the equilibrium state $\underline{x}_e$ is said *unstable*.

When the system is stable according to Lyapunov around an equilibrium point $\underline{x}_e$, the trajectory of the system state becomes arbitrarily close to $\underline{x}_e$, if the initial state is close enough to $\underline{x}_e$.

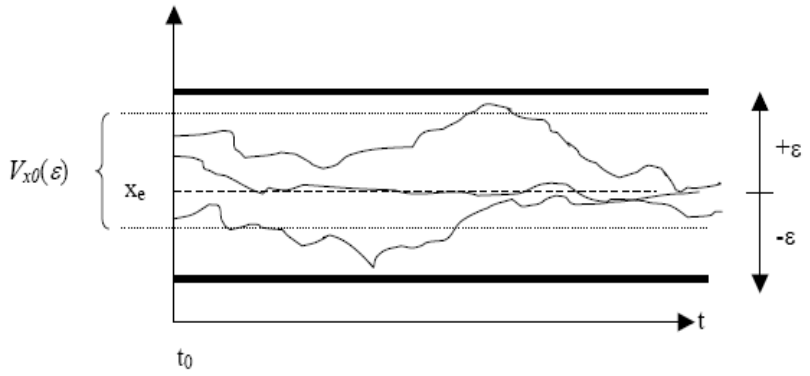

Figure B.1 Lyapunov stability

B.3.2 Asymptotic stability:

An equilibrium point $\underline{x}_e$ is said to be *asymptotically stable* if it is stable and if:

$$\exists\, \alpha > 0 : \left\| \underline{x}(0) - \underline{x}_e \right\| < \alpha \Rightarrow \lim_{t \to +\infty} \underline{x}(t) = \underline{x}_e \tag{B.7}$$

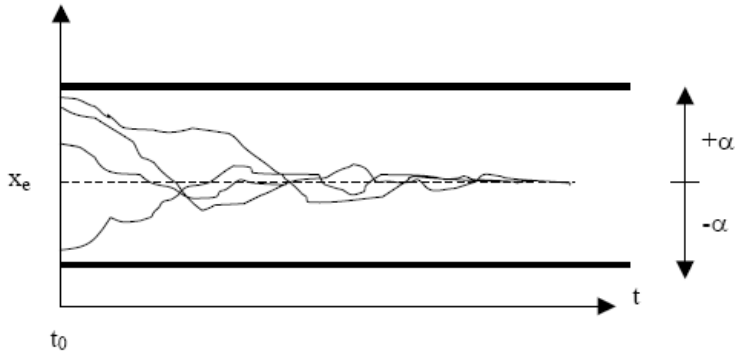

Figure B.2 Asymptotic stability

Asymptotic stability not only means that the equilibrium point $\underline{x}_e$ is stable but also means that there is a non-empty neighborhood of the equilibrium point such that any trajectory, with an initial state $\underline{x}_0$ belonging to that neighborhood, tends to $\underline{x}_e$ when $t \to +\infty$.

B.3.3 Exponential stability:

An equilibrium point $\underline{x}_e$ is exponential stable if there are two positive real numbers a and λ such as:

$$\forall t > 0,\ \exists r > 0,\ \forall \underline{x}_0 \in B(\underline{x}_e, r),\ \left\| \underline{x}(t) - \underline{x}_e \right\| \le a \cdot \left\| \underline{x}(0) - \underline{x}_e \right\| \cdot e^{-\lambda t} \tag{B.8}$$

where $B(\underline{x}_e,r)$ is a ball of center $\underline{x}_e$ and radius r. This means that the state vector under an initial condition $\underline{x}(0) \in B(\underline{x}_e, r)$ converges to $\underline{x}_e$ faster than an exponential function. The parameter λ is named the *rate of convergence*.

B.3.4 Global stability:

If the property of asymptotic stability towards an equilibrium state is satisfied whatever the initial state $\underline{x}(0)$ is, the equilibrium point is said to be *globally stable*.

Usually, if the asymptotic, exponential or global stability of an equilibrium point can be established, it is useful to determine the largest neighborhoods of the equilibrium point for which the property is satisfied. This will lead to defining *attraction areas* and *exponential stability areas* around an equilibrium point.

B.3.5 Stability of a trajectory:

In some cases where the system has no stable equilibrium point, it may be possible to find trajectories that do not diverge so far, they are said to be *stable trajectories*. Different cases can happen:

- the system admits a stable domain, if there is a non-empty open interval of R^n so that the trajectories from a initial point in this open interval are included in it during their whole evolution
- the system admits an attraction area, if there is an open interval R^n so that all trajectories, regardless of their origin, finish at the end of a finite time by returning to this open interval and stay there;
- the system admits a trajectory f_e stable, if for any given $\varepsilon > 0$, there is $a > 0$, so that if $\|f(0) - f_e(0)\| < a$, then for all $\|f(t) - f_e(t)\| < \varepsilon$.

In a similar way it is possible to define an attractive trajectory and the notions of asymptotic area or exponential (global or no) stability area around a given path.

To study more easily the stability of a dynamic system, Lyapunov introduced various auxiliary functions.

B.4 The Lyapunov Method

B.4.1 Lyapunov candidate functions:

Here $U : \underline{x} \in R^n \mapsto U(\underline{x}) \in R^+$ is a function such that:

i) $U(\underline{x})$ is continuously differentiable,

ii) $U(\underline{0}) = 0$ and $U(\underline{x}) > 0$ if $\underline{x} \neq 0$,

iii) there are two scalar functions a and b of P^+ in P^+, which are continuous, monotonic and increasing, such as

$$a(0) = b(0) = 0 \text{ and } \forall \underline{x} \in R^n \qquad a\left(\|\underline{x}\|\right) \leq U(\underline{x}) \leq b\left(\|\underline{x}\|\right) \tag{B.9}$$

then $U(x)$ is a candidate function of Lyapunov.

A candidate function of Lyapunov $U(\underline{x})$ defines the equation of a curve by $U(\underline{x})$ = constant, named Lyapunov equipotent, bounding convex domains around the origin if $D_1 = \{\underline{x} \mid U(\underline{x}) \leq c_1\}$, $D_2 = \{\underline{x} \mid U(\underline{x}) \leq c_2\}$ with $c_1 < c_2$, then $D_1 \subset D_2$.

B.4.2 Lyapunov Derivative:

Here $U : R^n \to R$ is a continuously differentiable function and the non-linear differential equation is $\dot{\underline{x}} = f(x), \quad \underline{x} \in R^n$.

Then we define $L_{fU}(\underline{x}) : \underline{x} \in R^n \mapsto L_{fU}(\underline{x}) \in R$ by:

$$L_{f_U}(\underline{x}) = \langle \nabla U(\underline{x}), f(\underline{x}) \rangle \tag{B.10}$$

where $\nabla U(\underline{x})$ means the gradient vector of U with respect to $\underline{x}$ and $\langle , \rangle$ denotes the scalar product on R^n. $L_{f_U}(\underline{x})$ is named the *Lie 1st order derivative* of $U(\underline{x})$ (also named Lyapunov derivative) or derivative of $U(\underline{x})$ along the trajectories of $\dot{\underline{x}} = f(\underline{x})$. This derivative corresponds to a time derivative of the composed function: $t \in i \mapsto U(\underline{x}(t)) \in i$. In fact, we have:

$$\langle \nabla U(\underline{x}), f(\underline{x}(t)) \rangle = \langle \nabla U(\underline{x}), \dot{\underline{x}}(t) \rangle = \frac{dU(\underline{x}(t))}{dt} \tag{B.11}$$

In the following part of this annex, the focus will be on the stability of autonomous systems of equation $\dot{\underline{x}} = f(\underline{x})$ which admits the origin as equilibrium point ($f(\underline{0}) = \underline{0}$).

B.4.3 Local asymptotic stability:

If there is a scalar function $U(\underline{x})$ in which the first partial derivatives are continuous and a neighborhood $V_{\underline{x}_e}$ of the equilibrium point $\underline{x}_e$ is such that:

1) U is a Lyapunov candidate function,

2) L_{f_U} , which is a derivative of $U(\underline{x})$ along the trajectories of $\dot{\underline{x}} = f(\underline{x})$, is negative or zero in all neighbourhood $V_{\underline{x}_e}$,

then $\underline{x}_e$ is a stable equilibrium point.

For any area bounded by an Lyapunov equipotent contained in $V_{\underline{x}_e}$:

$$\underline{x}(0) \in V_{\underline{x}_e} \Rightarrow \forall t > 0, \underline{x}(t) \in V_{\underline{x}_e} \tag{B.12}$$

If L_{f_U} is locally defined negative in $V_{\underline{x}_e}$ (i.e. $L_{fU}(\underline{x}) < 0$, $\forall x \in V_{\underline{x}_e} - \{\underline{x}_e\}$), then the stability is known as *locally asymptotic* in the part of the space bounded by a Lyapunov equipotent curve contained in $V_{\underline{x}_e}$:

$$\underline{x}(0) \in V_{\underline{x}_e} \Rightarrow \lim_{t \to +\infty} \underline{x}(t) = 0 \tag{B.13}$$

If the second condition is satisfied, it is possible to conclude of the stability of the equilibrium point, and if no conclusion can be made by using $U(\underline{x})$, it is possible to try to find a new Lyapunov candidate function to try to prove the stability of the equilibrium point.

B.4.4 Global asymptotic stability:

If there is a function U such that:

1) U is a Lyapunov candidate function,

2) $\dot{U}$, which is a derivative of $U(\underline{x})$ along the trajectories of $\dot{\underline{x}} = f(\underline{x})$, is defined negative,

3) The condition $\|\underline{x}\| \to +\infty$ implies that $U(\underline{x}) \to +\infty$,

then the origin is a globally and asymptotically equilibrium stable equilibrium point.

An important limitation of this approach is that it does not provide an infallible method for studying the nature of the equilibrium points and the associated stability areas of nonlinear systems. There is no general method for choosing a Lyapunov function and in many situations, physical considerations and past experience are useful to perform an adequate choice. Nevertheless, some methods have been designed to establish sufficient conditions of stability.

B.4.5 Examples of Lyapunov candidate function:

- Lyapunov quadratic candidate function: if a symmetric matrix P is defined positive, then $U(\underline{x}) = \underline{x}^T P \underline{x}$ is a Lyapunov candidate function. Here, the Lyapunov equipotent are ellipsoids of half-axes defined by the eigenvalues and eigenvector of P. The derivative of this Lyapunov function U is written as:

$$L_{fU}(\underline{x}) = \underline{x}^T P f(\underline{x}) + f(\underline{x})^T P \underline{x} \tag{B.14}$$

- Lyapunov candidate function is based on the norm of the maximum:

$$U(\underline{x}) = \max_{i=1,\cdots,n} |\underline{x}_i| \tag{B.15}$$

Here, the Lyapunov equipotent are hypercube indirectly parallel to the axes of the space vector and the derivative of Lyapunov is written:

$$L_{fU}(\underline{x}) = f_{i^*}(\underline{x}) \cdot \text{sign}(\underline{x}_{i^*}) \text{, where } i^* \text{ is that : } U(\underline{x}) = \max |\underline{x}_i| = \underline{x}_{i^*} \cdot \text{sign}(\underline{x}_{i^*}) \tag{B.16}$$

- Lyapunov candidate function is based on the dual norm of the maximum:

$$U(\underline{x}) = \sum_{i=1}^{n} |\underline{x}_i| \tag{B.17}$$

Here, the Lyapunov equipotentials are hypercubes of vertex positioned on the axes of the vector space. The derivative of Lyapunov is written as:

$$L_{fU}(\underline{x}) = \sum_{i=1}^{n} f_i(\underline{x}) \cdot \text{signe}(\underline{x}_i) \tag{B.18}$$

B.4.6 Krasovskii method:

This method consists in proposing a Lyapunov candidate function of the form $U(\underline{x}) = f(\underline{x})^T \; f(\underline{x})$ and in testing if this function is a Lyapunov function.

In fact we can show that if the matrix $F(\underline{x}) = A(\underline{x}) + A(\underline{x})^T$, where $A(\underline{x}) = [\partial f / \partial \underline{x}]$ is a Jacobian matrix, is defined negative in a neighborhood $V_{\underline{x}_e}$ of a final equilibrium point, then this equilibrium point is locally asymptotically stable and $U(\underline{x}) = f(\underline{x})^T f(\underline{x})$ is a Lyapunov function for this system . It can also be shown that, $V_{\underline{x}_e} \equiv R^n$ and $\lim U(\underline{x}) = +\infty$ when $\underline{x} \to +\infty$, then the equilibrium point is globally asymptotically stable.

B.5 Linear Systems Case:

In the case of linear systems, Lyapunov established the following resolution:

Lyapunov Theory: in the case of linear system:

$$\dot{\underline{x}} = A\,\underline{x} \text{ where } A \in R^{n\times m} \tag{B.19}$$

a necessary and sufficient condition for such system, which should be asymptotically stable around the origin, is that for any symmetric positive matrix Q ($Q = Q^T$, $Q > 0$), the symmetric matrix P, only solution of the Lyapunov algebraic equation:

$$A^T P + PA = -Q \tag{B.20}$$

should be defined positive.

Sufficient condition: Q should be a positive symmetric matrix (i.e. the matrix of a positive real quadratic form) and P should be a symmetric matrix defined positive solution of equation (B.20). Considering the Lyapunov candidate function as $U(\underline{x}) = \underline{x}^T P \underline{x}$, then we have:

$$L_{fU}(\underline{x}) = \dot{\underline{x}}^T Px + \underline{x}^T P\,\dot{\underline{x}} = \underline{x}^T (A^T P + PA)\underline{x} \tag{B.21}$$

and the system is asymptotically stable at origin.

Necessary Condition: If $\underline{V_i}$ is an eigenvector to the right of A with eigenvalue λ_i , it is necessary that it has a real part Re (λ_i), which is strictly negative, for there is asymptotic stability of the origin. In fact, the solution of equation (B.19) from an initial condition equal to $\underline{V_i}$ is given by:

$$\underline{x}(t) = \exp(\lambda_i\, t)\,\underline{V_i} \tag{B.22}$$

This condition implies the non-uniqueness of A.

Then, with solution P of equation (B.20) :

$$\frac{d}{dt}(\underline{\bar{x}}^T P\,\underline{x})_{\underline{x}=\underline{V_i}} = (\underline{\bar{x}}^T P\,\dot{\underline{x}})_{\underline{x}=\underline{V_i}} + (\underline{x}^T P\,\underline{x})_{\underline{x}=\underline{V_i}} = 2\mathrm{Re}(\lambda_i)(\underline{V_i}^T P\,\underline{V_i}) < 0 \tag{B.33}$$

where for a number (or vector) z, complex $\bar{z}$ that means its conjugate, was necessarily to ensure the asymptotic stability: $\underline{\bar{V}_i}^T P\,\underline{V_i} > 0$ for all eigenvector of A whose gather forms a base of R^n. A necessary condition is that the real matrix P should be positive.

ANNEX C

EXAMPLES OF NUMERICAL INTEGRATION METHODS AND EVALUATION

C.1 Introduction

In flight trajectory optimization problems, the aircraft dynamic is described by a group of differential equations, which leads to an initial value problem when we want to study the characteristic or performance of the aircraft starting from a given initial situation. This initial value problem exists not only in trajectory optimization domain, but also in control, mechanics, electric analysis, astral movement, etc, and most time its solution cannot be worked out in a closed form. To solve this problem there exist many numerical, such as Euler's method and improved Euler's method, Runge-Kutta Method, Milne-Simpson method, Hamming's method, etc. Generally, the more complex the method is, the less the error is. In Runge-Kutta method, the order of integration can be chosen according to this error requirement. It is widely used as a tool for solving ordinary differential equations in a numerical way.

C.2 Euler's Method

Supposing the system is described by following equation:

$$\dot{\underline{x}} = f(\underline{x}, \underline{u}) \text{ with } \underline{x}(t_0) = \underline{x}_0 \tag{C.1}$$

where $\underline{x}$ is the state vector, and $\underline{u}$ is control vector. The solution should be calculated over the given range $[t_0, t_f]$ under the certain initial condition x_0. No matter what kind of method is used to solve the problem, the integration range should be divided into small intervals by serials point t_i (i=0, 1, 2, …, n), whose value increases step by step. And the interval between the two adjacent points is called integration step, $h=t_{i+1}-t_i$, which could be fixed or variable.

Here Taylor expansion is used to approximate x at $t_1= t_0+h$ under the initial condition of $\underline{x}_0$:

$$\underline{x}(t_1) = \underline{x}(t_0 + h) = \underline{x}_0 + h \cdot \underline{x}'(t_0) + \frac{h^2}{2}\underline{x}''(t_0) + \cdots \tag{C.2-a}$$

and

$$\underline{\varepsilon}_1 = \frac{h^2}{2}\underline{x}''(t_0) + \cdots = O(h^2) \tag{C.2-b}$$

If h is small enough to make ε_1 less than some certain value, $\underline{x}(t_1)$ could be approximated by a simplified equation:

$$\underline{x}(t_1) = \underline{x}_0 + h \cdot \underline{x}'(t_0) + O(h^2) \approx \underline{x}_0 + h \cdot \underline{x}'(t_0) \tag{C.3}$$

Thus the state at each point can be calculated step by step from the initial point with the accumulated errors $\underline{\varepsilon}$.

$$\underline{\varepsilon}_{n+1} = (1 + h \cdot \frac{\partial f}{\partial \underline{x}})\underline{\varepsilon}_n + O(h^2) \tag{C.4}$$

This equation indicates that the dynamics of the error can be considered to be linear. If $\frac{\partial f}{\partial \underline{x}} < 0$ or $-2 < h\frac{\partial f}{\partial \underline{x}} < 0$, the error ε_{n+1} will converge absolutely.

To decrease the error, $\underline{x}(t_1)$ could be approximated by:

$$\underline{x}(t_1) = \underline{x}_0 + \frac{1}{2}h \cdot (\underline{x}'(t_0) + \underline{x}'(t_1)) + O(h^2) \approx \underline{x}_0 + \frac{1}{2}h \cdot (\underline{x}'(t_0) + \underline{x}'(t_1)) \tag{C.5}$$

here stage values should be predicted by (C.3), and thus $\underline{x}'(t_1)$ could be replaced with:

$$\underline{x}'(t_1) = f(\underline{x}(t_1)) \tag{C.6}$$

So the equation (C.5) is rewritten as:

$$\underline{x}(t_1) \approx \underline{x}_0 + \frac{1}{2}h \cdot (f(\underline{x}(t_0) + f(\underline{x}(t_0) + h \cdot f(\underline{x}(t_0))) \tag{C.7}$$

This method is called Trapezoidal method [ISERLES A.] or improved Euler's method. It is also called as a kind of second-order Runge-Kutta method [BOSEDE O. R.].

C.3 Runge-Kutta Method

Runge-Kutta method is widely used to solve ordinary differential equations. By using the Taylor series expansion about the $(n+1)^{th}$ step:

$$\underline{x}_{n+1} = \underline{x}(t_{n+1}) = \underline{x}(t_n + h) = \underline{x}_n + h \cdot \underline{x}'(t_n) + \frac{h^2}{2}\underline{x}''(t_n) + \cdots + \frac{1}{p!}h^p \underline{x}_n^{(p)} + O(h^{p+1}) \tag{C.8}$$

with equation (C.1), x_{n+1} is written as:

$$\underline{x}_{n+1} = \underline{x}_n + h \cdot f_n + \frac{h^2}{2}\left(\frac{df}{d\underline{x}}\right)_n + \cdots + \frac{1}{p!}h^p\left(\frac{d^{p-1}f}{d\underline{x}^{p-1}}\right) + O(h^{p+1}) \tag{C.9}$$

If the q-stage Runge-Kutta method is adpoted, which means that $\underline{x}_{n+1}$ is approximated by $\underline{X}_{n+1}$

$$\underline{X}_{n+1} = \underline{X}_n + h \cdot \sum_{i=1}^{q} \mu_i f\left(t_n + \lambda_i h, \underline{X}\left(t_n + \lambda_i h\right)\right) = \underline{X}_n + h \cdot \sum_{i=1}^{q} \mu_i k_i \tag{C.10}$$

Generally the higher stage number means more accuracy. And the increment between the two states is approximated by:

$$\int_{t_n}^{t_{n+1}} f(\underline{x}, \underline{u})\, dt \approx h \cdot \sum_{i=1}^{q} \mu_i f\left(t_n + \lambda_i h, \underline{X}\left(t_n + \lambda_i h\right)\right) \tag{C.11}$$

then

$$\underline{X}_{n+1} = \underline{X}_n + h \cdot \sum_{i=1}^{q} \mu_i f\left(t_n + \lambda_i h, \underline{X}\left(t_n + \lambda_i h\right)\right) = X_n + h \cdot \varphi(t_n, \underline{X}_n, h) \tag{C.12}$$

where $\varphi(t_n, \underline{X}_n, h) = \sum_{i=1}^{q} \mu_i k_i$, and

$$k_1 = f\left(t_n, \underline{X}_n\right) \tag{C.13-a}$$

$$k_i = f\left(t_n + \lambda_i h, \underline{X}_n + h\sum_{j=1}^{i-1} \eta_j k_j\right) \quad i = 2, \ldots, q \tag{C.13-b}$$

when q =1, it is identical to the Euler's method.

then

$$\underline{X}_{n+1} = \underline{X}_n + h \cdot \sum_{i=1}^{q} \mu_i k_i \tag{C.14}$$

We can write global truncation $\underline{e}_{n+1}$ and local truncation error $\underline{T}_{n+1}$ as:

$$e_{n+1} = \left\| \underline{x}_{n+1} - \underline{X}_{n+1} \right\| \tag{C.15-a}$$

$$T_{n+1} = \left\| \underline{x}_{n+1} - \underline{x}_n - h\varphi(t_n, \underline{X}_n, h) \right\| \tag{C.15-b}$$

If the pth-order method is adopted, the local truncation error $\underline{T}_{n+1}$ is $O(h^{p+1})$. With equation (C.12), equation (C.15-a) is written as

$$\begin{aligned} e_{n+1} &= \left\| \underline{x}_{n+1} - \underline{X}_{n+1} \right\| \\ &= \left\| \underline{x}_{n+1} - \underline{X}_n - h\varphi(t_n, \underline{X}_n, h) \right\| \\ &\le \left\| \underline{x}_{n+1} - \underline{x}_n - h\varphi(t_n, \underline{X}_n, h) \right\| + \left\| \underline{x}_n - \underline{X}_n \right\| + h \left\| \varphi(t_n, \underline{x}_n, h) - \varphi(t_n, \underline{X}_n, h) \right\| \end{aligned} \tag{C.16}$$

If a Lipschitz condition in $\underline{x}$ is satisfied $\left\| \varphi(t_n, \underline{x}_n, h) - \varphi(t_n, \underline{X}_n, h) \right\| = L \cdot \left\| \underline{x}_n - \underline{X}_n \right\|$,

$$e_{n+1} \le T_{n+1} + e_n + hLe_n \tag{C.17}$$

where L is the Lipschitz constant. And in the same way, we can get

$$\begin{aligned} e_n &\le T_n + e_{n-1} + hLe_{n-1} \\ &\vdots \\ e_1 &\le T_1 + e_0 + hLe_0 \end{aligned} \tag{C.18}$$

Here we define $e_0 = \left\| \underline{x}_0 - \underline{X}_0 \right\|$. Supposing the initial values are exact $\underline{X}_0$, global truncation error is

$$e_n \le \left(\frac{(1+hL)^n - 1}{L} \right) \frac{T_{n+1}}{h} \tag{C.19}$$

So the global truncation error of a p^{th} order method is $O(h^p)$. With different step length, the local truncation errors are different. The difference between them is always used to estimate the error. For a p^{th} order method, the n^{th} step integration is carried on with step length h and then with step length $\frac{h}{2}$ twice. After that there are two new states generated, $\underline{X}_{n+1}$ and $\underline{\tilde{X}}_{n+1}$,

whose local truncation errors are $O(h^{p+1})$ and $O(\left(\frac{h}{2}\right)^{p+1})$ respectively, so the local truncation error is estimated as

$$\frac{\underline{X}_{n+1} - \underline{\tilde{X}}_{n+1}}{2^{p+1} - 1} \tag{C.20}$$

This equation provides us a way to adapt the integration step h to satisfy error requirement.

ANNEX D

FEED-FORWARD NEURAL NETWORKS TRAINING

D.1 Feed-Forward Neural Networks

Multilayer neural networks have been proved to be able to perform function approximation with an adequate selection of neural network structure and with enough learning process even though the selection of structure and learning algorithm still strongly depend on empirical rules from trial-and-errors for different cases. This method is successfully used in many fields, such as expert system, pattern recognition, intelligent control, combinatorial optimization, predictive control, etc. The neural network principle and application have been enriched and combined with other technology in the last decades.

D.2 Feed-forward Neural Network with Backward Propagation Algorithm

An artificial neuron is described in figure D.1, where *x*, *w*, *b*, *y* are respectively the input, the weight, the threshold and the output.

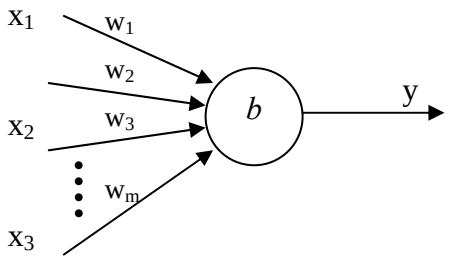

Figure D.1 Artificial neuron

The relation between input and output is given by

$$y = f(\sum_{i=1}^{m} x_i w_i - b) = f(\sum_{i=0}^{m} x_i w_i), \qquad (x_0 = -1, \qquad w_0 = b) \tag{D.1}$$

where *f* is the activation function. All neurons in the same layer usually have same activation function. The so-called sigmoid function, $f(x)=1/(1+exp(-x))$, is the most common activation function, then :

$$y = f(\sum_{i=1}^{m} x_i w_i - b) = \frac{1}{1+e^{-(\sum_{i=1}^{i=m} x_i w_i - b)}} = \frac{1}{1+e^{-\sum_{ii=01}^{m} x_i w_i}} \tag{D.2}$$

The neural network is composed of interconnected neurons, from one layer to the next in the case of feed-forward neural networks. The structure of a feed-forward artificial neural

network (ANN) is shown in figure D.2. In general a feed-forward ANN usually contains an input layer, a hidden layer and an output layer. Sometimes the hidden layer can be divided into several layers according to the degree of complexity. In general one hidden layer is enough for most system.

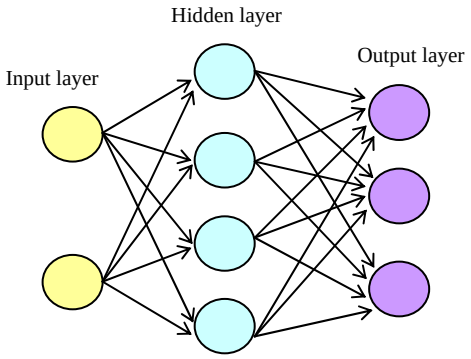

Figure D.2 The structure of a feed-forward ANN

Supposing x_j is input of the number j neuron in layer n, and y_i is output of the number i neuron in layer n-1which has m_{n-1} outputs, equation (D.1) can be rewritten as:

$$x_j = \sum_{i=1}^{m_{n-1}} y_i w_{ij} \tag{D.3}$$

where x_j is the weighted input of the neuron, and w_{ij} is the weight in the connection between the i^{th} neuron in layer n-1 and the j^{th} neuron in layer n. Considering a sigmoid activation function, the output of the j^{th} neuron is:

$$y_j = \frac{1}{1+e^{-x_j}} \tag{D.4}$$

For a 3-layer ANN, we obtain the relation between l^{th} output and the inputs x_{i0}, x_{i1}, x_{i2}, …, x_{im} of the ANN as follow:

$$y_{ol} = f_{ol}(\sum_j W_{olj} \cdot f_{hj}(\sum_k W_{hjk} \cdot f_{ik}(\sum_m W_{ikm} \cdot x_{im}))) \tag{D.5}$$

where:

y_{ol} -- the l^{th} output in output layer

f_{ol} -- the activation function of l^{th} neuron in output layer

W_{olj} – the weight between l^{th} neuron in output layer and j^{th} neuron in hidden layer

f_{hj} -- the activation function of j^{th} neuron in hidden layer

W_{hjk} – the weight between j^{th} neuron in hidden layer and k^{th} neuron in input layer

f_{ik} -- the activation function of k^{th} neuron in input layer

W_{ikm} – the weight between k^{th} neuron in input layer and m^{th} ANN input

If the desired output of neuron is y_d , the error of network can be calculated by

$$E = \frac{1}{2}\sum_j (y_j - y_{dj})^2 \tag{D.6}$$

So the error partial derivative, which illustrates the effect of y_j's variation to the error, is

$$E_{Y_j} = \frac{\partial E}{\partial y_j} = y_j - y_{dj} \tag{D.7}$$

and the effect of the total input to the error can be considered by

$$E_{X_j} = \frac{\partial E}{\partial x_j} = \frac{\partial E}{\partial y_j} \cdot \frac{\partial y_j}{\partial x_j} = E_{Y_j} \cdot y_j(1 - y_j) \tag{D.8}$$

Furthermore, when the weight changes, the error change of rate will be:

$$E_{W_{ij}} = \frac{\partial E}{\partial W_{ij}} = \frac{\partial E}{\partial x_j} \cdot \frac{\partial x_j}{\partial W_{ij}} = E_{X_j} \cdot y_i \tag{D.9}$$

When the output of a neuron in the last layer changes, the outputs of the connected neurons in the previous layers change correspondently. The equation can be obtained as :

$$E_{Y_i} = \frac{\partial E}{\partial y_i} = \sum_j \frac{\partial E}{\partial x_j} \cdot \frac{\partial x_j}{\partial y_j} = \sum_j E_{X_j} \cdot W_{ij} \tag{D.10}$$

The gradient descent is a common algorithm for optimization. We can adapt the weight matrix according to error change rate:

$$W_{ij}(n+1) = W_{ij}(n) + lr \cdot \delta_j \cdot y_j \tag{D.11}$$

where lr is learning rate of the network, and δ_j is error, whose definition is similar to E_{xj}, which is given in equation (D.7) and can be determined by equation (D.12):

$$\delta_j = \begin{cases} y_j(1 - y_j)(y_{dj} - y_{out}) & \text{if neuron } j \text{ is in output layer} \\ y_j(1 - y_j)\sum_k \delta_k W_{jk} & \text{if neuron } j \text{ is in hidden layer} \end{cases} \tag{D.12}$$

When the momentum factor, a, is introduced in to improve the learning performance, the equation of adapting weight is obtained as:

$$W_{ij}(n+1) = W_{ij}(n) + lr \cdot \delta_j \cdot y_j + a(W_{ij}(n) - W_{ij}(n-1)) \tag{D.13}$$

Normally the value of a is between 0 and 1.

In the Backward Propagation algorithm, the learning rates of all neurons are the same. It leads to a slow learning convergence speed and the deviation from the steepest descent direction. A feasible method to avoid these defects is determining the respective learning rate for each neuron according to previous solutions. And the activation function is modified as:

$$y_{oj} = \frac{2}{1+e^{-2(\sum_{i=1}^{m} y_{oi} w_{ij} - b)}} - 1 = \frac{2}{1+e^{-2\sum_{ii=01}^{m} x_i w_{ij}}} - 1 \tag{D.14}$$

So the error calculating equations are changed respectively:

$$\delta_{mj} = \begin{cases} (1+y_m)(1-y_m)(y_{dj} - y_{out}) & \text{if neuron m is in output layer} \\ (1+y_m)(1-y_m)\sum_k \delta_k W_{jk} & \text{if neuron m is in hidden layer} \end{cases} \tag{D.15}$$

The new weight for the next calculation is determined by equations (D.16):

$$W_{ij}(n+1) = W_{ij}(n) + lr_{ij} \cdot \sum_m \delta_{mj}(n) \cdot y_{omj}(n) \tag{D.16}$$

where,

$$lr_{ij}(n+1) = \begin{cases} lr_{ij}(n) \cdot a & if \sum_{\mathrm{m}} \delta_{mj}(n) \cdot y_{omi}(n) \cdot \Delta_1(n-1) > 0 \\ lr_{ij}(n) \cdot b & if \sum_{\mathrm{m}} \delta_{mj}(n) \cdot y_{omi}(n) \cdot \Delta_1(n-1) < 0 \\ lr_{ij}(n) & other \end{cases} \tag{D.17}$$

$$\Delta_1(n) = c \cdot \Delta_1(n-1) + (1+c)[\sum_m \delta_{mj}(n) y_{omi}(n)] \tag{D.18}$$

$$\Delta_1(0) = \sum_m \delta_{mj}(0) y_{omi}(0) \tag{D.19}$$

where, a>1, 0<b<1, 0<c<1.

D.3 The Neural Network Training Process

The neural networks are trained to find the adoptive weights and threshold value for approaching the relation between the inputs and outputs. The flow chart is shown in figure D.3. The structure of the neural networks is built according to the mathematic model of the controlled system. Then the first neural networks are initialized randomly for starting the training process. This training process is carried out according to (D.15)-(D.19) until the error requirement is satisfied. After that the trained networks should be validated by the validating

database. If it fails to validate, new neural networks should be built to find the solution of the problem. Figure D.3 displays the main steps of a general training process for a feed-forward neural network.

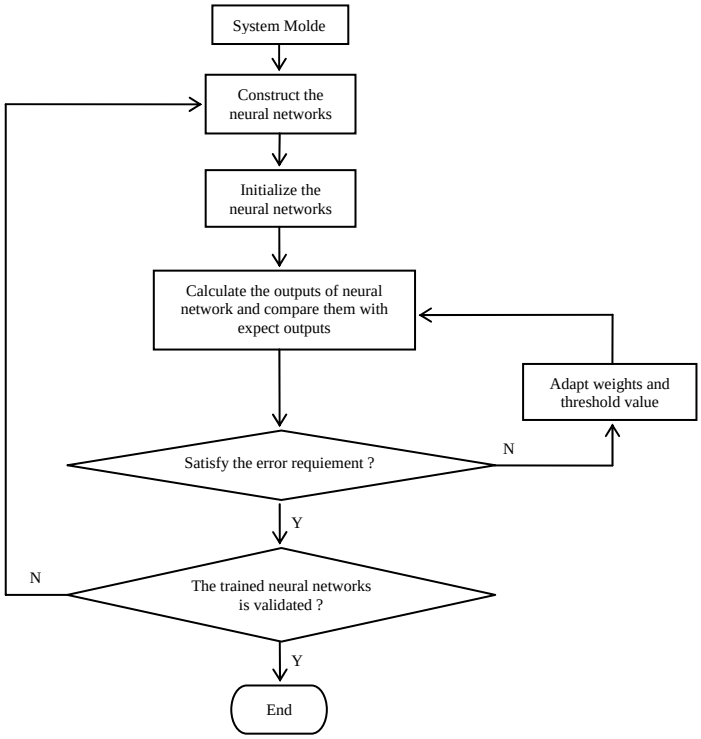

Figure D.3 Flow chart of general feed-forward neural networks training

REFERENCES

AAPID. *All engines-out landing due to fuel exhaustion*, Air Transat, Airbus A330-243 marks C-Gits, Lajes, Azores, Portugal, 24 August 2001. Aviation Accidents Prevention and Investigation Department, final investigation report 22/ACCID/2001.

AIRBUS[1]. Getting to grips with the cost index. *Customer services, airbus*, 1998, n°2, p. 23–33.

AIRBUS[2]. *A320 family instructor support*. Training & flight operations support division, Ref: UHG01041, Jan. 2001

AIRBUS[3]. *Aircraft maintenance manul*:A319/A320/A321. AIRBUS, France, 27-90-00

ANDREEVA-MORI A., SUZUKI S., ITOH E. Scheduling of arrival aircraft based on minimum fuel burn descents. *ASEAN engineering journal*, Jun. 2011.

ANSV. *Final report: Accident involving ART 72 aircraft registration marks RS-LBB* ditching off the coast of Capo Gallo (Palermo- Sicily) August 6th, 2005. Agenzia Nazionale per la Sicurezza del Volo.

ARDEMA M. D., ASUNCION B. C. Flight path optimization at constant altitude. *Variational and aerospace engineering*, Springer optimization and its applications, 2009, vol.33, p.21-32.

ARENDT D. 2001 Nall report : general aviation accident trends and factors for 2000. *AOPA Air Safety Foundation*, 2002, publisher: Bruce Landsberg.

ASSEO S. J. Terrain following/terrain avoidance path optimization using the method of steepest descent. *Aerospace and Electronics Conference*, 1988. NAECON 1988, proceeding of the IEEE 1988 National Date of Conference, 23-27 May 1988

BARRON R. Universal approximation bounds for superposition of a sigmoidal function. *IEEE Transactions on information theory*, 1993, vol.39, n°32, p. 930–945.

BASU J. K., BHATTACHARYYA D., KIM T. Use of artificial neural network in pattern recognition. *International journal of software engineering and its applications*, Apr. 2010, vol.4, n°2, p. 23–33.

BECKMAN M. J. *Dynamic Programming of economic decisions*. Berlin: Springer Verlag.

BELLMAN R.E.[1] *Dynamic Programming*. Princeton University Press, New Jersey, 1957.

BELLMAN R.E.[2], KALABA R., *Dynamic Programming and modern control theory*. Academic Press, New York, 1965.

BERTSEKAS D. P.[1] *Dynamic Programming and optimal control*. 2005, Athena Scientific.

BERTSEKAS D. P.[2], HOMER M.L., LOGAN D.A., PATEK S.D., SANDELL N.R. Missile defense and interceptor allocation by neuro-dynamic programming. *Systems, man and cybernetics, part A: Systems and humans, IEEE Tansactions on*, 2000, vol. 30, n°1, p. 42–51.

BERTSEKAS D. P.[3], *Neuro-Dynamic Programming*. Encyclopedia of optimization 2009, p. 2555-2560.

BETTS J. T[1]. Practical methods for optimal control using Nonlinear Programming. *Advances in design and control*, Society of Industrial and Applied Mathematics, 2001.

BETTS J. T[2]. Survey of numerical methods for trajectory optimization. *Journal of Guidance, Control, and Dynamics*, 1998, vol. 21, n°2, p. 193–207.

BHATTACHARYA R., SINGLA P. Nonlinear trajectory generation using global local approximations. *Proceedings of the 45th IEEE Conference on Decision & Control*, Dec 13-15, 2006, San Diego, CA, USA.

BISHOP C.M. *Neural networks for pattern recognition*. Clarendon Press. Oxford, 1995.

BOCK H.G., PLITT K.J. A multiple shooting algorithm for direct solution of optimal control problems. Institut fur Angewandte Mathematic, report 09.2/A-5, SFB 72, University of Bonn, in preprints of the 9th *IFAC World Congress*, Budapest, Hungary, 1984, vol. 9, p. 242–247.

BOLLINO K. P., LEWIS L. R., SEKHAVAT P., ROSS I. M. Pseudospectral optimal control: a clear road for autonomous intelligent path planning. *AIAA* Infotech@Aerospace 2007 Conference and Exhibit, Reston, VA, 7-10 May 2007.

BOSEDE O.R., EMMANUEL F. S., TEMITAYO O. J. On some numerical methods for solving initial value problems in Ordinary Differential Equations. *IOSR Journal of Mathmatics*, July-Aug. 2012, vo. 1, p.25-31.

BOTKIN N. D., TUROVA V. L. Application of dynamic programming approach to aircraft take-off in a windshear. *AIP Conference Proceedings*, Proc. 1479, 1226, 2012

BRUNT B. v. *The Calculus of Variations*. 2004, Springer. ISBN 0-387-40247-0, VII and VIII.

BRYSON A.E., HO Yu-Chi, *Applied optimal control*, Revised Printing, Hemisphere Publishing Corporation, 1975

BUCHANAN J. L. and TURNER P. R. Numerical methods and analysis. McGraw Hill, New York, 1992

BURGIN G. H., SCHNETZLER S. S. Artificial neural networks in flight control and flight management systems. *Aerospace and electronics conference*, NAECON 1990., proceeding of the IEEE 1990national, 21-25 May 1990, vol.2, p.567-573.

CALISE A. J.[1] Extended energy management methods for flight performance optimization. *AIAA Journal*, 1977, vol. 15, n°3, p. 314–321.

CALISE A. J.[2] Neural networks in nonlinear aircraft flight control. *Aerospace and electronic systems magazine*, IEEE, Jul. 1996, vol. 11, n°7, p.5–10.

CAMPBELL S. E., NEOGI Natasha A., and BRAGG Michael B. An optimal strategy for persistent contrail avoidance. *AIAA Guidence, Navigation and Control Conference and Exhibit*, Aug 2008, Honolulu, Hawaii.

CARTWRIGHT J. H. E., PIRO O. *The dynamics of Runge-Kutta Methods*. Int. J. Bifurcation and Chaos, 2, 427-449,1992, School of Mathematical Sciences, Queen Mary and Westfield College, University of London.

CHEN F. C. Back-propagation neural networks for nonlinear sef-tuning adaptive control. *Contro systems magazine*, IEEE, Apr. 1990, vol.10, n° 3, p. 44-48.

CHENG P., SHEN Z., LAVALLE S. M. RRT-based trajectory design for autonomous automobiles ans spacecraft. *Archives of control sciences*, 2001, vol. 11, n° 3- 4, p. 167-194.

CHEN L., NARENDRA K. S. Intelligent control using multiple neural networks. *International journal of adaptive control and signal processing*. 2003, vol.17, p. 417-430.

CHEN Y.H., CHERN J.S., HONG Z.C. Optimal turning of winged space vehicales at constant altitude. *Acta Astronautica*, Sept. 1996, vol. 39, n°6, p. 423-429.

CHIDRAWAR S., PATRE B. Generalized predictive control and neural generalized predictive control. *Leonardo journal of sciences*, 2008, vol.13, p. 133-152.

CLARKE F. The maximum principle in optimal control, then and now. *Control and cybernetics*, 2005, vol.34, n°31, p. 709-722.

CLEMENTS J. C. Minimum-time turn tr ajectories to fly-to points. *Optimal control applications and methods*, Jan./Mar. 1990, vol. 11, n°1, p. 39-50.

CONROY M. T. Aircraft addident that caused major changes to emergency response equipment and procedures. *The International Forum on Emergency and Risk Management*, Singapore Aviation Academy, 10-12 Jan. 2005.

CORONADO H., RODRIGEZ R., SLOSS T., SORLEY S. RAM air turbine – white team. [Report]. US: Duke University, 2008, http://www.mems.duke.edu/files/mems/RAT%20Blue%20Final_Report.pdf

COVERSTONE-CARROLL V. L. Near-ptimal low-thrust trajectories via micro-genetic Algorithms. *Journal of guidance, control, and dynamics*, 1997, vol. 20, n°1, p. 196-198.

CYBENKO G. Approximation by superpositions of a sigmoidal function. *Mathematics of control, signals and systems*. 1989, vol.2, n°4, p. 303-314.

DESOER C.A. Pontryagin's Maximum Principle and the principle of optimality. *Journal Franklin Inst.*, 1961,vol. 271, n°5, p. 361-367.

DICKMANNS E.D., WELL K.H. Parametrization of optimal control problems using piecewise polynomial approximation. *AIAA 74-822, AIAA Mechanics and control of Flight Conference*, 5-9 August, 1974, Anaheim, California.

DOUGUI N.E., DELAHAYE D., PUECHMOREL S., MONGEAU M. Light propagation algorithm for aircraft trajectory planning. *American Control Conference (ACC),* 29 Jun.-1 Jul. 2011, San Francisco, CA, USA, p.2143-2147

DREYFUSE S. E., LAW A. M., *The art and theory of dynamic programming*. Mathematics in science and engineering, vol.130, chapter 8, Academic Press, INC, 1977

ETKIN B. Dynamics of atmospheric flight. *John Wiley & Sons*, USA, first edition.

FAHROO F.[1], and ROSS I. M. Costate estimation by a legendre pseudo-spectra method. *Journal of Guidance, Control, and Dynamics*, March-April 2001,vol. 24, n° 2, p. 270–277.

FAHROO F.[2], and ROSS I. M. Direct trajectory optimization by a Chebyshev pseudospectral method. *Journal of Guidance, Control, and Dynamics*, 2002, vol. 25, n° 1, p. 160–166.

FAYE R.M., SAWADOGO S., MORA-CAMINO F. Flexible management of water resource system. *Applied mathematics and computation*167 (2005), p.516-527.

FETEIH S., BRECKENRIDGE G. Neural network based estimator for a maneuvering aircraft. *American control conference*, 2-4 Jun. 1993, p. 1380-1384.

FLIESS M., LEVINE J., MARTIN Ph., ROUCHON P. Flatness and defect of nonlinear systems: introductory theory and examples. *International journal control*, 1995, vol. 61, n°6, p. 1327-1361.

FUNAHASHI K. On the approximate realization of continuous mappings by neural networks. *Neural networks*, 1989, vol. 2, p.183-192.

GAO C., Hess R. (1993), Inverse Simulation of Large-Amplitude Aircraft Maneuvers, *Journal of Guidance, Control and Dynamics*, 1993, vol. 16, n°4, p. 733-737.

HAGELAUER P., MORA-CAMINO F., A soft dynamic programming approach for on-line aircraft 4D-trajectory optimization, *European Journal of Operational Research*, 16 May 1998, vol. 107, n° 1, p. 87–95.

HAMEL, P. G.[1], JATEGAONKAR, R. V. Evolution of flight vehicle system identification. *Journal of Aircraft*, Jan.-Feb. 1996, Vol. 33, n°14, p. 9-28.

HAMEL, P. G.[2], JATEGAONKAR, R. V. The role of system identification for flight vehicle applications- revisited. *RTO SCI Symposium on "System Identification for Integrated Aircraft Development and Flight Testing*", 5-7 May, 1998, Madrid, Spain, published in RTO MP-11.

HAMILTON J. A. Final report on Ethiopian Airlines B767-260ER (ET-AIZ) aircraft accident. Ethiopian Civil Aviation Authority Flight Safety Department, 20 May 1998.

HARGRAVES C.R., PARIS S.W., Direct trajectory optimization using nonlinear programming and collocation. *Journal of Guidance, Control, and Dynamics*, Jul.-Agu. 1987,vol. 10, n° 4, p. 338–342.

HORNIK K., STINCHCOMBE M., WHITE H. Multilayer feedforward networks are universal approximations. *Neural networks*, 1989, vol.2, p. 359-366.

HULL D. G., Conversion of optimal control problems into parameter optimization problems. *Journal of Guidance, Control, and Dynamics*, January-February 1997, vol. 20, n° 1, p. 57–60.

ICAO[1]. *2011 state of global aviation safety*. Published in Montreal, Canada, ICAO, 2011.

ICAO[2]. *Manual on volcanic ash, radioactive material and toxic chemical clouds*. Second edition , 2007, Doc 9691, AN/954, ICAO.

ISERLES A. *Numerical solution of differential equations*, Part III. Michaelmas 2007, Numerical analysis group, Centre for Mathematical Sciences, University of Cambridge, version 2.7182818284590, Sept. 2006.

IYER R. V., ARIZPE Rachelle, CHANDLER Phillip R. On the existence and uniqueness of minimum time optimal trajectory for a micro air vehicle under wind conditions. *Emergent Problems in Nonlinear Systems and Control*. Lecture notes in control and information science, 2009, vol. 393, p. 57-77.

JACOBSON David H., MAYNE David Q. *Differential dynamic programming*. New York, American Elsevier Pub. Co., 1970.

JARDIN M. R. and BRYSON Jr. A. E. Neighboring optimal aircraft guidance in winds. *Journal of Guidance, Control and Dynamics*, Jul.-Aug. 2001, vol. 24, n°4, p. 710-715.

KOBAYASHI T., SIMON D. L. A hybrid neural network-genetic algorithm technique for aircraft engine performance diagnostics. *AIAA-2001-3763*, ARL-TR-1266, Jul. 2001.

LAWDEN D.F., Optimal trajectories for space navigation. *Butterworth Mathematical Text*, Butterworth, London, 1963.

LIU Z., HOU M., WEN G. Experimental Determination of Aero-Engine Windmilling Drag. *Journal of Aerospace Power*, April 2006, vol.21, n°2, in Chinese.

LOONEY C. G. Neural works as expert systems. *Expert systems with applications*, 1993, vol. 6, n°2, p. 129-136.

LU W.[1], DUAN L., MORA-CAMINO F., ACHAIBOU K. Design of a genetic flight guidance system based on differential flatness and neural works. *Proceeding of the V International conference "System identification and control problems"*, SICPRO'06, 30 Jan.-2 Feb. 2006, Moscow(Russia).

LU W.[2], MORA-CAMINO F., ACHAIBOU A. Differential flatness and flight guidance: A neural adaptive approach. *Proceeding of AIAA Guidance, navigation and Control Conference*, 14-18 Aug. 2005, San Francisco (E.U)..

LU W.[3], MORA-CAMINO F., ACHAIBOU A. New approaches for flight guidance based on neural networks., *Proceeding of the IV International conference "System identification and control problems"*, SICPRO'05, 25-28 Jan. 2005, Moscow(Russia).

MAINE, R. E., ILIFF, K. W. Identification of dynamic systems - applications to aircraft. Part I : the output error approach. Dec. 1986, AGARD AC-300-Vol. 3, Part I.

MCGEE T. G., SPRY S., HEDRICK J. K. Optimal path planning in a constant wind with a bounded turning rate. Proc. *AIAA Guidance , Navigation, and Control (electronic), 2005, no. AIAA 2005-6186, San Francisco, California*, Aug. 2005.

MCLEAN D. *Automatic Flight Control System.* UK : Prentice Hall International, 1990, ch 2, p16-p60.

MELISSA J. P. *ICAO: Investigation of human factors in accidents and incidents*. Aviation knowledge, 2009.

MIELE A.[1], WANG T., WANG H., MELVIN W.W. Optimal penetration landing trajectories in the presence of windshear. *Journal of optimization theory and application*, Apr. 1988, vol. 57, n° 1, p. 1-40.

MIELE A.[2], WANG T., MELVIN W. W. Optimal take-off trajectories in the presence of windshear. *Journal of optimization theory and applications*, April 1986, vol. 49, n° 1, p. 1-45

MIELE A.[3], WANG T., MELVIN W. W. Quasi-steady flight to quasi-steady flight transition in a wind shear: trajectory optimization and guidance. *Journal of optimization theory and applications*, Aug. 1987, vol. 49, n° 2, p. 203-240

MORA-CAMINO F[1]. *Asservissements linéaires continues*. Synthèse d'un régulateur pour une servocommande aéronautique, IENAC 2004, Bureau d'études en automatique.

MORA-CAMINO F.[2], ACHAIBOU K., and OUATTARA B., Trajectory generation for relative guidance of merging aircraft. *Optimization and cooperative control strategies*, Lecture Notes in Control and Information Sciences, 2009,vol. 381, p. 151-166

MORA-CAMINO F.[3], ACHAIBOU A., MIQUEL T., FAYE R., OUATTARA B., SAWADOGO S. Minimum time trajectory generation for relative guidance of aircraft. *Inverse problems, design and optimization sympotium*, Rio de Janeiro, Brazil, 2004, (electronic).

NANDALAL K. D. W.,BOGARDI Janos J. *Dynamic Programming Based Operation of Reservoirs: Applicability and Limits*. 2007, chapter5.

NELSON, Robert C. *Flight Stability and Automatic Control*. US : McGraw-Hill Book Company, 1989, chaper 2,3, .

NG Hok K., GRABBE Shon, MUKHERJEE Avijit, Design and evaluation of Dynamic Programming flight routing algorithm using the convective weather avoicence model. *AIAA Guidence, Navigation and Control Conference*, Aug 2009, Chicago, Illinois.

NGO A. D. A fuel-optimal trajectory for a constrained hypersonic vehicle using a direcr transcription method. *2004 IEEE Aeropace Conference Proceedings*, p. 2704-2709.

NOTTROT R. Pontryagin's maximam principle for a constrained system of ordinary differential equations. *Journal of engineering mathematics*, Apr. 1968, vol.2, n°2, p. 109-121.

National transportation safety board (NTSB[1]). *Aircraft accident report*: Loss of thrust in both engines after encountering a flock of birds and subsequent ditching on the Hudson River. 4 May 2010, Notation 8082A, Washington.

NTSB[2]. *Aircraft accident report, Southern Airways*, Inc., DC-9-31, N1335u, New Hope, Georgia, April 4, 1977. Report No. NTSB-AAR-78-3, USA, Jan. 1978.

OLVER P. J. Applied mathmatics lecture notes. 14 Dec 2012, ch.20 p.1081-1142, www.math.umn.edu/~olver/appl.html

PONTRYAGIN L. S. The mathmatical theory of optimal processes. Gordon and Science Publishers, 1986.

PRATT R. W. *Flight Control System*. UK : the Institution of Electrical Engineers, Micheal Faraday House, 2000.

RAUWOLF G.A.; COVERSTONE-CARROLL, V. L. Near-optimal low-thrust orbit transfers generated by a genetic algorithm. *Journal of Spacecraft and Rockets*, vol. 33, n°6, p. 859-862.

RAYMER Daniel P. *Aircraft design: a conceptual approach*. American Institute of Aeronautics and Astronautics, Inc. 2nd edition, Washington, 1992, XII-297.

ROSS I. M. *A primer on pontryagin's principle in optimal control*. Collegiate Publishers,2009, chapter 2 Pontryagin's principle

SAGHAFI F., KHANSARI ZADEH S. M., ETMINAN BAKHSH V. Aircraft visual identification by neural networks. *Journal of aerospace science and technology*, Sep. 2008, vol.5, n°3, p.123-128.

SEYWALD H., KUMAR R.R. Method for automatic costate calculation, *Journal of Guidance, Control, and Dynamics*, November-Decedmber 1996, vol. 19, n°6, p.1252-1261.

SHAVER C. *A330-200 CBT NOTES*. June 3, 2002, Pilot assistance notes

SHI Y., XU M., WANG Z. Constrained trajectory optimization for hypersonic unpowered glider in near spece using Gauss Pseudospectral method. *2011 International Conference on Electronic & Mechanical Engineering and Information Technology*, 12-14 Aug. 2011, Harbin, Heilongjiang, p.3804-3807.

SLEIGHT P A, CARTER R D G. Report on the accident to Boeing 7777-236ER, G-YMMM, at London Heathrow Airport. *Department for Transportation* (Air Accidents Investigation Branch), 9 Feb. 2010, UK.

SMITH K., PALANISWAMI M., KRISHNAMOORTHY M. Neural techniques for combinatorial optimization with allplications. *IEEE transations on neural network*, Nov. 1998, vol 9, n°6, p.1301-11318.

SOLER M., OLIVARES A., STAFFETTI E. En-route optimal flight planning constrained to pass through waypoints using MINLP. *Ninth USA/Europe air traffic management research and development seminar (ATM2011)*, (electronic) , Berlin, 16 Jun. 2011.

Sourdine II Consortium, Identification document , Study of optimization proceDURes for decreasing the impact of noisE II, 2003. Report D1-1 Available at http://www.sourdine.org/pub-documents.html

STECK J.E., BALAKRISHNAN S.N. Use of Hopfield neural networks in optimal guidance. *Aerospace and electronic systems*, IEEE Transactions on, Jan 1994, vol.30, n°1, p.287 -293.

STRYK O. von, BULIRSCH R. Direct and indirect methods for trajectory optimization, *Annals of Operational Research*, 1992, vol.**37**, p.357-373.

SU M., WANG Y.J., LIU L., CHANG S.T. Design of reentry vehicle trajectory optimization based on improved particle swarm optimization algorithm. *Computing Technology and Automation*, 2011, vol. 39, n°4, p.55-59.

SUN W., YUAN Y. *Optimization theory and methods, Nonlinear Programming*. Springer optimization and its applications, 2006, vol. 1.

SUZUKI Shinji, TSUCHIYA Takeshi, ANDREEVA Adriana, Trajectory optimization for safe, clean and quiet flight, *ENRI international workshop on ATM/CNS*, Tokyo, Japan, Mar. 2009, (EIWAC 2009)

THE 2005 CONGRESS AND EXPOSITION ON NOISE CONTROL ENGINEERING, Containing aircraft noise levels at take-off: a mathematical programming approach. Fatiha NEJJARI, Xavier PRATS, Vicenc PUIG, Monique PILOT, Baba OUATTARA, Karim ACHAIBOU, Felix MORA-CAMINO. Rio de Janeiro, Internoise 2005.

VEELENTURF L.P.J. *Analysis and applications of artificial neural networks*. Prentice Hall International (UK) Limited, 1995, chapter 3, p.66-169.

VINH. Nguyen X. *Flight Mechanics of High-Performance Aircraft*. Cambridge University Press, 1993, chapter 5, p91-p104.

VISSER H.G. A 4-D trajectory optimization and guidance technique for terminal area traffic management. Report LR-769, June 1994, TU, Delft, Nederlands.

WALLER M.C., BLACKMAN D.R., BERREEN T.F. Aspects of Dynamic Programming in trajectory generation. *Australian Aeronautical Conference, 1989*: Research and Technology, the Next Decade, Melbourne, 9-11 Oct. 1989.

WANG H., YANG C.F., LIU H.J. Improved ant colony algorithm and its application on trajectory optimization. *Computer engineering and applications*, 2008, vol. 44, n° 28, p. 217-219.

WANG Z., WANG Y., QIAO W., LIU W. Extrapolating component maps into the low speed and simulation of windmilling performance of turbofan engine. *Journal of Propulsion Technology*, April 2006, vol.27, n°2, p146-p149.

WERBOS P. J. Backpropagation: basic and new development. *The handbook of brain theory and neural networks*, MIT Press, M.A. Aribib Ed., 1995, p.134-139

WILLIAMS M. The 156-tonne GIMILI GLIDER. *Flight safety Australia*. July-Aug. 2003, p. 22-27.

WU H.[1] Management of Emergency Trajectory for Transport Aircraft, MSc Repport, ENAC, Toulouse, September 2010.

WU H.[2], CHO N. C., BOUADI H., ZHONG L., MORA-CAMINO F. Dynamic Programming for Trajectory Optimization of Engine-Out Transportation Aircraft , *CCDC 2012*, Taiyuan , May 2012.

WU H.[3], MORA-CAMINO F. Glide control for engine-out aircraft. *AIAA Guidance, Navigation, and Control Conference*, 13-16 Aug. 2012, Minneapolis, Minnesota.

XIE F.Q., WU H., TANG L.L. Design of vehicle reentry trajectory optimization based on particle swarm optimization algorithm. *Computing Technology and Automation*, 2008, vol. 27, n° 4, p. 72-75.

XIE Y., ZHENG W., TANG G. Analysis of flight performance using neural networks. *Natural computation* (ICNC), *2012 Eighth international conference*, 29-31 May 2012, p. 380-384.

YANG X.X., JIANG Z.Y., ZHANG W.H. A particle swarm optimization algorithm based solid launch vehicle ascent trajectory optimal design. *Journal of Astronautics*, 2010,vol 5, p. 1304-1308

RÉSUMÉ

CONTRIBUTION À LA GESTION ET AU CONTRÔLE DE TRAJECTOIRE D'UN AVION AVEC PANNE TOTALE DES MOTEURS

CHAPITRE I

INTRODUCTION GÉNÉRALE

Le transport aérien a joué le long des dernières décennies un rôle important pour permettre la communication et le transport des biens et des personnes au sein d'une économie mondiale de plus en plus globalisée. Selon les statistiques de l'IATA (International Air Transport Association), 2,8 milliards de personnes ont voyagé sur 38 millions de vols en 2011. Ce nombre devrait augmenter considérablement à l'avenir. Selon les statistiques d'accidents mortels au cours des décennies, en comparant les différents moyens de transport (ferroviaire, maritime, routier et aérien), le transport aérien semble être le mode de transport le plus sûr. Grâce aux efforts des concepteurs d'avions, des avionneurs, des compagnies aériennes, des contrôleurs aériens, des règlements de transport aérien et d'autres, la probabilité d'accidents d'aéronefs avec victimes a été réduite à une valeur très faible. Bien que la sécurité de l'aviation a été de la plus haute priorité pour les organisations telles que ICAO (International Civil Aviation mondiale) et de l'IATA (International Air Transport Association), des catastrophes continuent de se produire de temps en temps. En général, ces catastrophes affectent tous les passagers et membres d'équipage de l'aéronef avec un nombre élevé de victimes et ont un effet très impressionnant pour le public.

Le niveau actuel de la sécurité est d’un accident mortel par million de vols. Il s'agit d'un objectif global qui a été fixée par l'OACI depuis des décennies. Des études montrent que les facteurs humains sont les contributeurs principaux aux accidents de transport aérien, en particulier lorsque certaines défaillances techniques ou plusieurs autres facteurs défavorables tels que la météo ou des problèmes de maintenance, apparaissent. Les pilotes jouent un rôle décisif dans la gestion des situations non standard pour lesquelles les systèmes automatiques n'ont pas été conçus pour faire face à eux. Ainsi, la conception de systèmes automatiques d’aide à la décision peuvent contribuer à gérer efficacement les situations critiques telles que la panne complète des moteurs.

Les moteurs sont essentiels pour la sécurité du vol. Sans leur fonctionnement sans défaillance, les avions sont incapables de se maintenir en vol. La panne des moteurs est un

facteur indéniablement dramatique pour la sécurité du vol puisque le domaine de vol de l'avion subit ensuite un rétrécissement dramatique alors que la disponibilité des actionneurs aérodynamiques est entravée par le déficit de puissance résiduelle disponible. De nombreux incidents et accidents résultent d'une panne de moteur et certains autres de la panne complète des moteurs.

C’est un cas très particulier de panne peu souhaitable, dans lequel tous les moteurs tombent en panne à un moment donné pendant le vol. On suppose que la panne moteur se produit lorsque l'avion a déjà acquis une certaine vitesse et altitude après le décollage ou est déjà en croisière ou est en train d'effectuer les premières étapes de la descente pour l'approche. Donc, ici, nous ne considérons pas le cas dans lequel un moteur en panne survient dans les premières étapes de montée ou de l'approche finale. Dans ces deux cas, la capacité de survie de l'avion est entièrement tributaire des compétences du pilote et sa réaction immédiate à cette situation catastrophique.

Il semble que dans le cas d’un arrêt total des moteurs, toute mauvaise décision prise par pilote peut avoir des conséquences catastrophiques, comme c'est le cas avec des situations de pannes moins critiques où un pour cent des accidents mortels est lié à l'action de pilote.

Il semble donc tout à fait intéressant d'essayer de développer une aide au pilotage pour cette situation. Cette nouvelle fonction pourrait être intégrée dans le système de guidage à côté du système de gestion de vol (FMS) de l'avion chargé lui de sélectionner un site d'atterrissage approprié et de calculer une trajectoire possible vers ce site. Ensuite, le système de guidage proposé travaillera en mode directeur de vol d'urgence en générant des indications pour que le pilote effectue une descente en toute sécurité et arrive avec une perspective de survie au site d'atterrissage.

Pour atteindre ce but, les étapes principales qui doivent être effectuées sont :

- Établir et analyser la dynamique de vol d'un avion de transport aérien avec panne moteur totale.

- Etudier les caractéristiques de planeur et les qualités de vol d'un avion de transport.

- Élaborer une méthode pour établir le domaine de vol plané à partir d'une situation donnée.

- Développer une méthode pour déterminer la trajectoire optimale de plané vers un lieu d'atterrissage en toute sécurité.

- Développer un système en ligne d'aide au vol plané.

Selon les objectifs mentionnés ci-dessus, la thèse a été divisée en plusieurs chapitres:

- Dans le chapitre I l'importance de l'optimisation du vol plané avec panne totale des moteurs est analysée.

- Dans le chapitre II, certaines situations de panne totale des moteurs sont analysées.

- Dans le chapitre III, la dynamique de vol des avions soumis à une panne totale moteur est étudiée.

- Dans le chapitre IV, les performances du vol plané, moteurs en panne, sont étudiés dans le but de trouver la zone accessible à l'avion.

- Dans le chapitre V la stabilité du vol plané est discutée.

- Dans le chapitre VI une étude des méthodes d'optimisation de trajectoire d'avion est développée.

- Dans le chapitre VII la méthode choisie pour l'optimisation de la trajectoire d'un avion en panne totale de moteurs est présentée et des résultats numériques sont affichés. Cela permet d'identifier le domaine sûr de descente et de construire la base de données correspondante.

- Dans le chapitre VIII un système en ligne d'aide au pilotage en vol plané est construit à partir de la base de données générée au chapitre VII et des résultats numériques ainsi que des interfaces possibles pour le système d'aide sont fournis.

- Enfin, la conclusion et les perspectives de cette étude sont présentées dans le chapitre IX.

CHAPITRE II

SITUATIONS DE PANNE TOTALE MOTEUR ET CONSÉQUENCES

Ce chapitre présente d'abord un aperçu des principaux événements rapportés de panne totale moteur ainsi qu'une brève analyse des conséquences pour les systèmes avion. Ensuite, il présente les principales conséquences de la panne totale des moteurs par rapport aux systèmes embarqués directement liées à la surviviabilité du vol dans cette situation. En effet, cette étude n'est pas consacrée à la sécurité ou à la conception des aéronefs et à l'analyse des risques des systèmes de bord, mais plutôt à la conception de dispositifs opérationnels et de méthodes de gestion pour cette situation catastrophique avec une certaine perspective de survie. Ainsi, après avoir décrit les principaux composants des systèmes hydrauliques d'un avion de transport, le fonctionnement d'un actionneur aérodynamique sous asservissement avec différentes conditions de pression est analysé. Cet aspect est essentiel afin de vérifier la maîtrise de l'appareil par ses surfaces aérodynamiques. Est également considérée dans ce chapitre, l'évolution de la température et de la pression de la cabine pendant le vol plané sans ou avec réduction de la climatisation, de sorte que la menace de santé qui en résulte pour les passagers et l'équipage est évaluée.

Il n'existe pas-de procédures d'urgences publiées par les avionneurs dans le cas de panne totale moteur. Cette situation est considérée comme extrêmement improbable (probabilité < 10-9 /heures de vol) avec des conséquences catastrophiques. Il existe des procédures en cas de panne d'un seul moteur pour un avion multi-moteur et jusqu'à deux moteurs en panne pour un avion quadrimoteur. En fonction de la phase de vol à laquelle arrive la panne moteur, les actions à entreprendre sont différentes. Au décollage, on réduit le taux de montée après la panne de moteur pour limiter la perte de vitesse, L'aide d'un HUD paraît ici très souhaitable. Si la panne partielle de moteur se produit au-delà, l'adoption de la vitesse green dot permettra d'avoir une distance maximale de vol de façon à choisir au mieux l'aéroport dátterrissaage. De l'étude développée dans ce chapitre, il en ressort que le principal effet sur les systèmes embarqués est la perte de la source d'énergie principale qui va gêner le pilote pour contrôler efficacement les surfaces aérodynamiques tout au long du vol plané et spécialement à

proximité de l’atterrissage. Le pilote automatique sera limité, les fonctions normales d'autoguidage ne seront pas disponibles. Les conséquences pour l'ambiance dans la cabine seront limitées à une température inconfortable et des conditions de pression variables, mais sans criticité. Les effets causés par la panne totale de moteurs pour l'alimentation électrique peuvent être limités par le fonctionnement d’équipements auxiliaires tels que la RAT et l'APU, fournissant une source auxiliaire d'alimentation pour les ordinateurs de vol et le contrôle des surfaces aérodynamiques principales.

CHAPITRE III

LA DYNAMIQUE DU VOL AVEC PANNE TOTALE MOTEUR

Dans ce chapitre, la dynamique d'un avion de transport en vol plané est considérée. Elle n’est pas trop différente de la dynamique du vol d'un avion de transport à moteur étudiée dans les ouvrages de référence. A première vue, la principale différence avec le vol plané est l'absence de poussée pour équilibrer la force de traînée qui est augmentée par la traînée des moteurs mis à l'arrêt par la panne.

Dans une première partie de ce chapitre, après avoir présenté les repères de référence utiles pour la présente étude, ainsi que les forces et moments externes appliqués à l'avion en vol plané, les équations de la dynamique de vol de l'avion en vol plané sont présentées. Dans la deuxième partie de ce chapitre, puisque l'avion en vol plané est particulièrement vulnérable par rapport au vent, les relations entre les angles d'attitude comme angle d'inclinaison, l'angle dassiette et de l’incidence par rapport à la vitesse et la vitesse du vent sont pris en considération. L'influence de la vitesse du vent sur la valeur de l'assiette est étudiée et une application numérique est développée.

Si la dynamique de vol moteur en panne est très similaire à la dynamique d'un aéronef à moteur, ce qui devient fondamental dans ce cas est la relation de l'avion avec l'air environnant et surtout le vent environnant. Il a été démontré dans la dernière partie de ce chapitre que l'avion en vol plané peut se trouver dans une situation critique par rapport au décrochage alors qu'il n'a aucun moyen de réagir à cette situation (pour un aéronef à moteur en marche, un

surplus de poussée permettra de réduire ce danger - Mode α-ground). Dans le chapitre suivant, les performances du vol plané d'un aéronef seront étudiées.

CHAPITRE IV

PERFORMANCES DU VOL PLANÉ DES AVIONS DE TRANSPORT

Sans puissance moteur, l'aéronef ne peut 'voler que sur une distance très limitée, qui dépend de l'énergie totale apparente (énergie potentielle et l'énergie cinétique) de l'appareil au début de la descente. Parmi les sites possibles d'atterrissage joignables identifiés, l'un d'eux est choisi en tenant compte de la configuration du terrain environnant ainsi que des informations sur le vent. Dans ce chapitre, les performances du vol plané d'un avion de transport sont analysées afin de déterminer la distance maximale atteignable. Pour cela, tout d'abord nous considérons la formulation d'un problème d'optimisation pour obtenir les conditions d'une distance maximale de descente. Puis une approche simplifiée considérant des conditions de vol plané au voisinage de l'équilibre est développée pour estimer la portée maximale et caractériser directement le taux de descente minimum.

Dans ce chapitre, les performances du vol plané en conditions de quasi équilibre pour un avion de transport ont été mises en place afin de déterminer le domaine de vol plané de l'avion sans moteur en opération. La formulation d'un problème d'optimisation pour obtenir la portée maximale de glissement a conduit à des conditions d'optimalité complexes, de sorte qu'une approche simplifiée considérant les conditions de vol plané au voisinage de l'équilibre ont été développés pour estimer la portée maximale et caractériser le taux de descente minimum. Maintenant, la question qui se pose est relative à la stabilité des trajectoires de vol plané quasi équilibrées, surtout lorsque l'avion rencontre des perturbations de vent, une situation qui est susceptible de se produire dans le vol plané sans moteur. Cette question est développée dans le chapitre suivant.

CHAPITRE V

STABILITÉ DU VOL PLANÉ POUR LES AVIONS DE TRANSPORT

Dans ce chapitre, la stabilité du vol plané autour de trajectoires de vol quasi équilibrées est étudiée. En général, l'atmosphère n'est pas complètement immobile et différentes configurations de vent produisant des perturbations peuvent être rencontrées lorsque l'avion se trouve toujours plus près du sol et probablement avec une faible vitesse le long de sa trajectoire de descente. Cette question est essentielle pour la sécurité de la trajectoire de descente car elle est directement liée à la contrôlabilité de la situation par le pilote, l'efficacité de ses actions de contrôle, ainsi que son degré d'implication dans la tâche de gestion du vol plané. L'annexe B présente les principaux concepts liés à la stabilité des systèmes non linéaires ainsi que l'approche de Lyapunov pour l'analyse de stabilité de ces systèmes.

Ici deux situations sont considérées suivant que la panne des moteurs affecte (par l'intermédiaire des circuits hydrauliques et électriques), la fonction de stabilisation longitudinale de l'avion ou non. Dans le premier cas, la stabilité dynamique autour de l'orientation des trajectoires stables glisse est étudiée tandis que dans le second cas, la période de stabilité dynamique est prise en compte.

Ce chapitre a démontré par l’analyse la stabilité du vol plané en présence de perturbations dues au vent. Les perturbations considérées bien que déterministes correspondent à des situations extrêmes dans lesquelles des impulsions pures de vitesse du vent sont appliquées à l'aéronef en vol planée. D'autres scenarios considérant des composantes stochastiques de la vitesse du vent pourraient être d'intérêt pour les études futures.

Dans le cas où le stabilisateur de tangage est hors service à la suite de l'extinction du moteur, il est apparu intéressant d'examiner la question de la stabilité du mode rapide (oscillation d’incidence) en lien direct avec le risque de décrochage et la difficulté de maîtriser l'avion en vol plané par le pilot . Dans le cas où les stabilisateurs de tangage

fonctionnent, la question a été considérée par rapport à la stabilité du vol plané autour des trajectoires de vol plané quasi équilibré.

Si dans le premier cas, les propriétés de stabilité naturelles des avions commerciaux permettent au pilote de gérer le vol plané, dans le second cas, il semble que l'intervention directe du pilote est nécessaire pour revenir à une situation stable de vol plané.

CHAPITRE VI

TECHNIQUES D'OPTIMISATION DE TRAJECTOIRE AVION

L’optimisation de trajectoire est le processus de génération d'une trajectoire réalisable qui minimise (ou maximise) un indice de performance ou critère d'optimisation. L’optimisation de trajectoire peut être vue comme un problème de commande optimale où la trajectoire à optimiser est représentée par l’évolution de son état. La génération d'une trajectoire de vol qui offre les meilleures performances par rapport aux coûts et aux services, joue un rôle important dans la conception des véhicules atmosphériques tels que les avions de transport ainsi que dans leur fonctionnement quotidien.

Les techniques qui sont aujourd'hui développées pour résoudre des problèmes d'optimisation se divisent en deux grandes classes:

- Les techniques de satisfaction des conditions d'optimalité issues de la théorie du contrôle optimal qui conduisent à la solution soit par des procédures analytiques soit numériques.
- Les techniques qui permettent de résoudre un problème approximé de commande optimale, grâce à l'utilisation d'une formulation de type programmation non-linéaire par des procédures numériques.

Les techniques de la première classe sont dits indirectes dans le sens où ils trouvent une solution aux conditions d'optimalité au cours de laquelle la différentielle de premier ordre de la mesure de la performance augmentée (le Hamiltonien), sa variation, est égale à zéro. Les techniques de la deuxième classe sont dites directes dans le sens où elles essaient de maximiser (ou minimiser) directement la mesure de la performance.

D'autres techniques, en général, issues de l'intelligence artificielle (algorithmes génétiques et d'autres techniques d'optimisation inspirées de la nature, exploration aléatoire, optimisation par essaim de particules, etc) ont été appliqués plus récemment à des problèmes d'optimisation de trajectoire. Ces techniques présentent un processus de recherche stochastique basé sur des primitives générales et leur efficacité est basée sur le caractère massif de leur calcul. En général, aucun aperçu de la structure de la solution n'est fourni par ces techniques qui sont en général assez complexes à programmer. Ensuite, un processus long et essentiellement empirique de validation et de mise au point doit être effectuée avec garantie limitée de succès.

De l'analyse effectuée dans ce chapitre, il semble que la technique de la programmation dynamique présente des caractéristiques intéressantes pour réaliser l'optimisation de trajectoires de vol plané:

- Le processus d'optimisation est totalement transparent et suit le principe d'optimalité de Bellman,
- La trajectoire optimale est construite par étapes,
- Les trajectoires partielles non optimales sont supprimées dès que possible.

Toutefois, deux difficultés se posent lors de l'application de la programmation dynamique : le volume de calculs et la taille de la mémoire nécessaire pour stocker les solutions partielles. Dans le chapitre suivant, il sera montré comment un algorithme d'optimisation de trajectoires de vol plané peut être développé par la programmation.

CHAPITRE VII

GÉNÉRATION DE TRAJECTOIRE DE VOL PLANÉ PAR LA PROGRAMMATION DYNAMIQUE

Dans ce chapitre, l'approche de programmation dynamique a été développée dans le but de produire des trajectoires optimales de vol plané à partir du niveau de croisière afin d'amener l'avion à proximité du site d'atterrissage choisi avec une situation de vol acceptable pour tenter l'atterrissage. Dans cette situation, un processus de programmation dynamique inverse

apparaît d'intérêt. Une première étape pour atteindre cet objectif de développement est de choisir une nouvelle variable indépendante, la distance au sol, afin que les étapes de la programmation dynamique puissant être définies conformément aux performances de vol et de sécurité. Ensuite, le choix d'un critère d'optimisation adéquat, ainsi que des contraintes d'état, est discuté afin de satisfaire efficacement aux objectifs essentiels de la manœuvre. Ensuite, il apparaît que la conception du processus de programmation dynamique inverse doit passer par différents choix empiriques de telle sorte que la charge de calcul qu'il génère reste acceptable, même dans un contexte hors ligne. Ces choix sont discutés en détail et les résultats numériques sont présentés.

Dans ce chapitre, le développement d'un processus de programmation dynamique inverse afin de générer des trajectoires optimales de glisse a été détaillé. En particulier, les différents moyens adoptés pour fixer le volume de calcul et de mémoire nécessaire pour construire des solutions ont été discutées et leur efficacité a été évalué. C'est le cas en particulier de:

La discrétisation spatiale proposée,

- La technique d'intégration numérique choisie et le pas d'espace,
- La fusion des états voisins,
- La règle de suppression d'états à chaque étape.

Lors de l'affichage des résultats numériques, il semble que ce qui était considéré dans un premier temps une difficulté pour l'application de l'approche de programmation dynamique inverse, peut-être, en fait, dans le contexte considéré comme opérationnel, une opportunité majeure. En effet, le processus de programmation développé, l’inversion dynamique, afin d'être aussi exhaustif et précis que possible pour fournir une solution optimale doit balayer tout le domaine possible du vol plané, générant non seulement la solution optimale en particulier, mais aussi un ensemble complet de trajectoires optimales, ou un ensemble de données de base, couvrant le domaine réalisable du vol plané et correspondant à différentes conditions initiales.

Dans le chapitre VIII un dispositif à base de réseaux de neurones sera introduit pour profiter pleinement de la base de données générée afin de proposer une nouvelle fonction pour aider le pilote à effectuer un vol plané avec les moteurs en panne qui soit satisfaisant.

CHAPITRE VIII

AIDE NEURONALE AU CONTRÔLE DU VOL PLANÉ

Dans le chapitre VII une approche de programmation dynamique inverse a été développée pour la conception de trajectoires optimales de vol plané à partir de conditions de croisière. Il semble que son application directe à la commande en temps réel est irréalisable compte tenu de la charge de calcul impliquée. Toutefois, le processus de programmation dynamique inverse génère au cours de son processus de recherche d'une base de données complète d'informations à propos d'un grand nombre de trajectoires possibles qui constituent une couverture par maillage serré, pour une masse d'aéronef donné, du domaine de vol plané.

Donc, dans ce chapitre, un nouvel outil a été développé pour tirer profit de cette base de données dans le but de fournir en ligne, des indications au pilote. L'objectif est d'aider le pilote à prendre des décisions de pilotage adéquates pour que l'avion suive une trajectoire sûre de vol plané menant à cibler le site avec une certaine probabilité d'atterrir avec succès. Cet outil est basé sur un réseau de neurones de type feed-forward qui doit être entrainé et validé sur un ensemble de trajectoires issues de la base de données générée. Des simulations numériques sont réalisées pour démontrer ce concept.

Ainsi, dans ce chapitre, un nouvel outil a été développé pour tirer profit de la base de données générée par le processus de programmation dynamique inverse décrit dans le chapitre précédent. L'objectif a été de concevoir un nouveau dispositif dont la fonction, de manière similaire aux fonctions d'un directeur de vol en vol normal, est d'aider le pilote à prendre des actions de pilotage adéquates pour que l'avion suive une trajectoire sûreté vol plané menant à rejoindre le site d’atterrissage avec une certaine probabilité de succès. Cet outil a été basé sur une structure de réseau de neurones de type feed-forward qui a été conçu, formée et validée

avec l'objectif de couvrir l'ensemble du domaine du vol plané de l'avion dans une situation de panne totale des moteurs.

Il a été constaté que la formation effective et la validation ultérieure de la structure du réseau de neurones sont des tâches complexes et doivent être atteintes grâce à la conception de plusieurs réseaux de neurones de type feed-forward dont l'unification globale est effectuée par un opérateur de type flou. Cependant, le module de calcul résultant, qui est essentiellement un interface d'entrée-sortie, peut être utilisé en ligne pour fournir des informations utiles pour le pilote manuel.

Plusieurs résultats de simulation ont été réalisés avec des vents différents (vents de face et vents arrières). Il semble que l'angle d'assiette nécessaire pour suivre une trajectoire sûre de vol plané souffre de fortes variations au cours de la manœuvre.

Enfin, un affichage de l'information générée pour le pilote est présenté. Il est proposé de fournir cette information au pilote à l'aide du Primary Flight Display. La valeur de référence de l'assiette y est comparée à l'assiette actuelle alors que l'information sur la situation de vol plané (en position, au delà, en deçà) et la vitesse et les limites des niveaux de vol sont affichées sur le panneau de l'annonciateur de mode, l'indicateur de vitesse et l'indicateur de niveau de vol. Selon ces informations de capacité d'atterrissage, le pilote pourra décider d'employer les aérofreins afin d'acquérir et maintenir au maximum la possibilité d'un atterrissage dans de bonnes conditions.

CHAPITRE IX

CONCLUSION GÉNÉRALE

La recherche d'une opération de plus en plus sûre du transport aérien sein du système de l'Aviation Civile est une entreprise sans fin pour les ingénieurs, les opérateurs et les responsables de la règlementation. Au cours de ces dernières décennies, de nouveaux dispositifs tels que les systèmes avertisseurs de proximité du sol, les systèmes anti-collision et d'autres ont été mis à la disposition des avions de transport exploités par l'Aviation Civile et ceci à un coût élevé par des processus complexes de développement impliquant la conception

et les études de définition, de sécurité, de faisabilité et d'intégration, les tests et la validation. La mise en place effective de ces systèmes, souvent poussée par des accidents dont l'apparition est liée à l'absence d'équipements équivalents, est en général difficile.

Le but de cette étude a été de faire une contribution initiale à la gestion et au contrôle de la situation critique de la panne totale des moteurs, ce qui peut être considéré, selon les statistiques, comme un événement rare, mais qui a connu récemment des réalisations spectaculaires avec des fins diverses. La contribution proposée est relative à la faisabilité d'un système d'aide au pilotage qui devrait permettre de générer l'attitude de référence à adopter de telle sorte que des trajectoires «sûres» de vol plané puissent être effectuées. Cela devrait être également un facteur limitant le stress du pilote au cours de cette situation critique et qui l'amènerait à entrer dans la phase finale d'atterrissage dans de meilleures conditions psychiques.

Tout d'abord, les conséquences à bord d'une situation de panne totale des moteurs pour un avion de transport ont été considérées pour obtenir une évaluation aussi bien des capacités restantes de commande de vol que des conditions de cabine pour les passagers et l'équipage.

Puis le vol plané sans moteur a été considéré du point de vue de la dynamique de vol et des contraintes de domaine de vol et enfin du point de vue des performances de vol, y compris la portée maximale du vol plané (le range) et le temps maximum de vol (endurance). Le concept de vol plané quasi stationnaire a été étudié et sa stabilité par rapport aux perturbations du vent a été étudiée, montrant que, dans cette situation, les actions du pilote sont nécessaires pour maintenir une trajectoire sûre de vol plané.

Puis, après avoir examiné les principales techniques d'optimisation de trajectoire disponibles dans la littérature scientifique pour faire face à la génération de trajectoires efficaces, la programmation dynamique inverse a été adoptée pour générer des trajectoires optimales de vol plané répondant à toutes les contraintes du domaine de vol. Le processus de la programmation dynamique inverse a été effectivement adapté au problème considéré, nécessitant l'introduction de nombreux paramètres pratiques pour rendre possible la tâche de calcul qui en résulte. L'adoption de l'approche de programmation dynamique inverse a conduit, lorsqu’elle est appliquée à la génération d'une base de données sur l'ensemble des trajectoires de vol plané sûres à partir de différentes situations de vol initial.

Enfin, une structure de réseau de neurones a été construite en utilisant cette base de données pour développer un système de décision en ligne pour aider le pilote à choisir l'angle d'assiette tout le long de la trajectoire de descente conduisant à une situation d'atterrissage avec une certaine perspective de survie. Une interface entre la fonction d'urgence proposée et le pilote a été également esquissée.

Cette étude pourrait être développée suivant plusieurs directions différentes de sorte qu'une gestion efficace et robuste et un système d’aide efficace dans le cas de la panne totale des moteurs transformés soit rendue possible. Des questions importantes telles que:

- Le choix d'un site d'atterrissage,

- L'efficacité des manœuvres latérales lors du vol plané sans moteur, y compris leurs conséquences en matière d'énergie totale, de vitesse et de portée maximale,

- Le développement de techniques d'estimation du vent, utiles, même en vol normal, et l'intégration de ces estimations dans le processus de calcul de l’assiette de référence,

- Le développement des moyens du bord pour estimer des paramètres de vol, y compris les valeurs actuelles des paramètres inertiels (moments d'inertie et masse) et des paramètres aérodynamiques (traînée supplémentaire des moteurs à l’arrêt en vol),

- L'adoption de versions améliorées de la méthode proposée de programmation dynamique inverse,

- Le développement d'un outil de développement d’une structure de réseaux de neurones pour mieux traiter la base de données de trajectoires générées par le processus de programmation dynamique inverse et d'améliorer le calcul de la valeur de référence de l'angle d’assiette longitudinale.

- Le développement par des spécialistes de l'interface homme-machine efficaces pour fournir les informations utiles au pilote pendant cette situation de pane critique du vol plané tous moteurs éteints.

- L'intégration à faible coût et complexité de cette nouvelle fonction dans les ordinateurs de bord responsables des protections de vol.

Il est intéressant de constater que bon nombre des propositions ci-dessus peuvent avoir des conséquences positives pour l'amélioration de l'efficacité d’autres fonctions préexistantes de de la conduite et la gestion automatique du vol.